New Amides, Amidinides, and Mixed-Metal Derivatives Thereof in Magnesium Chemistry

by

René B. Rowlings BSc (Hons)

A thesis submitted to the Department of Pure and Applied Chemistry,
University of Strathclyde, Glasgow, UK
In part of fulfilment of the requirements for the degree of Doctor of Philosophy.

September 1998

This thesis is dedicated to my grandmother, Mary R. L. Rowlings, for all her support, kindness and love given to me throughout my life.

Acknowledgements

I would like to thank the following people who have assisted me throughout my Ph.D.:

- Prof. Robert. E. Mulvey for his ever increasing enthusiasm, knowledge, dedication and above all, friendship, without whom this Ph.D. would not have been possible.

- The X-ray crystallographers, Dr Alan "R-factor". Kennedy, at Strathclyde University, for allowing me to commandeer the X-ray facility over the last 12 months. Also many thanks to Prof. Bill. Clegg, Lynne Horsburgh and Steve Liddle at the University of Newcastle.

- Dr. Dave R. "Angstrom" Armstrong for his unabating knowledge of theoretical chemistry, and above all his great sense of humour.

- The Heilbroner's past and present:

  Michael J. Ross, Fiona M. Mackenzie and Fiona J. Craig for making me feel one of the "family" and for initial help in the lab. Alan "Flying Scotsman" Robertson for running my NMR spectra, Allison Drummond for technical assistance and amusing conversation. Dr. Kenneth W. Henderson, for his knowledge of magnesium chemistry and Arlene E. McKeown for her friendship. Also the new blood Philip Rodger who will inherit the most exciting research area in main group chemistry.

  To my best friend John "Bon" Allan a "friend to the end" who gave me encouragement and the will to carry on.

- I would also like to acknowledge Beate Grünberg for making my final year a special one.

Finally, I acknowledge The EPSRC for making all this possible.

Published Papers

1) The first magnesium amide trimer, Magnesio 1,8-diaminonaphthalene.HMPA: Introducing an unprecedented cage assembly incorporating a Mg_3 triangle within a N_6 trigonal prism.
   W. Clegg, L. Horsburgh, R. E. Mulvey and R. B. Rowlings;
   J. Chem. Soc., Chem. Commun., (1996), 1739.

2) Synthesis and solid-state structures of three magnesium diamide complexes derived from $[RN(H)CH_2CH_2N(H)R]$ diamine precursors (R=Ph or $PhCH_2$).
   W. Clegg, L. Horsburgh, R. E. Mulvey, M. J. Ross, R. B. Rowlings and V. Wilson;
   Polyhedron., (1998), **17**, 1923.

3) Intermetallic lithium-magnesium hexamethyldisilazide: Synthesis and structure, discovery of an oxygen-centred variant, and a reaction with benzonitrile that produces a novel amidinate cage compound with a trigonal bipyramidal Li_4MgO core.
   A. R. Kennedy, R. E. Mulvey and R. B. Rowlings;
   J. Am. Chem. Soc., (1998), **120**, 7816.

4) Remarkable reaction of hetero-s-block-metal amides with molecular oxygen: Cationic $(NMNMg)_2$ ring products (M=Li or Na) with anionic oxo or peroxo cores.
   A. R. Kennedy, R. E. Mulvey and R. B. Rowlings;
   Angew. Chem. Int. Ed. Engl., (in press) paper no. Z11881.

5) Mixed-metal sodium-magnesium macrocyclic amide chemistry: A template reaction for the site selective di-deprotonation of arene molecules.
   D. R. Armstrong, A. R. Kennedy, R. E. Mulvey and R. B. Rowlings;
   Angew. Chem. Int. Ed. Engl., (in press) paper no. Z12273.

Conference Presentations

1) Monomers, dimers and trimers.
   R. E. Mulvey and R. B. Rowlings;
   30th USIC conference, University of St. Andrews, 1996.

2) Fused-ring structures of magnesium diamide dimers.
   R. E. Mulvey and R. B. Rowlings;
   214th ACS National Meeting, Las Vegas, U.S.A.
   Abstract No. INOR 250, 1997.

3) Macrocyclic amide ring systems containing
   a mixture of s-block metals (Oral).
   A. R. Kennedy, R. E. Mulvey and R. B. Rowlings
   32nd USIC conference, University of Strathclyde, 1998.

Abstract

Research has been directed towards the development of organonitrogen-magnesium chemistry, focusing on amide ligands mainly, and on amidinide ligands to a lesser extent. New compounds have been characterised by elemental analyses and NMR spectroscopic studies and seventeen of them have been crystallographically authenticated by X-ray diffraction.

Within the area of dianionic ligands, it has been found that deprotonating 1,8-diaminonaphthalene twice with dibutylmagnesium leads to [{(1,8-$C_{10}H_6(NH)_2$)Mg.HMPA}$_3$.2THF], the first magnesium amide trimer, having an unprecedented N_6Mg_3 cage structure. In contrast, treating the diamines N,N'-diphenylethylenediamine or N,N'-dibenzylethylenediamine with the same reagent in the same stoichiometry produces [{MgN(Ph)CH_2CH_2N(Ph).2THF(1.5THF)}$_2$], [{MgN(CH_2Ph)CH_2CH_2N(CH_2Ph).HMPA}$_2$], or [MgN(Ph)CH_2CH_2N(Ph).2HMPA], which adopt more conventional dimeric ring or monomeric structures. Also, the novel magnesium aluminate salt, [Mg(HMPA)$_4$.2AlMe$_4$], has been synthesised serendipitously from an attempt to make a mixed-metal diamide complex.

Within the area of monoanionic ligands, two structurally related mixed lithium-magnesium amides, [{$(Me_3Si)_2N$}$_3$LiMg] and [{(c-C_6H_{11})$_2$N}$_3$LiMg.THF], based on discrete (NLiNMg) cyclic cores, have been prepared. Further exploration of the hexamethyldisilazide has opened up a remarkable new area of macrocyclic chemistry. Thus, magnesium-substituted derivatives of classical alkali metal amide ring structures, [{$(Me_3Si)_2N$}$_4$$Li_2Mg_2(O_2)_x(O)_y$] and [{$(Me_3Si)_2N$}$_4$$Na_2Mg_2(O_2)_x(O)_y$], having oxo or peroxo core dianions for charge balance, have been established. The tetramethylpiperidide analogue, [{Me_2CCH$_2$CH$_2$CH$_2$(Me)$_2$CN}$_4$$Li_2Mg_2$(O)], has also been made. In an extension of this work, a larger twelve-membered $(N_6Na_4Mg_2)^{2+}$ cationic ring system have been realised through [{Me_2C(CH$_2$)$_3$(Me)$_2$CN}$_6$$Na_4Mg_2$\{$C_6H_3(CH_3)$\}] and [{$Me_2$C(CH$_2$)$_3(Me)_2$CN}$_6$$Na_4Mg_2(C_6H_4)$}].

This ring acts as a templating host for the selective di-deprotonation of toluene and benzene respectively, the dianions of which occupy the ring centre. Possible insight into the mechanism of arene incorporation in these macrocycles is gained through the structure of $[\{(Me_3Si)_2N\}_6K_2Mg_2.4\{C_6H_5(CH_3)\}]$, the first potassium amido magnesate species.

Finally, two magnesium and one lithium-magnesium amidinide structures, $[\{PhNC(Ph)NPh\}_2Mg.2DMSO.C_6H_5CH_3]$ $[\{PhNC(Ph)NPh\}_2Mg.2HMPA.C_6H_5CH_3]$ and $[\{PhC(NSiMe_3)_2\}_4Li_4Mg(O)]$ respectively, have been reported.

Contents

Copyright	i
Dedication	ii
Acknowledgements	iii
Published Papers	iv
Conference Presentations	v
Abstract	vi-vii
Contents	viii-x
Figure and Scheme Legends	xi-xiv

Chapter One - General Introduction

1.1	Lithium Amides	1
1.2	Uses of Lithium Amides	1-3
1.3	Structural Considerations	4
1.3.1	Uncomplexed Lithium Amides	4-8
1.3.2	Complexed Lithium Amides	9-13
1.4	Magnesium Amides	14
1.4.1	Preparation of Alkyl/Aryl Magnesium Amides	14-15
1.4.2	Preparation of Magnesium Bis(amides)	15
1.4.3	Preparation of (Amido) Magnesium Halides	16
1.5	Uses of Magnesium Amides	1-21
1.6	Solid-State Structures of Magnesium Amides	21-22
1.6.1	Magnesium Bis(amides)	23-27
1.6.2	Alkyl Magnesium Amides	28-30
1.6.3	Miscellaneous Magnesium Amide Compounds	30-31
1.7	Chapter One References	32-34

Chapter Two – Structural Chemistry of Magnesium Involving Dianionic Ligands

2.1	Introduction	35-42
2.2	Chapter Two Experimental	43-59
2.3	Chapter Two Discussion	60
2.3.1	Synthesis and Analysis of Compounds 2A-2D	60-63
2.3.2	X-ray Crystallography of Compounds 2A-2D	64-70
2.3.3	Synthesis and Analysis of Compound 2E	71-72
2.3.4	X-ray Crystallography of Compound 2E	73-74
2.4	Chapter Two Conclusions	75
2.5	Chapter Two Further Work	76
2.6	Chapter Two References	77-78

Chapter Three (Part 1) – Structural Chemistry of Mixed Lithium/Magnesium Complexes

3.1	Introduction	79-82
3.1.1	Lithium Organomagnesates	83-84
3.1.2	Lithium Amidomagnesates	85-86
3.1.3	Lithium Oxomagnesates	86-87
3.1.4	Lithium Halomagnesates	88-89
3.2	Chapter Three Experimental (Part1)	90-103
3.3	Synthesis and Analysis of Compounds 3A and 3B	104-106
3.4	X-ray Crystallography of Compounds 3A and 3B	107-109
3.5	Synthesis and Analysis of Compound 3C	109-110
3.6	X-ray Crystallography of Compound 3C	111-114
3.7	Synthesis and Analysis of Compound 3D	115-117
3.8	X-ray Crystallography of Compound 3D	118-122

Chapter Three (Part 2) – Macrocyclic Amide Ring Systems Containing a Mixture of S-Block Metals

3.9	Introduction	123
3.10	Chapter Three Experimental (Part 2)	124-140
3.11	Synthesis and Analysis of Compounds 3E and 3F	141-145
3.12	X-ray Crystallography of Compounds 3E and 3F	146-150
3.13	Synthesis and Analysis of Compounds 3G and 3H	151-154
3.14	X-ray Crystallography of Compounds 3G and 3H	155-158
3.15	X-ray Crystallography of Compound 3I	159-161
3.16	Chapter Three Conclusions	162-163
3.17	Chapter Three Further Work	164-165
3.18	Chapter Three References	166-169

Chapter Four – Miscellaneous N-Mg Bonded Structures

4.1	Introduction	170
4.2	Chapter Four Experimental	171-179
4.3	Synthesis and Analysis of Compounds 4A and 4B	180-181
4.4	X-ray Crystallography of Compounds 4A and 4B	182-184
4.5	Synthesis and Analysis of Compound 4C	185-186
4.6	X-ray Crystallography of Compound 4C	186-188
4.7	Chapter Four Conclusions	189
4.8	Chapter Four Further Work	190
4.9	Chapter Four References	191

Appendices 192-202

Legends

Chapter One

Figures

1.1	Crystal structure of the eight-membered ring system, $[Me_2CCH_2CH_2CH_2C(Me)_2NLi]_4$ **1**	5
1.2	Crystal structures of (a) $[(Me_3Si)_2NLi]_3$ **2**, (b) $[(PhCH_2)_2NLi]_3$ **3** and $[PhCH_2(Me_3Si)NLi]$ **5**	6
1.3	Crystal structures of unsolvated ladders (a) $[\{Li(NHCH_2CH_2NH_2)\}_\infty]$ **6** and (b) $[Li(Dipp)NCH_2CH_2N(Dipp)Li]_2$ **7**	8
1.4	Axial view of the helical structure of LDA **8**	8
1.5	Structures of selected solvated limited length ladders (a) $[\{LiN(CH_2)_3CH_2\}_2.TMEDA]_2$ **9** and (b) $[\{LiN(CH_2)_3CH_2\}_3.PMDETA]_2$ **10**	9
1.6	Structure of the lithium amide.amine complex **11**	10
1.7	Crystal structure of $[\{(PhCH_2N(H)Li)_2.H_2NCH_2Ph\}_\infty]$ **13**	11
1.8	Structure of dimeric $[(PhCH_2)_2NLi.HMPA]_2$ **14**	11
1.9	Structure of dimeric $[Ph(Me)NLi.TMEDA]_2$ **15**	12
1.10	Structures of monomeric (a) $[(Me_3Si)_2NLi.TMEDA]$ **16** and (b) [Ph(Naphthyl)NLi.PMDETA] **17**	13
1.11	Crystal structure of the β-H intermediate $[\{(Me_3Si)_2NMg[\mu\text{-}OC(H)Ph_2]\cdot(O{=}CPh_2)\}_2]$ **19**	17
1.12	Basic structural motifs adopted by magnesium amides	21
1.13	Examples of two and three-coordinate magnesium amides	23
1.14	Structure of monomeric $[Mg\{N(2\text{-}pyr)Ph\}_2.2THF]$ **39**	26
1.15	Crystal structures of (a) $[\{Mg[\mu\text{-}N(Ph)_2][N(Ph)(2\text{-}pyr)]\}_2]$ **25** and (b) $[Mg_3\{\mu\text{-}N(H)Dipp\}_4\{N(SiMe_3)_2\}_2]$ **26**	27
1.16	Structures of (a) monomeric $[EtMg(NC_{28}H_{40}).2THF]$ **42** and (b) dimeric $[Bu^sMg\{\mu\text{-}N(SiMe_3)_2\}]_2$ **43**	29
1.17	Crystal structure of dodecameric $[\{DippN(H)MgEt\}_{12}]$ **47**	30
1.18	Structure of the Hauser base, $[Mg(\mu\text{-}Cl)\{N(SiMe_3)_2\}.OEt_2]_2$ **48**	31

Schemes

1.1	Differences in reactivity of *n*-BuLi (top) and $[(Pr^i)_2NLi]$ (bottom)	2
1.2	Three fundamental C-C bond formation reactions	2
1.3	Some structures of uncomplexed lithium amides	4
1.4	'Ring Laddering' of dimeric $(NLi)_2$ rings	7
1.5	Mechanism of β-H transfer (hydrolysis not shown)	17
1.6	Reaction of $(TMP)_2Mg$ with amide-activated strained systems	19
1.7	Mechanism for the formation of β-amino dithioacetals	20

Chapter Two

Figures

2.1	Crystal structure of the hexameric magnesium cage compound $[\{o\text{-}C_6H_4(NH^-)_2\}Mg.THF]_6$ **54**	37
2.2	Dimeric structure of $[Mg\{\mu\text{-}N(SiMe_3)C_6H_4N(SiMe_3)\text{-}o\}(OEt_2)]_2$ **55**	37
2.3	Crystal structures of (a) $[(Et_2OMg)_6(NPh)_4Br_4]$ **59** and (b) $[(THF)MgNPh]_6$ **60**	40
2.4	The mixed Al-Mg imide $[(HAlN^tBu)_3\{MgN^tBu(THF)\}]$ **61**	41
2.5	Crystal structure of the mixed amido-nitrido cage $[Mg_6N(NH^tBu)_9]$ **62**	42
2.6	Crystal structure of trimeric $[\{(1,8\text{-}C_{10}H_6(NH)_2)Mg.HMPA\}_3.2THF]$ **2A**	46
2.7	Crystal structure of the five-coordinate dimer $[\{MgN(Ph)CH_2CH_2N(Ph).2THF(1.5THF)\}_2]$ **2B**	49
2.8	Crystal structure of dimeric $[\{MgN(CH_2Ph)CH_2CH_2N(CH_2Ph).HMPA\}_2]$ **2C**	52
2.9	Crystal structure of one independent monomer $[MgN(Ph)CH_2CH_2N(Ph).2HMPA]$ **2D**	55
2.10	Crystal structure showing cation moiety in $[\{Mg(HMPA)_4.2AlMe_4]$ **2E**	58
2.11	Alternative view of **2A**, highlighting the N_6Mg_3 cage arrangement	64
2.12	Structure of $[MeMg\{N(Me)CH_2CH_2NMe_2\}]_2$ **45**	66
2.13	Structural formulae of N,N'-diphenylethylenediamine and N,N'-dibenzylethylenediamine	66
2.14	Trans-5-4-5-fused ring systems of 2B and 2C showing (a) exo and (b) endo orientation of C(2) atom respectively	67
2.15	Crystal structure of $[PhLiNCH_2CH_2NLiPh.3HMPA]$ **63**	70
2.16	^1H NMR spectrum of $[Mg(HMPA)_4.2AlMe_4]$ **2E**, in d_5-pyr at 300K	72

2.17 Structure of $[Mg\{AlMe_4\}_2]$ **64** 73

Schemes

2.1 Unique bonding mode exhibited by dicarbanions 36
2.2 The formation of a magnesium imide via a six-membered transition state 38
2.3 Preparation of magnesium imide complexes derived from aniline 39
2.4 Typical transfer reactions using $[(THF)MgNPh]_6$ **60** 40
2.5 Possible route to the formation of **2E** 71

Chapter Three

Figures

3.1 Metallation of isopropylbenzene using a superbasic mixture of Bu^nLi / Bu^tOK in THF 80
3.2 Pictorial representation of possible intermediates involved in superbases 80
3.3 Crystal structures of (a) $[Li_2Mg\{N(CH_2CH_2NMe_2)CH_2Ph\}_4]$ **78**, (b) $[Li_2Mg\{N(Bzl)_2\}_4]$ **79** and (c) $[LiMg\{N(Bzl)_2\}_3.py]$ **80** 86
3.4 Crystal structures of (a) $[LiMg_4O\{o\text{-}Me(C_6H_4)O\}_7.4THF]$ **81** and (b) $[Li(TMEDA)]_2[Mg\{o\text{-}Me(C_6H_4)O\}_4]$ **82** 87
3.5 Crystal structures of (a) $[Li(THF)_2(\mu\text{-}Br)_2Mg\{C(SiMe_3)_3\}.THF]$ **84** and (b) $[Mg_2Cl_3.THF_6][Li\{nido\text{-}[2,3\text{-}(SiMe_3)_2C_2B_4H_4]\}][ZrCH_2SiMe_3(Cl)]$ **85** 89
3.6 Crystal structure of $[\{(Me_3Si)_2N\}_3LiMg]$ **3A** 93
3.7 Crystal structure of $[\{(c\text{-}C_6H_{11})_2N\}_3LiMg.THF]$ **3B** 96
3.8 Crystal structure of $[\{(Me_3Si)_2N\}_4Li_2Mg_2(O_2)_x(O)_y]$ **3C** 99
3.9 Crystal structure of $[\{PhC(NSiMe_3)_2\}_4Li_4Mg(O)]$ **3D** 103
3.10 ^1H NMR spectrum of $[\{(Me_3Si)_2N\}_3LiMg]$ **3A** in d_8-toluene at 300K 106
3.11 ^1H NMR spectrum of $[\{(Me_3Si)_2N\}_4Li_2Mg_2(O_2)_x(O)_y]$ **3C** in d_8-toluene at 300K 110
3.12 ^1H NMR spectrum of $[\{PhC(NSiMe_3)_2\}_4Li_4Mg(O)]$ **3D** in d_5-pyridine at 300K 116
3.13 View showing the central Li_4MgO core of structure **3D** 118
3.14 The two distinct NCN amidinate ligands present in structure **3D** 120
3.15 Crystal structure of $[Os_3(\mu\text{-}H)(CO)_9\{PhNC(Ph)NH\}]$ **115** 122
3.16 Crystal structure of $[\{Me_2\overline{CCH_2CH_2CH_2(Me)_2CN}\}_4Li_2Mg_2(O)]$ **3E** 127
3.17 Crystal structure of $[\{(Me_3Si)_2N\}_4Na_2Mg_2(O_2)_x(O)_y]$ **3F** 130

3.18 (a) Crystal structure of $[\{Me_2\overline{CCH_2CH_2CH_2(Me)_2CN}\}_6Na_4Mg_2\{C_6H_3(CH_3)\}]$ **3G** (in black and white) 133

3.18 (b) Crystal structure of $[\{Me_2\overline{CCH_2CH_2CH_2(Me)_2CN}\}_6Na_4Mg_2\{C_6H_3(CH_3)\}]$ **3G** (in colour) 134

3.19 Crystal structure of $[\{Me_2\overline{CCH_2CH_2CH_2(Me)_2CN}\}_6Na_4Mg_2(C_6H_4)]$ **3H** 138

3.20 Crystal structure of $[\{(Me_3Si)_2N\}_6K_2Mg_2.4\{C_6H_5(CH_3)\}]$ **3I** 140

3.21 ^{1}H NMR spectrum of compound **3E** in d_8-toluene at 300K 143

3.22 ^{7}Li NMR spectrum of compound **3E** in d_8-toluene at 300K 145

3.23 Crystal structure of the macrocyclic complex [12]mercuracarborand-4 148

3.24 Space filling representations of compounds **3C**, **3E** and **3F** 150

3.25 ^{1}H NMR spectrum of dimetallated toluene section of **3G** in d_6-DMSO at 300K 153

3.26 Side-view of macrocyclic ring structure **3G** 155

3.27 Relative energies of toluene-based dianions in kcal mol^{-1} 157

3.28 View of heterobimetallic ring fragment 159

Schemes

3.1 Various lithium organomagnesates 83

3.2 Addition across benzonitrile using a trimethylsilyl amide 117

3.3 Formal representation of oxide / peroxide incorporation into heterobimetallic cationic rings 149

3.4 Presumed template reaction for the formation of **3H** 158

Chapter Four

Figures

4.1 Crystal structure of $[\{PhNC(Ph)NPh\}_2Mg.2DMSO.C_6H_5CH_3]$ **4A** 173

4.2 Crystal structure of one independent monomer of $[\{PhNC(Ph)NPh\}_2Mg.2HMPA.C_6H_5CH_3]$ **4B** 176

4.3 Crystal structure of $[\{(Me_3Si)_2NMgN(H)C_6H_5.THF\}_2]$ **4C** 179

4.4 Idealised coordination geometries in amidinide monomers 182

4.5 Orbital representation of four-membered MgNMgN central ring 188

Chapter One

Chapter One - General Introduction

The research presented in this thesis is based mainly on the structural determinations of both magnesium amides and mixed lithium-magnesium amide complexes. Therefore by way of a general introduction, the separate areas of lithium amide chemistry and magnesium amide chemistry are now discussed in turn.

1.1 Lithium Amides

Since the preparation of lithamide, $[(H_2NLi)_n]$[1], over a hundred years ago, many compounds belonging to this class have since been prepared, primarily on account of their great synthetic applicability.

These organonitrogen-metal compounds are formed from the replacement of the acidic H on the parent amine by a lithium atom. This deprotonation is carried out using a commercial alkyllithium reagent (RLi), the reaction of which is fast even at low temperatures (equation 1.1).

$$RLi + R^1R^2NH \longrightarrow R^1R^2NLi + RH \qquad (1.1)$$

where usually R = Me, Bu^n, Ph

1.2 Uses of Lithium Amides

After alkyllithium reagents[2], e.g. *n*-BuLi, bulky lithium amide compounds, e.g. $[(Pr^i)_2NLi]$, are the second most utilised class of organolithium reagent used in modern synthetic chemistry. This is a consequence of their strong Brønsted basicity coupled with poor nucleophilicity (scheme 1.1), which makes them attractive for use in regio / stereoselective syntheses.

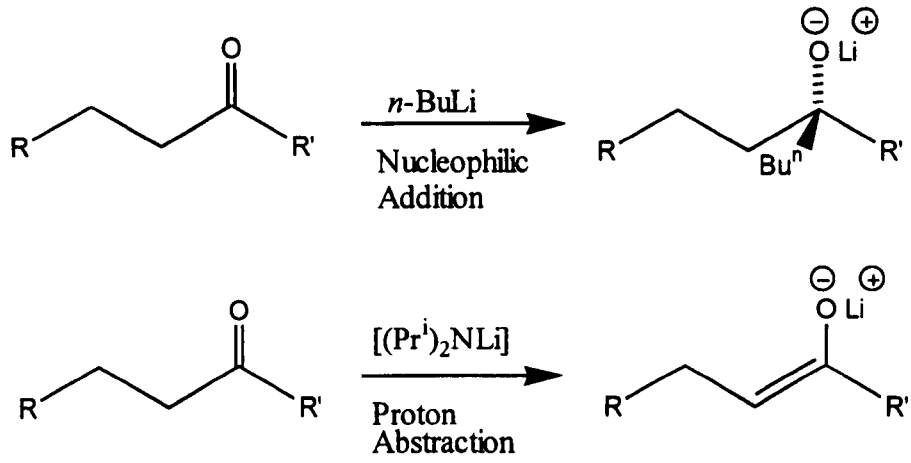

Scheme 1.1- Differences in reactivity of n-BuLi (top) and [(Pr^i)$_2$NLi] (bottom)

By far the most widely used application of lithium amides is in natural product synthesis[3]. The deprotonation of a carbonyl compound (e.g. a ketone, aldehyde or ester) possessing α-hydrogen atoms results in the formation of an enolate anion. This fundamental intermediate reacts with electrophilic carbon centres resulting in C-C bond formation. Three well documented C-C bond forming reactions are highlighted in scheme 1.2.

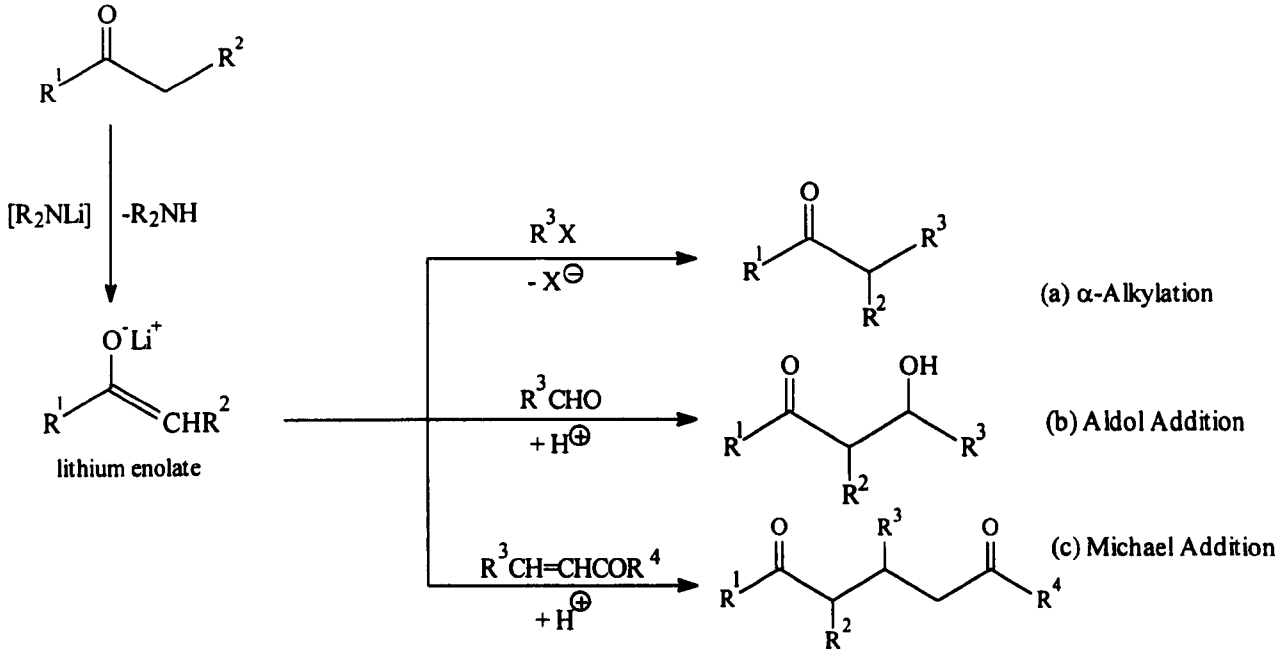

Scheme 1.2- Three fundamental C-C bond formation reactions

Within the realms of inorganic chemistry, lithium amides are found to be excellent transmetallating agents for the formation of other main group and transition metal amides[4]. The driving force for reaction is the production of a lithium halide salt (LiX) possessing a large lattice energy of formation (equation 1.2).

$$n\,[R^1R^2NLi] \;+\; MX_n \longrightarrow [(R^1R^2N)_nM] \;+\; n\,LiX \qquad (1.2)$$

where, M = main group / transition metal; X = halide

In a recent study by Collum *et al*[5], polyamine solvated $[(Pr^i)_2NLi]$ complexes were found to be excellent dehydrohalogenating reagents (equation 1.3).

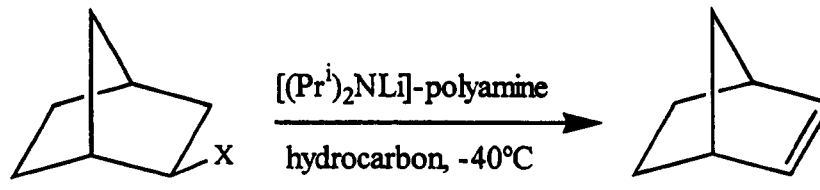

(1.3)

where, polyamine = TMEDA, TMCDA, PMDETA

Although having been known for over a century[4], lithium amides have only recently been isolated and crystallographically characterised. The first single crystal structure to be obtained was that of $[\{(Me_3Si)_2NLi\}_3]$[6] in 1978. Since then, the number of lithium amide single crystal structures has rapidly increased and have been the subject of several reviews[7]. Isolation of crystalline products rather than *in situ* use offers the luxury of reagent purity, accurate stoichiometric control and a better understanding of reaction mechanisms.

1.3 Structural Considerations

1.3.1 Uncomplexed Lithium Amides

Uncomplexed lithium amides can form ring oligomers or ladder type structures depending on the size of the R groups attached to the amido nitrogen centre as illustrated by the selection shown in scheme 1.3, where n represents the state of association.

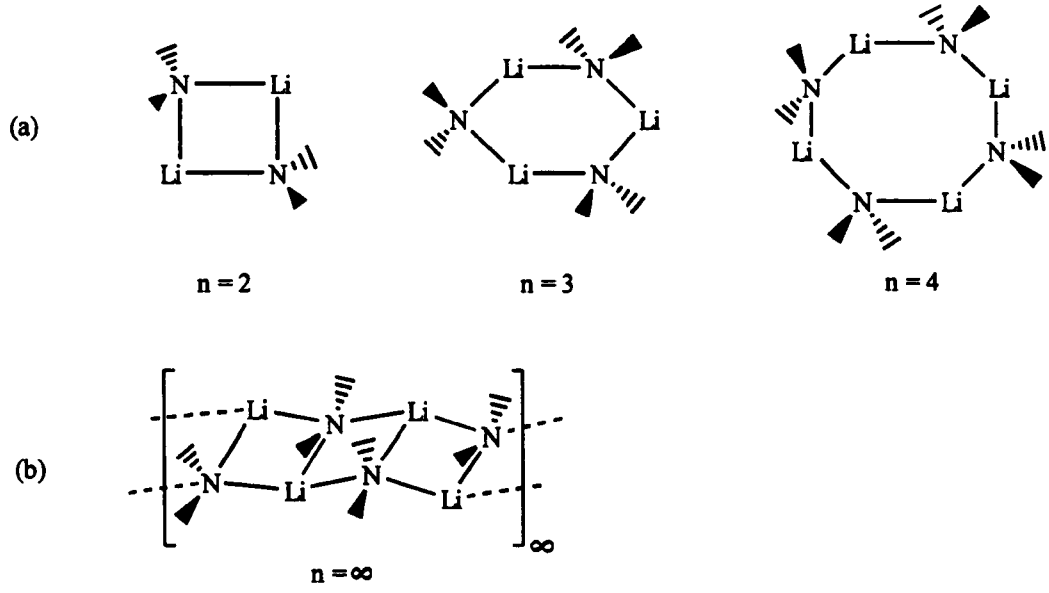

Scheme 1.3- Some structures of uncomplexed lithium amides

Discrete, singular rings are preferentially formed when R^1 and R^2 are bulky, because they fill much of the lateral space around the ring (scheme 1.3(a)). A 'classic' example is that of $[Me_2CCH_2CH_2CH_2C(Me)_2NLi]_4$ **1**[8], which consists of a planar eight-membered $(NLi)_4$ ring, where each piperidine ring lies in a chair conformation staggered to one another (figure 1.1).

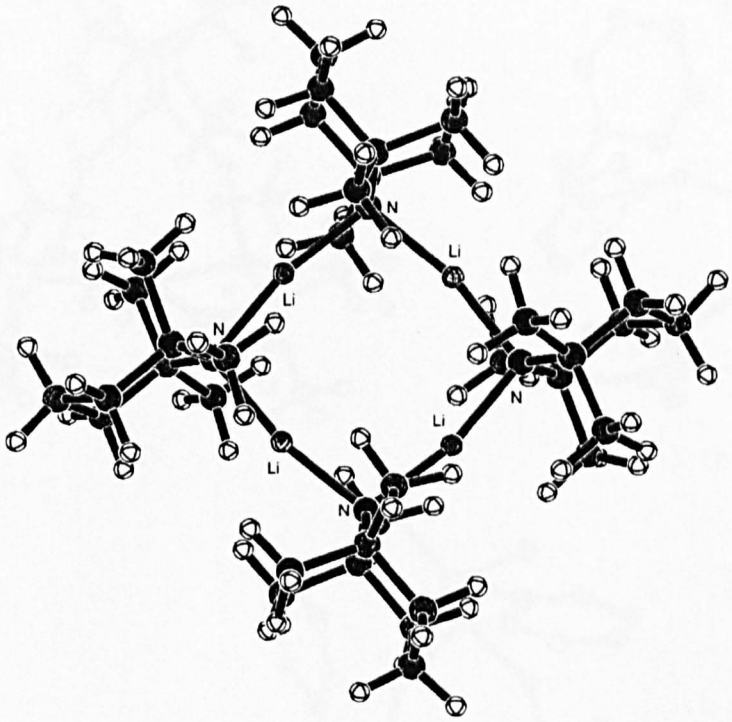

Figure 1.1- Crystal structure of the eight-membered ring system, $[Me_2CCH_2CH_2CH_2C(Me)_2NLi]_4$ ***1***

When sterically less demanding anions are employed, the formation of smaller trimeric rings (n=3) is favoured, examples being $[(Me_3Si)_2NLi]_3$[6], **2** (figure 1.2(a)), $[(PhCH_2)_2NLi]_3$[9,10], **3**, (figure 1.2(b)), $[(Me_3Ge)_2NLi]_3$[11], **4** and $[PhCH_2(SiMe_3)NLi]_3$[12], **5**, (figure 1.2(c)). The benzyl groups present in structures **3** and **5**, pivot towards the lithium cations allowing for favourable Li···C agostic interactions. These interactions are observed at three distinct sites on the benzyl moiety, at the *ortho*-, *ipso*- and *benzylic* carbons [mean agostic distances in **3** and **5** respectively: Li···*ortho*-C, 2.80Å, 2.58Å; Li···*ipso*-C, 2.80Å, 2.45Å; Li···*benzylic*-C, 2.81Å, 2.65Å]. The existence of these interactions help to offset the formal low coordination number (2) of the lithium centre.

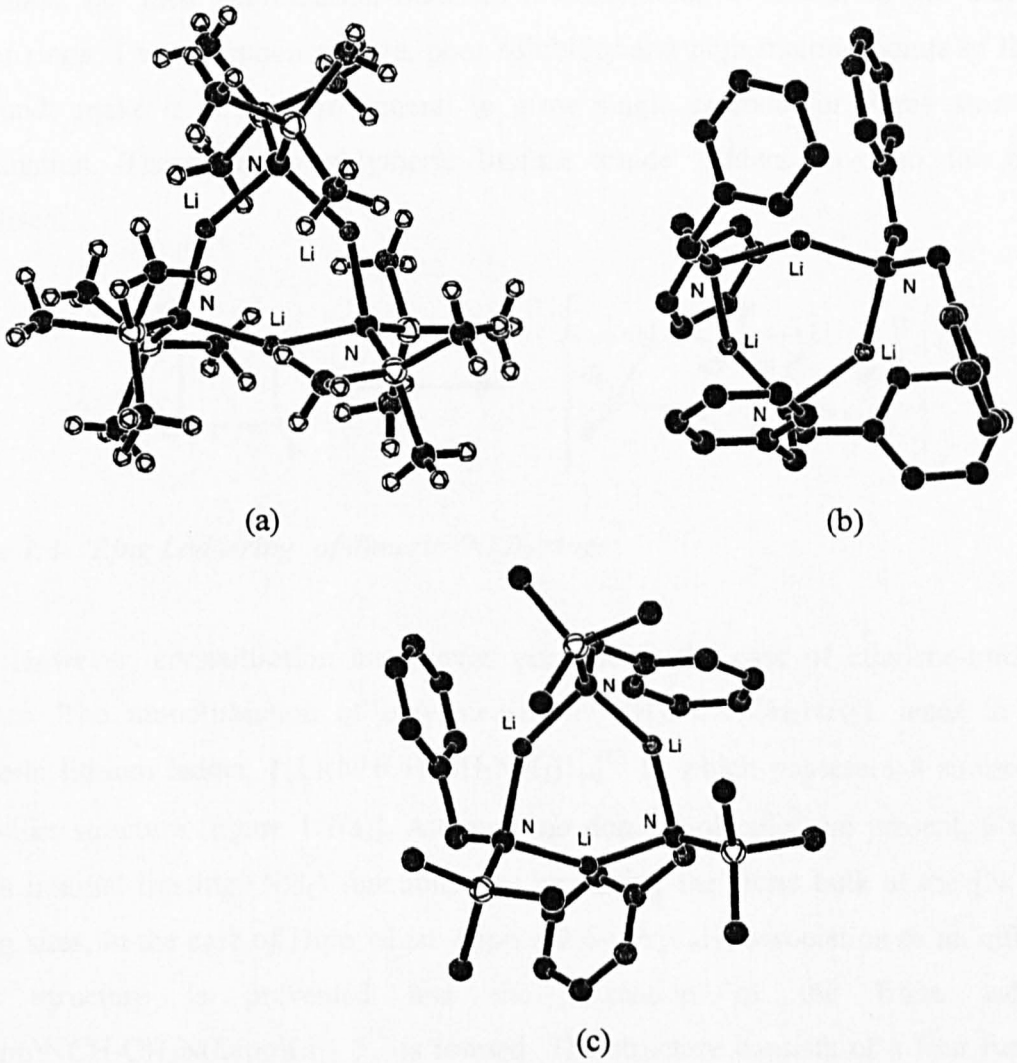

*Figure 1.2- Crystal structures of (a) $[(Me_3Si)_2NLi]_3$, **2**, (b) $[(PhCH_2)_2NLi]_3$, **3** and $[PhCH_2(Me_3Si)NLi]_3$, **5**, (in **3** and **5** hydrogen atoms are omitted for clarity)*

The sp^3 nature of the anionic nitrogen within the singular ring structures of lithium amides causes the R groups to project above and below the $(NLi)_n$ ring. When small or flat anions are incorporated, ladder structures form (scheme 1.3(b)). Association of dimeric $(NLi)_2$ rings occurs laterally along the N-Li ring edges by a process called 'Ring Laddering' (scheme 1.4). The driving force for the laddering process can be attributed to the need for both lithium and nitrogen to maximise their number of polar

interactions, i.e. their coordination numbers increase relative to that in the discrete singular rings. The amorphous nature, poor solubility and high melting points of these compounds make it difficult in general to grow single crystals for X-ray structure determination. Therefore no polymeric lithium amide ladders have so far been crystallised.

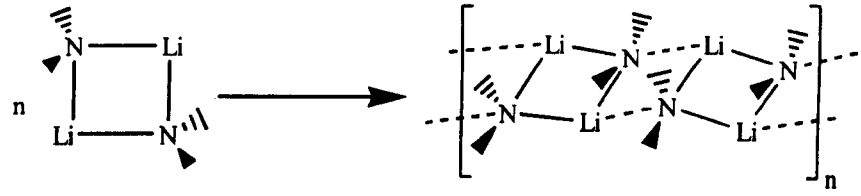

Scheme 1.4- 'Ring Laddering' of dimeric $(NLi)_2$ rings

However, crystallisation has proved possible in the case of ethylene-bridged diamines. The monolithiation of ethylenediamine, $[H_2NCH_2CH_2NH_2]$, leads to the polymeric lithium ladder, $[\{Li(NHCH_2CH_2NH_2)\}_\infty]$[13] **6**, which possesses a sinusoidal ribbon-like structure (figure 1.3(a)). Although no donor molecules are present, **6** does possess internal ligating (NH_2) functions. By increasing the steric bulk at the $[N(H)^-]$ binding sites, in the case of Dipp where Dipp = 2,6-i-$Pr_2C_6H_3$ association to an infinite ladder structure is prevented and the formation of the finite ladder, $[Li(Dipp)NCH_2CH_2N(Dipp)Li]_2$ **7**[14] is formed. The structure consists of a four runged ladder, whereby the lithium centres attain coordinative saturation (four at external rung sites and three at internal sites) through agostic interaction with the bulky amide moieties (figure 1.3(b)).

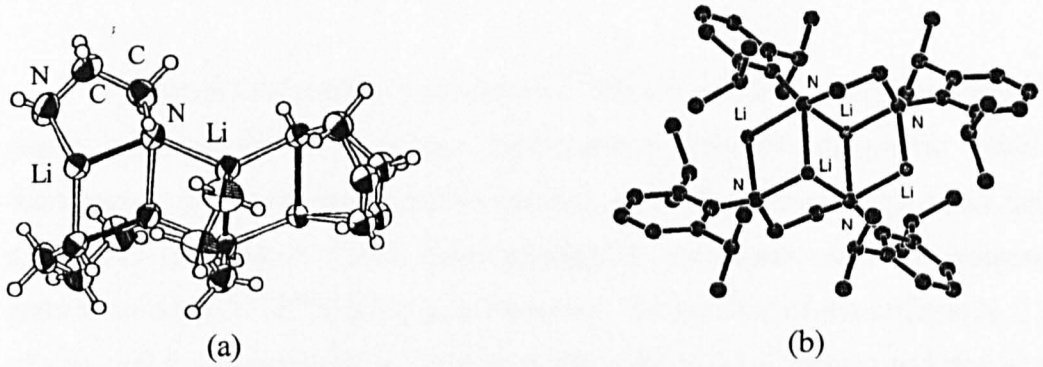

*Figure 1.3- Crystal structures of unsolvated ladders (a) $[\{Li(NHCH_2CH_2NH_2)\}_\infty]$ **6** and (b) $[Li(Dipp)NCH_2CH_2N(Dipp)Li]_2$ **7**, (in **7** hydrogen atoms are omitted for clarity)*

Finally, the crystal structure of lithium diisopropylamide, $[(Pr^i)_2NLi]_\infty$, **8**, commonly known as (LDA), is polymeric[15]. Instead of an infinite ladder array, LDA crystallises as an unprecedented infinite helical assembly of near linear N-Li-N with eight N-Li bonds per helix twist (figure 1.4). Each two-coordinate lithium centre takes part in alternating short and slightly longer N-Li bonds throughout the spiral structure.

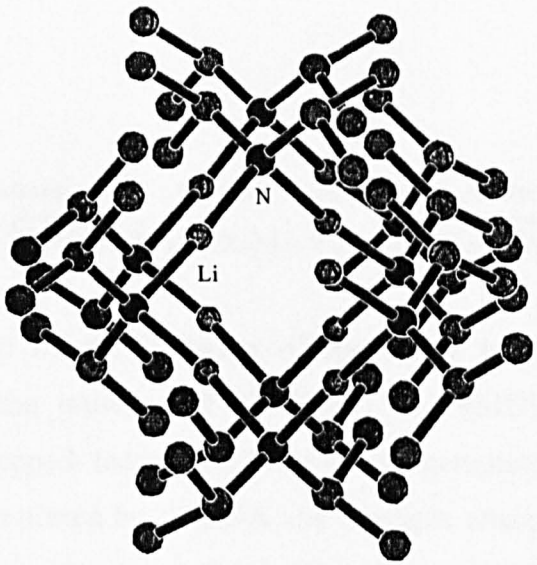

*Figure 1.4- Axial view of the helical structure of LDA, **8**, (hydrogen atoms are omitted for clarity)*

1.3.2 Complexed Lithium Amides

As mentioned earlier uncomplexed lithium amides possessing relatively small amide units usually form arene / hydrocarbon insoluble polymeric materials. The introduction of Lewis base (donor) solvents (L) effects dissolution such that smaller aggregates are formed. These lower aggregated complexes can be represented by the general formula, $[R^1R^2NLi.(L)_x]_n$, x represents the number of donor ligands. The degree of association is dependent on both the steric bulk of the R groups and that of the donor molecule. When the Lewis base:Li ratio is less than 1 (i.e. L:Li <1) ladders of limited length typically form. Two such examples, **9** and **10** are shown in figure 1.5.

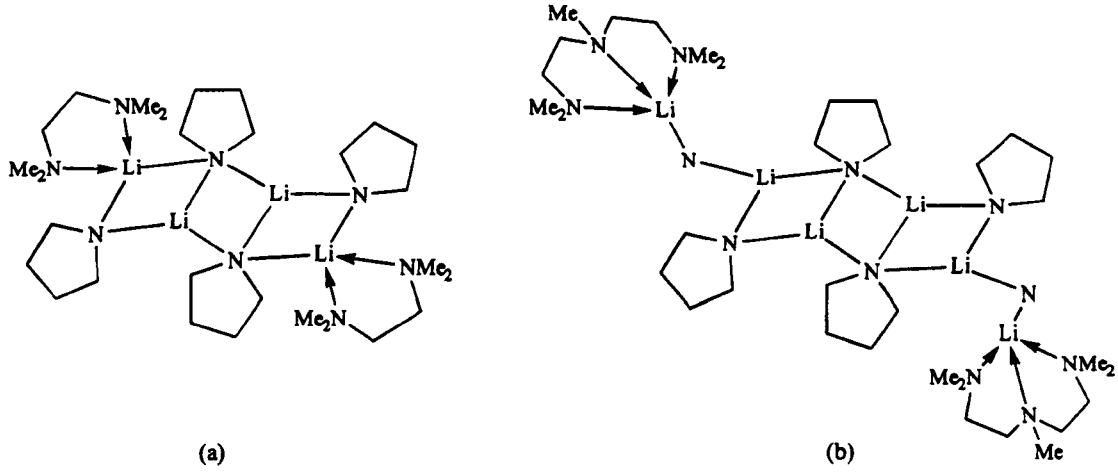

Figure 1.5- Structures of selected solvated limited length ladders (a) $[\{Li\overline{N(CH_2)_3CH_2}\}_2.TMEDA]_2$ 9 and (b) $[\{Li\overline{N(CH_2)_3CH_2}\}_3.PMDETA]_2$ 10

These were prepared by the lithiation of the cyclic secondary amine pyrrolidine, $[H_2\overline{C(CH_2)_3NH}]$ in the presence of TMEDA[16] and PMDETA[17] respectively. Each structure is a finite stepped- ladder consisting of four complete rungs. In **9** the outermost lithium atoms are complexed by TMEDA and therefore attain a coordination number of four, while the lithium atoms in the inner rungs remain uncomplexed and three-coordinate. In contrast, **10** can be regarded as a six-rung ladder with the two outermost

rungs partially broken so as to accommodate the bulky PMDETA donor ligands and allow the lithium centres to achieve a more favourable four-coordination.

As well as stepped-ladder arrangements, solvated finite ladders with "concave" backbones are also possible as evident from the structures of $[LiN(CH_2)_4CH_2.HN(CH_2)_4CH_2]_4$ **11**[18] (figure 1.6) and $[\{LiN(SiMe_3)CH_2\}_2.OEt_2]_2$ **12**[19] (not shown). In both cases solvation by donor molecules occurs only at the terminal lithium centres leaving the central lithiums uncomplexed. However, in structure **11** solvation by two piperidine molecules, i.e. the amine lithiated in the reaction, at each outermost lithium renders a coordination number of four, whereas in **12** the solvation by one ether molecule results in a coordination number of three. The lithium centres at the internal rung positions are three coordinate in each case.

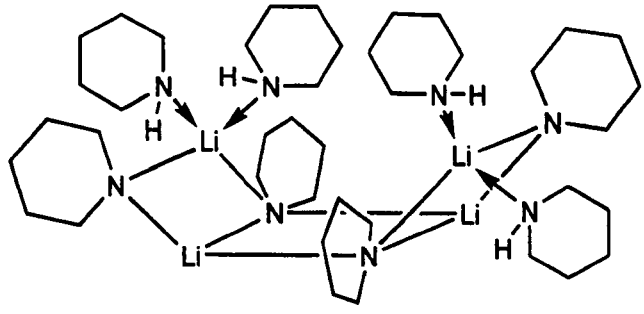

Figure 1.6- Structure of the lithium amide.amine complex 11

In light of structure **11**, the use of primary amines as donor molecules has recently been investigated and shown to form polymeric ladders. In the presence of excess benzylamine, lithium benzylamide forms a remarkable hemi-solvated polymeric ladder structure[20], $[\{(PhCH_2N(H)Li)_2.H_2NCH_2Ph\}_\infty]$ **13** (figure 1.7). Curiously, solvation occurs regioselectively along one edge of the ladder only, with the amine ligands positioned alternatively above and below the $[(NLi)_2]_\infty$ ladder framework. The lithium centres that have donor attached are four coordinate, while the unsolvated lithiums are three coordinate. This inequivalency in coordination environment makes the

ladder twist in a cisoid-transoid conformation, where cisoid represents the case when the two N-H groups lie on the same side of the $(NLi)_2$ ring.

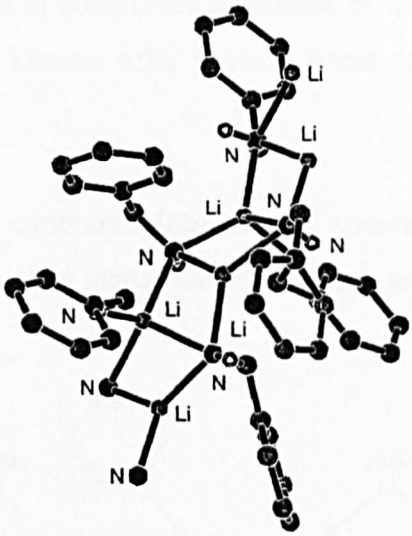

Figure 1.7- Crystal structure of $[\{(PhCH_2N(H)Li)_2.H_2NCH_2Ph\}_\infty]$ ***13****, (hydrogen atoms are omitted for clarity)*

When the Lewis base:Li ratio is 1:1 or greater (i.e. Lewis base:Li ≥1), dimers and monomers (contact ion pairs C.I.Ps or solvent separated ion pairs S.S.I.Ps) form as long as the amide function is bulky. In the vast majority of complexed dimeric lithium amide structures, the lithium centre is three coordinate. This is rather low for lithium, which normally prefers a coordination number of four or higher. To understand why this lower coordination number is favoured consider, $[(PhCH_2)_2NLi.HMPA]_2$ **14**[9,10] (figure 1.8).

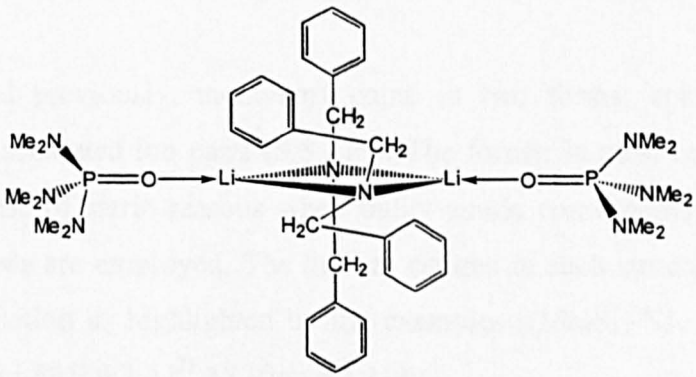

Figure 1.8- Structure of dimeric $[(PhCH_2)_2NLi.HMPA]_2$ **14.**

The presence of HMPA molecules bound to the lithium atoms in the $(NLi)_2$ ring sterically 'block' either side of the dimer making lateral association impossible. At present there are no examples of complexed tetrameric or trimeric ring structures known in lithium amide chemistry. Dimers offer a much larger coordination arc at the metal centre for solvation.

In discrete dimeric structures lithium can sometimes attain a coordination number of four, in particular when planar amide functions are employed (figure 1.9).

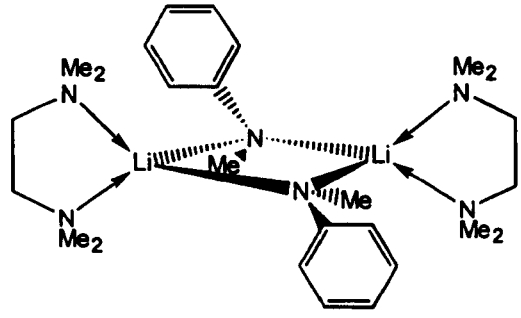

*Figure 1.9- Structure of dimeric [Ph(Me)NLi.TMEDA]$_2$ **15***

For example, in the structure of [Ph(Me)NLi.TMEDA]$_2$ **15**[21], four coordination is feasible due to the lack of steric hindrance exhibited by the planar amido constituents, thus the didentate TMEDA molecules can bind to lithium unperturbed.

As mentioned previously, monomers come in two forms: contact ion pairs (C.I.Ps) and solvent separated ion pairs (S.S.I.Ps). The former is most common. These normally arise because of steric reasons when bulky amide constituents and / or high denticity donor ligands are employed. The lithium centres in such structures can attain three or four coordination as highlighted by the examples [$(Me_3Si)_2$NLi.TMEDA][7] **16** and [Ph(Naphthyl)NLi.PMDETA][21] **17** (figure 1.10).

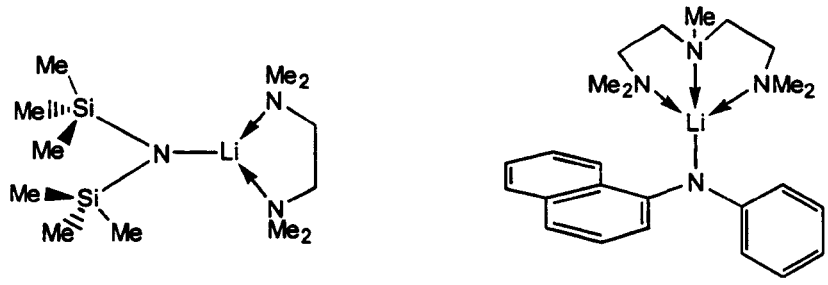

(a) (b)

*Figure 1.10- Structures of monomeric (a) [$(Me_3Si)_2NLi.TMEDA$] **16** and (b) [Ph(Naphthyl)NLi.PMDETA] 17*

Solvent separated ion pairs are rare. They usually only form when more exotic donor ligands are employed such as macrocyclic polyethers. These donors encapsulate the metal severing any bonding with the anion. One such example is $[Mes_2BNSiPh_3]^-[Li(12\text{-crown-}4)_2]^+$ **18**[22].

1.4 Magnesium Amides

This section will deal with alkyl / arylmagnesium amide complexes, [R'_2NMgR], magnesium bis(amide) complexes, [$(R'_2N)_2Mg$], and a brief mention of (amido)magnesium halide compounds, [R'_2NMgX].

In contrast with the ever increasing number of publications concerning Grignard reagents[23] and to a lesser extent diorganylmagnesium species[24], magnesium amide compounds, in particular bis(amide) compounds have received little attention both structurally and synthetically. This is somewhat surprising considering the vast utility shown by their lithium amide counterparts (section 1.2, pg.1). Synthetic studies have shown that magnesium amide compounds exhibit differing selectivity, lower reactivity and a higher thermal stability compared to lithium amides[25]. Considering these advantages it is surprising that greater scrutiny has not been focused on the synthetic utility of these species.

The preparations, synthetic uses and solid-state structures of each magnesium amide class will now be considered separately.

1.4.1 Preparation of Alkyl/Arylmagnesium Amide Compounds

Alkyl / arylmagnesium amide compounds, (R'_2NMgR), can be prepared by two general methods. The simplest preparation, which was first reported in 1903[26], involves reaction of a diorganylmagnesium base, [R_2Mg], with one equivalent of amine (equation 1.4).

$$R_2Mg + R'_2NH \longrightarrow R'_2NMgR + RH \qquad (1.4)$$

R' can be a wide range of organic substituents except Me[27], as a disproportionation reaction occurs, resulting in the formation of a polymeric bis(dimethylamido)magnesium product.

Preparation can also be achieved by the transmetallation of an alkali metal amide, R'_2NM, (where M= Li or Na) using a Grignard reagent (equation 1.5).

$$R'_2NH + RM \longrightarrow R'_2NM \xrightarrow{RMgX} R'_2NMgR + MX \qquad (1.5)$$

where M = Na, Li ; X = halide

1.4.2 Preparation of Magnesium Bis(amides)

Historically, magnesium bis(amide) compounds, were prepared from the direct reaction of magnesium metal with free amine under high temperature and pressure conditions[28,29] (200°C, 200Kgcm^{-3}). Today, such compounds can be readily prepared using commercially available diorganylmagnesium reagents, such as *n,s*-Bu_2Mg (equation 1.6).

$$R_2Mg + 2\,R'_2NH \longrightarrow (R'_2N)_2Mg + 2\,RH \qquad (1.6)$$

where R= *n,s*-Bu

However, difficulties have been seen to arise in some instances[29] where the thermodynamic stability of the 'intermediate' alkyl(amido) species overrides the reaction with a further equivalent of amine e.g. as in $[\{PhCH_2(Me_2N(CH_2)_2)NMg^nBu\}_2]$[30].

1.4.3 Preparation of (Amido)magnesium Halides

Known also as 'Magnesylamines', and 'Hauser bases', (amido)magnesium halide compounds were first prepared by Meunier nearly a century ago[26]. Since then, they have been the subject of only intermittent interest[31]. They are easily prepared from the equimolar reaction of a Grignard reagent with secondary amine (equation 1.7).

$$R'_2NH + RMgX \longrightarrow R'_2NMgX + RH \qquad (1.7)$$

1.5 Uses of Magnesium Amides

Compared to the nearly ubiquitous lithium amides, the use of analogous magnesium amides in synthetic chemistry is still in its infancy. This section will consider the utility of these compounds as promising reagents in carrying out organic transformations.

In 1978, Ashby *et al* found that (amido)magnesium hydrides, $[R'_2NMgH]$[32], and alkylmagnesium amide compounds, $[R'_2NMgR]$[33], were good stereoselective reducing agents upon reaction with cyclic ketones. This stereoselectivity was found to be greatly enhanced when bulky amide substituents were employed. After hydrolysis, the main product was shown to be that of the equatorial alcohol (attack from the least sterically demanding side) in yields of up to 100%.

Magnesium bis(amide) compounds such as magnesium diisopropylamide, $[(Pr^i_2N)_2Mg]$[34], have also been employed to effect the reduction of aldehydes and ketones. It was postulated that a hydride was transferred from the carbon β to the metal centre via a six-membered transition state (scheme 1.5).

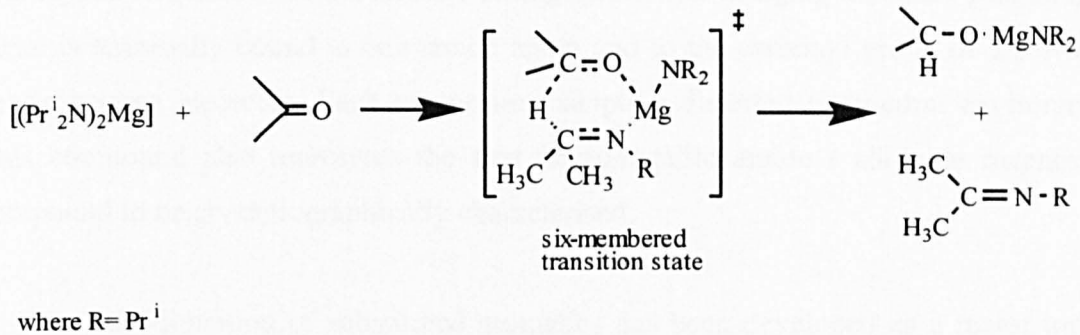

Scheme 1.5- Mechanism of β–H transfer (hydrolysis not shown)

The above mechanism was confirmed recently by Henderson *et al*[35] who obtained a crystal structure (figure 1.11) of the intermediate hydride transfer product from the reaction of the alkyl magnesium amide compound, [$(Me_3Si)_2NMgBu^s$], with benzophenone ($Ph_2C{=}O$). In this case the hydride was transferred from the β-C of the alkyl function.

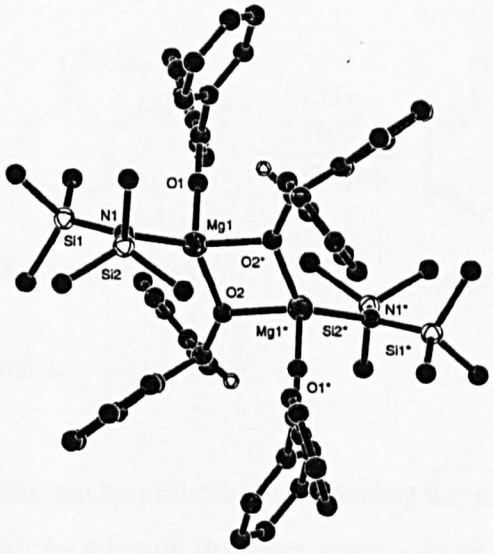

*Figure 1.11- Crystal structure of the β-H intermediate [{$(Me_3Si)_2NMg[\mu$-$OC(H)Ph_2]\cdot(O{=}CPh_2)\}_2$] **19**, (hydrogen atoms are omitted for clarity)*

The crystal structure shows a dimeric arrangement with bridging alkoxide anions. Each metal is terminally bound to one amide anion and to the carbonyl group of a solvating benzophenone molecule. Each magnesium adopts a distorted tetrahedral environment. This compound also represents the first homometallic amide / alkoxide magnesium compound to be crystallographically characterised.

Ortho-lithiation of substituted aromatics has been developed as a major tool in organic synthesis[36]. It has been extended to include lithiation of activated vinyl[37], allylic[38] and strained saturated systems[39]. Lithiations are often carried out at low temperatures (-78°C) due to the instability of both the lithium reagent and intermediate lithiated species. Eaton *et al*[25(a)] demonstrated that ortho-magnesiation offers a more attractive pathway of ortho metallation since both the magnesium base and intermediate magnesiated species are more thermally stable. Ortho-lithiation reactions are not usually suitable when ester functions are present as nucleophilic attack often results[40]. However, methyl and ethyl esters have found to be unreactive to magnesiation[25(a)] (equation 1.8).

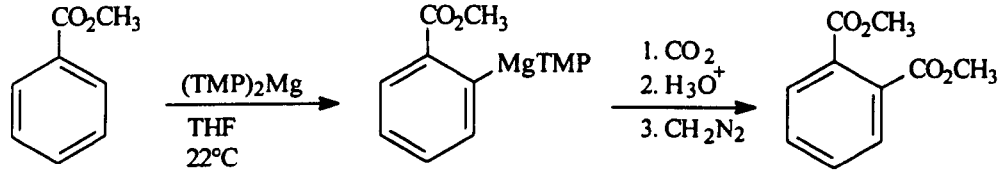

(1.8)

methyl benzoate amido-Grignard species dimethyl *o*-phthalate

where, TMP = 2,2,6,6-tetramethylpiperidide

The bulky amide function inhibits nucleophilicity by lessening the ability of the metal to complex with the ester substrate. As a result, the ester group can co-exist with the metal amide for some time prior to work up.

Difficulties can arise when ortho-lithiation is required twice on a doubly activated ring system[41]. The polar nature of the first C-Li bond usually deactivates the

remaining C-H bonds to further lithiation. This process has shown to be more easily accomplished with the involvement of magnesium, due to the less polar C-Mg bonds involved (equation 1.9).

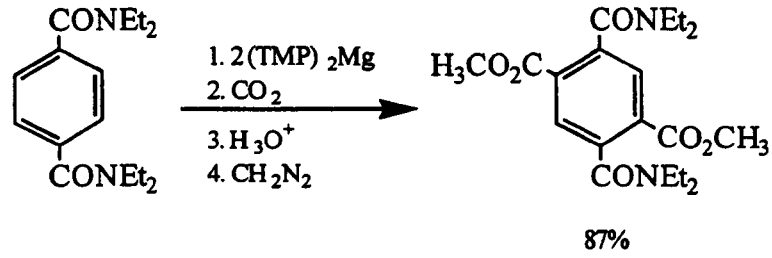

(1.9)

Amide-activated strained systems which have s-rich, acidity enhanced C-H bonds such as cyclopropane and cubane derivatives, also react well with bulky magnesium amide bases[25(a)] (scheme 1.6).

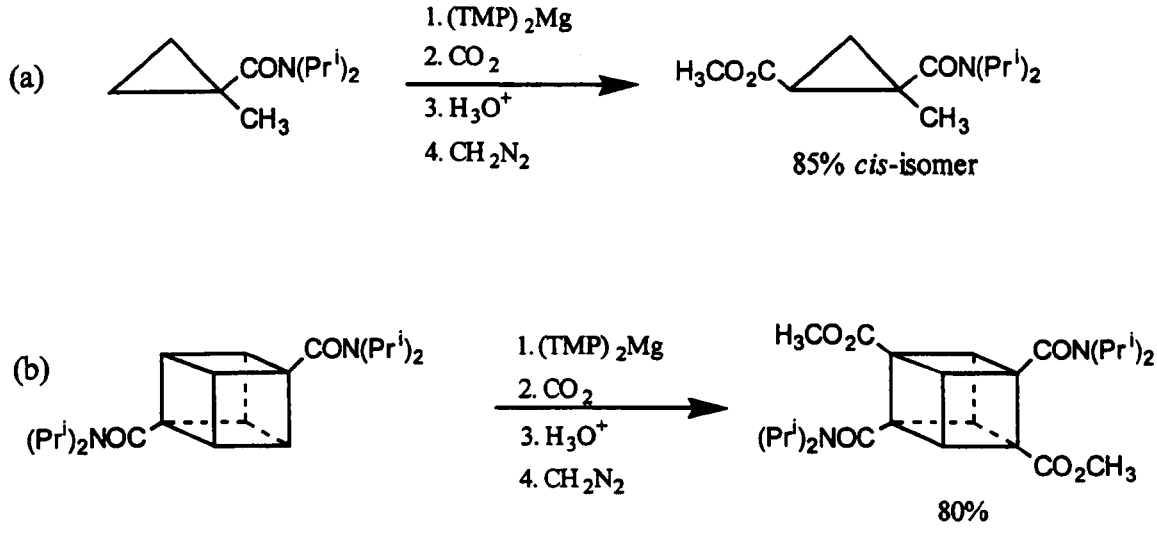

Scheme 1.6- Reaction of (TMP)$_2$Mg with amide-activated strained systems

The acid-catalysed condensation of carbonyl compounds with thiols[42] has been the general method for preparing dithioacetals for many years. Dithioacetals have been found to be important functionalities in the formation of carbon-carbon bonds[43].

Kobayashi *et al* found a new route to these compounds by the reaction of substituted sulphoxides[44] (bearing α-hydrogen atoms) with magnesium amides.

When vinyl sulphoxides are employed, β-aminodithioacetals result. These are potentially useful not only in synthetic organic chemistry but also in medicinal chemistry due to their biological activities[45]. The preparation of dithioacetals by this method occurs via a complex mechanism as illustrated by scheme 1.7 (mechanism for β-amino dithioacetal formation is shown).

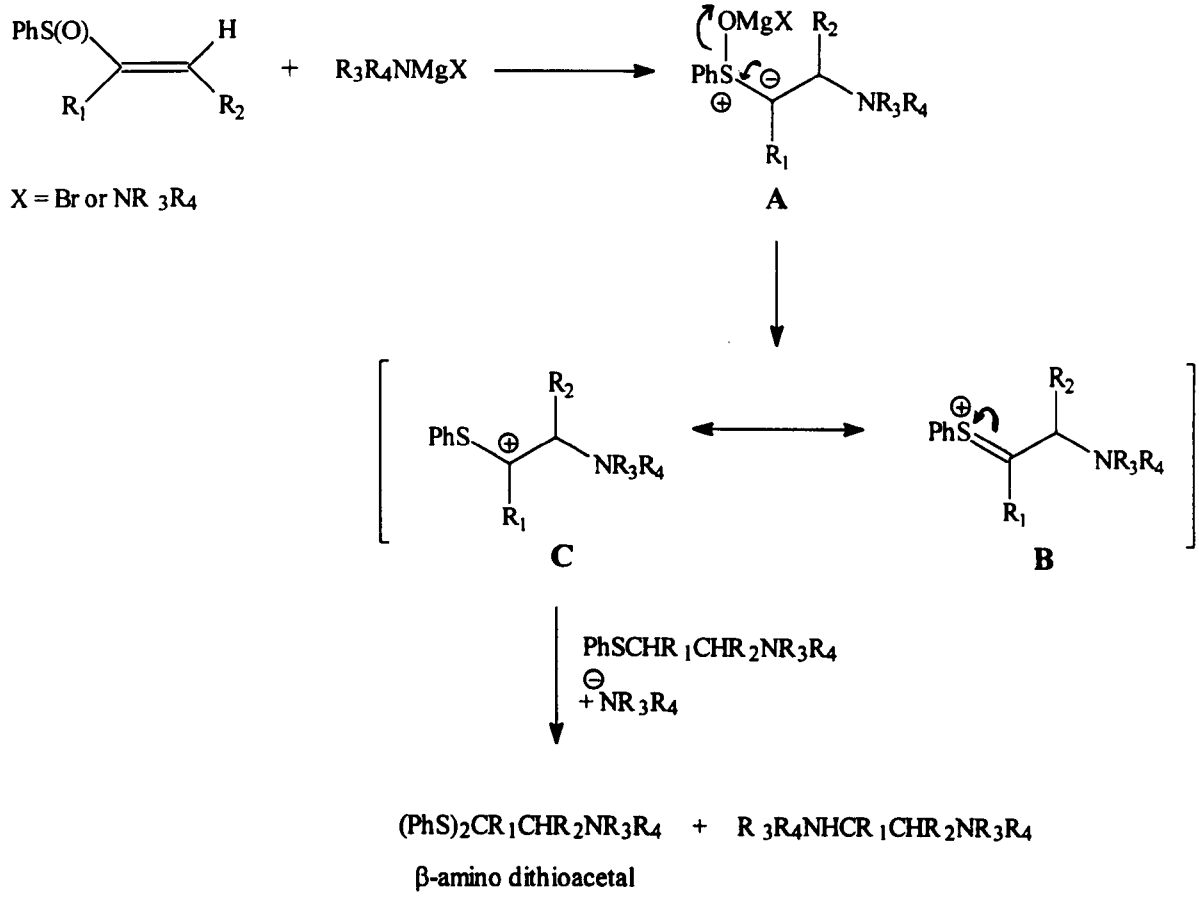

Scheme 1.7- Mechanism for the formation of β-amino dithioacetals

Conjugate addition of an amide group to the β-C results in the formation of ylide species, (A), which then gives the sulphonium ion intermediate, (B). The stabilised

carbonium ion, (C), then undergoes nucleophilic attack by substituted sulphide (produced by the reduction of vinyl sulphoxide with excess amide reagent). The resultant products are that of the β-amino dithioacetal along with substituted amine.

1.6 Solid-State Structures of Magnesium Amides

The basic structural feature exhibited by magnesium amides is the presence of four-membered azamagnesacyclic MgNMgN rings. The high bridging ability of the amide units usually induces the formation of insoluble polymeric materials. The presence of large R groups and / or donor solvents inhibits this aggregation process making structural analysis possible.

The most common structural types exhibited by magnesium amides are dimers, with a central MgNMgN ring containing electron precise bonds, and monomers with terminal N-Mg bonds (figure 1.12). In both cases the favoured coordination number of magnesium is four occupying a distorted tetrahedral geometry. Table 1.1 shows a catalogue of all crystallographically determined magnesium amide compounds presently known in the literature (note that this excludes those consisting of dianionic ligands, these will be discussed in chapter two). Highlights from the table will be now discussed in detail.

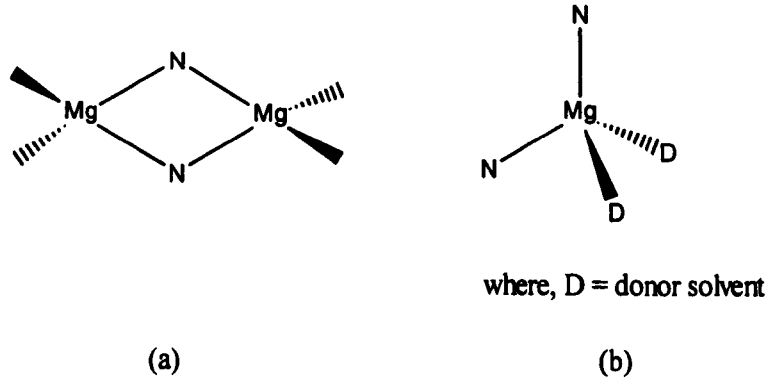

Figure 1.12- Basic structural motifs adopted by magnesium amides

Unsolvated Magnesium bis amides	Compound Number	Association	Ref.
$[Mg\{N(SiMePh_2\}_2]$	**(20)**	1	46
$[Mg\{N(8\text{-quinolyl})(SiMe_3)\}_2]$	**(21)**	1	47
$[Mg\{N(CH_2Ph)_2\}_2]_2$	**(22)**	2	48
$[Mg\{N(SiMe_3)_2\}_2]_2$	**(23)**	2	49
$[Mg\{N(c\text{-}C_6H_{11})_2\}_2]_2$	**(24)**	2	50
$[\{Mg[\mu\text{-}N(Ph)_2][N(Ph)(2\text{-pyr})]\}_2]$	**(25)**	2	51
$[Mg_3\{\mu\text{-}N(H)Dipp\}_4\{N(SiMe_3)_2\}_2]$	**(26)**	3	50
$[Mg(NH_2)_2]_\infty$	**(27)**	∞	52
Solvated Magnesium bis amides	**Compound Number**	**Association**	**Ref.**
$[Mg\{N(SiMe_3)_2\}_2.2THF]$	**(28)**	1	53
$[Mg\{N(SiMe_3)_2\}_2.2(2,3,5\text{-collidine})]$	**(29)**	1	54
$[Mg\{N(SiMe_3)_2\}_2.2(2\text{-picoline})]$	**(30)**	1	54
$[Mg\{N(SiMe_3)_2\}_2.2(3,5\text{-lutidine})]$	**(31)**	1	54
$[Mg\{N(SiMe_3)_2\}_2.(2,3,5\text{-collidine})]$	**(32)**	1	54
$[Mg\{N(SiMe_3)_2\}_2.(2\text{-picoline})]$	**(33)**	1	54
$[Mg\{N(SiMe_3)_2\}_2.(2,6\text{-lutidine})]$	**(34)**	1	54
$[Mg\{N(CH_2Ph)_2\}_2.TMEDA]$	**(35)**	1	55
$[Mg\{N(CH_2Ph)_2\}_2.2HMPA]$	**(36)**	1	55
$[Mg(tmdbtd).THF]$	**(37)**	1	56
$[Mg\{N(H)Mes\}_2.2HMPA]$	**(38)**	1	50
$[Mg\{N(2\text{-pyr})Ph\}_2.2THF]$	**(39)**	1	30
$[Mg\{N(CH_2Ph)_2\}_2.HMPA]_2$	**(40)**	2	55
$[Mg\{N(CH_2Ph)_2\}_2.THF]_2$	**(41)**	2	55
Alkyl Magnesium Amides	**Compound Number**	**Association**	**Ref.**
$[EtMg(NC_{28}H_{40}).2THF]$	**(42)**	1	57
$[Bu^sMg\{\mu\text{-}N(SiMe_3)_2\}]_2$	**(43)**	2	58
$[Bu^tMg\{\mu\text{-}N(H)Bu^t\}.THF]_2$	**(44)**	2	50
$[MeMg\{N(Me)CH_2CH_2NMe_2\}]_2$	**(45)**	2	59
$[Bu^nMg\{N(CH_2CH_2Me_2)PhCH_2\}]_2$	**(46)**	2	30
$[EtMg\{N(H)Dipp]_{12}$	**(47)**	12	50
Miscellaneous Magnesium Amide Compounds	**Compound Number**	**Association**	**Ref.**
$[Mg(\mu\text{-}Cl)\{N(SiMe_3)_2\}.OEt_2]_2$	**(48)**	2	46
$[Br_2Mg_2\{N_2C_{12}H_8\}.(THF)_6]$	**(49)**	2	60
$[MeSi\{Bu^tNMgN(SiMe_3)_2\}_3]$	**(50)**	3	61

Table 1.1- Crystallographically characterised magnesium amides

1.6.1 Magnesium Bis(amides)

Magnesium bis(amide) compounds $[R_2N(R'_2N)Mg]$ can be separated into two distinct categories, namely, homoleptic or heteroleptic. These terms are used when two identical amide functions i.e. (R = R') and two dissimilar amide functions i.e. (R ≠ R') respectively are bound to magnesium. The former category is by far the most common and will be considered first.

When bulky amide ligands are involved, magnesium usually favours a coordination number of less than four (figure 1.13).

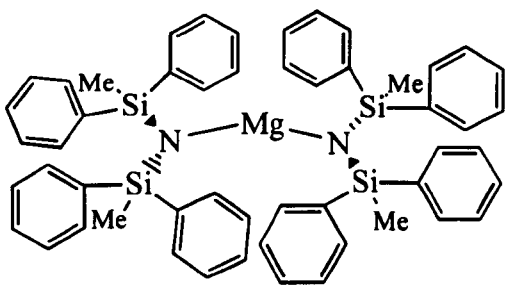

$[Mg\{N(SiMePh_2)_2\}_2]$ **20**

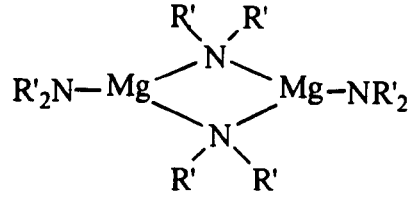

$[\{(R'_2N)_2Mg\}_2]$

where R'= CH_2Ph **22**, $SiMe_3$ **23** or *c*-C_6H_{11} **24**

Figure 1.13- Examples of two and three-coordinate magnesium amides

The silylamide $[Mg\{N(SiMePh_2)_2\}_2]$[46] **20** represents a rare example of two coordination for a magnesium amide in the solid state (note that $[Mg\{N(SiMe_3)_2]$ adopts a similar two-coordinate structure in the gas phase[62]). The extremely bulky nature of the $[^-N(SiMePh_2)_2]$ anions causes the N-Mg-N angle to deviate from linearity [N-Mg-N 162.8(3)°]. Compounds **22**[48], **23**[49] and **24**[50] are related dimeric structures whereby each magnesium centre is three-coordinate in a distorted trigonal-planar environment. Important bond distances and angles are shown in table 1.2.

Amide Group	Mean N_{br}-Mg bond distance (Å)	Mean N_t-Mg bond distance (Å)	Mean ring Mg-N_{br}-Mg angle (°)	Mean ring N_{br}-Mg-N_{br} angle (°)
$-N(CH_2Ph)_2$	2.09	1.94	85.8	94.2
$-N(SiMe_3)_2$	2.15	1.98	84.2	95.8
$-N(c\text{-}C_6H_{11})_2$	2.11	1.95	86.7	93.3

Where br = bridging and t = terminal

*Table 1.2- Key geometrical parameters for the three-coordinate dimers **22-24***

From the comparative data, it is observed that in all cases the terminal N_t-Mg bond distances are significantly shorter than their bridging counterparts [range N_t-Mg,1.94-1.98Å c.f. N_{br}-Mg, 2.09-2.15Å] indicating that the terminal anions bind more strongly to the magnesium centres. Turning to bond angles, the endocyclic angles at magnesium are larger than those at nitrogen [range N_{br}-Mg-N_{br}, 93.3°-95.8° c.f. Mg-N_{br}-Mg, 84.2°-86.7°] indicating that the repulsion between both bridging anions forces the N-Mg-N angle to increase.

Generally, in the presence of donor solvent, the coordinatively unsaturated three-coordinate dimers (**22** and **23**) readily deaggregate to more favoured four-coordinate monomeric species (**28-31**)[53,54], (**35-36**[55]) where magnesium adopts a distorted tetrahedral geometry. This is illustrated in equation 1.10 for the case of magnesium bis[bis(trimethylsilyl)] amide.

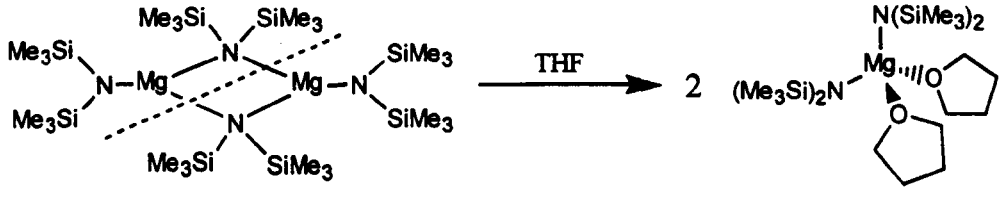

(1.10)

23 **28**

Recently, it was shown that sublimation[54] of the four-coordinate monomers $[Mg\{N(SiMe_3)_2\}_2.2(2,3,5\text{-collidine})]$ **29** and $[Mg\{N(SiMe_3)_2\}_2.2(2\text{-picoline})]$ **30**, affords the monomeric, three-coordinate variants **32** and **33**, (equation 1.11 shows the case of the 2-picoline compound **30** → **33**), which were characterised by X-ray diffraction.

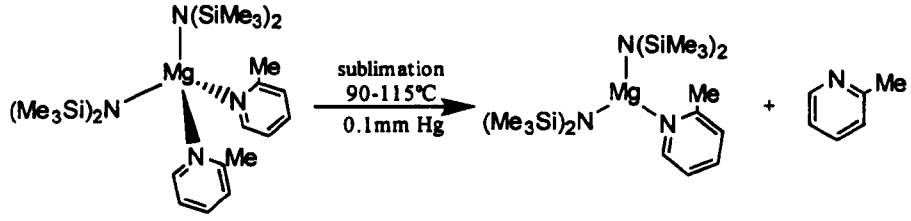

(1.11)

The sum of the angles about the central magnesium in $[Mg\{N(SiMe_3)_2\}_2.(2\text{-picoline})]$ **33**, is 359.5(2)° which indicates a near perfect planar geometry. The N-Mg-N angle between the anions was found to be the largest [137.3(2)°]. Interestingly, the plane of the 2-picoline donor ligand was found to lie approximately planar to the plane of the three N atoms so as to avoid steric interactions with the silyl methyl groups.

Depending on the nature of the amide function, coordination numbers greater than four are possible in the monomeric state, in particular when internal ligating groups are present. One such example is $[Mg\{N(2\text{-pyr})Ph\}_2.2THF]$[30] **39** which possesses internal ligating (2-pyr) functions. In this structure the magnesium atom is located at the centre of a distorted octahedron (figure 1.14), made up of pairs of amido-N, pyridyl-N and THF molecules all arranged in a *trans* conformation. The internal ligation of the 2-pyridyl unit at magnesium creates two essentially planar MgNCN four-membered rings. The dimensions of these rings signify that the metal has a greater affinity for the amido-N, as indicated by the shorter bond lengths [$Mg\text{-}N_{anionic}$ 2.105(2)Å c.f. $Mg\text{-}N_{pyridyl}$ 2.182(2)Å]. The O-Mg bond distances in **39** are found to be longer than for those found in the bis THF complex $[Mg\{N(SiMe_3)_2\}_2.2THF]$ **28** i.e. [**39** O-Mg, 2.12(2)Å c.f. **28** O-Mg, 2.093(5)Å].

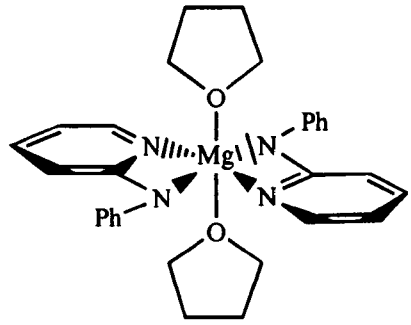

Figure 1.14- Structure of monomeric [Mg{N(2-pyr)Ph}$_2$.2THF] 39

As mentioned previously, heteroleptic magnesium bis(amide) complexes are magnesium compounds with two different amide functions attached. At the time of writing only two such compounds have been reported. Each one is now discussed in turn.

The secondary amine derivative [{Mg[μ-N(Ph)$_2$][N(Ph)(2-pyr)]}$_2$][51] **25** (figure 1.15(a)) displays a conventional dimeric arrangement with each magnesium in a four-coordinate, distorted tetrahedral geometry. The amido N-atoms of the central planar azamagnesacyclic MgNMgN ring belong to the [$^-$N(Ph)$_2$] anions, while the didentate [$^-$N(Ph)(2-pyr)] anions occupy the terminal positions. Interestingly, the N-Mg bond distances are asymmetric within the central ring [short edges, 2.080(5)Å; long edges, 2.119(5)Å] and the endocyclic N-Mg-N, Mg-N-Mg angles are perfectly right angled [90.0(2)°].

The second heteroleptic bis amide [Mg$_3${μ-N(H)Dipp}$_4${N(SiMe$_3$)$_2$}$_2$][50] **26**, (figure 1.15(b)), which is formally derived from a mixture of primary and secondary amines, possesses a novel linear trimeric array of two fused (NMg)$_2$ rings [torsion angle between (NMg)$_2$ rings 75.0°]. The details of the structure can be rationalised on the basis of metal coordination numbers and steric effects of the ligands. The more bulky [$^-$N(SiMe$_3$)$_2$] anions preferentially occupy terminal positions whereas the less bulky

primary amide functionalities [μ-N(H)Dipp] assume a bridging role. The terminal three-coordinate and bridging N-Mg bond distances have similar dimensions to those in the aforementioned three-coordinate dimers **22-24**. [i.e. mean N_t-Mg, bond distances 1.966(6)Å; mean N_{br}-Mg bond distances 2.102(6)Å c.f. table 1.2, pg.24]. The internal endocyclic MgNMgN bond angles are found to straddle 90° [i.e. N_{br}-Mg-N_{br}, 89.5(2)°/90.6(2)°; Mg-N_{br}-Mg, 90.3(2)°/89.5(2)°].

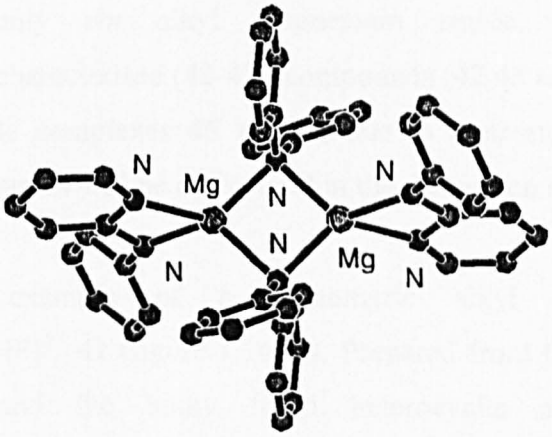

(a)

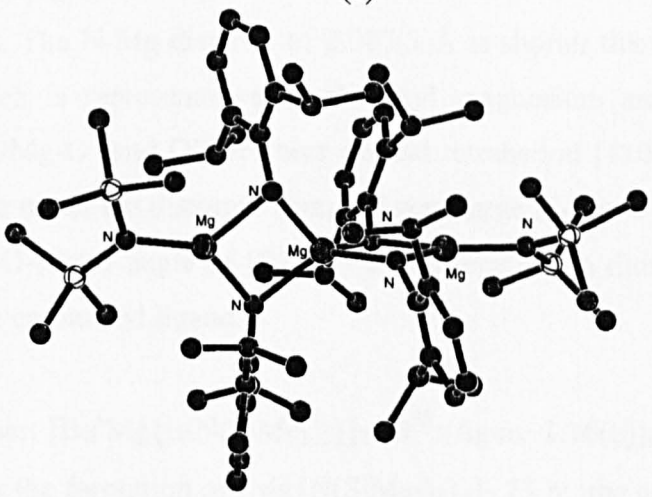

(b)

*Figure 1.15- Crystal structures of (a) [{Mg[μ-N(Ph)$_2$][N(Ph)(2-pyr)]}$_2$] **25** and (b) [Mg$_3${μ-N(H)Dipp}$_4${N(SiMe$_3$)$_2$}$_2$] **26**, (hydrogen atoms are ommited for clarity)*

1.6.2 Alkyl Magnesium Amides

Similar to the aforementioned bis(amide) compounds, alkyl magnesium amide complexes tend to form four-coordinate dimeric arrangements in the presence of bulky amide groups. Since N is more electronegative than C, amido bridges are found in preference to the alkyl analogues.

To date, only six alkyl magnesium amide complexes have been crystallographically characterised (**42-47**), compounds (**42**,**43** and **47**) will be considered in this section, while complexes **45** and **46** due to their structural similarities with selected dianionic systems will be considered in the discussion section of chapter two.

The only example of a monomeric alkyl magnesium amide is $[EtMg(NC_{28}H_{40}).2THF]$[57] **42** (figure 1.16(a)). Prepared from the equimolar reaction of diethylmagnesium and the bulky fused heterocyclic amine, 1,3,6,8-tetra-tert-butylcarbazole. Magnesium attains a coordination number of four by solvation of two THF molecules. The N-Mg distance of 2.087(3)Å is shorter than the C-Mg distance of 2.141(4)Å which is representative of all alkyl magnesium amide complexes. Bond angles about N-Mg-O (and O') are near perfect tetrahedral [110.3(1)°] while the other angles about the metal are distorted from the very large N-Mg-C angle of [125.2(2)°] to the very small O-Mg-O angle of [89.0(1)°]. Aggregation to dimer is precluded by the large size of the carbazolyl ligand.

The dimer, $[Bu^sMg\{\mu\text{-}N(SiMe_3)_2\}]_2$ **43**[58] (figure 1.16(b)), can be regarded as an intermediate for the formation of $[Mg\{N(SiMe_3)_2\}_2]_2$ **23** by the equimolar reaction of *n*, *s*-dibutylmagnesium [*n*,*s*-Bu_2Mg] and bis(trimethylsilyl) amine [$HN(SiMe_3)_2$]. This reaction illustrates selective metallation whereby the kinetic *sec*-Bu product is crystallised in preference to the *n*-Bu isomer. **43** is isostructural with the aforementioned bis(amide) compounds **22-24** where each magnesium is three-coordinate and in a distorted trigonal planar geometry. The C-Mg distances are shorter than the

corresponding N-Mg distances [2.08(1)Å c.f. 2.118(4)Å]. The internal bond angles of the central MgNMgN ring straddle 90°, the larger angles being situated at the metal [mean Mg-N-Mg 87.1(2)°; N-Mg-N 92.9(2)°].

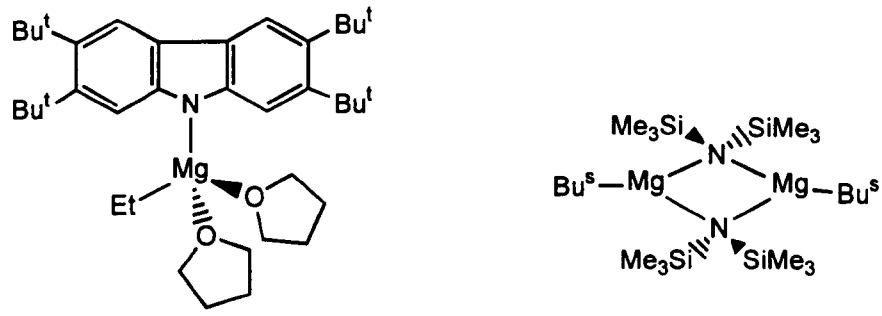

(a) (b)

Figure 1.16- Structures of (a) monomeric [EtMg(NC$_{28}$H$_{40}$).2THF] ***42*** *and (b) dimeric [Bu^{s}Mg{μ-N(SiMe$_3$)$_2$}]$_2$* ***43***

A unique example of an alkylmagnesium amide complex accommodating both bridging amido and alkyl substituents is [{DippN(H)MgEt}$_{12}$] **47**[50] (figure 1.17). The structure of **47** represents a remarkable dodecameric ring assembly of twelve magnesium atoms associated in a bowed disk arrangement; at present it is the largest oligomer so far characterised in magnesium amide chemistry The structure can also be viewed as a circular array of twelve fused MgNMgC rings. For steric reasons the ethyl groups are disposed toward the circle interior while the bulky amide moieties point outwards. Although both N and C bridge the magnesium centres, large differences can be seen in their lengths [mean N-Mg 2.085Å; C-Mg 2.17Å]. The asymmetrical MgNMgC rings cause significant distortions in the endocyclic ring angles, the angles at magnesium deviating largely from an ideal tetrahedral geometry [mean N-Mg-C, 95.67°]. Similarly the angles at C and N deviate markedly from their ideal sp^3 environments [mean Mg-C-Mg, 80.39°; Mg-N-Mg, 87.41°].

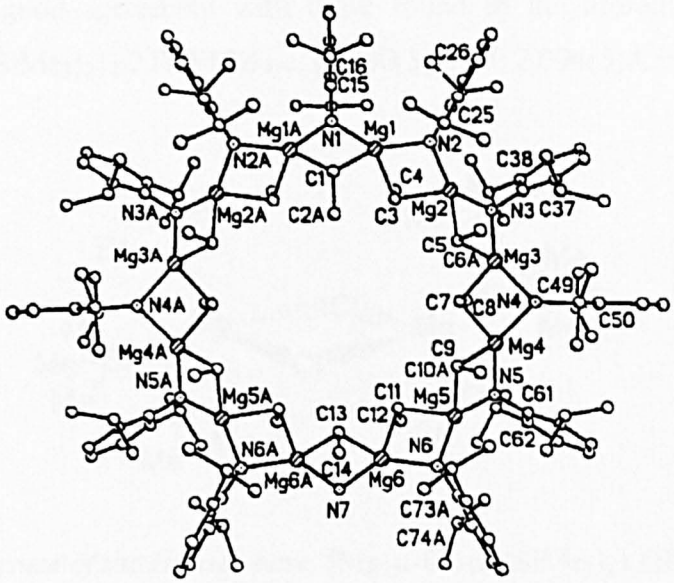

*Figure 1.17- Crystal structure of dodecameric [{DippN(H)MgEt}$_{12}$] **47**, (hydrogen atoms are omitted for clarity)*

1.6.3 Miscellaneous Magnesium Amide Compounds

From this category only the Hauser base compound [Mg(μ-Cl){N(SiMe$_3$)$_2$}.OEt$_2$]$_2$ **48**[46] (figure 1.18) will be discussed as it represents the only one of its kind to be found in the literature.

Complex **48** has a dimeric structure with chloride anions preferentially bridging the magnesium centres and amide ligands occupying terminal positions. Halide bridged dimers, although uncommon in structural magnesium amide chemistry, have been found in some crystallised dimeric Grignard reagents e.g. [EtMg(Br).NEt$_3$]$_2$[63(a)] and [CH$_2$=CHCH$_2$Mg(Cl).TMEDA][63(b)]. The terminal N-Mg bond distances are similar to the three-coordinate dimeric structure of [Mg{N(SiMe$_3$)$_2$}$_2$]$_2$ **23** i.e. [1.907(7)Å c.f. 1.98Å in **23**]. Four-coordination at the magnesium centres is complete with the presence of terminally solvating ether ligands. The bond angles within the central (MgCl)$_2$ ring indicate an almost perfect square [Cl-Mg-Cl, 90.9(1)°; Mg-Cl-Mg, 89.1(1)°]. The O-Mg

distances are in good agreement with those found in the aforementioned bis THF complex [Mg{N(SiMe$_3$)$_2$}$_2$.2THF] **28** i.e. [2.000(3)Å c.f. 2.094(5)Å in **28**].

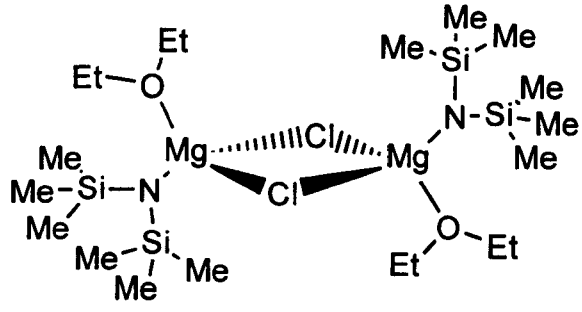

Figure 1.18- Structure of the Hauser base, [Mg(μ-Cl){N(SiMe$_3$)$_2$}.OEt$_2$]$_2$ **48**

1.7 Chapter One References

[1] A. W. Titherley; *J. Chem. Soc.*, (1894), **65**, 504.

[2] B. J. Wakefield; Organolithium methods, Academic Press, London, (1988).

[3] Reviews: (a) M. Majewski and D. M. Cleave; *J. Organomet. Chem.*, (1994), **470**, 1;
(b) D. Seebach; *Angew. Chem.,Int. Ed. Engl.*, (1988), **27**, 1624.

[4] M. F. Lappert, P. P. Power, A. R. Sanger and R. C. Srivastava; *Metal and Metalloid Amides*, Ellis Horwood Ltd., John Wiley & Sons., (1980), **2**, 31.

[5] J.F. Remenar and D. B. Collum; *J. Am. Chem. Soc.*, (1998), **120**, 4081.

[6] R. D. Rodgers, J. L. Atwood and R. Grüning; *J. Organomet.Chem.*, (1978), **157**, 229.

[7] Reviews: (a) R. E. Mulvey; *Chem. Soc. Rev.*, (1991), **20**, 167;
(b) K. Gregory, P. v. R. Schleyer and R. Snaith; *Adv. Inorg. Chem.*, (1991), **37**, 47.

[8] M. F. Lappert, M. J. Slade, A. Singh, J. L. Atwood, R. D. Rodgers and R. Shakir; *J. Am. Chem. Soc.*, (1983), **105**, 302.

[9] D. R. Armstrong, R. E. Mulvey, G. T. Walker, D. Barr and R. Snaith; *J. Chem. Soc., Dalton Trans.*, (1988), 617.

[10] D. Barr, W. Clegg, R. E. Mulvey and R. Snaith; *J. Chem. Soc., Chem. Commun.*, (1984), **285**, 287.

[11] M. Rannenberg, H. D. Hausen and J. Weilden; *J. Organomet. Chem.*, (1989), 376, C27.

[12] D. R. Armstrong, D. R. Baker, F. J. Craig, R. E. Mulvey, W. Clegg and L. Horsburgh; *Polyhedron.*, (1996), **15**, 3533.

[13] G. R. Kowach, C. J. Warren, R. C. Haushalter and F. J. Disalvo; *Inorg. Chem.*, (1998), **37**, 156.

[14] H. Chen, R. A. Bartlett, H. V. R. Dias, M. M. Olmstead and P. P. Power; *Inorg Chem.*, (1991), **30**, 2487.

[15] N. D. R. Barnett, R. E. Mulvey, W. Clegg and P. A. O'Neil; *J. Am. Chem. Soc.*, (1991), **113**, 8187.

[16] D. R. Armstrong, D. Barr, W. Clegg, S. M. Hodgson, R. E. Mulvey, D. Reed, R. Snaith and D. S. Wright; *J. Am. Chem. Soc.*, (1989), **111**, 4719.

[17] D. R. Armstrong, D. Barr, W. Clegg, R. E. Mulvey, D. Reed, R. Snaith and K. Wade; *J. Chem. Soc., Chem. Commun.*, (1986), 869.

[18] G. Boche, I. Langlotz, M. Marsch, K. Harms and N. E. S. Nudelman; *Angew. Chem. Int. Ed. Engl.*, (1992), **31**, 1205.

[19] M. G. Gardiner and C. L. Raston; *Inorg. Chem.*, (1996), **35**, 14, 4162.

[20] A. R. Kennedy, R. E. Mulvey and A. Robertson; *J. Chem. Soc., Chem. Commun.*, (1998), 89.

[21] D. Barr, W. Clegg, R. E. Mulvey, R. Snaith and D. S. Wright; *J. Chem. Soc., Chem. Commun.*, (1987), 716.

[22] P. P. Power; *Acc. Chem. Res.*, (1988), **21**, 147.

[23] (a) W. E. Lindsell, in G. Wilkinson, F. G. A. Stone and E. W. Abel (eds.); *Comprehensive Organometallic Chemistry*, Vol 1, Pergamon Press, Oxford, 1982, Chapter 4;

(b) C. H. Heathcock, in B. M. Trost and I. Fleming (eds.); *Comprehensive Organic Chemistry*, Vol 2, Pergamon Press, Oxford, (1991), Chapter 1.6.

[24] (a) J. J. Eisch and R. Sanchez; *J. Organomet. Chem.*, (1985), **296**, C27;

(b) P. R. Markies, G. Schat, O. S. Akkerman, F. Bickelhaupt, W. J. J. Smeets, P. Van. Der. Sluis and A. L. Spek., *J. Organomet. Chem.*, (1990), **393**, 315;

(c) Review: P. R. Markies, G. Schat, O. S. Akkerman, F. Bickelhaupt, W. J. J. Smeets, P. Van. Der. Sluis and A. L. Spek., *Adv. Organomet. Chem.*, (1991), **32**, 147.

[25] (a) P. E. Eaton, C. H. Lee and Y. Xiong; *J. Am. Chem. Soc.*, (1989), **111**, 8016;

(b) D. Bonafoux, M. Bordeau, C. Biran, P. Cazeau and J. Dunogues; *J. Org. Chem.*, (1996), **61**, 5532.

[26] L. Meunier; *Compt. Rend.*, (1903), **136C**, 758.

[27] G. E. Coates and D. Ridley; *J. Chem. Soc., (A).*, (1967), 56.

[28] A. Terent'ev; *Bull. Soc. Chim. Fr.*, (1924), **35**, 1164.

[29] G. Dozzi, G. Del. Piero, M. Cesari and S. Cucinella; *J. Organomet. Chem.*, (1980), **190**, 229.

[30] K. W. Henderson, R. E. Mulvey, W. Clegg and P. A. O'Neil; *J. Organomet.Chem.*, (1992), **439**, 237.

[31] P. A. Petyunin; *Russ. Chem. Rev. (Engl. Transl.).*, (1962), **31**, 100.

[32] E. C. Ashby, J. J. Lin and A. B. Goel; *J. Org. Chem.*, (1978), **43**, 1564.

[33] E. C. Ashby and F. G. Willard; *J. Org. Chem.*, (1978), **43**, 4094.

[34] R. Sanchez and W. Scott; *Tetrahedron Lett.*, (1988), **29**, 139.

[35] K. W. Henderson, J. F. Allan and A. R. Kennedy; *J. Chem. Soc., Chem. Commun.*, (1997), 1149.

[36] For reviews see: (a) H. W. Gschwend and H. R. Rodriguez; *Org. React.* (N.Y), (1979), **26**, 1;

(b) V. Snieckus; *Heterocycles*, (1980), **14**, 1649;

(c) N. S. Narasimhan and R. S. Mali; *Synthesis*, (1983), 957;

(d) P. Beak and V. Snieckus; *Acc. Chem. Res.*, (1982), **15**, 306;

(e) P.Beak and A. I. Meyers; *Acc. Chem. Res.*, (1986), **19**, 356.

[37] (a) P. G. McDougal and J. G. Rico; *Tetrahedron Lett.*, (1984), **25**, 5977;

(b) P. Beak, D. J. Kempf and K. D. Wilson; *J. Am. Chem. Soc.*, (1985), **107**, 4745.

[38] P. Beak, J. E. Hunter, Y. M. Jun and A. P. Wallin; *J. Am. Chem. Soc.*, (1987), **109**, 5403.

[39] (a) P. E. Eaton and G. Castaldi; *J. Am. Chem. Soc.*, (1985), **107**, 724;

(b) P. E. Eaton, R. G. Daniels, D. Casucci, G. T. Cunkel; *J. Org. Chem.*, (1987), **52**, 2100.

[40] P. Beak and C. J. Upton; *J. Org. Chem.*, (1975), **40**, 1094.

[41] (a) V. Snieckus, R. J. Mills, R. F. Horvath and M. P. Sibi; *Tetrahedron Lett.*, (1985), **26**, 1145;

(b) P. E. Eaton and R. M. Martin; *J.Org. Chem.*, (1988), **53**, 2728.

[42] A. Padwa and K. E. Krumpe; *Tetrahedron*, (1992), **48**, 5385. And references cited therein.

[43] (a) T. Ibata and H. Nakano; *Chem. Express.*, (1989), **4**, 93;

(b) T. Ibata and H. Nakano; *Bull. Chem. Soc. Jpn.*, (1990), **63**, 3096;

(c) T. Ibata and H. Nakano; *Bull. Chem. Soc. Jpn.*, (1992), **65**, 3088;

(d) Recent review: Y. Vallee and A. Bulpin; *Comprehensive Organic Functional Group Transformations*; G. W. Kirby, (Ed.), Elsevier: Oxford, (1995), **4**, 243.

[44](a) K. Kobayashi, M. Kawakita, T. Mannami, O. Morikawa and H. Konishi; *Chem. Lett.*, (1994), 1551;

(b) K. Kobayashi, M. Kawakita, K. Yokota, T. Mannami, K. Yamamoto, O. Morikawa and H. Konishi; *Bull. Chem. Soc. Jpn.*, (1995), ***68***, 1401.

[45] M. B. Green and W. L. Jenkins; *J. Sci. Food. Agric.*, (1958), 536;

Japan. Soda. Co. Ltd., Japan, 44, Patent 56991963; *Chem. Abstr.* (1864), **60**, 4720h.

[46] R. A. Bartlett, M. M. Olmstead and P. P. Power; *Inorg. Chem.*, (1994), **33**, 4800.

[47] L.M. Englehardt, P. C. Junk, W. C. Patalinghug, R. E. Sue, C. L. Raston, B. W. Skelton and A. H. White; *J. Chem. Soc., Chem. Commun.*, (1991), 930.

[48] W. Clegg, K. W. Henderson, R. E. Mulvey and P. A. O'Neil; *J. Chem. Soc., Chem. Commun.*, (1994), 769.

[49] M. Westerhausen and W. Schwarz; *Z. anorg. allg. Chem.*, (1992), **609**, 39.

[50] M. M. Olmstead, W. J. Grigsby, D. R. Chacon, T. Hascall and P. P. Power; *Inorg. Chim. Acta.* (1996), **251**, 273.

[51] K. W. Henderson, R. E. Mulvey, W. Clegg and P. A. O'Neil; *Polyhedron*, (1993), **12**, 2535.

[52] H. Jacobs; *Anorg. Chem.*, (1971), **382**, 97.

[53] D. C. Bradley, M. B. Hursthouse, A. A. Ibrahim, K. M. A. Malik, M. Motevalli, R. Moseler, H. Powell, J. D. Runnacles and A. C. Sullivan; *Polyhedron*, (1990), **9**, 2959.

[54] J. L. Sebestl, T. T. Nadasdi, M. J. Heeg and C. H. Winter; *Inorg. Chem.*, (1998), **37**, 1289.

[55] K. W. Henderson, R. E. Mulvey, F. J. Craig, W. Clegg and L. Horsburgh; *Inorg. Chem.*, (1997), **36**, 6238.

[56] F. Corazza, C. Floriani, A. Chiesi-Villa, C. Guastini and S. Ciurli; *J. Chem. Soc., Dalton. Trans.*, (1988), 2341.

[57] N. Kuhn, M. Schulten, R. Boese and D. Bläser; *J. Organomet. Chem.*, (1991), **421**, 1.

[58] L. M. Englehardt, B. S. Jolly, P. C. Junk, C. L. Raston, B. W. Skelton and A. H. White; *Aust. J. Chem.*, (1986), **39**, 1337.

[59] V. R. Magnuson and G. D. Stucky; *Inorg. Chem.*, (1969), **8**, 1427.

[60] P. C. Junk, C. L. Raston, B. W. Skelton and A. H. White; *J. Chem. Soc., Chem. Commun.*, (1987), 1162.

[61] M. Veith, A Spaniol, J. Pöhlmann, F. Gross and V. Huch; *Chem. Ber.*, (1993), **126**, 2625.

[62] T. Fjelberg and R. A. Andersen; *J. Mol. Struct.*, (1984), **125**, 287.

[63] (a) J. Toney and G. D. Stucky; *J. Chem. Soc., Chem. Commun.*, (1967), 1168.

(b) M. Marsch, K. Harms, W. Massa and G. Boche; *Angew. Chem. Int. Ed. Engl.*, (1987), **26**, 696.

Chapter Two

Chapter Two – Structural Chemistry of Magnesium Involving Dianionic Ligands

Aims

- To give a brief review of magnesium cage structures based on dianionic ligands.
- To discuss the synthesis, analysis and characterisation of new magnesium diamide complexes derived from primary and secondary diamines.

2.1 Introduction

The chemistries of magnesium and lithium exhibit many similarities as a consequence of their 'diagonal relationship' within the Periodic Table. However, a marked difference can be seen in the structural nature of certain complexes that they form. In general, organolithium complexes form a wide variety of cage architectures[1], whereas organomagnesium complexes do not. This difference can, in part, be attributed to the different valencies involved. Lithium can be thought of as possessing a formal 1+ charge and magnesium a 2+ charge. Thus, to gain electroneutrality lithium requires one anion and magnesium two anions. As a result, lithium has more room in its coordination sphere for the formation of three-dimensional cage contacts compared to that of magnesium is sterically encumbered. As well as steric factors, Lewis acidity plays an important role in aggregate formation. Magnesium is a stronger Lewis acid than lithium and therefore magnesium possesses a higher affinity for hard Lewis bases such as THF. This explains why in organomagnesium chemistry, lower aggregates such as disolvated monomers are formed readily. It is only in special cases that higher aggregates form.

Magnesium structural chemistry seems to be dominated by its preference to form four-coordinate, distorted tetrahedral metal environments in monomeric, dimeric and polymeric arrangements. In comparison to organolithium structural chemistry, that of

magnesium appeared to be rather banal and largely predictable. A strong hint that organomagnesium structural chemistry has the possibility of more variety was provided by Bickelhaupt *et al* in 1993[2,3]. Three cyclic bifunctional organomagnesium.THF complexes, *o*-phenylenemagnesium **51**, naphthalene-1,8-diylmagnesium **52** and *cis*-diphenylvinylenemagnesium **53**, were prepared by them and they established for the first time the existence of tetrameric cage architectures with C-Mg bonded cores.
The interesting feature in all three compounds is the unique bonding mode exhibited by the dicarbanion. This is shown schematically below.

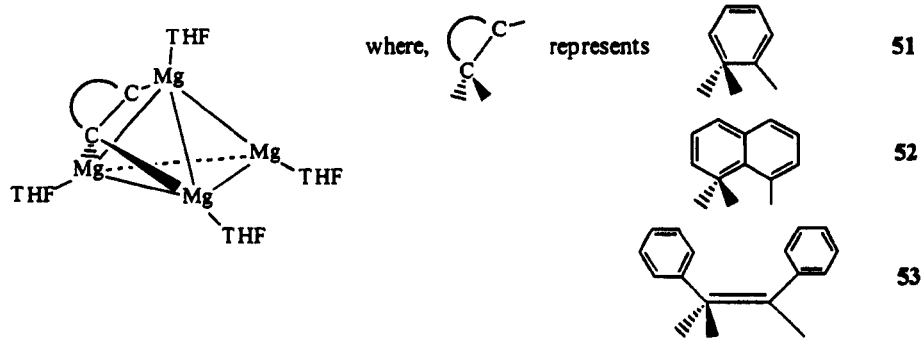

Scheme 2.1- Unique bonding mode exhibited by dicarbanions

Each organic moiety is bound to one face of a Mg_4 tetrahedron. One carbon of the dicarbanion is σ-bound (C_σ) to one magnesium centre; and the other carbon bridges in a μ^2-fashion (C_μ) to the remaining two magnesium centres of the triangular tetrahedron face. Bridging occurs via electron deficient three-centre, two-electron bonds.

Stimulated by the above report, Mulvey *et al*[4] prepared an organonitrogen derivative by doubly deprotonating the primary diamine *o*-phenylenediamine, [*o*-$C_6H_4\{NH_2\}_2$], using the diorganylmagnesium base, *n,s*-Bu_2Mg, in THF. The product is the first octahedral magnesium amide cage species, [{*o*-$C_6H_4(NH)_2$}Mg.THF]$_6$ **54** (figure 2.1). The cage is built up of a (distorted) Mg_6 octahedron, interpenetrated with a (distorted) N_{12} cuboctahedron constructed from six divalent [{*o*-$C_6H_4\{N(H)^-\}_2$] bridges. This preference, to form a more open hexameric cage over the tetrameric alternative is

linked to the number of atoms between the anionic centres. In the $C^{-}\cdots C^{-}$ examples there are no or only one atom between the C^{-} anions, whereas in the aforementioned amide two atoms separate the $N^{-}\cdots N^{-}$ anions. This results in longer $N^{-}\cdots N^{-}$ distances by comparison. Hence there is reduced steric congestion about each magnesium centre.

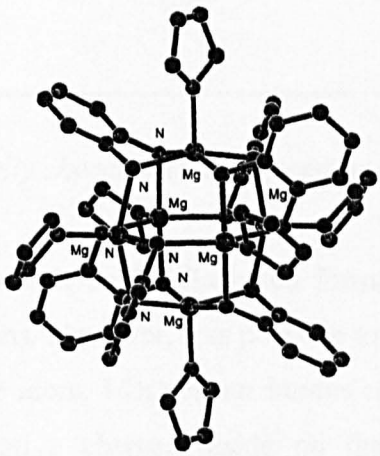

*Figure 2.1- Crystal structure of the hexameric magnesium cage compound [{o-$C_6H_4(NH^{-})_2$}Mg.THF]$_6$ **54**, (hydrogen atoms are omitted for clarity)*

In another *o*-phenylene compound, [Mg{μ-N($SiMe_3$)C_6H_4N($SiMe_3$)-*o*}(OEt_2)]$_2$ **55** (figure 2.2), Lappert *et al*[5] showed that upon increasing the steric bulk about the anionic nitrogen centre, by replacing a -H by a -$SiMe_3$ group, resulted in the formation of a less structurally interesting dimeric arrangement.

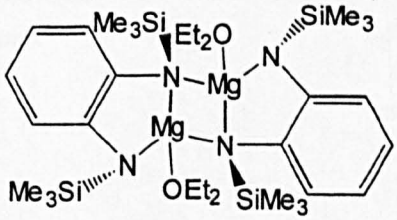

*Figure 2.2- Dimeric structure of [Mg{μ-N($SiMe_3$)C_6H_4N($SiMe_3$)-o}(OEt_2)]$_2$ **55***

Veith *et al* also found that monomeric and dimeric arrangements were formed by metallating large chelating silazane ligands, as shown in table 2.1.

Metallated Silazane Complex	Complex Number	Association Number	Ref.
$[Me_2Si(NBu^t)_2Mg.THF]_2$	(56)	2	6
$[(MeSi)_2(BrMg)_2(NBu^t)_4]$	(57)	2	7
$[\{([NBu^t][Me]Si)[NBut]_2\}$-Mg.2THF]	(58)	1	8

Table 2.1-Crystallographically characterised magnesium silazide complexes

The dianionic compounds so far discussed formally have one negative charge located on two different atoms. However, it is possible to have the two negative charges formally located on a single atom. Magnesium imides represent an example of such a species whereby both negative charges reside on the one nitrogen centre. These complexes were first identified in 1978 by Ashby and Willard[9] from the thermal decomposition of alkylmagnesium amide complexes ($RMgNR'_2$). Kinetic and stereochemical studies indicated that imide formation went via a six-membered transition state. One such reaction is shown in scheme 2.2 involving [N-(*threo*-1,2-diphenyl-1-propyl)anilino]methylmagnesium, which ultimately produces *cis*-1,2-diphenylpropene as well as the imide.

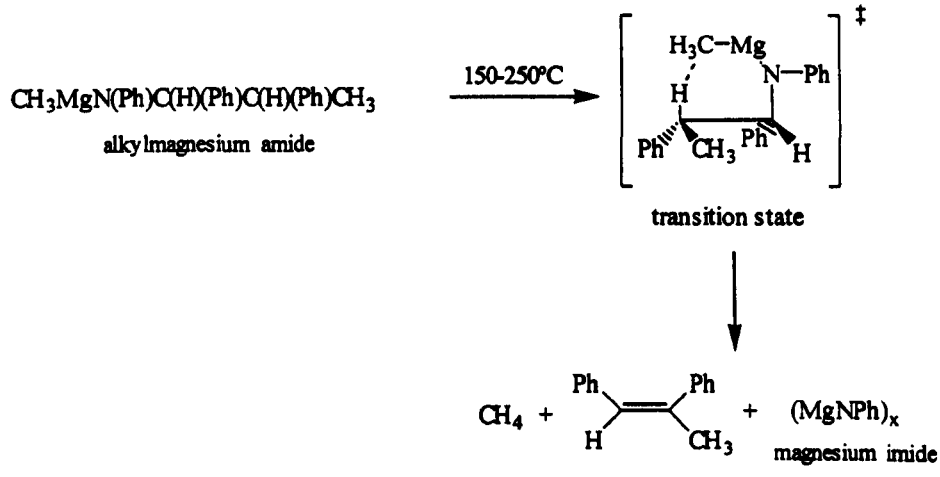

Scheme 2.2- The formation of a magnesium imide via a six-membered transition state

More recent work by Power *et al* has shown that the two major products obtained from the reaction of a Grignard reagent (RMgX) or dialkylmagnesium species (R_2Mg) with aniline are the magnesium imide compounds **59**[10] and **60**[11], shown in scheme 2.3 (a) and (b).

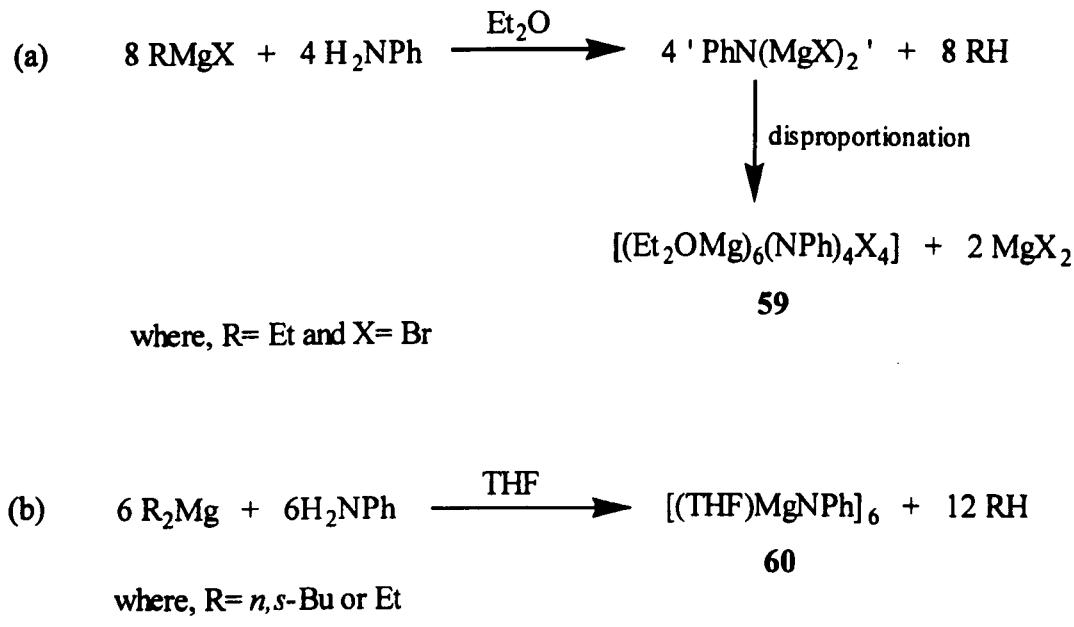

Scheme 2.3- Preparation of magnesium imide complexes derived from aniline

Reactions of this type involving Grignard reagents were first reported by Meunier[12] in 1903, although no crystallographic studies were possible at that time. The proposed product was the doubly deprotonated imidobis(magnesium halide) species '$PhN(MgX)_2$'. Power *et al* found that this complex disproportionated upon crystallisation from ether to give the structure $[(Et_2OMg)_6(NPh)_4Br_4]$ **59** and $MgBr_2$. This complex possesses an adamantane-like Mg_6N_4 framework. The six, octahedrally disposed Mg^{2+} cations are associated with four bridgehead $(NPh)^{2-}$ moieties. The overall charge balance of the compound is provided by four Br^- ions, which cap the four hexagonal faces of the Mg_6N_4 array. The halide 'free' species $[(THF)MgNPh]_6$ **60** possesses an entirely different structural motif. It features a distorted hexagonal-prismatic framework of alternating magnesium and nitrogen atoms. Both magnesium

and nitrogen are four-coordinate in distorted tetrahedral arrangements. The framework can be thought of as consisting of two slightly puckered (towards chair conformation) hexagonal Mg_3N_3 arrays bound together. Within the rings the average N-Mg distance (2.05Å) is found to be slightly shorter than the average N-Mg distance between the rings (2.08Å).

The 1-naphthyl derivative[13] has been prepared similarly using the same methodology shown in scheme 2.3 equation (b) and is found to be isostructural to **60**.

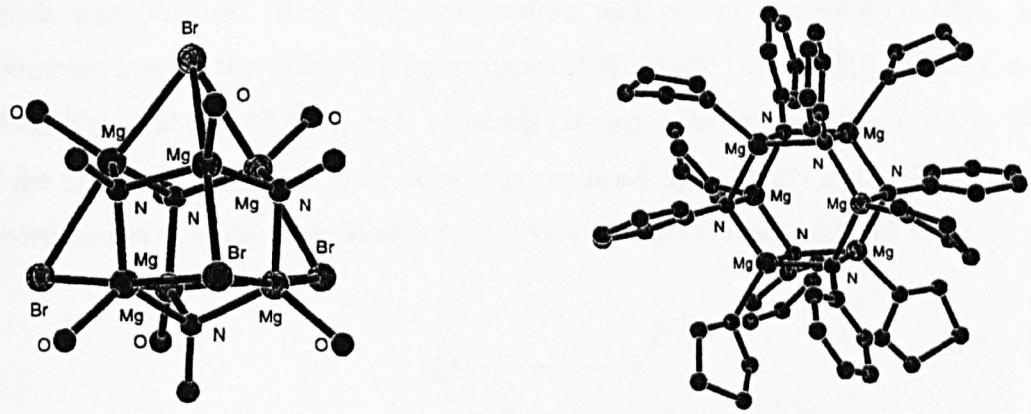

*Figure 2.3- Crystal structures of (a) $[(Et_2OMg)_6(NPh)_4Br_4]$ **59**, (central core shown) and (b) $[(THF)MgNPh]_6$ **60**, (hydrogen atoms are omitted for clarity)*

Compound **60** has been found to be an excellent imide transfer reagent[13], as illustrated in scheme 2.4.

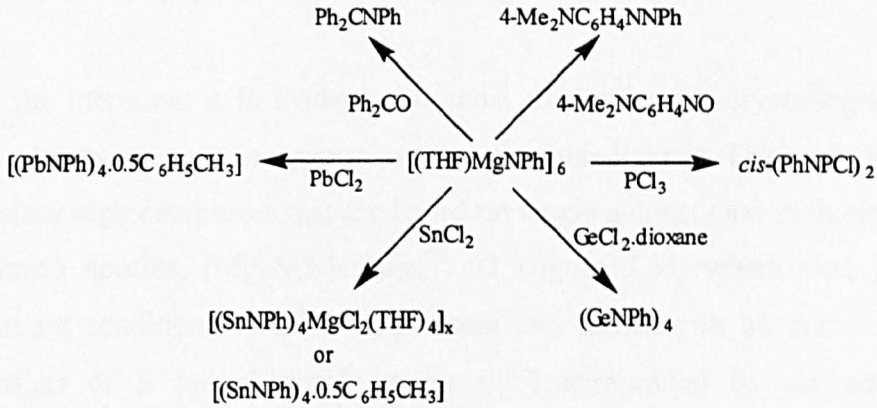

*Scheme 2.4 – Typical transfer reactions using $[(THF)MgNPh]_6$ **60***

The inherent stability of these magnesium imide species is thought to lie primarily with the presence of the arene rings which stabilise the 2- charge present on the ring-bound nitrogen centre. This could explain why very few magnesium imides formed from aliphatic amines exist, i.e. they would be less stabilised electronically.

The only such example that has been crystallographically characterised is the mixed aluminium-magnesium imide, $[(HAlN^tBu)_3\{MgN^tBu(THF)\}]$[14] **61** (figure 2.4) which was obtained using high temperature and pressure conditions. The structure resembles that of the poly(alkyliminoalane) derivatives[15] $(RAlNR')_n$, where n= 4 e.g. $(HAlN^iPr)_4$ and $(MeAlN^iPr)_4$ both of which possess a cubane skeleton $(AlN)_4$. In **61** one of the corners of a $(HAlN^tBu)_4$ cubane is replaced by a $\{MgN^tBu(THF)\}$ moiety. The incorporation of a larger metal results in severe distortion from an ideal cube.

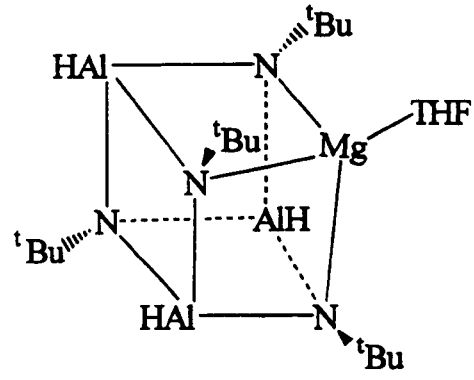

Figure 2.4- The mixed Al-Mg imide $[(HAlN^tBu)_3\{MgN^tBu(THF)\}]$ 61

From the literature, it is evident that most of the known crystallographically characterised magnesium cage complexes involve dianionic ligands. There are, however, a few magnesium cage complexes that are based on single anions. One such example is the amido-nitrido species, $[Mg_6N(NH^tBu)_9]$[16] **62** (figure 2.5), which was prepared fortuitously under conditions of high temperature and pressure in an autoclave. The structure consists of a central nitride anion (N^{3-}) surrounded by six equidistant magnesium centres in near perfect trigonal prismatic geometry. In addition to the central

nitride anion, each magnesium is tetrahedrally bound to three bridging nitrogens from the amine, giving rise to nine four-membered N-Mg planar rings.

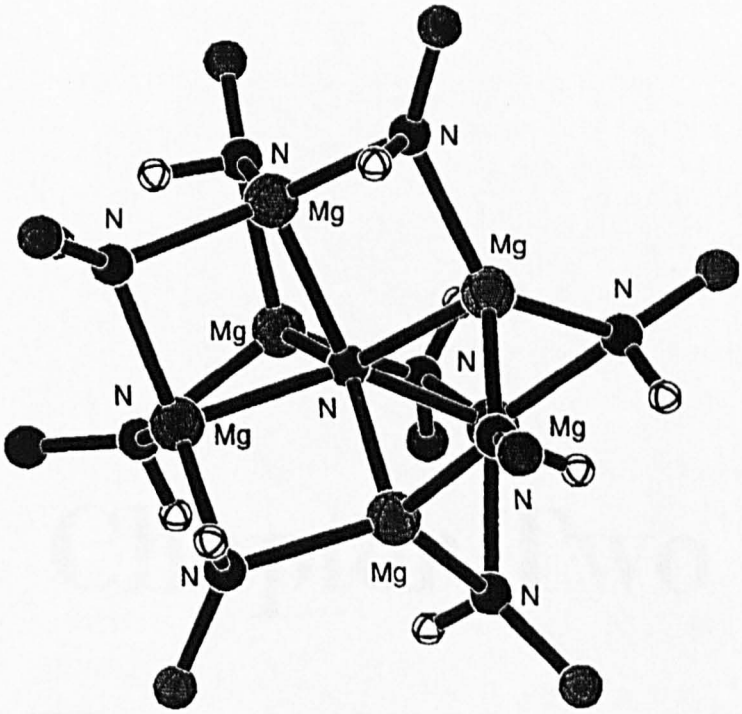

*Figure 2.5- Crystal structure of the mixed amido-nitrido cage [$Mg_6N(NH^tBu)_9$] **62**, (central core shown)*

Chapter Two

Experimental

2.2 Chapter Two Experimental

Reaction 2.1: Synthesis of [{(1,8-$C_{10}H_6(NH)_2$)Mg.HMPA}$_3$.2THF], 2A

Solid 1,8-diaminonaphthalene (1.58g, 10mmol) was charged to a Schlenk tube. To this was added an equimolar amount of DBM (10mmol in heptane, 10ml of a 1.0 M solution). No reaction was observed. The heptane solvent was then removed and replaced with THF (15ml). Immediately an extremely vigorous reaction ensued, with the formation of an off-white precipitate. Complete dissolution of the solid occurred upon addition of HMPA (3.5ml, 20mmol). The resultant green solution was left to cool to room temperature over a period of 24 hrs, producing large colourless needle crystals which were then subsequently isolated and washed with THF. They were subsequently identified as the title complex, [{(1,8-$C_{10}H_6(NH)_2$)Mg.HMPA}$_3$.2THF] **2A**.

Yield: 1.70g (38.0%) based on consumption of DBM

Melting Point: >300°C (no sign of decomposition)

Elemental analysis: $C_{48}H_{78}Mg_3N_{15}O_3P_3.2C_4H_8O$

Calculated C, 55.0; H, 7.8; N, 17.2; Mg, 6.0; O, 6.5; P, 7.5%

Found C, 51.0; H, 7.3; N, 17.7; Mg, 6.0%

Infrared / cm^{-1} (nujol mull)

2900v.s/br, 1550s, 1520s, 1460m/s, 1440s, 1340s, 1200m, 1100s, 1070s, 1040s, 980s, 800v.s, 770s, 750s, 730s, 700s, 620v.s, 520s, 500s

On exposure to air a broad signal was observed at 3710br corresponding to [$Mg(OH)_2$] and a further two bands were observed at 3450m, 3330br corresponding to asymmetric and symmetric –NH_2 stretching bands of the regenerated amine.

^{1}H NMR (400MHz, d_5-pyridine, 300K)

Chemical shift δ/ppm	Splitting pattern	Relative integral	Assignment
7.31	multiplet	—	*m, o* or *p*-Ph (pa)
7.03	triplet	1H	*meta*-Ph
6.90	doublet	—	*o or p*-Ph (pa)
6.76	doublet	1H	*o* or *p*-Ph
6.29	doublet	1H	*o* or *p*-Ph
5.84	broad singlet	—	NH_2 (pa)
4.08	singlet	1H	N-H
3.67	multiplet	2H	CH_2O, THF
2.05	doublet	9H	$O{=}P(NMe_2)_3$
1.64	multiplet	2H	CH_2, THF

Where (pa) represents: small quantity of unreacted parent amine [1,8-diaminonaphthalene] of negligible integral.

^{13}C NMR spectrum (^{1}H-decoupled, 100MHz, d_5-pyridine, 300K)

1,8-diamidonaphthalene carbon skeleton;

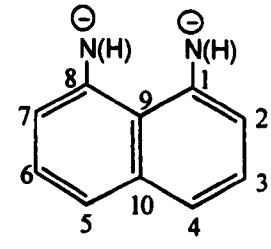

Chemical shift δ/ppm	Assignment
162.0	*ipso*-C (1) and (8)
140.4	C- (10)
127.2	C-(3) and (6)
120.7	C-(9)
118.8	C-(2) and (7) or C-(4) and (5)
109.1	C-(2) and (7) or C-(4) and (5)
68.3	CH_2O, THF
36.2	$O{=}P(NMe_2)_3$
26.3	CH_2, THF

Crystal structure

X-ray crystallographic studies of a selected crystal with dimensions 0.30x0.33x0.40mm were undertaken. These divulged the trimeric, five-coordinate magnesium bis(amide) cage structure, $[\{(1,8\text{-}C_{10}H_6(NH)_2)Mg.HMPA\}_3.2THF]$ **2A** (figure 2.6). The final R factor was 0.0565. Other crystallographic parameters are presented in Appendix III.

Table 2.2: Selected bond distances (Å) in **2A**

Mg(1)-O(1)	1.930(2)	**Mg(2)-O(2)**	1.916(2)	**Mg(3)-O(3)**	1.933(2)
Mg(1)-N(1)	2.189(3)	**Mg(1)-N(2)**	2.153(2)	**Mg(1)-N(5)**	2.164(2)
Mg(1)-N(6)	2.168(2)	**Mg(2)-N(1)**	2.165(3)	**Mg(2)-N(2)**	2.178(2)
Mg(2)-N(3)	2.150(2)	**Mg(2)-N(4)**	2.157(2)	**Mg(3)-N(3)**	2.166(3)
Mg(3)-N(4)	2.168(3)	**Mg(3)-N(5)**	2.153(3)	**Mg(3)-N(6)**	2.150(2)
O(1)-P(1)	1.494(2)	**O(2)-P(2)**	1.483(2)	**O(3)-P(3)**	1.489(2)

Table 2.3: Selected range of bond angles (°) in **2A**

O—Mg—N	107.17(10)-115.56(10)	**N—Mg—N** ^{s}	73.54(9)-74.77(9)
N—Mg—N ^{d*}	88.31(9)-91.07(9)	**N—Mg—N** ^{d**}	135.84(10)-137.61(10)
Mg—N—Mg	83.62(9)-84.96(9)	**Mg(1)-O(1)-P(1)**	151.2(2)
Mg(2)-O(2)-P(2)	171.0(2)	**Mg(3)-O(3)-P(3)**	167.5(2)

Where s = same ligand; d* = different ligand-*cis*; d** = different ligand-*trans*.

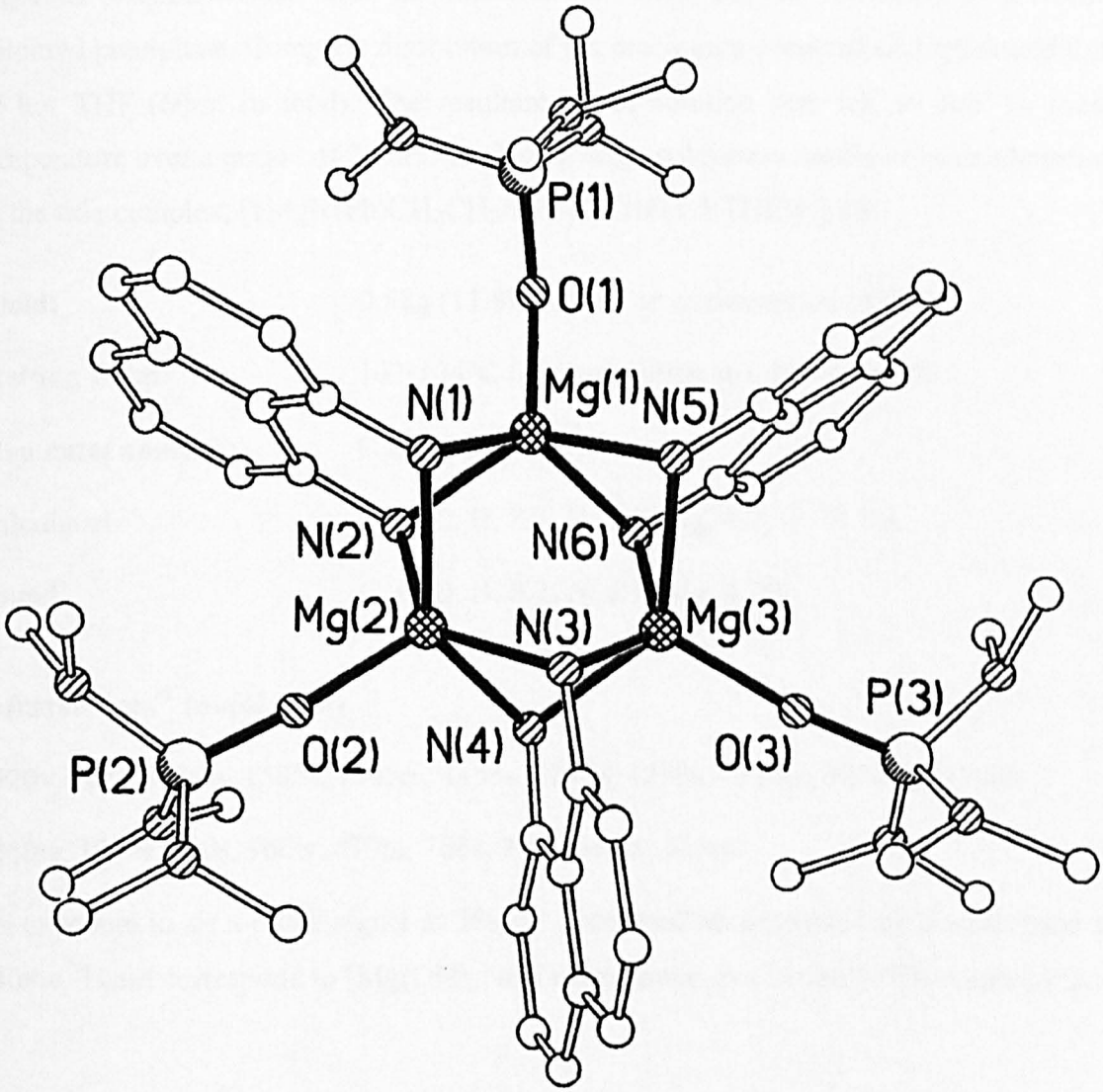

Figure 2.6- Crystal structure of trimeric [{(1,8-$C_{10}H_6(NH)_2$)Mg.HMPA}$_3$.2THF] **2A**, *(hydrogen atoms are omitted for clarity)*

Reaction 2.2- Synthesis of [{MgN(Ph)CH_2CH_2N(Ph).2THF(1.5 THF)}$_2$], 2B

To a chilled solution of N,N'-diphenylethylenediamine (2.12g,10mmol) in THF (10ml) was added DBM (10mmol in heptane, 10ml of a 1.0 M solution). Immediately, a vigorous reaction ensued with the liberation of butane and the formation of a cream-coloured precipitate. Complete dissolution of the precipitate occurred on further addition of hot THF (60ml in total). The resultant green solution was left to cool to room temperature over a period of 24 hrs, producing large colourless needle crystals identified as the title complex, [{MgN(Ph)CH_2CH_2N(Ph).2THF(1.5 THF)}$_2$] 2B.

Yield:	0.58g (11.8%) based on consumption of DBM
Melting Point:	102-104°C (decomposition to a brown solid)
Elemental analysis:	$C_{56}H_{84}Mg_2N_4O_7$
Calculated	C, 69.2; H, 8.7; N, 5.8; Mg, 4.9; O, 11.5%
Found	C, 69.0; H, 8.2; N, 6.1; Mg, 4.3%

Infrared / cm^{-1} (nujol mull)

2920v.s/br, 2825v.s, 1585s, 1485m, 1455s, 1315s, 1290s, 1230m, 1210w, 1170m, 1080w, 1030s, 990s, 960w, 870m, 760s, 700s, 560w, 510m

On exposure to air a broad signal at 3690br developed accompanied by a weak band at 3408w. These correspond to [$Mg(OH)_2$] and regenerated free amine [-NH] respectively.

^{1}H NMR (400MHz, d_6-DMSO, 300K)

Chemical shift δ/ppm	Splitting pattern	Relative integral	Assignment
7.07	multiplet	2H	*meta*-Ph
6.58	multiplet	2H	*ortho*-Ph
6.53	multiplet	1H	*para*-Ph
3.61	triplet	4H	CH_2O, THF
3.20	singlet	2H	CH_2
1.77	triplet	4H	CH_2, THF

*Please note, that THF of crystallisation was not present in this particular batch of complex **2B**.

Suitable ^{13}C {^{1}H} spectra were not recorded due to the poor solubility of the compound.

Crystal structure

X-ray crystallographic studies of a selected crystal with dimensions 0.65x0.42x0.41mm were undertaken. These divulged the dimeric, five-coordinate magnesium bis(amide) structure [{MgN(Ph)CH_2CH_2N(Ph).2THF(1.5 THF)}$_2$], **2B** (figure 2.7). The final R factor was 0.0742. Other crystallographic parameters are presented in Appendix III.

Table 2.4: Selected bond distances (Å) in **2B**

Mg—N(1)	2.290(2)	**Mg—O(1)**	2.083(2)
Mg—N(1A)	2.099(2)	**Mg—O(2)**	2.167(2)
Mg-N(2)	2.040(2)		

Table 2.5: Selected bond angles (°) in **2B**

N(2)—Mg—O(1)	109.26(9)	**N(2)—Mg—N(1A)**	127.58(9)
O(1)—Mg—N(1A)	122.64(9)	**N(2)—Mg—O(2)**	100.35(9)
O(1)—Mg—O(2)	81.59(8)	**N(1A)—Mg—O(2)**	94.13(8)
N(2)—Mg—N(1)	84.22(8)	**O(1)—Mg—N(1)**	91.34(8)
N(1A)—Mg—N(1)	87.64(8)	**O(2)—Mg—N(1)**	172.52(8)
Mg—N(1)—Mg(A)	92.36(8)		

Symmetry transformations used to generate equivalent atoms, A: -x+1, -y+1, -z+1

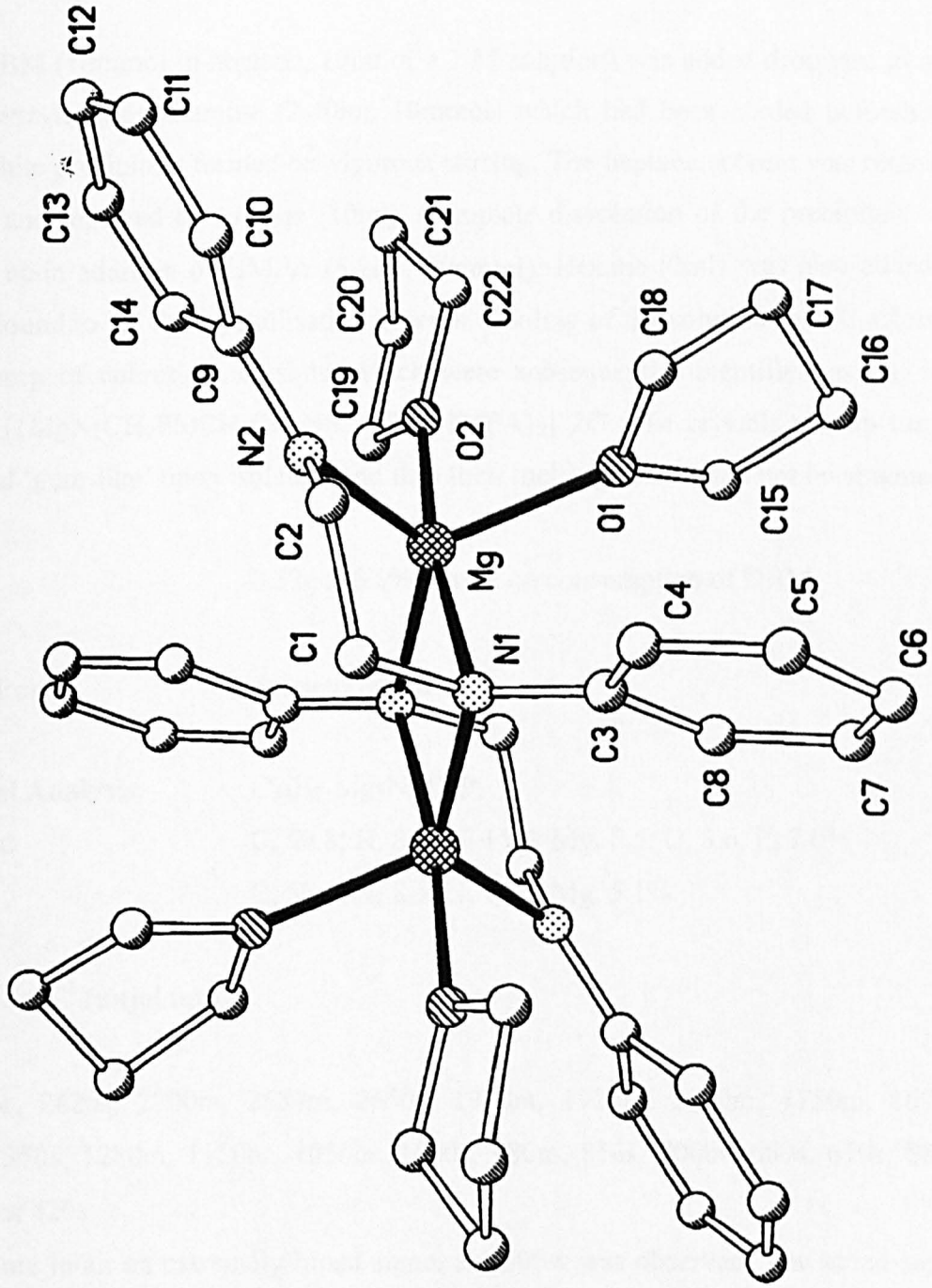

Figure 2.7- Crystal structure of the five-coordinate dimer [{MgN(Ph)CH$_2$CH$_2$N(Ph).2THF(1.5 THF)}$_2$] ***2B****, (hydrogen atoms are omitted for clarity)*

Reaction 2.3: Synthesis of [{MgN(CH_2Ph)CH_2CH_2N(CH_2Ph).HMPA}$_2$], 2C

DBM (10mmol in heptane, 10ml of a 1 M solution) was added dropwise to neat N,N'-dibenzylethylenediamine (2.40ml, 10mmol) which had been cooled beforehand. An off-white precipitate formed on vigorous stirring. The heptane solvent was removed *in vacuo* and replaced by toluene (10ml). Complete dissolution of the precipitate was achieved upon addition of HMPA (5.2ml, 30mmol). Hexane (2ml) was also added as this was found to aid the crystallisation process. Cooling of the solution to 5°C afforded a large crop of colourless crystals, which were subsequently, identified as the title complex [{MgN(CH_2Ph)CH_2CH_2N(CH_2Ph).HMPA}$_2$] **2C**. The crystals readily turned brown and 'gum-like' upon isolation and thus their melting point could not be obtained.

Yield: 0.57g (36.5%) based on consumption of DBM

Melting Point: not determined

Elemental Analysis: $C_{44}H_{72}Mg_2N_{10}O_2P_2$

Calculated C, 59.8; H, 8.2; N, 15.9; Mg, 5.5; O, 3.6; P, 7.0%

Found C, 58.7; H, 8.5; N, 15.3; Mg, 5.1%

Infrared / cm^{-1} (nujol mull)

2900v.s/br, 2820s, 2700m, 2680m, 2650s, 1970m, 1920m, 1860m, 1750m, 1675s, 1480w, 1350s, 1280m, 1150br, 1050br, 1000s, 980m, 810s, 700br, 650s, 610s, 580s, 540s, 460s, 420s

On exposure to air an extremely broad signal at 3300w was observed. The broad signal is due to hydrolysis and can be identified as a H_2O band. Unfortunately, due to its broadness, the N-H stretch is masked.

^{1}H NMR (400MHz, d_6-DMSO, 300K)

Chemical shift δ/ppm	Splitting pattern	Relative integral	Assignment
7.28	multiplet	4H	*o/m*-Ph
7.21	multiplet	1H	*para*-Ph
3.65	singlet	2H	CH_2
2.57	singlet	2H	CH_2CH_2
2.52	doublet	9H	$O{=}P(NMe_2)_3$

Suitable ^{13}C {^{1}H} spectra were not recorded due to the poor solubility of the compound.

Crystal structure

X-ray crystallographic studies of a selected crystal with dimensions 0.78x0.44x0.20mm were undertaken. These divulged the dimeric, four-coordinate magnesium bis(amide) structure, [{$MgN(CH_2Ph)CH_2CH_2N(CH_2Ph)$.HMPA}$_2$] **2C** (figure 2.8). The final R factor was 0.0752. Other crystallographic parameters are presented in Appendix III.

Table 2.6: Selected bond distances (Å) in **2C**

Mg—N(1)	2.113(2)	**Mg—N(2)**	1.982(3)
Mg—N(1A)	2.077(2)	**Mg—O(1)**	1.938(2)

Table 2.7: Selected bond angles (°) in **2C**

O(1)—Mg—N(2)	117.86(10)	**O(1)—Mg—N(1A)**	116.35(10)
N(2)—Mg—N(1A)	112.75(10)	**O(1)—Mg—N(1)**	123.18(9)
N(2)—Mg—N(1)	87.83(10)	**N(1A)—Mg—N(1)**	93.76(9)
Mg—N(1)—Mg(A)	86.24(9)		

Symmetry transformations used to generate equivalent atoms, A: -x+1, -y+2, -z

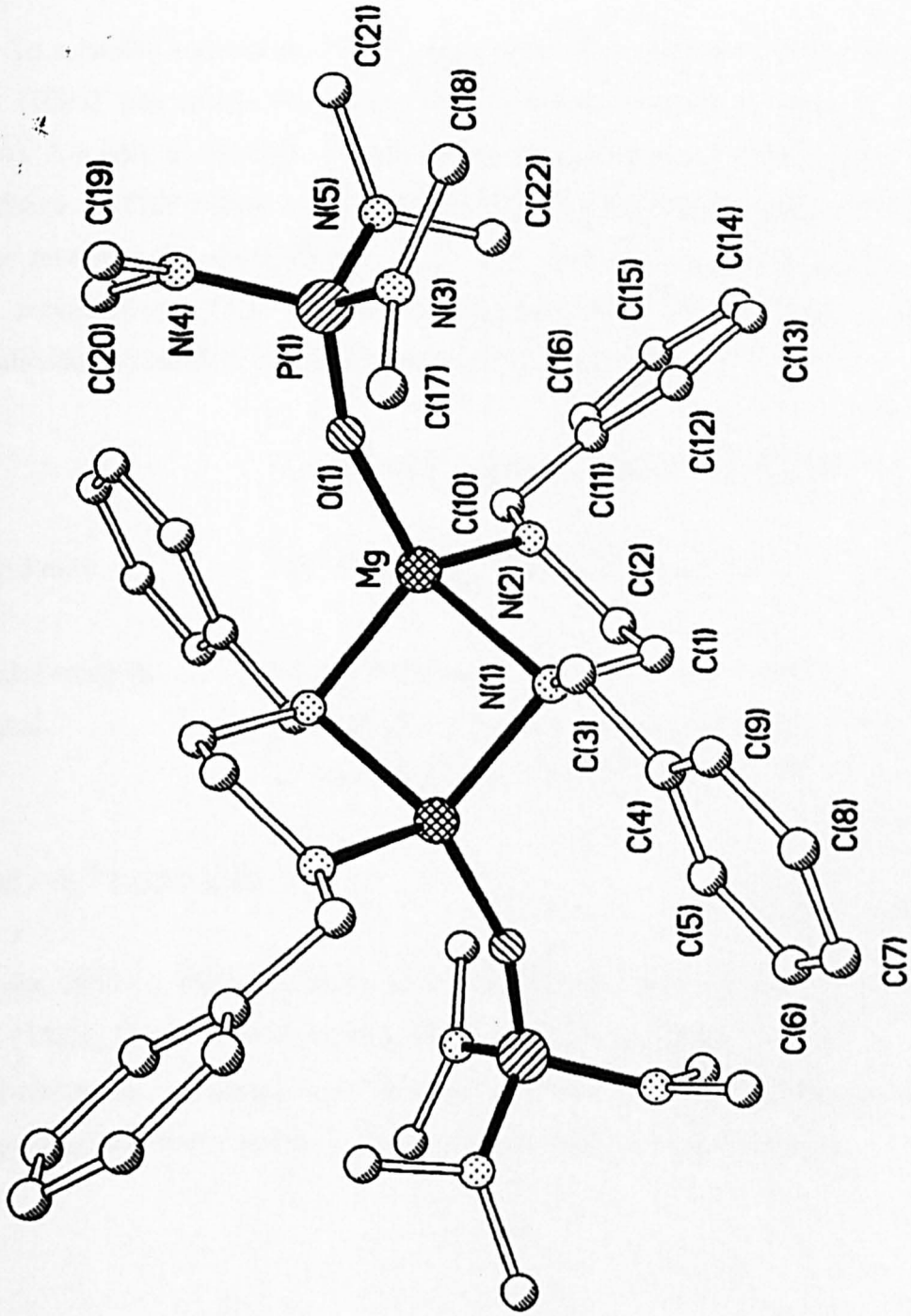

*Figure 2.8- Crystal structure of dimeric [{MgN(CH$_2$Ph)CH$_2$CH$_2$N(CH$_2$Ph).HMPA}$_2$] **2C**, (hydrogen atoms are omitted for clarity)*

Reaction 2.4: Synthesis of [MgN(Ph)CH_2CH_2N(Ph).2HMPA], 2D

To a chilled suspension of N,N'-diphenylethylenediamine (2.120g, 10mmol) in hexane (10ml) was added, dropwise, DBM (10mmol in heptane, 10ml of a 1.0 M solution). A mildly exothermic reaction ensued producing an amorphous solid. Neither the addition of THF (10ml) or of pyridine (10ml) could dissolve this solid. To the pyridine mixture was added HMPA (8ml). This gave a brown solid initially, before rapidly precipitating a solid. Pale brown/colourless needle crystals were obtained by recrystallising this solid in a toluene/HMPA (5ml/1ml) mixture.

Yield:	2.55g (43.0%) based on consumption of DBM
Melting Point:	195°C (decomposition to brown solid)
Elemental analysis:	$C_{26}H_{50}MgN_8O_2P_2$
Calculated	C, 52.7; H, 8.4; N, 18.9; Mg, 4.1; O, 5.4; P, 10.5%
Found	C, 52.2; H, 7.5; N, 19.3; Mg, 3.4%

Infrared / cm^{-1} (nujol mull)

2910v.s/br, 2850v.s, 1587m, 1536m, 1485, 1456s/br, 1374m, 1334m, 1319m, 1295m, 1191m, 1172m, 1096w, 1060w, 983s/br, 837w, 813w, 742s, 690w

On exposure to air two signals were observed at 3700w and 3308s/br. These bands can be assigned to [$Mg(OH)_2$] and the secondary amine N-H stretch respectively.

^{1}H NMR (400MHz, d_6-DMSO, 300K)

Chemical shift δ/ppm	Splitting pattern	Relative integral	Assignment
7.04	triplet	2H	*meta*-Ph
6.55	doublet	2H	*ortho*-Ph
6.50	triplet	1H	*para*-Ph
3.17	singlet	2H	CH_2CH_2
2.49	doublet	18H	$O{=}P(NMe_2)_3$

Suitable $^{13}C\ \{^1H\}$ spectra were not recorded due to the poor solubility of the compound.

Crystal structure

X-ray crystallographic studies of a selected crystal with dimensions 0.83x0.58x0.31mm were undertaken. These divulged the monomeric, four-coordinate magnesium bis(amide) structure, [$MgN(Ph)CH_2CH_2N(Ph)$.2HMPA], **2D** (figure 2.9). The final R factor was 0.0439. Other crystallographic parameters are presented in Appendix III.

Table 2.8: Selected bond distances (Å) in **2D**

Mg(1)—N(7)	2.031(3)	**Mg(1)—N(8)**	2.024(3)
Mg(1)—O(1)	1.960(2)	**Mg(1)—O(2)**	1.944(2)

Table 2.9: Selected bond angles (°) in **2D**

O(2)—Mg(1)—O(1)	101.74(10)	**O(2)—Mg(1)—N(8)**	118.75(11)
O(1)—Mg(1)—N(8)	116.22(11)	**O(2)—Mg(1)—N(7)**	115.92(11)
O(1)—Mg(1)—N(7)	118.08(10)	**N(8)—Mg(1)—N(7)**	87.03(11)

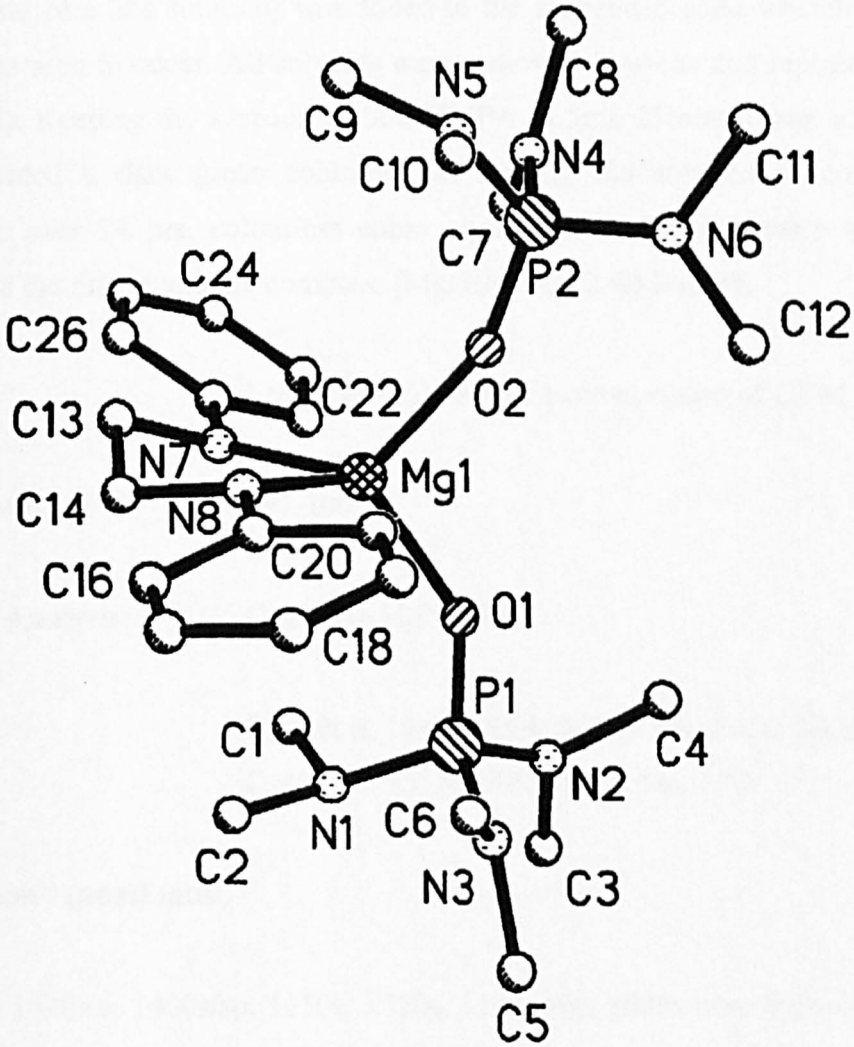

Figure 2.9- Crystal structure of one independent monomer [MgN(Ph)CH$_2$CH$_2$N(Ph).2HMPA] ***2D****, (hydrogen atoms omitted for clarity)*

Reaction 2.5: Synthesis of [Mg(HMPA)$_4$.2AlMe$_4$] 2E

DBM (10mmol in heptane, 10ml of a 1.0 M solution) was added dropwise to a stirred, chilled solution of o-phenylenediamine (1.08g, 10mmol) in THF (10ml). An exothermic reaction ensued with the formation of a white precipitate. $AlMe_3$ (20mmol in hexane, 10ml of a 2M solution) was added to the suspended solid whereby no visible reaction was seen to occur. All solvents were removed *in vacuo* and replaced with neat THF (20ml). Keeping the suspension hot, HMPA (4.5ml, 25mmol) was added slowly, which afforded a dark green solution. On leaving the solution to cool to room temperature over 24 hrs, colourless cubic crystals formed which were subsequently identified as the title aluminate complex, [Mg(HMPA)$_4$.2AlMe$_4$], **2E**.

Yield: 1.96g (21.4%) based on consumption of DBM

Melting Point: 197-200°C

Elemental Analysis: $C_{32}H_{96}Al_2MgN_{12}O_4P_4$

Calculated: C, 42.0; H, 10.6; N, 18.4; Al, 5.9; Mg, 2.6; O 7.0; P, 13.5%

Found: C, 41.1; H, 9.1; N, 18.5; Al, 5.8; Mg, 2.3%

Infrared / cm^{-1} (nujol mull)

2900v.s/br, 1490v.s, 1400s/sp, 1350s, 1250s, 1100m/br, 1000v.s/sp, 920w/sp, 900w/sp, 850v.s/br, 620v.s/br

On exposure to air, very broad hydrolysis bands appeared between 3100-3700br [Mg(OH)$_2$, Al(OH)$_3$ and H_2O].

^{1}H NMR (400MHz, d_5-pyridine, 300K)

Chemical shift δ/ppm	Splitting pattern	Relative integral	Assignment
2.58	doublet	3H	$O{=}P(NMe_2)_3$
-0.17	sextet	1H	$AlMe_4$

Average $^2J_{H\text{-}Al}$ = 6.4Hz

^{13}C NMR spectrum (^{1}H-decoupled, 100MHz, d_5-pyridine, 300K)

Chemical shift δ/ppm	Assignment
35.9	$O{=}P(NMe_2)_3$
-3.62	$AlMe_4$

Average $J_{C\text{-}Al}$ = 70.84Hz

Crystal structure

X-ray crystallographic studies of a selected crystal with dimensions 0.40x0.30x0.30mm were undertaken. These divulged the magnesium tetramethyl aluminate salt [$Mg(HMPA)_4.2AlMe_4$], **2E** (figure 2.10). The final R factor was 0.0582. Other crystallographic parameters are presented in Appendix III.

Table 2.10: Selected bond distances (Å) in **2E**

Mg—O(1)	1.885(3)	**Al(1)—C(25)**	2.013(4)
Mg—O(2)	1.903(2)	**Al(1)—C(26)**	2.011(5)
Mg—O(3)	1.899(3)	**Al(1)—C(27)**	2.010(4)
Mg—O(4)	1.900(2)	**Al(1)—C(28)**	2.014(5)

Table 2.11: Selected bond angles (°) in **2E**

O(1)—Mg—O(3)	108.63(13)	**O(1)—Mg—O(2)**	112.05(13)
O(1)—Mg—O(4)	109.28(12)	**O(3)—Mg—O(2)**	107.85(12)
O(3)—Mg—O(4)	107.67(12)	**O(4)—Mg—O(2)**	111.22(11)

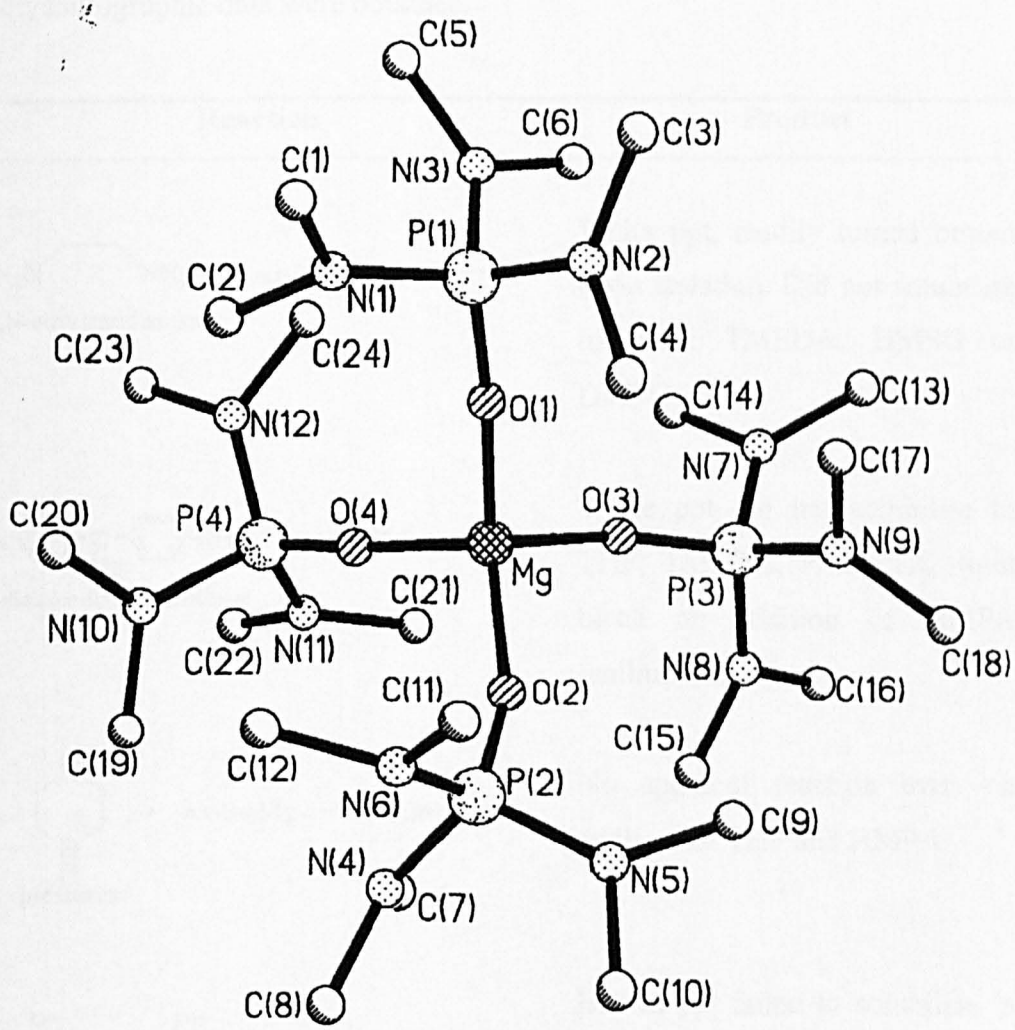

Figure 2.10- Crystal structure showing cation moiety in [Mg(HMPA)$_4$.2AlMe$_4$] 2E, (hydrogen atoms are omitted for clarity)

Reactions 2.6- Other dianionic systems

Here is presented a summary of other reactions that were carried out involving the double deprotonation of primary and secondary diamines. The products obtained in each case were found to be extremely insoluble, presumably because they are, polymeric materials, which failed to solubilise in excess donor solvents. Hence no useful analytical or crystallographic data were obtained.

Reaction	Product
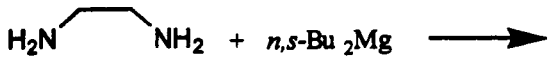 N,N-ethylenediamine	White ppt, readily turned brown upon isolation. Did not solubilise in THF, TMEDA, DMSO or DMPU.
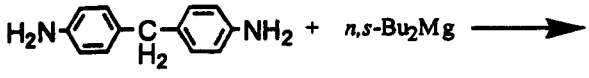 4,4'-diaminodiphenylmethane	White ppt did not solubilise in THF, TMEDA, PMDETA, went black on addition of HMPA 'aniline-black'.
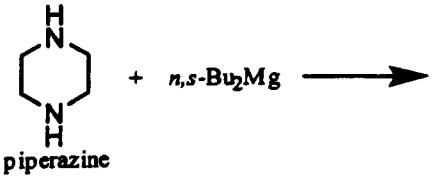 piperazine	No apparent reaction even on addition of THF and HMPA.
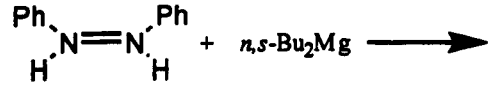 diphenylhydrazine	Brown ppt failed to solubilise in HMPA, PMDETA, DMSO or TMEDA

Table 2.12- Other reactions involving $1^y/2^y$ diamines (ppt = precipitate)

Chapter Two

Discussion

2.3 Chapter Two Discussion

Discussion will concentrate on the syntheses and characterisation of the novel trimeric amide cage compound [{(1,8-$C_{10}H_6(NH)_2$)Mg.HMPA}$_3$.2THF] **2A** along with the more conventional dimeric and monomeric amide arrangements of [{MgN(Ph)CH_2CH_2N(Ph).2THF(1.5THF)}$_2$] **2B**, [{MgN(CH_2Ph)CH_2CH_2N(CH_2Ph).HMPA}$_2$] **2C** and [MgN(Ph)CH_2CH_2N(Ph).2HMPA] **2D**. In an aside to the main theme of the chapter, the last part of the discussion will briefly deal with the tetramethyl aluminate salt, [Mg(HMPA)$_4$.2$AlMe_4$] **2E**, prepared fortuitously from the reaction of [*o*-$C_6H_4(NH)_2Mg]_\infty$ with trimethylaluminium ($AlMe_3$) in the presence of HMPA.

2.3.1 Synthesis and Analyses of Complexes 2A-2D

Complexes **2A-2D** were prepared by a simple, facile, magnesium-hydrogen exchange process (equation 2.1) using the commercial dialkylmagnesium reagent, DBM (which contains a statistical mixture of *n*-Bu and *sec*-Bu groups together with 5% of *n*-octyl groups).

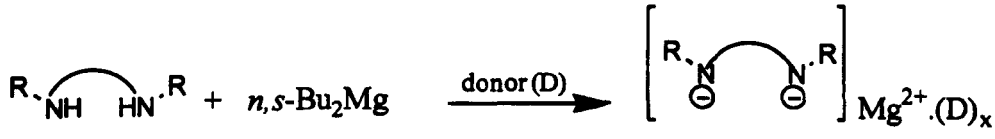

(2.1)

R = H(**2A**), Ph(**2B**,**D**), CH_2Ph(**2C**)
D = THF(**2B**), HMPA(**2A**,**C**,**D**)
x = 1(**2A**,**C**) or 2(**2B**,**D**)

In each case, donor solvent (D) was required to effect dissolution of the metallated diamine precipitates. For compounds **2C** and **2D**, three and five molar equivalents of HMPA were required respectively. Compound **2B** on the otherhand required over 70 molar equivalents of the weaker donor, THF. Thus, the opportunity for stoichiometric

control on the degree of solvation was denied. Upon isolation, the colourless crystals of **2A** readily went green which is thought to be the result of a surface radical reaction with minute traces of oxygen. Crystals of compound **2C** rapidly turned gum-like, and as a result could not be forced down a capillary tube for melting point determination. Satisfactory elemental analyses was obtained in each case, but on repeat preparations of **2B** varying amounts of THF was present in the lattice, causing rapid weight loss of the sample. This led to unreliable analyses. Infrared spectroscopy was used only to determine if the respective diamine had been successfully metallated. Thus, on exposure to air, the compounds hydrolysed resulting in the formation of a broad band around 3700cm^{-1}(br) due to H_2O and $Mg(OH)_2$ as well as with bands corresponding to the regeneration of free amine i.e. **2A**, -NH_2: 3450cm^{-1}(m) (asymmetric), 3330cm^{-1}(br) (symmetric); **2B**, -NH: 3408cm^{-1}(w); **2C**, masked by H_2O; **2D**, -NH: 3308cm^{-1}(s/br).

^{1}H NMR spectra unequivocally determined the empirical formulae of all the compounds **2A-2D**. The metallated N-H protons in compound **2A**, are observed to undergo a large low frequency shift in comparison to those present in the parent amine i.e. 5.84ppm in amine c.f. 4.08ppm in compound **2A**. This is to be expected as metallation replaces a proton on the primary (–NH_2) function by a formal negative charge, thus the remaining N-H proton becomes more shielded and hence lies further upfield. The protons on the arene rings experience only small low frequency shifts in comparison to the parent amine i.e. *m*-Ph on amine lies at 7.31ppm whereas compound **2A** the *m*-Ph lies at 7.03ppm. The donor molecule HMPA is clearly observed as a doublet at 2.05ppm. In this particular batch of **2A**, small amounts of unreacted diamine was found to be present as well as THF of crystallisation (2 molecules per trimer) i.e. at 3.67ppm (CH_2O) and 1.64ppm (CH_2).

Turning to $^{13}C\{^1H\}$ NMR spectroscopy, the carbon skeleton of 1,8-diamidonaphthalene is shown below together with the numbering scheme.

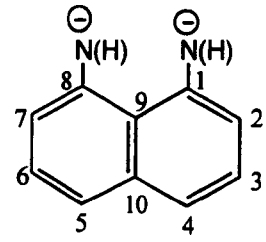

In the parent amine, the *ipso*-carbons (1 and 8) reside at 147.4ppm. These carbons are affected most upon metallation resulting in a large high frequency shift to 162.0ppm. The quaternary carbons (9) and (10) were distinguished by considering resonance forms, whereby the negative charge was found to reside on C (9) but not C (10). Thus C (9) lies at a lower frequency than C (10) i.e. C (10) at 140.4ppm c.f. C (9) at 120.7ppm. The corresponding quaternary carbons on the parent amine were found only slightly upfield by comparison i.e. 138.5ppm and 118.1ppm respectively. Carbons (3) and (6) were found to have similar chemical shifts to those in the parent amine i.e. 127.3ppm in amine c.f. 127.2ppm in compound **2A**. The chemical shifts of carbons (2)/(7) and carbons (4)/(5) were only 9.7ppm apart so could not be unambiguously assigned. The methyl groups from HMPA were easily detected at 36.2ppm. THF of crystallisation was found at 68.3ppm (OCH_2) and 26.3ppm (CH_2).

In compounds **2B-2D**, the absence of broad N-H signals at 5.62ppm and 1.98ppm in [$PhN(H)CH_2CH_2N(H)Ph$] and [$PhCH_2N(H)CH_2CH_2N(H)CH_2Ph$] respectively, indicated metallation had gone to completion. In compound **2B** the *ortho*-Ph were observed to have moved slightly upfield in comparison to that of the parent amine i.e. 6.61ppm in amine c.f. 6.58ppm in **2B**. Similarly, a small low frequency shift was observed for the ethylene protons i.e. 3.23ppm in amine c.f. 3.20ppm in **2B**. In the particular batch of compound **2B** that was prepared for NMR, only directly bound THF of solvation was present, (no THF of crystallisation), as evidenced by the relative integrals of the signals at 3.61ppm and 1.77ppm. The chemical shifts of the amide units in both dimeric **2B** and monomeric **2D** are observed to be only 0.03ppm apart, indicating that the state of aggregation does not significantly affect the chemical environments of these protons (table 2.13).

Compound	*m*-Ph / (ppm)	*o*-Ph / (ppm)	*p*-Ph / (ppm)	CH_2 / (ppm)
2B	7.07	6.58	6.53	3.20
2D	7.04	6.55	6.50	3.17

*Table 2.13- Comparison of amide chemical shifts in compounds **2B** and **2D***

On comparing the ^{1}H NMR spectra of the dimers **2B** and **2C** in d_6-DMSO an interesting correlation can be made. In compound **2C**, the presence of a benzyl $-CH_2$ group causes greater charge localisation on the nitrogen centre (i.e. charge cannot delocalise into the phenyl ring). This increase in negative charge causes greater shielding of the ethylene protons and a corresponding deshielding of the phenyl protons with comparison to **2B** (table 2.14).

Structure	CH_2CH_2 / (ppm)	*o*-/*m*-/*p*-Ph / (ppm)
2B	3.20	7.07 – 6.53
2C	2.57	7.28 – 7.21

*Table 2.14- Comparison of amide chemical shifts in compounds **2B** and **2C***

2.3.2 X-ray Crystallography of Compounds 2A-2D

Our research group has been interested in constructing N-Mg bound cage architectures based on dianionic amide ligands (i.e. derived from organic diamines). Success was first achieved in 1994[4] with the preparation of the first octahedral Mg_6 cage, $[\{o\text{-}C_6H_4(NH)_2\}Mg.THF]_6$ **54** (figure 2.1, pg.37), from the double deprotonation of *o*-phenylenediamine, $[o\text{-}C_6H_4(NH)_2]$ in THF solution. The molecular design of the anion is thought to be the controlling factor in its cage construction. Firstly, a bifunctional anion is involved. Secondly, the ligand backbone is planar. Thirdly, the steric bulk about the metal binding sites $[N(H)^-]$ is kept to a minimum with the presence of small hydrogen atoms. And finally, only two carbon atoms separate the anionic centres. In this present work we explored the possibility of keeping the first three criteria constant but increasing the number of carbon atoms separating the anionic centres by one (to three atoms in total). This prompted the use of 1,8-diaminonaphthalene, $[1,8\text{-}C_{10}H_6(NH_2)_2]$, which consequently led to the formation of $[\{(1,8\text{-}C_{10}H_6(NH)_2)Mg.HMPA\}_3.2THF]$ **2A**.

Determined by X-ray crystallography, the structure of **2A** (figure 2.6, pg.46) is shown to possess an unprecedented N_6Mg_3 cage arrangement. The magnesium atoms are arranged in an almost perfect equilateral Mg_3 triangle (side lengths 2.903Å, 2.913Å, 2.916Å; endocyclic angles, 59.7°, 60.1° and 60.2°) which is encapsulated within, and staggered with respect to, the six N corners of a trigonal prism which makes up the open cage structure (figure 2.11).

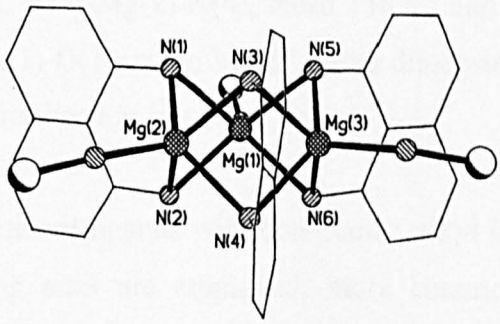

*Figure 2.11- Alternative view of **2A**, highlighting the N_6Mg_3 cage arrangement*

At the time of writing, only two other trimeric amido species are known in the literature, namely, $[MeSi\{(Bu^t)NMgN(SiMe_3)_2\}_3]$[17] **50** which adopts a tricyclic SiN_3Mg_3 skeleton and $[Mg_3(\mu\text{-NH-Dipp})_4\{N(SiMe_3)_2\}_2]$[18] **26** (figure 1.15(b), pg.27), which is composed of three planar $(NMg)_2$ rings fused in a linear arrangement (as opposed to three distorted, four-membered $(NMg)_2$ fused rings present in the core structure of **2A**).

The magnesium centres in **2A** occupy a five-coordinate, distorted square-based pyramidal geometry. The N_4 rectangular base is made up of two short intra-ligand contacts (mean, 2.61Å) and two long inter-ligand contacts (mean, 3.06Å). An apical O atom (from HMPA) takes up the fifth coordination site. This coordination geometry bears a similarity to that in $[\{o\text{-}C_6H_4(NH)_2\}Mg.THF]_6$ **54** ; however a difference can be seen in the bonding mode of the dianion, as each intra ligand N-N unit bridges two Mg centres in **2A** compared with three in **54**. There is also a similarity in the N-Mg bond distances which can be attributed to the coordinative equivalency exhibited in both structures i.e. **2A**, mean N-Mg 2.163Å; **54**, mean N-Mg 2.152Å. Moreover, the O-Mg bond distances in **2A** are found to be significantly shorter than those found in **54** (**2A**, mean O-Mg 1.926Å; **54**, mean O-Mg 2.091Å). This difference is a result of the differing donor strengths exhibited by HMPA and THF (where HMPA is the strongest). Turning to bond angles, there are four distinct categories, which can be identified about the metal centre: (1) where the dianionic ligand chelates in a η^2-fashion, e.g. N(1)-Mg(1)-N(2), mean 74.2°; (2) those made with edges within the trigonal faces of the N_6 prism, e.g. N(1)-Mg(1)-N(5), mean 90.1°; those made with diagonal pairs within rectangular faces of the N_6 prism, e.g. N(1)-Mg(2)-N(4), mean 136.8°; and finally (4) those involving O atoms, e.g. N(1)-Mg(1)-O(1), mean 111.6°. More dimensions are given in tables 2.2 and 2.3 of the experimental section (pg.45).

When bifunctional ligands with non-planar, alkyl bridges and bulky substituents at the metal binding sites are employed, more common dimeric arrangements are favoured, as exemplified by the structure of $[MeMg\{N(Me)CH_2CH_2NMe_2\}]_2$ **45**[19] (figure 2.12).

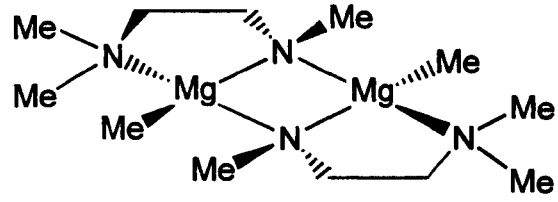

Figure 2.12- Structure of [MeMg{N(Me)CH$_2$CH$_2$NMe$_2$}]$_2$ ***45***

Using this notion, we decided for comparison to synthesise such dimeric architectures using the secondary diamine precursors, N,N'-diphenylethylenediamine and N,N'-dibenzylethylenediamine (figure 2.13). This proved successful.

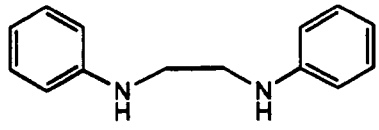

N,N'-diphenylethylenediamine

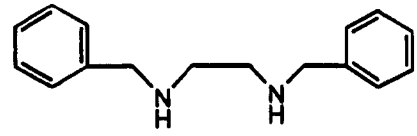

N,N'-dibenzylethylenediamine

Figure 2.13- Structural formulae of N,N'-diphenylethylenediamine and N,N'-dibenzylethylenediamine

Magnesiation and subsequent addition of donor molecules led to the formation of compounds [{MgN(Ph)CH$_2$CH$_2$N(Ph).2THF(1.5THF)}$_2$] **2B**, [{MgN(CH$_2$Ph)CH$_2$CH$_2$N(CH$_2$Ph).HMPA}$_2$] **2C** and [MgN(Ph)CH$_2$CH$_2$N(Ph).2HMPA] **2D**.

The crystal structures of **2B** and **2C** are both centrosymmetric dimers constituting a central planar (NMg)$_2$ cyclic ring. On opposite sides of this ring lies two five-membered $\overline{\text{MgNCCN}}$ chelate rings, lying *trans* to one another. The *trans*-5.4.5-fused ring frameworks shown in both **2B** and **2C** show subtle differences upon close examination: the additional steric interference (i.e. a methylene group) present on the amido substituent in **2C**, causes the flap at the C(2) apex to position *endo* (figure

2.14(b)) with respect to the central ring; whereas in **2B** the flap at the C(2) apex is positioned in an *exo* conformation (figure 2.14(a)).

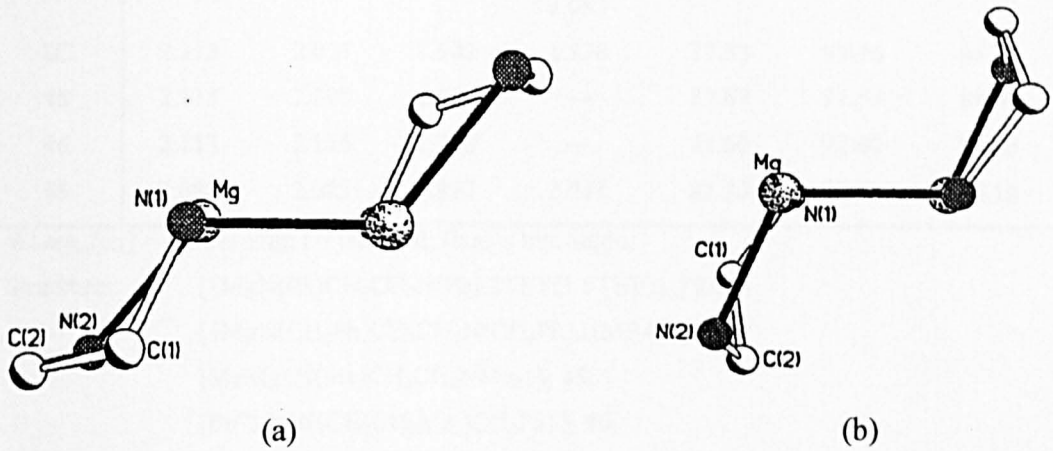

*Figure 2.14- Trans-5.4.5-fused ring systems of **2B** and **2C** showing (a) exo and (b) endo orientation of C(2) atom respectively*

A more obvious difference between the structures is that the magnesium centres in **2B** are five-coordinate, arranged in a distorted trigonal bipyramidal geometry [axial atoms N(1) and O(2)], whereas in **2C** a four-coordinate, distorted tetrahedral geometry is preferred. The higher coordination number experienced by the magnesium atoms in **2B** can be explained as a result of decreased steric bulk about the anionic N centre, which in turn allows coordination by two THF solvent molecules. Hitherto, **2B** is the only literature example of a crystallised, dimeric, five-coordinate magnesium amide. It has been shown previously that other 5.4.5-fused ring systems e.g. $[MeMg\{N(Me)CH_2CH_2NMe_2\}]_2$ **45**[19] and $[Bu^nMg\{N(CH_2CH_2Me_2)CH_2Ph\}]_2$ **46**[20] have a steric preference for four-coordinate magnesium geometries. The structure of **46** bears some similarity to **2C** as the presence of the benzyl moiety causes a similar *endo* conformation of the C(2) apex. Individual bond lengths and angles for structures **2B** and **2C** are presented in the experimental section (tables 2.4-2.7, pg.48 and 51). In table 2.15 the structural parameters of **2B** and **2C** are compared with those of other 5.4.5-fused ring systems.

Structure	N—Mg (c.r) / (Å)	N'—Mg (c.r) / (Å)	N—Mg (t) / (Å)	O—Mg donor / (Å)	N-Mg-N (b.a) / (°)	N-Mg-N' (c.r) / (°)	Mg-N-Mg (c.r) / (°)
2B	2.290	2.099	2.040	2.167 2.083	84.22	87.64	92.36
2C	2.113	2.077	1.982	1.938	87.83	93.76	86.24
45	2.113	2.100	2.186	—	83.67	91.54	88.46
46	2.113	2.116	2.200	—	84.60	92.40	87.60
55	2.082	2.085	1.997	2.041	87.80	93.90	86.10

Where, (c.r) = central ring; t = terminal; (b.a) = bite angle.

Structures: $[\{MgN(Ph)CH_2CH_2N(Ph).2THF(1.5THF)\}_2]$ **2B**,
$[\{MgN(CH_2Ph)CH_2CH_2N(CH_2Ph).HMPA\}_2]$ **2C**,
$[MeMg\{N(Me)CH_2CH_2NMe_2\}]_2$ **45**,
$[Bu^nMg\{N(CH_2CH_2Me_2)CH_2Ph\}]_2$ **46**,
$[Mg\{\mu\text{-}N(SiMe_3)C_6H_4N(SiMe_3)\text{-}o\}(OEt_2)]_2$ **55**.

Table 2.15- Comparison of selected bond distances (Å) and angles (°) in various 5.4.5-fused ring systems

From the comparative data, similarities are observed: the non-equivalent N-Mg distances within the central $(NMg)_2$ rings show little variation throughout the series [range 2.077-2.290Å]; the bite angles of the diamine ligands [N(1)MgN(2)] span a narrow range [84.22-87.83°]. The five-coordinate dimer **2B**, is the only structure in the series that displays wider endocyclic bond angles at N [92.36° c.f. 87.64° at Mg] located within the central $(NMg)_2$ ring. In keeping with the unsymmetrical character of its $(NMg)_2$ cyclic core, the two O-Mg (THF) distances are of different length i.e. the equatorial O(1) is 0.084Å shorter than the axial one involving O(2). As expected the stronger oxygen donor HMPA present in **2C** forms the shortest O-Mg bond [1.983Å] in the dimer series.

Although structure **2D** possesses both the same dianion and degree of solvation as **2B**, the employment of the stronger donor, HMPA, in the former causes deaggregation to a monomeric four-coordinate species, which crystallises as two independent monomers of nearly identical molecular structure in the unit cell (only one

monomer is shown in figure 2.9, pg.55). In comparison with **2B**, the metal-diamide bond distances are shorter [mean 2.023Å] and more symmetrical in the monomer. The bite angle is also wider in **2D** [mean 87.02°]. There exists a twist in the $NC(H)_2C(H)_2N$ bridge [e.g. N—C—C—N torsion angles 46.1° and 44.5° in both monomers] so as to prevent eclipsing of the methylene units; this in turn forces the attached phenyl rings out of co-planarity [dihedral angles 36.9° and 35.8°]. Two HMPA ligands complete the distorted tetrahedral geometry with almost identical O-Mg bond lengths [i.e. for one monomer O(1)-Mg(1) 1.960Å, O(2)-Mg(1) 1.944Å]. Both HMPA molecules are separated by a mean O-Mg-O angle of 100.12°, the N-Mg-O angle by comparison is larger at 117.75°. A recent example of a four-coordinate bis-HMPA solvated monomer is that of $[Mg\{N(H)Mes\}_2.2HMPA]$[18] **38** (where Mes = 2,4,6-$Me_3C_6H_2$-): its O-Mg bond distances [mean 1.973 Å] and O-Mg-O bond angles [mean 102.9°] were found to be within good agreement with those found in **2D**

Monomeric magnesium amide complexes have been shown to adopt a variety of coordination numbers depending on both the nature of the amide ligand and degree of solvation. By far the most common is a coordination number of four where the magnesium lies in a distorted tetrahedral environment. Structure **2D** represents one such compound but is a rare example of a monomeric magnesium amide derived from a dianion.

For completeness it should be mentioned that dilithiation of N,N'-diphenylethylenediamine has been carried out by Snaith *et al.* The product crystallises as the monomeric, dinuclear sesqui-HMPA solvate, $[PhLiNCH_2CH_2NLiPh.3HMPA]$[21] **63** (figure 2.15). Its salient feature is an N_2Li_2 double bridge, which bears similarity to the C_2Li_2 "ion-triplet" structures encountered in many dilithiated hydrocarbons[(22-25)]. The N-Li distances within the N_2Li_2 'butterfly' shaped ring are asymmetric due to twisting of the $NC(H)_2C(H)_2N$ bridge [N(1)-Li(1), 2.055(8)Å; N(2)-Li(1), 2.137(7)Å; N(1)-Li(2), 2.146(9)Å; N(2)-Li(2), 2.088(8)Å]. Two HMPA ligands are attached terminally to the lithium atoms [O(2)-Li(1), 1.888(6)Å; O(3)-Li(2), 1.868(7)Å]. The third HMPA ligand

on the otherhand bridges both lithium centres forming three co-fused "butterfly" frameworks [asymmetric O-Li distances O(1)-Li(1), 2.068(8)Å; O(1)-Li(2), 1.994(7)Å]. In this diamide system, there can be no equivalent magnesium structure on account of the formal 2+ charge on the alkaline-earth metal cation; hence **2D** adopts a simpler single ion-pair arrangement.

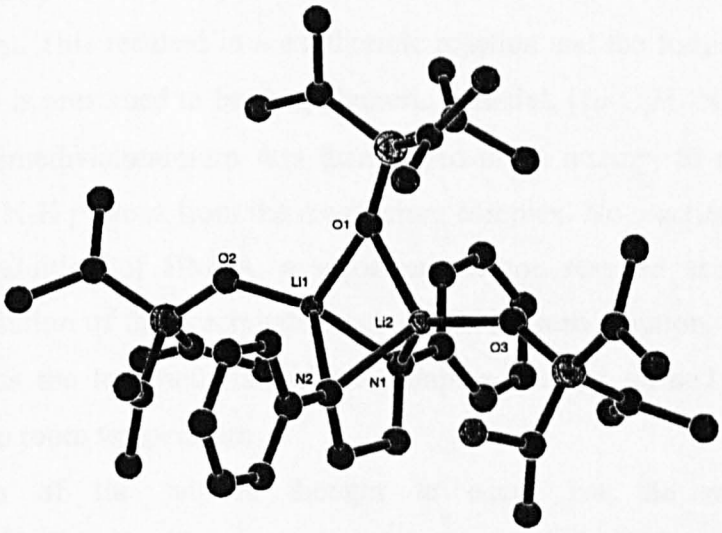

Figure 2.15- Crystal structure of [PhLiNCH$_2$CH$_2$NLiPh.3HMPA] ***63****, (hydrogen atoms are omitted for clarity)*

2.3.3 Synthesis and Analysis of Compound 2E

The aim of reaction 2.5 was to prepare a mixed magnesium / aluminium analogue of the aforementioned cage complex $[\{o\text{-}C_6H_4(NH)_2\}Mg.THF]_6$ **54**. Instead of the desired product, the formation of the magnesium tetramethylaluminate complex, $[Mg(HMPA)_4.2AlMe_4]$ **2E**, resulted.

To a solution of o-phenylenediamine in THF was added one equivalent of dibutylmagnesium. This resulted in a exothermic reaction and the formation of a white precipitate which is presumed to be the polymeric material, $[\{o\text{-}C_6H_4(NH)_2\}Mg]_\infty$. Two equivalents of trimethylaluminium was then added in an attempt to remove the two remaining acidic N-H protons from the magnesium complex. No reaction was observed. However upon addition of HMPA, a vigorous reaction resulted accompanied with subsequent dissolution of the precipitate to give a dark green solution. Crystals, which were identified as the tetramethylaluminate complex, readily formed on leaving the solution to cool to room temperature.

Formation of the salt is thought to occur via the reactive species $[AlMe_2.2HMPA]^+[AlMe_4]^-$ which is produced by asymmetric HMPA cleavage of the Al_2Me_6 dimer (scheme 2.5).

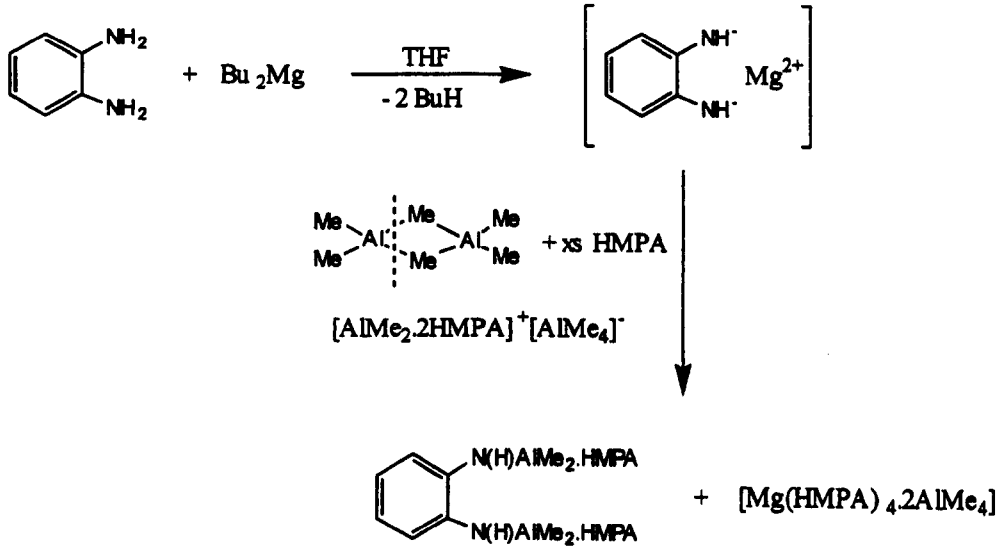

Scheme 2.5- Possible route to the formation of 2E

Following isolation of the crystals, the filtrate was kept in an attempt to identify the amido-species in solution. Unfortunately, upon removal of solvent, the green oil turned black. The ^{1}H NMR spectrum carried out on this oil proved to be uninformative due to poor quality of resolution (very noisy base-line).

Compound **2E** gave satisfactory elemental analyses. Analysis by infrared spectroscopy showed that on exposure to air, **2E** readily hydrolysed to give a broad band in the region 3100-3700cm^{-1} indicating the presence of [$Mg(OH)_2$, $Al(OH)_3$ and H_2O].

The information in both the ^{1}H and $^{13}C\{H\}$ NMR spectra, recorded in d_5-pyr, were found to be consistent with the formula found in the crystal structure. No signals were observed in the aromatic region. Coupling of the appropriate nuclei to the ^{27}Al nucleus was observed, resulting in the formation of a sextet splitting pattern [$^{2}J_{H\text{-}Al}$ = 6.4 Hz and $J_{C\text{-}Al}$ = 70.8 Hz respectively].

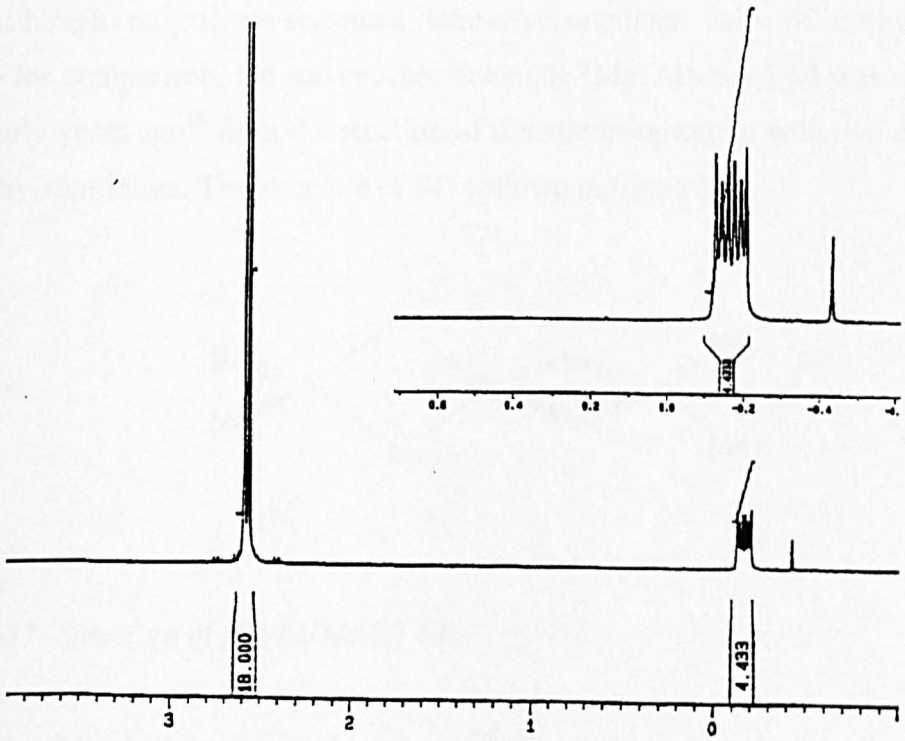

Figure 2.16- ^{1}H NMR spectrum of [Mg(HMPA)$_4$.2AlMe$_4$] 2E, in d_5-pyr at 300K

2.3.4 X-ray Crystallography of Compound 2E

The crystal structure of compound **2E** represents a solvent-separated ion pair (S.S.I.P) with one divalent cation [$\{Mg(HMPA)_4\}^{2+}$] and two [$AlMe_4^-$] anions. This compound is believed to be the first crystallographically characterised magnesium (S.S.I.P) tetramethylaluminate salt.

The magnesium centre is surrounded by four HMPA ligands, which occupy a distorted tetrahedral environment. Both the O-Mg bond distances and O-Mg-O bond angles lie within short ranges [O-Mg, 1.885(3)-1.903(2)Å; O-Mg-O, 107.7(12)°-112.1(13)°]. Similarly, short ranges are observed for the bond distances and angles within both distorted tetrahedral anions [**1**: C-Al, 2.010(4)-2.014(5)Å; C-Al-C, 106.9°-111.7(2)°; **2**: C-Al, 1.999(5)-2.013(4)Å; C-Al-C, 107.5(2)°-112.0(2)°].

Although no solvent-separated tetra-alkylaluminate salts of magnesium are available for comparison, the solvent-free analogue [$Mg\{AlMe_4\}_2$] **64** was crystallised nearly thirty years ago[26] from the reaction of dimethylmagnesium with two equivalents of trimethylaluminium. The structure of **64** is shown in figure 2.17.

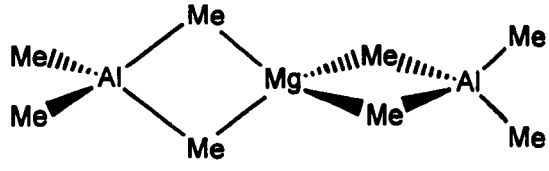

*Figure 2.17- Structure of [$Mg\{AlMe_4\}_2$] **64***

The comparable electropositive character of both magnesium and aluminium gives an essentially covalent structure with electron-deficient, three-centre two electron bonds. This electron-deficient character is noticeable in the structure itself with an average

metal-carbon-metal bridge angle of 77.7° and a metal-metal approach of 2.70Å which are similar to those parameters found in trimethylaluminium [Al-C-Al, 74.7°; Al···Al, 2.60 Å].

Recently, Fiona Craig[27] of our laboratory crystallised a series of solvent-separated and partially solvent-separated tetramethylaluminate salts involving the group 1 metals sodium and potassium. These are shown in table 2.16 along with dimensions of the $AlMe_4^-$ anion involved.

Structure	Compound Number	Mean C-Al Bond Distance (Å)	Range C-Al-C Bond Angles (°)
$[\{Na(TMEDA)_2\}\{AlMe_4\}]$	**(65)**	2.000	107.2-112.3
$[\{K(PMDETA)_2\}\{AlMe_4\}]$	**(66)**	2.000	106.3-111.9
$[\{K(TMEDA)_2\}\{AlMe_4\}]$	**(67)**	1.997	107.2-114.9
$[\{K(18\text{-crown-}6)\}\{AlMe_4\}]$	**(68)**	2.018	107.8-111.2

Table 2.16- Important parameters for $AlMe_4$ anion in selected tetramethyl aluminate salts

Structures **65** and **66** are solvent-separated ion pairs, where the chelating donor ligands, TMEDA and PMDETA surround the metal cation respectively. The sodium cation in **65** is bound to two TMEDA ligands resulting in a four-coordinate, distorted square-planar geometry. In contrast, the larger potassium cation in **66** is encapsulated by two tridentate PMDETA ligands which form an irregular N_6 coordination polyhedron. The structures of **67** and **68** represent partially solvent separated ion pairs. The potassium cations in both cases are coordinatively unsaturated; thus the $AlMe_4^-$ anions act as bridging ligands resulting in the formation of polymeric chains [K···Me-Al; **67**, 3.377(3)Å, **68**, 3.181(2)Å].

2.4 Chapter Two Conclusions

Magnesiation of the bicyclic primary diamine, 1,8-diaminonaphthalene, has led to the formation of the unprecedented, trimeric, magnesium amide cage assembly, $[\{(1,8\text{-}C_{10}H_6(NH))\}Mg.HMPA\}_3.2THF]$ **2A** which consists of a central Mg_3 triangle encapsulated by an N_6 trigonal prism. Corresponding magnesiation of the alkyl bridged secondary diamines, N, N'-diphenylethylenediamine and N, N'-dibenzylethylenediamine has led to the formation of the more conventional dimeric, 5.4.5-fused ring structures $[\{MgN(Ph)CH_2CH_2N(Ph).2THF(1.5THF)\}_2]$ **2B** and $[\{MgN(CH_2Ph)CH_2CH_2N(CH_2Ph).HMPA\}_2]$ **2C**. Additionally the monomeric complex $[\{MgN(Ph)CH_2CH_2N(Ph)\}.2HMPA]$ **2D** has been prepared whereby the central magnesium adopts a four-coordinate, distorted tetrahedral geometry.

In a study examining reactions of the magnesium dianionic cage compound $[\{o\text{-}C_6H_4(NH)_2\}Mg.THF]_6$ with trimethylaluminium in the presence of HMPA, the first solvent separated, magnesium tetramethyl aluminate salt $[Mg(HMPA)_4.\ 2AlMe_4]$ **2E** has been prepared.

2.5 Chapter Two Further Work

The reactivity of the magnesium cage complex, [{(1,8-$C_{10}H_6(NH)_2$)Mg.HMPA}$_3$.2THF] **2A** requires investigation e.g. can the remaining N-H protons be removed using a strong base such as *t*-BuLi, *n*-BuNa, *n*-BuK or a mixed RLi / *t*-BuOK superbase to form a mixed metal imide species. Magnesiation studies on 1,2- and 2,3- diaminonaphthalenes (shown below) should be carried out to see whether other analogous magnesium cage complexes can be formed (amide or imide).

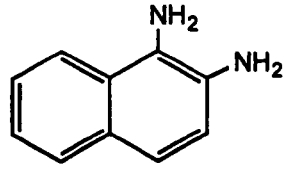

1,2-diaminonaphthalene

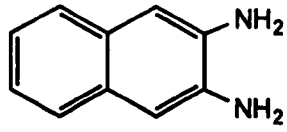

2,3-diaminonaphthalene

Research should also be carried out on bulky primary amine systems (e.g. $DippNH_2$) to ascertain whether other imide complexes can be formed.

Investigations on the preparation of the magnesium tetramethylaluminate salt [$Mg(HMPA)_4.2AlMe_4$] **2E** are required to see if amide function from [{*o*-$C_6H_4(NH)_2$.Mg}$_\infty$] is required for its formation. Reaction should thus be repeated using pre-formed [$Mg(AlMe_4)_2$] **64** and reacting with HMPA. Additionally, it would be interesting to carry out the synthesis of **2E** in the presence of a crown-ether ligand rather than HMPA to see whether a polymeric species involving bridging $AlMe_4$ groups would be produced.

2.6 Chapter Two References

[1] For Reviews: (a) E. Weiss; *Angew. Chem. Int. Ed. Engl.*, (1993), **32**, 1501;
(b) W. N. Setzer and P. v. R. Schleyer; *Adv. Organomet. Chem.*, (1985), **24**, 353.

[2] M. A. G. M. Tinga, O. S. Akkerman, F. Bickelhaupt, E. Horn and A. L. Spek; *J. Am. Chem. Soc.*, (1991), **113**, 3604.

[3] M. A. G. M. Tinga, G. Schat, O. S. Akkerman, F. Bickelhaupt, E. Horn, H,. Kooijmann, W. J. J. Smeets and A. L. Spek; *J. Am. Chem. Soc.*, (1993), **115**, 2808.

[4] W. Clegg, M. Frank, R. E. Mulvey and P. A. O'Neil; *J. Chem. Soc., Chem. Commun.*, (1994), 97.

[5] A. Duff, P. Hitchcock, M. F. Lappert, R. G. Taylor and J. A. Segal; *J. Organomet. Chem.*, (1985), **293**, 271.

[6] M. Veith, W. Frank, F. Tollner and H. Lange; *J. Organomet. Chem.*, (1987), **326**, 315.

[7] M. Veith; *Adv. Organomet. Chem.*, (1990), **31**, 269.

[8] M. Veith, F. Goffing and V. Huch; *Z. Naturforsch.*, (1988), **43b**, 846.

[9] E. C. Ashby and F. G. Willard; *J. Org. Chem.*, (1978), **43**, 4750.

[10] T. Hascall, M. M. Olmstead and P. P. Power; *Angew. Chem. Int. Ed. Engl.*, (1994), **33**, 1000.

[11] T. Hascall, K. R-Senge and P. P. Power; *Angew. Chem. Int. Ed. Engl.*, (1994), **33**, 356.

[12] L. Meunier; *Compt. Rend.*, (1903), **136C**, 758.

[13] W. J. Grigsby, T. Hascall, J. J. Ellison, M. M. Olmstead and P. P. Power; *Inorg. Chem.*, (1996), **35**, 3254.

[14] G. Del. Piero, M. Cesari, S. Cucinella and A. Mazzei; *J. Organomet. Chem.*, (1977), **137**, 265.

[15] G. Del. Piero, M. Cesari, G. Dozzi and A. Mazzei; *J. Organomet. Chem.*, (1977), **129**, 281.

[16] G. Dozzi, G. Del. Piero, M. Cesari and S. Cucinella; *J. Organomet. Chem.*, (1980), **190**, 229.

[17] M. Veith, A. Spaniol, J. Pöhlmann, F. Gross and V. Huch; *Chem. Ber.*, (1993), **126**, 2625.

[18] M. M. Olmstead, W. J. Grigsby, D. R. Chacon, T. Hascall and P. P. Power; *Inorganica. Chimica. Acta.*, (1996), **251**, 273.

[19] V. R. Magnuson and G. D. Stucky; *Inorg. Chem.*, (1969), **8**, 1427.

[20] K. W. Henderson, R. E. Mulvey, W. Clegg and P. A. O'Neil., *J. Organomet. Chem.*, (1992), **439**, 237.

[21] D. R. Armstrong, D. Barr, A. T. Brooker, W. Clegg, K. Gregory, S. M. Hodgson, R. Snaith and D. S. Wright; *Angew. Chem. Int. Ed. Engl.*, (1990), **29**, 410.

[22] (a) E. D. Jemmis, J. Chandrasekhar and P. v. R. Schleyer; *J. Am. Chem. Soc.*, (1979), **101**, 2848;
(b) P. v. R. Schleyer and A. J. Kos; *J. Chem. Soc., Chem. Commun.*, (1982), 448.

[23] U. Schubert, W. Neugebauer and P. v. R. Schleyer; *J. Chem. Soc., Chem. Commun.*, (1982), 1184.

[24] P. v. R. Schleyer, *Pure. Appl. Chem.*, (1983), **55**, 355; (1984), **56**, 151. And references therein.

[25] A. Streitwieser; *Acc. Chem. Res.*, (1984), **17**, 353. And references therein.

[26] J. L. Atwood and G. D. Stucky; *J. Am. Chem. Soc.*, (1969), 2538.

[27] (a) F. J. Craig, Ph.D. Thesis, University of Strathclyde, (UK), 1997;

(b) F. J. Craig, A. R. Kennedy, R. E. Mulvey and M. D. Spicer; *J. Chem. Soc., Chem. Commun.*, (1996), 1951.

Chapter Three

Chapter Three (Part 1) – Structural Chemistry of Mixed Lithium/Magnesium Complexes

Aims

- To give a brief review of all known mixed lithium / magnesium complexes presently available in the literature.
- To discuss the synthesis, analysis and characterisation of several new, mixed lithium / magnesium complexes, including the unprecedented, oxo-centred, N-silylated benzamidinate, $[\{PhC(NSiMe_3)_2\}_4Li_4MgO]$.

3.1 Introduction

The beginning of mixed s-block chemistry can be traced back almost 50 years when Wittig[1] reported the synthesis of "diphenyllithium sodium". This somewhat ill-defined compound was found to be a better nucleophilic reagent than normal phenyllithium in the reaction with benzophenone. This observation demonstrated for the first time that intermetallic (mixed-metal) systems display differing chemical behaviour in comparison to their single-metal counterparts. In 1967, Schlosser[2] recognised that other mixed s-block compounds namely alkyllithium / heavier alkali metal (sodium or potassium) alkoxide combinations, so called "superbases", were reagents of excellent deprotonating ability. In one such study[3], the metallation of isopropylbenzene was investigated, with a superbasic mixture of *n*-butyllithium and potassium *t*-butoxide, (*n*-BuLi / *t*-BuOK), in various solvent media (figure 3.1). Metallation was found to preferentially occur on the aromatic ring (*meta* and *para* positions) rather than on the more acidic benzylic group.

In a recent review by Lochmann[4], several possible mechanisms for superbasic behaviour are discussed. One hypothesis suggests that the potassium alkoxide and alkyllithium reagent form a mixed aggregate (A), i.e. before complete transmetallation

to the organopotassium and lithium alkoxide reagent, this intermediate then reacts with the organic substrate via a multicentred transition state (B) (figure 3.2).

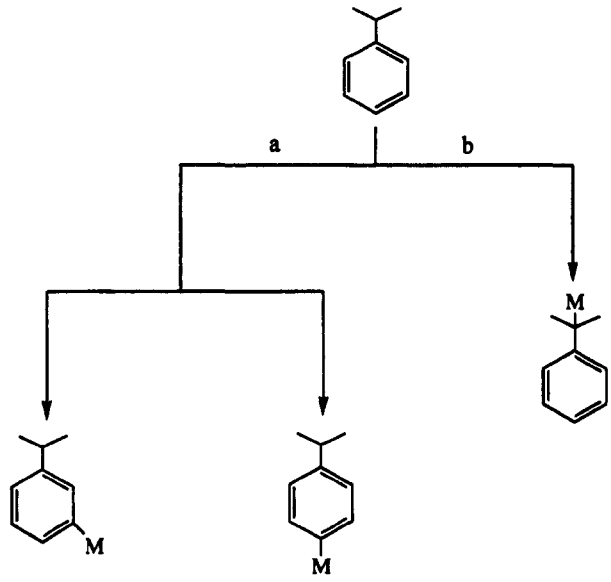

	a : b	*meta* : *para*
Bu^nLi / Bu^tOK	95 : 5	65 : 35

Figure 3.1- Metallation of isopropylbenzene using a superbasic mixture of n-BuLi / t-BuOK in THF

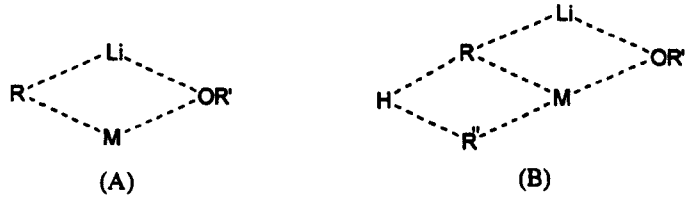

Figure 3.2- Pictorial representation of possible intermediates involved in superbases

It can be thus appreciated that the 'superbase', exhibits differing chemical reactivity in comparison to the organopotassium and organolithium reagents on there

own. As a consequence they offer major practical advantages. This synergistic effect offered by the incorporation of two alkali metals in close proximity clearly activates the superbase; however, the true nature of this reactivity remains poorly understood.

As well as superbases, organometallates, commonly known as '*ate*' complexes[5] are finding increasing use in modern synthetic chemistry[6]. Such compounds are prepared simply by mixing stoichiometric amounts of their constituent components and were initially considered as "double compounds" e.g. $NaEt.ZnEt_2$ **69**[7]. However it is only with the aid of X-ray crystallography that the true nature of these compounds is coming to light. Typically these compounds can be partitioned, although sometimes only formally, into a complex organometallate ion, and a counterion[8]. Solvation of this counterion is often observed, and in the case of sterically demanding donor ligands, solvent-separated ion-pairs are generally formed. Numerous classes of 'ate' complexes have been reported[9] and include; cuprates, e.g. $[\{Li(Et_2O)\}(CuPh_2)]_2$ **70**[10], lithates, e.g. $[Na(TMEDA)]_3[LiPh_4]$ **71**[11] and borates, e.g. $[Li(BMe_4)]_4$ **72**[10].

The research detailed in this chapter concerns the synthesis and characterisation of compounds containing a mixture of lithium and magnesium, and therefore can be termed lithium magnesates. One method of preparing these complexes (equation 3.1) is by simply mixing a diorganomagnesium reagent with an organolithium reagent, usually in the presence of a donor solvent.

$$\text{'RLi'} + \text{'}R_2Mg\text{'} \longrightarrow \text{'}[Li^+(MgR_3)^-]\text{'} \qquad \textbf{(3.1)}$$

A search of the Cambridge Crystallographic Database[12] revealed only thirteen structurally characterised mixed lithium / magnesium complexes. These can be divided into several distinct categories, depending on the R group, as shown in table 3.1.

Li-C-Mg Bonds	Compound Number	Ratio Li : Mg	Ref.
$[Li(TMEDA)]_2[MgMe_4]$	**(73)**	2 : 1	13
$[Li(TMEDA)]_2[Ph_2MgPh_2MgPh_2]$	**(74)**	2 : 2	14
$[Li(TMEDA)_2][(TMEDA)LiBzl_2MgBzl_2]$	**(75)**	2 : 1	15
$[Li(THF)_{0.6}(Et_2O)_{0.4}][Mg(2,4,6\text{-}i\text{-}Pr_3C_6H_2)_3]$	**(76)**	1 : 1	16
$[Li_2\{(PhC{\equiv}C)_3Mg(TMEDA)\}_2]$	**(77)**	2 : 2	15
Li-N-Mg Bonds	**Compound Number**	**Ratio Li : Mg**	**Ref.**
$[Li_2Mg\{N(CH_2CH_2NMe_2)CH_2Ph\}_4]$	**(78)**	2 : 1	17
$[Li_2Mg\{N(Bzl)_2\}_4]$	**(79)**	2 : 1	18
$[LiMg\{N(Bzl)_2\}_3.py]$	**(80)**	1 : 1	18
Li-O-Mg Bonds	**Compound Number**	**Ratio Li : Mg**	**Ref.**
$[LiMg_4O\{o\text{-}Me(C_6H_4)O\}_7.4THF]$	**(81)**	1 : 4	19
$[Li(TMEDA)]_2[Mg\{o\text{-}Me(C_6H_4)O\}_4]$	**(82)**	2 : 1	19
$[Li(py)_2]_2\text{-}\mu\text{-}Mg[\{Ph_2SiO\}_2O][\{Ph_2SiO\}_3O]$	**(83)**	2 : 1	20
Li-Hal-Mg Bonds	**Compound Number**	**Ratio Li : Mg**	**Ref.**
$[Li(THF)_2(\mu\text{-}Br)_2Mg\{C(SiMe_3)_3\}.THF]$	**(84)**	1 : 1	21
$[Mg_2Cl_3.THF_6][Li\{nido\text{-}[2,3\text{-}(SiMe_3)_2C_2B_4H_4]\}][ZrCH_2SiMe_3(Cl)]$	**(85)**	1 : 2	22

Where Hal = halogen

Table 3.1- X-ray characterised mixed lithium/magnesium compounds

Highlights from the table will now be discussed in detail.

3.1.1 Lithium Organomagnesates

Lithium organomagnesates possess a variety of interesting structures, where the magnesium centre(s) can attain various coordination numbers (in the range, 3-5). The state of aggregation in such complexes is not only dependent on the donor solvent but also on the steric bulk of the R groups involved. This can be seen in scheme 3.1.

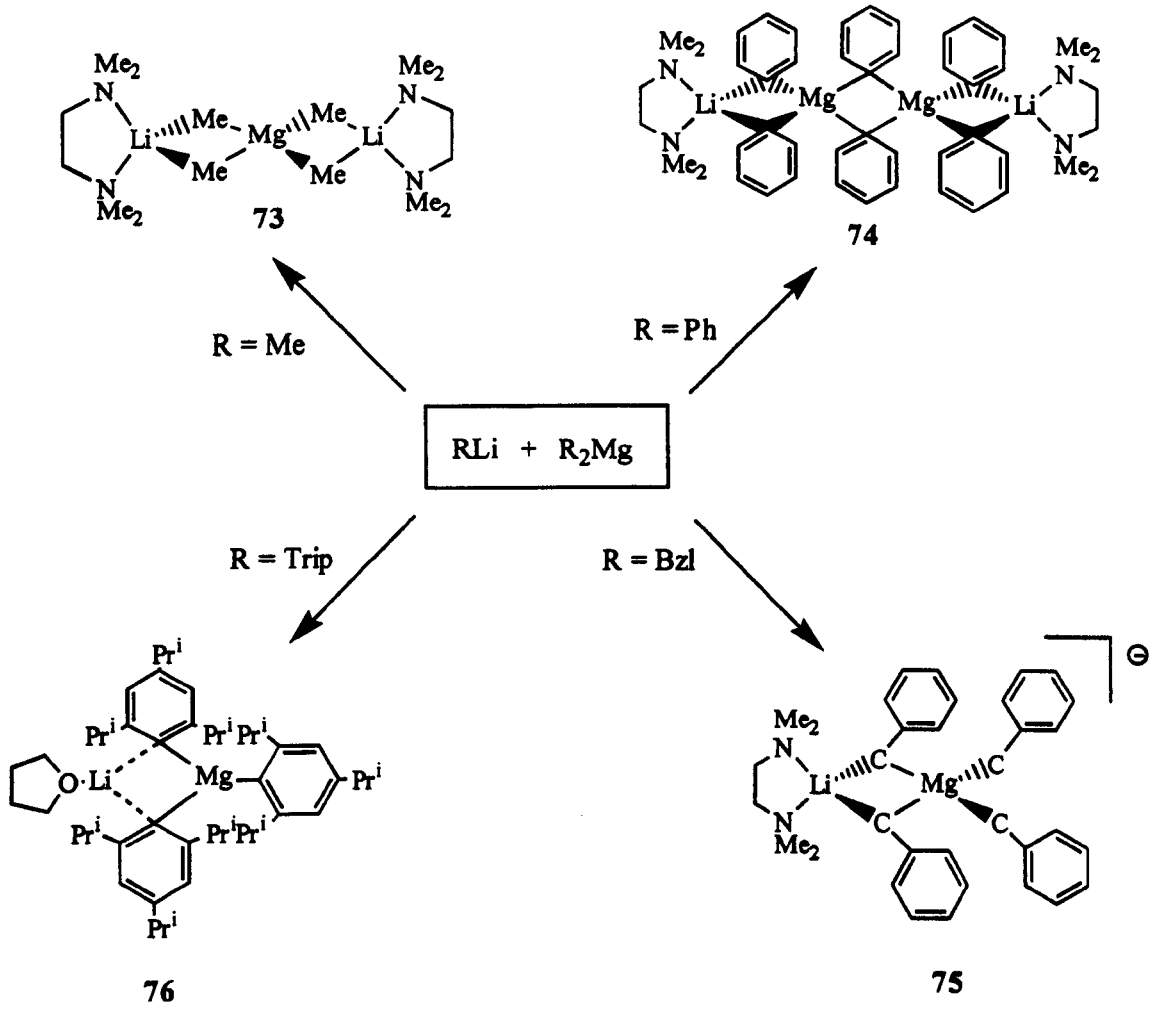

Scheme 3.1- Various lithium organomagnesates

When small or flat R groups is involved, fused ring oligomers form e.g., as in $[Li(TMEDA)]_2[MgMe_4]$[13] **73** and $[Li(TMEDA)]_2[Ph_2MgPh_2MgPh_2]$[14] **74**. In both these structures lithium and magnesium are four-coordinate adopting distorted tetrahedral environments. However the ratio of these metals are different i.e. 2Li:1Mg in **73** but 2Li:2Mg in **74**. As a consequence of this, the central magnesate units attain different structural features. In **73** the central core consists of a tetrahedral tetramethylmagnesate unit whereas in **74** there is a central $(CMg)_2$ ring made up of asymmetrical C-Mg bonds [2.29Å and 2.33Å]. The lithium centres in both cases are solvated by the didentate donor TMEDA.

With bulkier R groups, smaller, charge separated, aggregates are favoured e.g. $[Li(TMEDA)_2][(TMEDA)LiBzl_2MgBzl_2]$[15] **75** and $[Li(THF)_{0.6}(Et_2O)_{0.4}][Mg(2,4,6\text{-i-}Pr_3C_6H_2)_3]$[16] **76**. The structure of **75** is that of a solvent separated ion pair (S.S.I.P) arrangement. The anion consists of a MgCLiC ring where magnesium is bound to two bridging and two terminal benzyl groups, resulting in a four-coordinate distorted tetrahedral geometry [C_{br}-Mg, 2.32Å and 2.31Å; C_t,-Mg, 2.22Å and 2.26Å] . The lithium that belongs to the lithium moiety also attains four-coordination by ligation of a TMEDA molecule. Two TMEDA molecules surround the lithium cation. On the otherhand complex **76** is a contact ion pair (C.I.P) structure between $[Mg(2,4,6\text{-i-}Pr_3C_6H_2]^-$ and $[Li(THF)_{0.6}(Et_2O)_{0.4}]^+$. Due to the size of the substituted phenyl ring, magnesium attains only a three-coordinate geometry, angles at which display considerable distortion from ideal trigonal values (i.e. 105.0°, 121.8° and 133.2°). The C-Mg bridging bonds are considerably longer than that found for the terminal C-Mg bond i.e. [mean C_{br}-Mg, 2.23Å c.f. C_t-Mg, 2.15Å]. The lithium also adopts a three-coordinate geometry bound to two bridging (2,4,6-i-$Pr_3C_6H_2$) functions and a terminal monodentate donor molecule, either THF or Et_2O.

3.1.2 Lithium Amidomagnesates

At present, only three crystal structures of this type can be found in the literature namely, $[Li_2Mg\{N(CH_2CH_2NMe_2)CH_2Ph\}_4]$[17] **78**, $[Li_2Mg\{N(Bzl)_2\}_4]$[18] **79** and $[LiMg\{N(Bzl)_2\}_3.py]$[18] **80** (figure 3.3).

Both **78** and **79** consist of two fused heterometallic $\overline{MgNLiN}$ rings bound through a single four-coordinate, distorted tetrahedral magnesium centre [mean N-Mg-N: **78**, 111.2°, **79**, 109.7°] resulting in a lithium to magnesium ratio of 2:1. The presence of intramolecular donor (NMe_2) side arms in structure **78** allows the lithium cations to attain a four-coordinate distorted tetrahedral geometry [mean N-Li-N 109.4°]. However, in structure **79** the lithium cations are unsolvated, and therefore have a two-coordinate environment [mean N-Li-N 103.0°]. As a consequence of this relatively low coordination state the lithium draws the amido anions towards itself, thus relieving steric congestion at magnesium, hence shorter N-Li bond distances [mean 1.99Å] in comparison to the N-Mg bond distances [mean 2.10Å]. On the otherhand **78** possesses similar metal-amido bond distances but longer contacts are observed between lithium and the tertiary amine group i.e. [N-Mg, 2.09Å, N_{br}-Li, 2.09Å, N_t-Li, 2.13Å].

On preparing **79** in the presence of pyridine, solvation at lithium occurs producing the dimeric 1:1 complex, $[LiMg\{N(Bzl)_2\}_3.py]$ **80**. The subsequent increase in coordination number of the lithium centre (from two to three) lessens its pull on the bridging amido anions, resulting in longer N-Li bonds and shorter N-Mg bond distances [N-Li 2.04Å, N_{br}-Mg 2.05Å] with comparison to the unsolvated analogue. Alternatively, the increased steric bulk at lithium pushes the amide ligands closer to magnesium. This increased 'congestion' about the magnesium centre results in the lower coordination number of three arranged within a distorted trigonal planar geometry [N-Mg-N 99.4°, 138.1° and 122.35°].

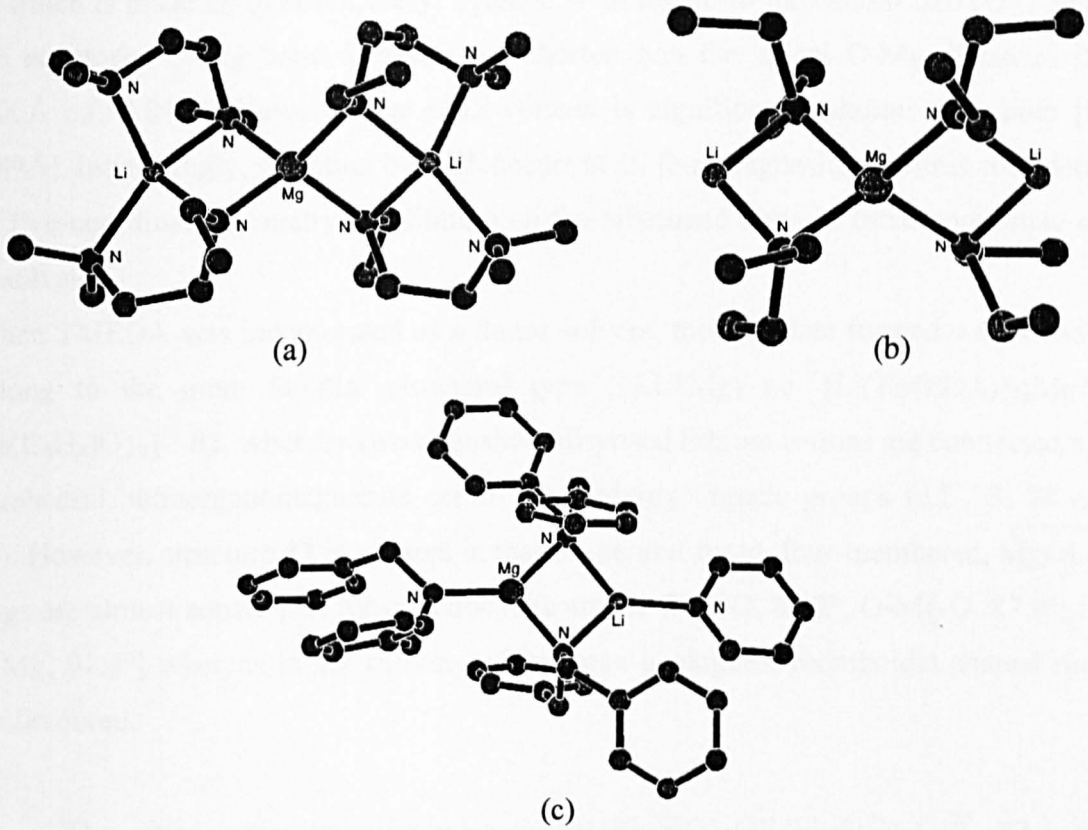

*Figure 3.3- Crystal structures of (a) $[Li_2Mg\{N(CH_2CH_2NMe_2)CH_2Ph\}_4]$ **78**, (b) $[Li_2Mg\{N(Bzl)_2\}_4]$ **79** and (c) $[LiMg\{N(Bzl)_2\}_3.py]$ **80**, (in **78** and **79** the phenyl rings are omitted for clarity)*

3.1.3 Lithium Oxomagnesates

Lithium magnesates derived from oxo anions are a relatively new addition to this series. The three reported crystal structures appeared in 1994.

Two of these structures were derived from the aryl oxide, *o*-cresol, [*o*-$CH_3C_6H_4OH$] in different donor solvents (figure 3.4). When THF was employed, the remarkable cage complex, $[LiMg_4O\{o\text{-}Me(C_6H_4)O\}_7.4THF]$[19] **81** resulted, which remains without precedent in composition, stoichiometry (1Li:4Mg) and structure when compared in general to other lithium magnesates. The principal feature of the molecular structure of **81** is a oxo-centred, distorted trigonal bipyramidal $LiMg_4$ core, the periphery

of which is made up of seven cresyl ligands. With regard to the central oxo (O^{2-}) anion, the equatorial O-Mg bond distances are shorter than the apical O-Mg distances [i.e. 2.00Å c.f. 2.04Å]. However, the O-Li contact is significantly shorter than both [i.e. 1.89Å]. Interestingly, solvation by THF occurs at all four magnesium centres completing its five-coordinate geometry, the lithium on the otherhand remains three-coordinate and unsolvated.

When TMEDA was incorporated as a donor solvent, the cresylate formed was found to belong to the more familiar structural type (2Li:1Mg) i.e. $[Li(TMEDA)]_2[Mg\{o\text{-}Me(C_6H_4)O\}_4]$[19] **82**, whereby two oppositely disposed lithium cations are connected to a tetrahedral, tetraorganomagnesate centre via bridging organic groups (c.f. **73**, **78** and **79**). However, structure **82** is unusual in that the central fused, four-membered, MgOLiO rings are almost square [i.e. mean endocyclic angles O-Li-O, 88.2°; O-Mg-O, 87.9°; Li-O-Mg, 91.4°] whereas in the carbon and nitrogen analogues, rhomboidal shaped rings are favoured.

The third structure, $[Li(py)_2]_2\text{-}\mu\text{-}Mg[\{Ph_2SiO\}_2O][\{Ph_2SiO\}_3O]$[20] **83**, (not shown) is derived from the dilithiated siloxide, $[(Ph_2SiOLi.THF)_2O]$ and exhibits the same basic features as complex **82** i.e. 2Li:1Mg stoichiometry.

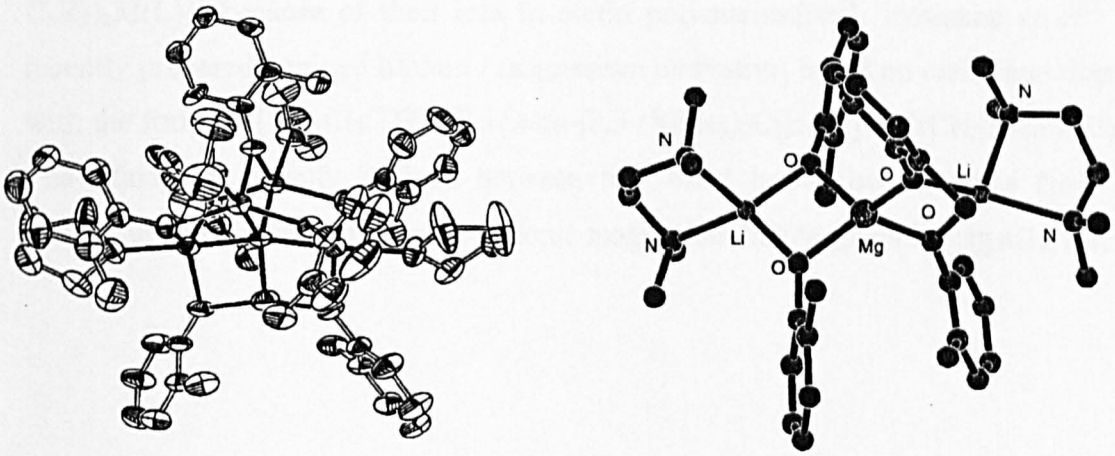

(a) (b)

*Figure 3.4- Crystal structures of (a) $[LiMg_4O\{o\text{-}Me(C_6H_4)O\}_4.4THF]$ **81** and (b) $[Li(TMEDA)]_2[Mg\{o\text{-}Me(C_6H_4)O\}_4]$ **82**, (hydrogen atoms are omitted for clarity)*

3.1.4 Lithium Halomagnesates

Lithium magnesate structures containing bridging halide anions are relatively scarce: only two $[Li(THF)_2(\mu\text{-}Br)_2Mg\{C(SiMe_3)_3\}.THF]$[21] **84** and $[Mg_2Cl_3.THF_6][Li\{nido\text{-}[2,3\text{-}(SiMe_3)_2C_2B_4H_4]\}][ZrCH_2SiMe_3(Cl)]$[22] **85** (figure 3.5), have so far been reported in the literature.

Structure **84** adopts a dimeric arrangement with a Li:Mg ratio of 1:1. Both the lithium and magnesium centres have four-coordinate, distorted tetrahedral environments. The lithium is terminally bound to two THF solvent molecules, whereas magnesium is terminally bound to a THF and a tris(trimethylsilyl)methyl group. Both metals are bridged by two bromide anions, to form a central, four-membered LiBrMgBr ring, the endocyclic angles of which are larger at the metals i.e. [Br-Mg-Br, 98.0°; Br-Li-Br, 101.0° c.f. mean Li-Br-Mg, 80.0°]. The mean Br-Mg distance [2.53Å] is found to be a little shorter than that found in the dimeric Grignard reagent, $[\{MgEtBr(OPr^i_2)\}_2]$[23] [2.58Å].

At present there is a great deal of interest in complexes of the type $[(\eta^5\text{-}C_5R_5)_2M(L)]^+$ because of their role in olefin polymerisation[24]. Hosmane *et al*[22] have recently prepared a mixed lithium / magnesium derivative, based on carborane dianions, with the formula $[Mg_2Cl_3.THF_6][Li\{nido\text{-}[2,3\text{-}(SiMe_3)_2C_2B_4H_4]\}][ZrCH_2SiMe_3(Cl)]$ **85**. The lithium is equally bridged between two basal bound boron atoms from each carborane and is also bound to the cationic magnesium halide species, $[Mg_2Cl_3(THF)_6]^+$.

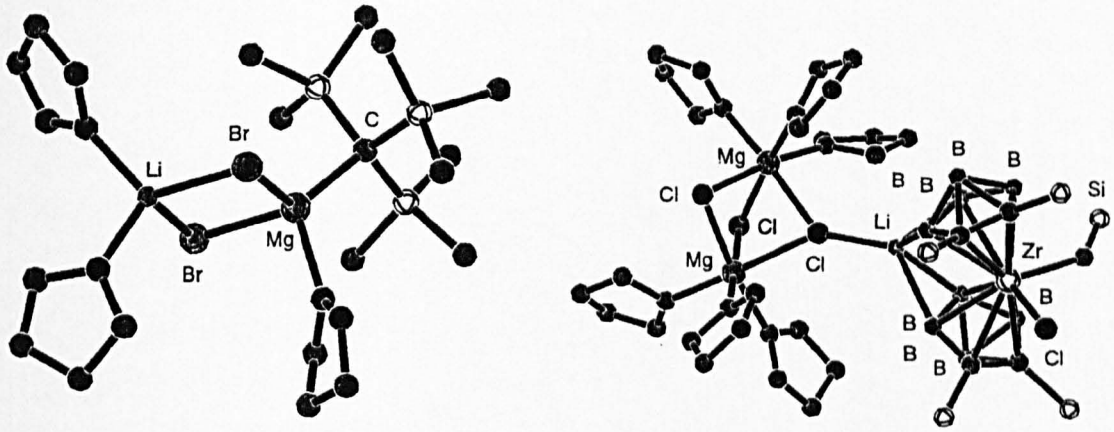

(a) (b)

Figure 3.5- Crystal structures of (a) $[Li(THF)_2(\mu\text{-}Br)_2Mg\{C(SiMe_3)_3\}.THF]$ ***84*** *(hydrogen atoms are omitted for clarity) and (b) $[Mg_2Cl_3.THF_6][Li\{nido\text{-}[2,3\text{-}(SiMe_3)_2C_2B_4H_4]\}][ZrCH_2SiMe_3(Cl)]$* ***85*** *(methyl substituents on silicon atoms are omitted for clarity)*

Chapter Three

Experimental (Part 1)

3.2 Chapter Three Experimental (Part 1)

Reaction 3.1: Synthesis of [{$(Me_3Si)_2N$}$_3$LiMg] 3A

The magnesium bis(amide) precursor, was prepared beforehand by the reaction of DBM (5mmol in heptane, 5ml of a 1M solution) with two equivalents of the bis(trimethylsilyl)amine, [$(Me_3Si)_2NH$], (2.1ml, 10mmol). The colourless solution was then refluxed for 4 hours. On cooling to ambient temperature, large colourless crystals of [{$(Me_3Si)_2N$}$_2$Mg] were formed. These were subsequently washed with hexane, isolated, and set aside for later use. The lithium amide precursor, [$(Me_3Si)_2NLi$], was prepared *in situ* by treating the chilled amine, [$(Me_3Si)_2NH$], (2.1ml, 10mmol) with *n*-BuLi (10mmol in hexane, 6.9ml of a 1.45M solution). To another Schlenk tube was added the pure crystalline magnesium bis(amide), (1.72g, 5mmol) which was dissolved in toluene (10ml). This solution was then transferred via cannula to the lithium amide solution. The resultant mixture was stirred at ambient temperature for 1 hour, then placed in a freezer at –30°C. After 24 hours, colourless crystals were obtained which were identified at the title complex, [{$(Me_3Si)_2N$}$_3$LiMg] **3A**.

Yield:	0.34g (9.9%) based on consumption of Mg bis(amide)
Melting Point:	120°C(decomp.)
Elemental Analysis:	$C_{18}H_{54}N_3LiMgSi_6$
Calculated	C, 42.2; H, 10.6; N, 8.2; Li, 1.4; Mg, 4.7; Si, 32.9%
Found	C, 40.6; H, 9.3; N, 7.4; Li, 1.3; Mg, 4.0%

Infrared / cm^{-1} (nujol mull)

1780w, 1766w, 1590w/br, 1250v.s, 956s/br, 855w, 835s/br, 790w, 760w, 666m

On exposure to air sharp signals appeared at 3699s and 3680s corresponding to the formation of [$Mg(OH)_2$] and [LiOH] respectively. A broad signal was also evident at 3386br corresponding to regeneration of free amine [N-H].

^{1}H NMR (400MHz, d_8-toluene, 300K)

Chemical shift δ/ppm	Splitting pattern	Relative integral	Assignment
0.28	singlet	1H	t-$SiMe_3$
0.21	singlet	2H	br-$SiMe_3$

Where t = terminal and br = bridging

^{13}C NMR spectrum (^{1}H-decoupled, 100MHz, d_8-toluene, 300K)

Chemical shift δ/ppm	Assignment
7.05	t-$SiMe_3$
5.53	br-$SiMe_3$

^{1}H NMR (400MHz, d_5-pyridine, 300K)

Chemical shift δ/ppm	Splitting pattern	Relative integral	Assignment
0.60	singlet	—	$SiMe_3$

^{13}C NMR spectrum (^{1}H-decoupled, 100MHz, d_5-pyridine, 300K)

Chemical shift δ/ppm	Assignment
7.66	$SiMe_3$

^{13}C-^{29}Si, ^1J, 52Hz

^{7}Li NMR spectrum in d_5-pyridine at 300K, 155.50 MHz (externally referenced to LiCl in D_2O, 0.0ppm)

Sharp singlet at 3.20ppm

Crystal structure

X-ray crystallographic studies of a selected crystal with dimensions 0.20x0.20x0.20mm were undertaken. These divulged the dimeric, mixed magnesium/lithium amide, $[\{(Me_3Si)_2N\}_3LiMg]$ **3A** (figure 3.6). The final R factor was 0.0581. Other crystallographic parameters are presented in Appendix III.

Table 3.2: Selected bond distances (Å) in **3A**

Mg(1)-N(1)	2.125(4)	**Li(1)-N(1)**	2.021(8)	**Li(1)···C(7)**	2.320(9)
Mg(1)-N(2)	2.103(4)	**Li(1)-N(2)**	2.017(9)	**Mg(1)···C(11)**	2.830(6)
Mg(1)-N(3)	1.998(4)	**Li(1)···C(1)**	2.294(10)		

Table 3.3: Selected bond angles (°) in **3A**

N(3)-Mg(1)-N(1)	132.2(16)	**N(2)-Li(1)-C(1)**	130.2(4)
N(3)-Mg(1)-N(2)	131.3(16)	**N(1)-Li(1)-C(1)**	85.2(3)
N(2)-Mg(1)-N(1)	96.5(15)	**N(2)-Li(1)-C(7)**	84.6(3)
N(2)-Li(1)-N(1)	102.8(4)	**N(1)-Li(1)-C(7)**	139.5(4)
Mg(1)-N(1)-Li(1)	80.0(3)	**Mg(1)-N(2)Li(1)**	80.6(2)

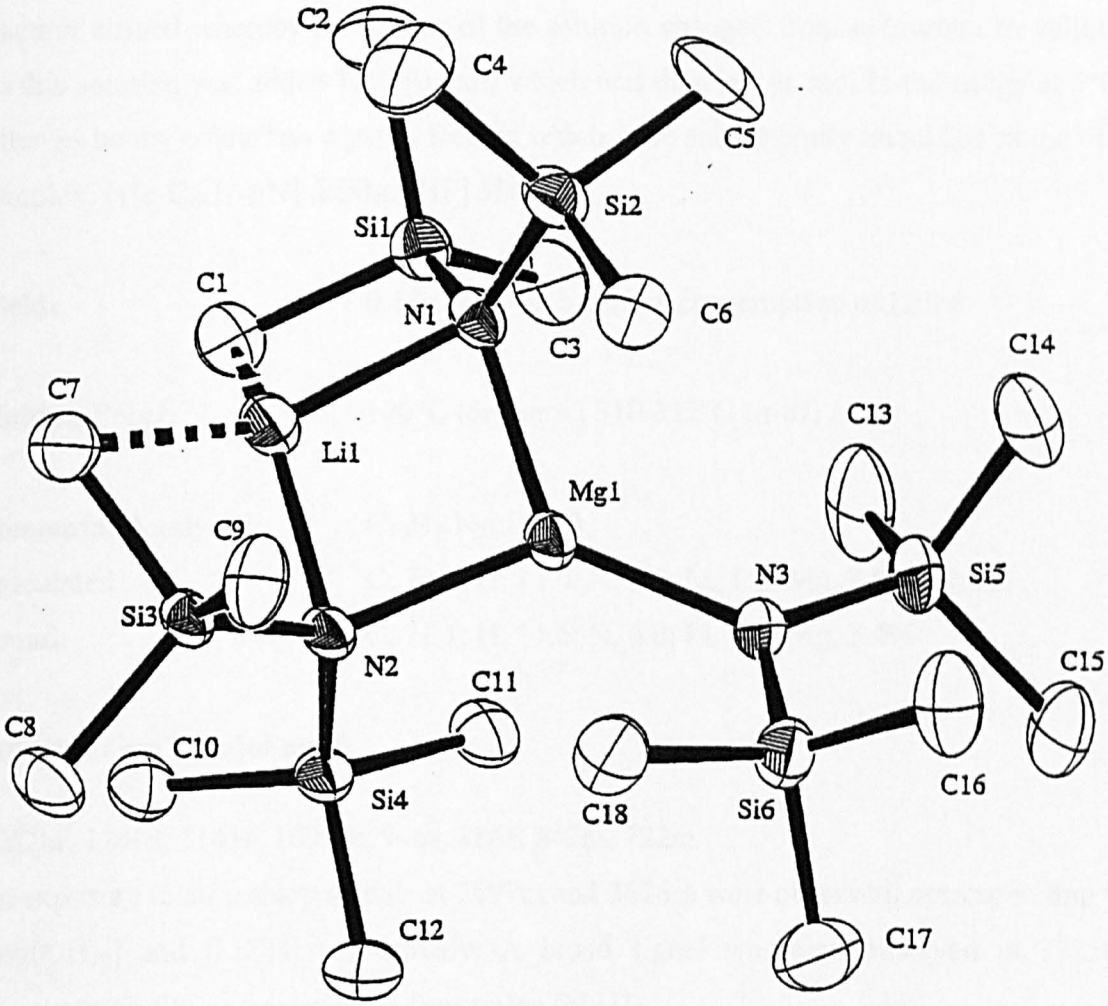

*Figure 3.6- Crystal structure of [{(Me$_3$Si)$_2$N}$_3$LiMg] **3A**, (hydrogen atoms are omitted for clarity)*

Reaction 3.2: Synthesis of [{(*c*-C_6H_{11})$_2$N}$_3$LiMg.THF] 3B

n-BuLi (5mmol in hexane, 3.5ml of a 1.45M solution) was added to a stirred solution of DBM (5mmol in heptane, 5ml of a 1M solution). To the stirred, cooled mixture of metal alkyls was added dicyclohexylamine, (3.0ml, 15mmol). A vigorous reaction ensued whereby the colour of the solution changed from colourless to yellow. To this solution was added THF (0.4ml) which was then left to cool in the fridge at 5°C. After 24 hours, colourless crystals formed which were subsequently identified as the title complex, [{(*c*-C_6H_{11})$_2$N}$_3$LiMg.THF] **3B**.

Yield: 0.48g (14.9%) based on consumption of DBM

Melting Point: 100°C (decomp.) 310-312°C (melt)

Elemental Analysis: $C_{40}H_{74}N_3LiMgO$

Calculated C, 74.6; H, 11.6; N, 6.5; Li, 1.1; Mg, 3.8; O, 2.5%

Found C, 71.1; H, 11.6; N, 6.0; Li, 0.9; Mg, 3.4%

Infrared / cm^{-1} (nujol mull)

2662br, 1240s, 1141s, 1096br, 946s, 886s, 842m, 722m

On exposure to air a sharp signals at 3697m and 3676m were observed, corresponding to [Mg(OH)$_2$] and [LiOH] respectively. A broad signal was also observed at 3325br corresponding to regeneration of free amine [N-H].

^{1}H NMR (400MHz, d$_8$-toluene, 300K)

Chemical shift δ/ppm	Splitting pattern	Relative integral	Assignment
3.83	multiplet	2H	OCH_2(THF)
2.52	multiplet	2H	CH_2(THF)
1.90-0.99	broad multiplets	33H	*c*-C_6H_{11}

^{13}C NMR spectrum (^{1}H-decoupled, 100MHz, d_8-toluene, 300K)

Chemical shift δ/ppm	Assignment
66.5	OCH_2(THF)
26.4	CH_2(THF)
57.0-14.6	*c*-C_6H_{11}

Crystal structure

X-ray crystallographic studies of a selected crystal with dimensions 0.60x0.40x0.30mm were undertaken. These divulged the dimeric, mixed magnesium/lithium amide, [{(*c*-$C_6H_{11})_2N\}_3$LiMg.THF] **3B** (figure 3.7). The final R factor was 0.0686. Other crystallographic parameters are presented in Appendix III.

Table 3.4: Selected bond distances (Å) in **3B**

Mg(1)-N(1)	1.956(4)	**Li(1)-N(2)**	2.085(11)
Mg(1)-N(2)	2.041(5)	**Li(1)-N(3)**	2.079(12)
Mg(1)-N(3)	2.067(5)	**Li(1)-O(1)**	1.945(10)

Table 3.5: Selected bond angles (°) in **3B**

N(1)-Mg(1)-N(2)	131.7(3)	**O(1)-Li(1)-N(2)**	132.5(7)
N(1)-Mg(1)-N(3)	127.5(2)	**Mg(1)-N(2)-Li(1)**	81.0(3)
N(2)-Mg(1)-N(3)	100.11(18)	**Mg(1)-N(3)-Li(1)**	80.5(3)
O(1)-Li(1)-N(3)	129.2(6)		

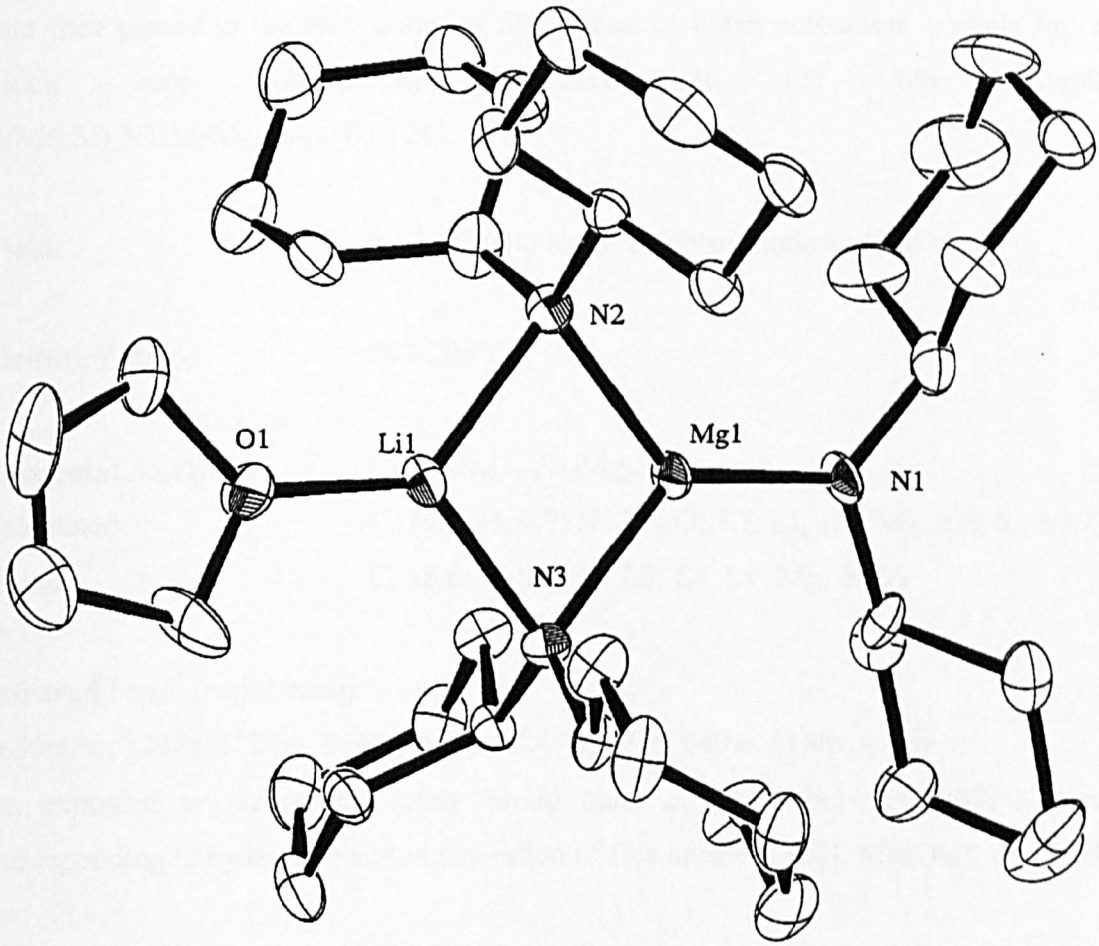

*Figure 3.7- Crystal structure of [{(c-C_6H_{11})$_2$N}$_3$LiMg.THF] **3B**, (hydrogen atoms are omitted for clarity)*

Reaction 3.3: Synthesis of $[\{(Me_3Si)_2N\}_4Li_2Mg_2(O_2)_x(O)_y]$ 3C

Equimolar amounts of *n*-BuLi (10mmol in hexane, 7.7ml of a 1.3M solution) and DBM (10mmol in heptane, 10.4ml of a 0.96M solution) were mixed in a Schlenk tube and chilled. Bis(trimethylsilyl)amine, $[(Me_3Si)_2NH]$, (6.3ml, 30mmol) was then added to the mixture whereby a vigorous reaction ensued. The reaction mixture was stirred for 1 hour then placed in the refrigerator at 5°C. After 24 hours colourless crystals formed, which were subsequently identified as the title complex, $[\{(Me_3Si)_2N\}_4Li_2Mg_2(O_2)_x(O)_y]$ **3C**.

Yield: 0.17g (5.0%) based on consumption of DBM

Melting Point: 203-205°C

Elemental Analysis: $C_{24}H_{72}N_4O_{1.4}Li_2Mg_2Si_8$

Calculated C, 39.5; H, 9.9; N, 7.7; O, 3.7; Li, 1.9; Mg, 6.6; Si, 30.7%

Found C, 38.8; H, 9.7; N, 7.3; Li, 1.9; Mg, 6.9%

Infrared / cm^{-1} (nujol mull)

1650m/br, 1248s, 1200m, 974br, 954w, 824v.s, 670s, 640w, 518m, 475w

On exposure to air an extremely broad band appeared between 3071-3731cm^{-1} corresponding to hydrolysis and regeneration of free amine [LiOH, $Mg(OH)_2$ and N-H].

^1H NMR (400MHz, d_8-toluene, 300K)

Chemical shift δ/ppm	Splitting pattern	Relative integral	Assignment
0.29	singlet	2.5H	$SiMe_3$ (peroxide)
0.27	singlet	1H	$SiMe_3$ (oxide)

^{13}C NMR spectrum (^{1}H-decoupled, 100MHz, d_8-toluene, 300K)

Chemical shift δ/ppm	Assignment
6.20	$SiMe_3$ (peroxide)
6.10	$SiMe_3$ (oxide)

^{7}Li NMR spectrum in d_5-pyridine at 300K, 155.5 MHz (externally referenced to LiCl, in D_2O, 0.0ppm)

Sharp singlet at 2.97ppm

Crystal structure

X-ray crystallographic studies of a selected crystal with dimensions 0.60x0.55x0.25mm were undertaken. These divulged the, mixed oxide/peroxide, magnesium/lithium amide, $[\{(Me_3Si)_2N\}_4Li_2Mg_2(O_2)_x(O)_y]$ **3C** (figure 3.8). The final R factor was 0.0357. Other crystallographic parameters are presented in Appendix III.

Table 3.6: Selected bond distances (Å) in **3C**

M(1)-O(1)	2.023(2)	**M(1)-N(1)**	2.113(2)	**M(2)-O(1*)**	2.024(2)
M(1)-O(1*)	2.013(2)	**M(1)-N(2)**	2.113(2)	**M(2)-O(2)**	1.854(6)
M(1)-O(2)	1.872(6)	**M(2)-O(1)**	2.012(2)	**M(2)-N(2)**	2.135(2)
M(2)-N(3)	2.124(2)	**O(1)-O(1*)**	1.551(4)		

Where M1 is the Mg(1)/Li(1) site and M(2) is the Mg(2)/Li(2) site.

Table 3.7: Selected bond angles (°) in **3C**

N(1)-M(1)-N(2)	166.62(8)	**M(1)-N(2)-M(2)**	76.58(7)
N(2)-M(2)-N(3)	166.89(8)	**M(2)-N(3)-M(1*)**	76.96(10)
M(1)-N(1)-M(1*)	77.31(10)		

Where M1 is the Mg(1)/Li(1) site and M(2) is the Mg(2)/Li(2) site.

Symmetry transformations used to generate equivalent atoms: (*) = 3/2-x, y, 1/2-z

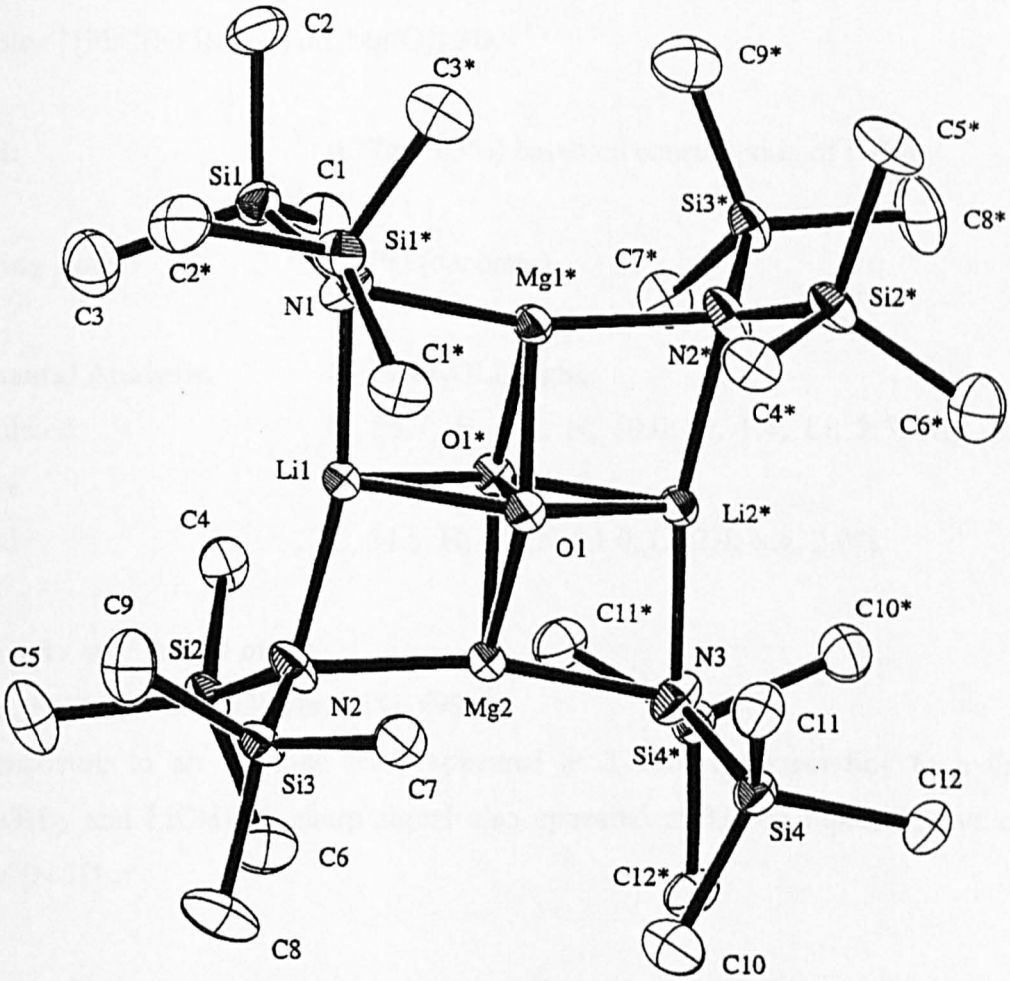

*Figure 3.8- Crystal Structure of [{(Me₃Si)₂N}₄Li₂Mg₂(O₂)ₓ(O)ᵧ] **3C**, (hydrogen atoms are omitted for clarity)*

Reaction 3.4: Synthesis of [{PhC(NSiMe$_3$)$_2$}$_4$Li$_4$Mg(O)] 3D

Equimolar amounts of *n*-BuLi (10mmol in hexane, 7.7ml of a 1.3M solution) and DBM (10mmol in heptane, 10.4ml of a 0.96M solution) were mixed in a Schlenk tube and chilled. Bis(trimethylsilyl)amine, [(Me$_3$Si)$_2$NH], (6.3ml, 30mmol) was then added to the mixture whereby a vigorous reaction ensued. To this solution benzonitrile (3.0ml, 30mmol) was added, again resulting in a vigorous reaction, which produced a pale orange solution. On leaving this solution to stand at ambient temperature for several days, colourless needle crystals formed. These were subsequently identified as the title complex [{PhC(NSiMe$_3$)$_2$}$_4$Li$_4$Mg(O)] **3D**.

Yield: 0.77g(13.3%) based on consumption of DBM

Melting Point: 178°C (decomp.)

Elemental Analysis: $C_{52}H_{92}N_8OLi_4MgSi_8$

Calculated C, 55.7; H, 8.3; N, 10.0; O, 1.4; Li, 2.5; Mg, 2.1; Si, 20.0%

Found C, 54.5; H, 8.3; N, 11.0; Li, 2.4; Mg, 2.0%

Infrared / cm^{-1} (nujol mull)

1662s, 1245v.s, 983s, 838s/br, 758s, 699s/w

On exposure to air a broad band appeared at 3700br corresponding to hydrolysis [Mg(OH)$_2$ and LiOH]. A sharp signal also appeared at 3384m representative of free amine [N-H].

^{1}H NMR (400MHz, d_5-pyridine, 300K)

Chemical shift δ/ppm	Splitting pattern	Relative integral	Assignment
7.46	doublet	2H	*ortho*-Ph
7.36-7.29	overlap. multiplets	3H	*m*-/*p*-Ph
0.015	singlet	18H	$SiMe_3$

^{13}C NMR spectrum (^{1}H-decoupled, 100MHz, d_5-pyridine, 300K)

Chemical shift δ/ppm	Assignment
178.4	N---C---N
149.3	*ipso*-Ph
128.2	*m*-/*p*-Ph
126.6	*ortho*-Ph
126.4	*m*-/*p*-Ph
3.6	$SiMe_3$

^{7}Li NMR spectrum in d_5-pyridine at 300K, 155.5 MHz (externally referenced to LiCl, in D_2O, 0.0ppm)

Sharp singlet at 3.41ppm

Crystal Structure

X-ray crystallographic studies of a selected crystal with dimensions 060x0.24x0.15mm were undertaken. These divulged the novel, mixed, magnesium/lithium benzamidinate, $[\{PhC(NSiMe_3)_2\}_4Li_4Mg(O)]$ **3D** (figure 3.9). The final R factor was 0.0571. Other crystallographic parameters are presented in Appendix III.

Table 3.8: Selected bond distances (Å) in **3D**

Mg(1)-O(1)	**1.850(6)**	**Li(1)-O(1)**	**1.799(11)**	**Li(2)-O(1)**	**1.919(11)**
Mg(1)-N(1)	**2.099(4)**	**Li(1)-N(2)**	**2.105(10)**	**Li(2)-N(3)**	**2.118(10)**
Mg(1)···N(2)	**2.471(4)**	**Li(1)-N(3)**	**2.076(9)**	**Li(2)-N(4*)**	**2.207(10)**

Table 3.9: Selected bond angles (°) in **3D**

N(1)-Mg(1)-N(1*)	111.2(3)	**N(2)-Li(1)-N(3)**	148.9(4)
O(1)-Mg(1)-N(1)	124.4(13)	**Mg(1)-O(1)-Li(1)**	92.0(3)
O(1)-Li(1)-N(2)	102.4(4)	**Mg(1)-O(1)-Li(2)**	141.7(3)
O(1)-Li(1)-N(3)	105.2(4)	**Li(1)-O(1)-Li(2*)**	93.6(4)

Symmetry transformations used to generate equivalent atoms: (*) = -x, y, 1/2-z

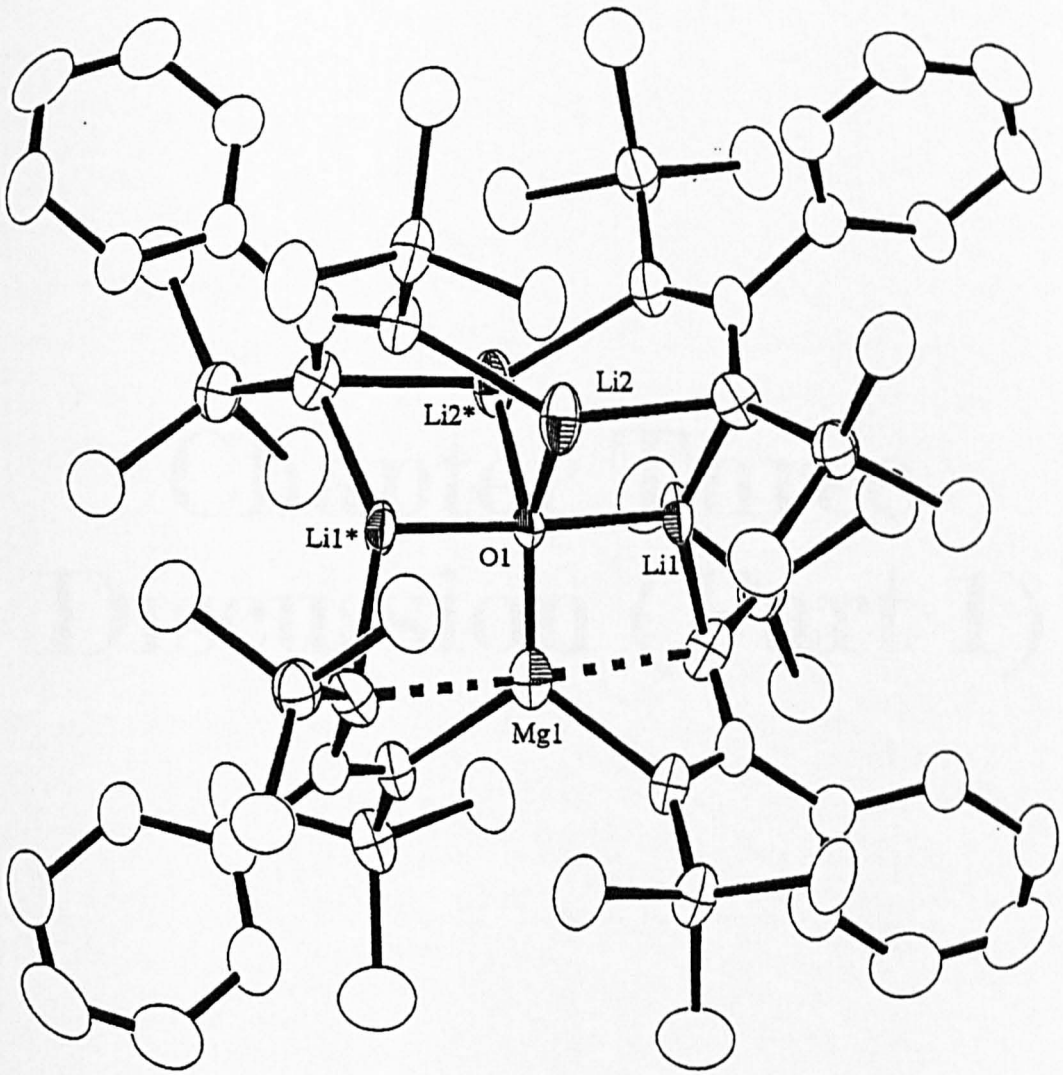

Figure 3.9- Crystal structure of [{PhC(NSiMe$_3$)$_2$}$_4$Li$_4$Mg(O)] ***3D****, (hydrogen atoms are omitted for clarity)*

Chapter Three
Discussion (Part 1)

3.3 Synthesis and Analysis of Compounds 3A and 3B

The heterobimetallic complex, $[\{(Me_3Si)_2N\}_3LiMg]$ **3A**, could only be crystallised from solutions containing a 2:1 stoichiometry of lithium amide to magnesium bis(amide). It was imperative to make the magnesium bis(amide) precursor, $[\{(Me_3Si)_2N\}_2Mg]$ in a pure crystalline state prior to reaction with the lithium amide. This was carried out by adding two equivalents of the bis(trimethylsilyl)amine to one equivalent of dibutylmagnesium in heptane then refluxing for 4 hours (equation 3.2). This avoided the possibility of forming the alkyl(amido) intermediate, $[\{(Me_3Si)_2NMgBu\}_2]$[25], a known structurally characterised compound. Finally the magnesium bis(amide) crystals were dissolved in toluene and transferred via cannula to the lithium amide which was generated *in situ* by lithiation of the parent amine (equation 3.3). This method of reacting two monometallic bis(trimethylsilyl) amides to form a heterobimetallic composite has previously been reported by Williard *et al*[26] in his work on mixed alkali-metal systems.

$$n,s\text{-}Bu_2Mg + 2(Me_3Si)_2NH \longrightarrow [\{(Me_3Si)_2N\}_2Mg] + 2\,BuH \qquad (3.2)$$

$$2\,n\text{-}BuLi + 2(Me_3Si)_2NH \longrightarrow 2[(Me_3Si)_2NLi] + 2\,BuH \qquad (3.3)$$

$$\downarrow [\{(Me_3Si)_2N\}_2Mg]$$

$$[\{(Me_3Si)_2N\}_3LiMg]] + [(Me_3Si)_2NLi]$$

The preparation of $[\{(c\text{-}C_6H_{11})_2N\}_3LiMg.THF]$ **3B** was carried out by adding three equivalents of dicyclohexylamine to a stirred, chilled, 1:1 mixture of *n*-butyllithium and dibutylmagnesium. A vigorous reaction ensued whereby the solution changed colour from colourless to yellow. Colourless crystals formed over a period of 30 minutes at ambient temperature, however when analysed by X-ray diffraction, they were identified as the magnesium bis(amide) complex, $[\{(c\text{-}C_6H_{11})_2N\}_2Mg]$[27]. The

reaction was repeated, in the additional presence of THF (0.4ml), but no crystalline product was observed to form at room temperature. Thus the solution was placed in the fridge at 5°C. After a period of 24 hours, small colourless crystals formed. A melting point analysis confirmed that these crystals were not the aforementioned magnesium bis(amide) i.e. [bis(amide), m.p. 240°C (decomp.) c.f. new product, m.p. 100°C (decomp.), 310-312°C melt]. An X-ray analysis established that the new crystals were, $[\{(c\text{-}C_6H_{11})_2N\}_3LiMg.THF]$ **3B**, (equation 3.4).

$$n\text{-BuLi} + n,s\text{-}Bu_2Mg + 3\,(c\text{-}C_6H_{11})_2NH \xrightarrow{THF} [\{(c\text{-}C_6H_{11})_2N\}_3LiMg.THF] \qquad (3.4)$$

Satisfactory elemental analyses were obtained for both compounds **3A** and **3B**. The presence of both lithium and magnesium in compounds **3A** and **3B** was confirmed using infrared spectroscopy, whereby on exposure to air the metal-hydroxide bands appeared [$Mg(OH)_2$: **3A**, 3699cm^{-1}, **3B**, 3697cm^{-1}; LiOH: **3A**, 3680cm^{-1}, **3B**, 3676cm^{-1}] accompanied by bands corresponding to regeneration of 'free' amine. AAS spectrophotometry quantified the amount of each metal present, which was found to correspond to that in the crystal structures.

The ^{1}H NMR spectrum of complex **3A** was initially carried out in d_5-pyridine but was found to be uninformative as it revealed only a single resonance in the alkyl region. It was then decided to prepare the sample in d_8-toluene, whereby two signals of relative integral 2:1 appeared in this region (figure 3.10). Both of these signals have different chemical shifts than those exhibited by the monometallic (trimethylsilyl) amide complexes i.e. (**3A**, 0.21ppm and 0.28ppm respectively c.f. $[(Me_3Si)_2NLi]$, 0.10ppm; $[\{(Me_3Si)_2N\}_2Mg]$, 0.32ppm and 0.44ppm). The $^{13}C\{^1H\}$ NMR spectrum, which was run in d_8-toluene also, confirmed the presence of two distinct methyl (Me_3Si-) groups [5.53ppm (br), 7.05ppm (t)]. The NMR data confirmed the structure found in the solid state, where two chemically equivalent $[(Me_3Si)_2N\text{-}]$ groups bridge the pair of metal centres, while another binds terminal to the magnesium centre.

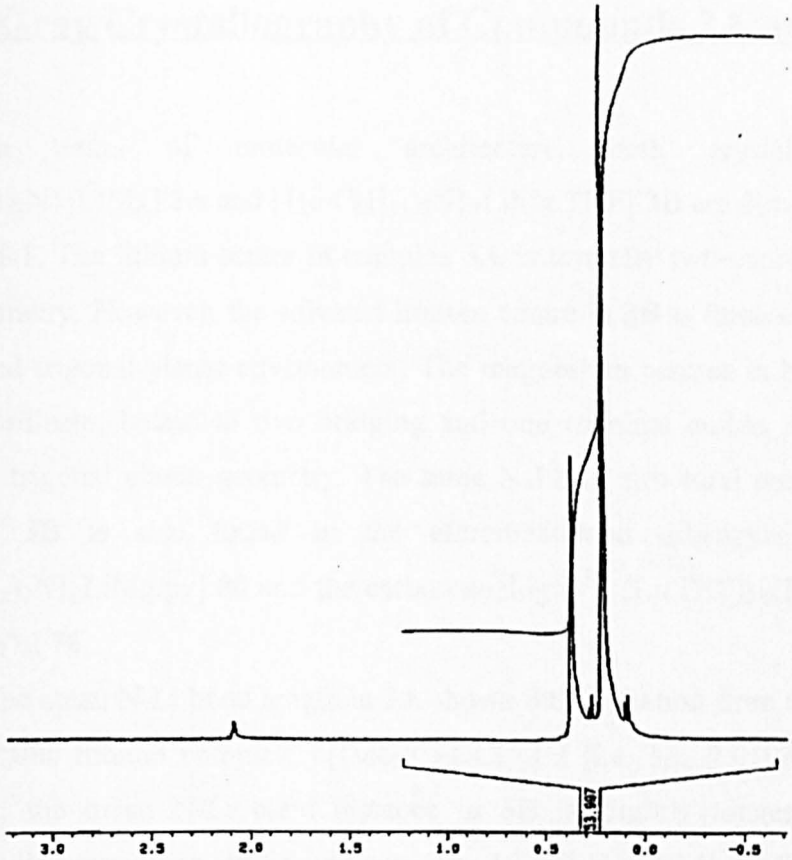

Figure 3.10- ^{1}H NMR spectrum of [{(Me$_3$Si)$_2$N}$_3$LiMg] 3A in d$_8$-tol at 300K

Both the ^{1}H and ^{13}C NMR spectra of, [{(*c*-C_6H_{11})$_2$N}$_3$LiMg.THF] **3B**, proved to be rather complicated. In the alkyl region of the ^{1}H NMR spectrum many overlapping multiplets were present which were assigned to the cyclohexyl groups (in the range 0.99-1.90ppm). It was not thought important to resolve these. However THF could easily be distinguished by the presence of two small multiplets at 2.52ppm (CH_2) and 3.83ppm (OCH_2) respectively. Integration of these signals and the cyclohexyl ones gave a ratio of 4:33, which is what would be expected for a dimer with three dicyclohexyl amide units and one THF molecule. The ^{13}C NMR data were just as difficult to assign, again the carbon signals were close together over a short range (14.6-57.0ppm), only the THF could be determined accurately (these come at 26.4ppm and 66.5ppm).

3.4 X-ray Crystallography of Compounds 3A and 3B

In terms of molecular architecture, both crystal structures of, [{$(Me_3Si)_2N$}$_3$LiMg] **3A** and [{$(c\text{-}C_6H_{11})_2N$}$_3$LiMg.THF] **3B** are dinuclear with a Li:Mg ratio of 1:1. The lithium centre in complex **3A** is formally two-coordinate possessing a bent geometry. However, the solvated lithium centre in **3B** is three-coordinate adopting a distorted trigonal planar environment. The magnesium centres in both complexes are three-coordinate, bound to two bridging and one terminal amide unit, arranged in a distorted trigonal planar geometry. The same N_3LiMg structural motif present in both **3A** and **3B** is also found in the aforementioned dibenzylamido derivative[18], [{$(PhCH_2)_2N$}$_3$LiMg.py] **80** and the carbon analogue[16], [Li(THF)$_{0.6}$(Et_2O)$_{0.4}$][Mg(2,4,6-i-$Pr_3C_6H_2$)$_3$] **76**.

The mean N-Li bond length in **3A** shows little variation from that in the trimeric, homometallic lithium complex, [{$(Me_3Si)_2NLi$}$_3$] **2** [i.e. **3A**, 2.019Å c.f. 2.00Å in **2**]. However, the mean N-Li bond distance in **3B** is slightly longer than that in the corresponding tetrameric, all lithium complex, [{$(c\text{-}C_6H_{11})_2NLi$}$_4$][28] [i.e. **3B**, 2.082Å c.f. 1.959Å]. The N-Li bond lengths in both **3A** and **3B** can also be compared with those in the dimeric THF[(25,29)] and ether[30] complexes of lithium bis(trimethylsilyl)amide [i.e. which measure 2.025Å and 2.055Å respectively]. The lithium centres in these solvates have a formal coordination number of three and are only marginally longer than those found for **3A**. This suggests that the lithium centre in **3A** is receiving extra stabilisation besides that from the bridging amido groups. On close examination of the structure the two methyl groups (C1 and C7) on Si1 and Si3 respectively, which lie on opposite sides of the NLiNMg ring, are observed to interact in an intermolecular fashion with the lithium centre. The C1···Li1 and C7···Li1 distances are short [i.e. 2.294(10)Å and 2.320(9)Å respectively]. These C-Li contacts can be placed in the same category as the formal electron-deficient bonds found in alkyllithiums such as [(EtLi)$_4$][31] and [(*t*-BuLi)$_4$][32] [mean C-Li distances, 2.25Å and 2.246Å respectively]. The two hydrogen atoms attached to C1 (H1A, H1C) and the two H atoms attached to C7 (H7B, H7C) also form short contacts with Li1 [i.e. 2.195Å, 2.173Å, 2.266Å and 2.160Å respectively].

Pseudo-agostic interactions of this type have been found in other alkali metal complexes where the metal is in a low coordination state and highly-polarised $Si^{\delta+}$-$CH_3^{\delta-}$ units are available for coordination. As well as intermolecular coordination (shown in complex **3A**) intramolecular coordination is also possible and has been exhibited by some alkali metal hypersilanides[33]. As mentioned previously, the lithium centre in compound **3B** is three-coordinate, whereby the third coordination site is occupied by the oxygen donor, THF. The O-Li bond length is found to be significantly longer than that found in the aforementioned lithium arylmagnesate complex, $[Li(THF)_{0.6}(Et_2O)_{0.4}][Mg(2,4,6\text{-}i\text{-}Pr_3C_6H_2)_3]$ **76** [i.e. **3B**, 1.945(10)Å c.f. **76**, 1.858(8)Å]. This difference in length can be attributed to the different anions involved, the amide anions in **3B** will satisfy the lithium better than the carbon analogue, thus the THF molecule will not be pulled in as close by comparison.

The mean μN-Mg bond distance in compound **3A** is found to be in good agreement with that found in the homoleptic magnesium bis(amide), $[\{(Me_3Si)_2N\}_2Mg]$ **23** [i.e. **3A**, 2.114Å c.f. 2.151Å in **23**]. Complex **3B**, on the otherhand, has a mean (N-Mg bond length similar to that found in the pyridine solvate $[\{(PhCH_2)_2N\}_3LiMg.py]$ **80** [i.e. **3B**, 2.054Å c.f. 2.045Å in **80**]. The shorter, terminal N-Mg distances in both **3A** and **3B** [i.e. **3A**, 1.998(4)Å, **3B**, 1.956(4)Å], are in good agreement with those found in $[\{(Me_3Si)_2N\}_2Mg]_2$ **23** [1.975(7)Å], $[\{(c\text{-}C_6H_{11})_2N\}_2Mg]_2$ **24** [1.94(3)Å] and $[\{(PhCH_2)_2N\}_3LiMg.py]$ **80** [1.945(3)Å].

Turning to bond angles, compound **3A** and **3B** possess similar endocyclic angles at magnesium and nitrogen [i.e. **3A**, at Mg 99.5(2)°, at N 80.0(3)°; **3B**, at Mg 100.11(18)°, at N 80.8(3)°]. However a slight difference is observed in the angles at lithium [i.e. in **3A**, 102.8(4)°; in **3B**, 98.3(4)°]. Complex **3B** shows greater similarity with compound **80** [at Mg 99.40(1)°, at N 80.5(2)° and at Li 99.6(2)°].

Complexes **3A** and **3B** represent two new additions to the family of lithium amidomagnesates with lithium to magnesium ratios of 1:1. Complex **3A** is particularly

novel as it represents one of the few lithium magnesate structures which is formally unsolvated, to compensate for this it features agostic-type interaction with its amido functions.

3.5 Synthesis and Analysis of Compound 3C

In another attempt to prepare $[\{(Me_3Si)_2N\}_3LiMg]$ **3A**, the metal alkyls were used instead of the respective amide complexes. To a 1:1 mixture of *n*-BuLi/*n,s*-Bu_2Mg, three equivalents of the silyl amine were added (equation 3.5). A vigorous reaction ensued whereby the solution was left to cool in the fridge at 5°C. After 24 hours, small colourless crystals were observed to have formed.

$$n,s\text{-}Bu_2Mg + n\text{-}BuLi + 3\,(Me_3Si)_2NH \xrightarrow{\text{trace of } O_2} z\,[\{(Me_3Si)_2N\}_4Li_2Mg_2(O_2)_x(O)_y] + z\,BuH + \text{other products} \quad (3.5)$$

On analysis, the crystals were found not to be that of complex **3A**, but instead were that of an oxygen contaminated derivative of formula, $[\{(Me_3Si)_2N\}_4Li_2Mg_2(O_2)_x(O)_y]$ **3C**. The precise composition of the relative quantities of peroxide and oxide was established using X-ray crystallography. For the particular crystal reported here, the oxygen content was found to be mainly in the form of peroxide [i.e. with x = 0.715(7); y = 0.285(7)]. The formation of compound **3C** was found to be totally reproducible, however the yields were consistently small [range 1-5%]. No other products were found to crystallise from the solutions. As mentioned previously, the crystals of compound **3C** are colourless like the oxygen-free complex **3A**. Both can be distinguished using melting point analysis: compound **3C** melts 80°C higher at 203-205°C.

Satisfactory elemental analyses were obtained. On exposure to air the infrared spectrum revealed a broad hydrolysis band between 3071-3731cm^{-1}, which can be attributed to both the metal hydroxides, H_2O and the regeneration of free amine.

The ^{7}Li NMR spectrum revealed only one type of lithium present in the sample at 2.97ppm. An attempt at ^{17}O NMR was carried out on a concentrated sample in d_5-pyridine, which proved fruitless as no signals were observed, this can be attributed to the low natural abundance of the ^{17}O isotope (0.037%) whereby enrichment of the sample needs to be carried out (time did not allow this here).

The ^{1}H NMR spectrum of **3C** was found to consist of two singlet resonances only 0.02ppm apart (i.e. at 0.29 and 0.27ppm) in an approximate ratio of 2.5:1.0 (figure 3.11). These signals were found to possess different chemical shifts in comparison to lithium bis(trimethylsilyl)amide, magnesium bis[bis(trimethylsilyl)amide] and the mixed metal analogue **3A**. The structure of **3C** can be assumed to be retained in solution as the ^{1}H NMR signals integrate to the same ratio of peroxide to oxide present in the crystal (i.e. x = 0.715, y = 0.285). This is also supported by the $^{13}C\{^{1}H\}$ NMR spectrum, which displays only two signals that are only 0.1ppm apart (i.e. at 6.20 and 6.10ppm).

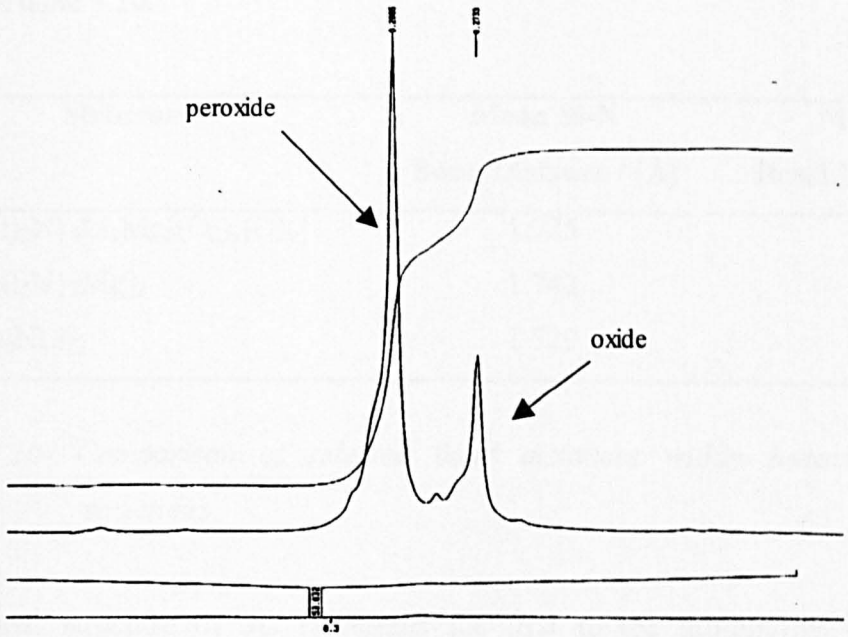

*Figure 3.11- ^{1}H NMR spectrum of $[\{(Me_3Si)_2N\}_4Li_2Mg_2(O_2)_x(O)_y]$ **3C**, in d_8-toluene at 300K*

3.6 X-ray Crystallography of Compound 3C

The basic molecular structure of **3C** (figure 3.8, pg.99, note that only the peroxide component shown) is that of a planar eight-membered $(NM)_4$ cyclic ring. The two lithium and two magnesium centres are indistinguishable due to mutual substitution disorder. On free refinement occupations, 51%Li and 49%Mg were obtained. Thus on grounds of chemical sense, the metal occupancy sites in the structure were set at 50%Li and 50%Mg. The core of the structure is occupied by a peroxide molecule (note that the other 30% of molecules in bulk lattice contain oxide) which is side-on coordinated to all four metal centres in a square planar-type arrangement. Unfortunately, dimensions within the metal oxygen core cannot be discussed due to the two types of substitution disorder present. The periphery of **3C** is occupied by Me_3Si groups (from the amide) which render the molecule lipophilic. The Si-N and Si-C bond distances are equivalent within standard deviations to the monometallic bis(trimethylsilyl) amide compounds, as shown in table 3.10.

Structure	Mean Si-N Bond Distance / (Å)	Mean Si-C Bond Distance / (Å)
$[\{(Me_3Si)_2N\}_4Li_2Mg_2(O_2)_x(O)_y]$	1.725	1.872
$[\{(Me_3Si)_2N\}_2Mg]_2$	1.742	1.857
$[(Me_3Si)_2NLi]_3$	1.729	1.867

Table 3.10- Comparison of selected bond distances within hexamethyldisilazide structures

The crystal structure of **3C** represents the first mixed lithium/magnesium, mixed amide/peroxide composition. At present few main group element 1,2-μ-peroxide structures are known. The first structure of a lithium peroxide[34], that of $[LiOOBu^t]_{12}$ **86**, was published as recently as 1996. Its structure was found to be that of a dodecameric

ring where each lithium ion bridges the two oxygen atoms of a peroxide unit. The crystal structure of the monometallic lithium mixed peroxide-siloxide species, $[(Me_3SiOLi)_4(Li_2O_2)\{(Me_3Si)_2NLi\}.2THF]$[35] **87** has also appeared recently which was prepared by air-oxidation of dilithium hydrazide, $[(Me_3Si)_2N_2Li_2]$. Here **87** contains the same amide unit as complex **3C** whereby the peroxide anion is side-on coordinated by three lithium centres.

Crystal structures containing adventitious oxygen have been known for over 30 years, the first being when Stucky *et al*[36] reported the Grignard oxidation product, $[Mg_4Br_6(O).4Et_2O]$ **88**, prepared by exposing an ether solution of PhMgBr to the open atmosphere. Since then there have been growing reports of oxygen contamination in early main group compounds. The only other example of a mixed lithium/magnesium oxygen contaminated complex is that of the aforementioned cresylate, $[LiMg_4O\{o\text{-}Me(C_6H_4)O\}_7.4THF]$ **81** (pg.87) where an oxide anion occupies the centre of the trigonal bipyramidal $LiMg_4$ cage. Several barium oxide-containing cage species are also known, one example being the aryl oxide, $[(PhO)_{14}H_2Ba_8(O)_2.6HMPA.2PhMe]$[37] **89**. In many structures, the incorporation of "Li_2O" molecular units verifies the strong oxophilic nature of lithium. An early example of this type of incorporation is found in the dilithiosulphone complex, $[\{[PhSO_2\text{-}C(SiMe_3)]Li_2\}_6Li_2O.(THF)_{10}]$[38] **90**. More recent examples with progressively larger cage sizes are the primary amide, $[\{(c\text{-}C_5H_9)N(H)Li\}_{12}Li_2O]$[39] **91**, the phosphanediide, $[\{[Pr^i_2(Mes)Si]P\}_8Li_{16}.Li_2O]$[40] **92** and the arsanediide, $[\{[Me_2(Pr^iMe_2C)Si]As\}_{12}Li_{24}.Li_2O]$[40] **93**. The mixed lithium-potassium, oxide-alkoxide cage complex, $[(Bu^tO)_8Li_8K_2(O).(TMEDA)_2]$[41] **94** has also been reported. In the presence of moisture, main group compounds readily hydrolyse forming complexes containing hydroxide anions e.g. the heterotrianionic, mixed lithium-potassium compound $[(C_6H_{11}O)_4(t\text{-}C_6H_9O)_4Li_4K_4.KOH.(THF)_5]$[42] **95** and the heterobianionic, all lithium complex, $[(t\text{-}BuOLi)_{10}(LiOH)_6]$[43] **96**. Alkoxide structures containing peroxide anions are also known e.g. as in the barium diketonate, $[(THD)_{10}Ba_6(O_2)(H_2O)_6]$[44] **97** where HTHD = 2,2,6,6-tetramethylheptane-3,5-dione.

Complexes containing square planar oxygen (peroxide or oxide) are relatively uncommon. Compound **3C** represents the first mixed group1/2 example. In the literature, this coordination mode of oxygen is mainly limited to complexes containing transition metals e.g. as in the tetranuclear vanadium complex, $[(NBu^n_4)_2\{V_4O(edt)_2Cl_8]$[45] **98** where edt = ethane-1,2-dithiolate, the niobium cluster anion[46], $[Nb_4OCl_8\{(PhC)_4\}_2Mg(THF)_3\}]^-$ **99** and the neutral mixed sodium-niobium complex, $[Na_2\{Nb_4OCl_8[(PhC)_4\}_2](THF)_6.(C_6H_6)_2]$[47] **100**.

In most of the examples considered so far, the source of oxygen contamination is not known with any degree of certainty. This picture is not any clearer, in the selected cases when oxygen contamination has been deliberate. Illustrative of this has been the deliberate insertion of dioxygen into alkyl-magnesium bonds which gives alkoxide formation in the alkylamide system, $[Me_2Al(NPr^i_2)_2Mg(OMe)]$[48] but alkyl peroxide functions in the tris(pyrazolyl)hydroborato system[49], $[(HB(3\text{-}Bu^t\text{-}pz)_3\}MgOOR]$ where R = Me, Et, Pr^i and Bu^t. In the latter system, the position of oxygen insertion was identified using ^{17}O NMR.

In the preparation of complex **3C**, the source of oxygen contamination is thought to be dioxygen rather than moisture. By triply distilling and degassing (using freeze-pump-thaw techniques) the amine prior to use, it was hoped that the formation of **3C** would not occur. This was not the case, though much smaller yields were obtained. Possible sources of contamination are thought to be from the "oxygen-free" blanket gas and more realistically from the molecular sieve (as this was used straight from the oven) which was used to dry the amine. Our suspicions that dioxygen was the cause was realised, when deliberate addition of dioxygen was carried out. On repeating the reaction a $CaCl_2$ drying tube was placed at the mouth of the Schlenk, thus allowing air to enter but not moisture. After 24 hours at 5°C, a large batch of complex **3C** had formed with a yield of 10% (double that which was obtained previously).

The bulky trimethylsilyl substituents in structure **3C** are thought responsible for the larger percentage of peroxide present in relation to oxide. One would expect from thermodynamic considerations that the latter would be more favoured in the presence of small Li^+ and Mg^{2+} counterions. In this case the peroxide incorporation is presumed to be the kinetic product, where the large amide groups shield the peroxide anion from any bimolecular process that would abstract an oxygen atom to form O^{2-}. A similar kinetic-thermodynamic argument has been put forward to explain the formation of the bis(1,2-μ-peroxo)-bridged tin amide complex[50], $[Sn\{N(SiMe_3)_2\}_2(\mu\text{-}O_2)]_2$ **101**. However, the reaction is different as the metal, tin, is changing oxidation state from II to IV, an occurrence of which does not transpire in lithium or magnesium chemistry.

The relatively low yields obtained in the preparation of **3C** suggest that it is only a minor product. It is assumed that the solution contains a mixture of soluble products including that of the intermetallic amide, $[\{(Me_3Si)_2N\}_3LiMg]$ **3A**. This solution should also contain relatively small amounts of the oxidised product, $(Me_3Si)_2N\text{-}N(SiMe_3)_2$ as dioxygen is formally reduced.

The discovery of $[\{(Me_3Si)_2N\}_4Li_2Mg_2(O_2)_x(O)_y]$ **3C** led to an in-depth study of selected mixed group1/magnesium amide systems using the bulky secondary amines, bis(trimethylsilyl)amine and 2,2,6,6-tetramethylpiperidine. These are discussed separately in part 2 of this chapter.

3.7 Synthesis and Analysis of Compound 3D

In this part of the work, it was decided to investigate the reactivity of the oxidation product, $[\{(Me_3Si)_2N\}_4Li_2Mg_2(O_2)_x(O)_y]$ **3C**. The type of reaction carried out was that of addition across benzonitrile (PhC≡N). The low yield of **3C** made it impractical to use isolated material. Hence by deliberately omitting degassing procedures **3C** was prepared *in situ*. To an oxidised mixture of 1 *n*-BuLi / 1 *n,s*-Bu_2Mg / 3 $(Me_3Si)_2NH$ was added three molar equivalents of benzonitrile. Immediately a vigorous reaction ensued whereby the solution changed colour from colourless to orange. On leaving the solution at ambient temperature for several days, colourless needle crystals formed. These were subsequently identified as the novel, oxo-centred, tetralithium-monomagnesium, N-silylated benzamidinate, $[\{PhC(NSiMe_3)_2\}_4Li_4Mg(O)]$ **3D** (equation 3.6).

$$n,s\text{-}Bu_2Mg + n\text{-}BuLi + 3(Me_3Si)_2NH + 3\ PhC{\equiv}N \xrightarrow{\text{trace of } O_2} x[\{PhC(NSiMe_3)_2\}_4Li_4Mg(O)] + y\ BuH + \text{other products} \quad (3.6)$$

As far as we are aware, there is no precedent in this branch of chemistry for using a mixed metal reagent to generate a mixed metal product. However, it is not certain that compound **3D** is prepared directly from **3C** as the solution may contain a mixture of oxide species as well as the oxygen-free intermetallic complex **3A**.

Elemental analysis proved successful. Metal analysis of compound **3D** indicated a lithium to magnesium ratio of 4:1 which was later confirmed by X-ray crystallography. The infrared spectrum of **3D** displayed a very sharp signal at 1662s which can be assigned to the stretching frequency of the N=C=N unit. On exposure to air, hydrolysis resulted, indicated by a broad band centred at 3700br corresponding to a

mixture of $Mg(OH)_2$, LiOH and H_2O. This was accompanied by a signal at 3384m corresponding to that of the regenerated amidine [N-H].

On examination of the crystal structure of **3D**, two chemically distinct benzamidinate functions can be found. However, in both the ^1H and $^{13}C\{^1H\}$ NMR spectra, only one type of benzamidinate group was detected in d_5-pyridine solution. This suggests that the nature of the N---C---N bonding within the cage is insensitive to the metal set which coordinates to it, resulting in predominantly ionic bonding. Such a distinction between the ligands could not be made even at low temperature (188K). From the ^1H NMR spectrum (figure 3.12), a singlet was observed at 0.015ppm, which was assigned to the protons present on the trimethylsilyl groups. In the aromatic region, overlapping multiplets corresponding to the *meta-* and *para-* protons from the phenyl rings are observed (7.36-7.29ppm). The *ortho*-Ph protons are found to lie at a higher frequency (7.46ppm).

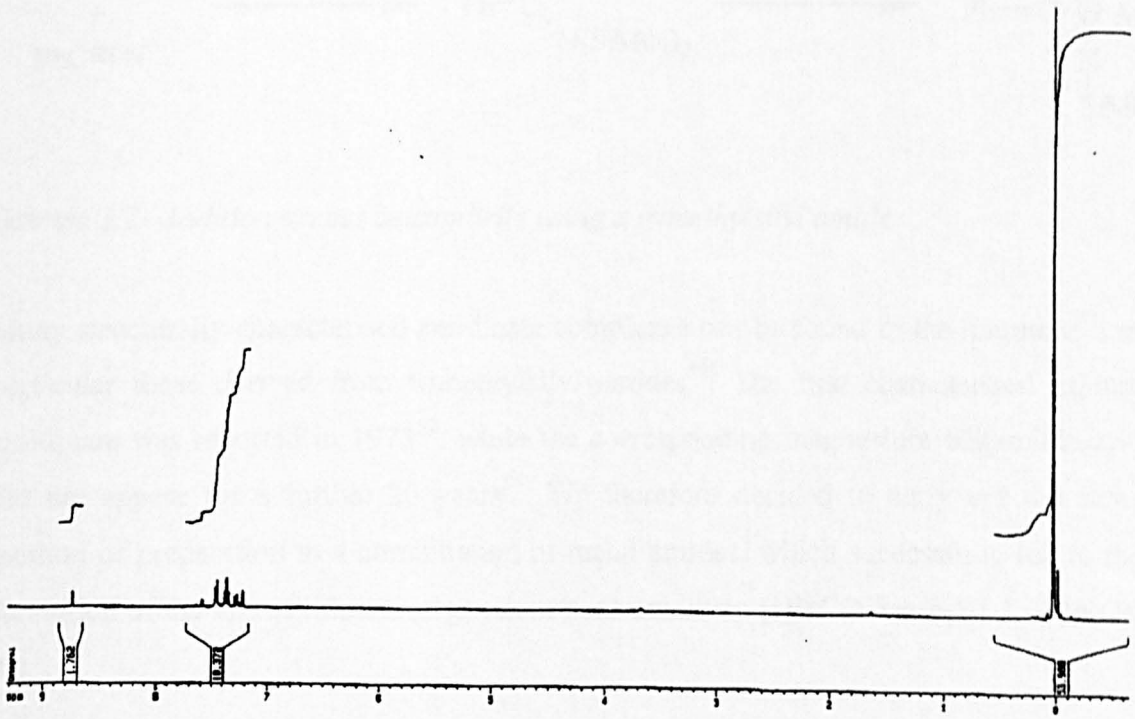

*Figure 3.12- ^1H NMR spectrum of $[\{PhC(NSiMe_3)_2\}_4Li_4Mg(O)]$ **3D** in d_5-pyridine at 300K*

From the $^{13}C\{^{1}H\}$ NMR spectrum the trimethylsilyl, *ipso*-C and aza-allyl carbons, N---C---N, were easily identified at 3.6, 149.3 and 178.4ppm respectively. In an attempt to distinguish the carbons on the phenyl ring, a ^{13}C-^{1}H correlated spectrum was run. This allowed the *ortho*-carbon at 126.6ppm to be distinguished, but not the *meta*- and *para*- carbons, which were only 1.8ppm apart.

The synthesis of compound **3D** was carried out several times and proved reproducible. However, yields were variable (maximum, 13%, based on dibutylmagnesium consumption). No rationale can, as yet be offered to explain the curious ratio of 4Li to 1Mg found in complex **3D**, prepared from a 1:1 stoichiometry. The four benzamidinate ligands present in this structure are formed from a well documented two-step addition/migration mechanism as shown in scheme 3.2.

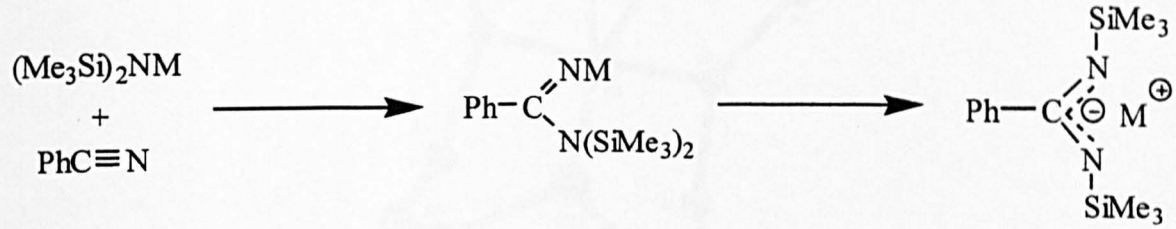

Scheme 3.2- Addition across benzonitrile using a trimethylsilyl amide

Many structurally characterised amidinate complexes can be found in the literature[51], in particular those derived from trimethylsilyl amides[52]. The first characterised lithium amidinate was reported in 1973[53], while the corresponding magnesium bis(amidinates) did not appear for a further 20 years[54]. We therefore decided to carry out the same method of preparation to a combination of metal amides, which successfully led to the formation of the mixed lithium/magnesium benzamidinate $[\{PhC(NSiMe_3)_2\}_4Li_4Mg(O)]$ **3D**.

3.8 X-Ray Crystallography of Compound 3D

The unique structure of [{PhC(NSiMe$_3$)$_2$}$_4$Li$_4$Mg(O)] **3D** (figure 3.9, pg.103) was revealed using X-ray crystallography. The unprecedented amidinate cage assembly is built around a central oxide anion, whereby four lithiums and one magnesium cation are arranged in a distorted trigonal bipyramidal geometry. Within this central core, both Li1 and Li1* define axial sites, and Mg1/Li2/Li2* define the equatorial plane (figure 3.13).

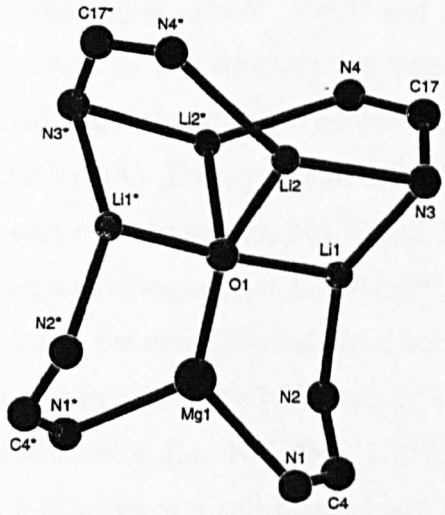

*Figure 3.13- View showing the central Li$_4$MgO core of structure **3D***

Disorder within this metal-oxide core limits the precision of the bond distances and bond angles (tables 3.8, 3.9, pg.102). The unprecedented cage structure is completed by the coordination of four benzamidinate ligands, which bind to the metal centres through bonds of considerable π character. This bonding mode is observed on examination of the NCN-metal fragments, where each metal atom in **3D** lies either above or below the NCN plane. In contrast, the NCN-metal fragments in purely σ-bonded systems are planar or approximately so. In the structure of **3D** there are two distinct types of amidinate-metal attachment (figure 3.14). In the first type, the NCN unit

assumes a bridging role, where each of the N atoms (N1, N2) coordinate to a single metal centre (Mg1 and Li1 respectively). The torsion angles Mg1N1C4N2 [15.0(5)°] and Li1N2C4N1 [49.6(6)°] clearly display a deviation from planarity. In the second type, the NCN ligand exhibits an unusual triangular-face capping mode, where N3 bridges the lithium centres Li1 and Li2, with torsion angles of 36.3(6)° (Li1N3C17N4) and 36.6(6)° (Li2N3C17N4). On the otherhand, N4 is bound terminally to a unique third lithium centre Li2* with a torsion angle of 10.3(8)° (Li2*N4C17N3). Thus as a result, N3 has a four-coordinate distorted tetrahedral geometry, while the remaining N atoms are three-coordinate possessing either distorted trigonal planar (N1 and N4) or pyramidal (N2) geometries [i.e. sum of bond angles, 359.6°, 359.7° and 350.4° respectively]. Both the magnesium and lithium centres in this structure are three-coordinate. The solitary magnesium occupies a distorted trigonal planar environment (note, that the magnesium binds only weakly to N1 at 2.471(4)Å). The equatorial Li2 possesses greater pyramidal character than axial Li1 [i.e. sum of bond angles, 344.9° and 356.5° respectively]. This, in part, reflects the sharper equatorial-equatorial Li2O1Li2* bond angle [76.7(7)° c.f. 83.2(4)° for Li1O1Li2], as well as the asymmetrical fit of each NCN ligand. The near-equivalent bond lengths within each half of the NCN unit of each benzamidinate ligand indicates almost uniform delocalisation [i.e. N1C4N2, 1.337(6)/1.331(6)Å; N3C17N4, 1.327(6)/1.328(6)Å]. This is indicative of a substantial ionic contribution to the metal-ligand bonding which is greatly enhanced by the strongly polarising trimethylsilyl groups attached to each N centre. The bond angles within the NCN three atom units show only a slight deviation from that of an ideal trigonal planar geometry (120°) [i.e. N1C4N2, 119.2(4)°; N3C17N4, 121.9(4)°], which suggests that the π-bonding is essentially maximised. The bulky trimethylsilyl groups and phenyl rings occupy the periphery of the cage structure in orientations least likely to disrupt the N---C---N bonding set.

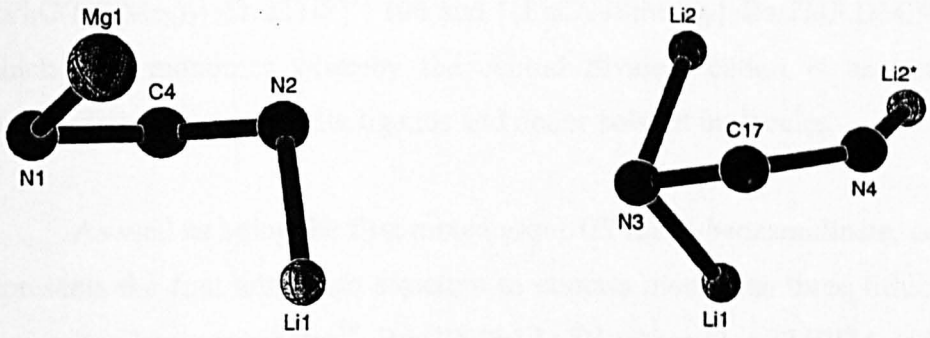

Figure 3.14- The two distinct NCN amidinate ligands present in structure 3D

The metal-oxide Li_4MgO core of structure **3D** bears comparison with that of the mixed-metal cresylate, $[LiMg_4O\{o\text{-}Me(C_6H_4)O\}_7.4THF]$ **81** (figure 3.4(a), pg.87), where a reversal in metal stoichiometry exists i.e. 1Li:4Mg in **81** c.f. 4Li:1Mg in **3D**. The shorter metal-oxide bond lengths present in complex **3D** indicate a more compact structure in comparison to **81** [i.e. **3D**, O(1)-Mg(1), 1.850(6)Å, O(1)-Li(1), 1.799(7)Å, O(1)-Li(2), 1.919(11)Å c.f. **81**, O-Mg, 2.002(4)Å/2.041(2)Å, O-Li, 1.89(2)Å].

At present only three magnesium amidinate crystal structures are reported in the literature: the monometallic bis(amidinate), $[\{PhC(NSiMe_3)_2\}_2Mg.N{\equiv}CPh]$[54] **102** prepared from the reaction of magnesium bis[bis(trimethylsilyl)amide] with three equivalents of benzonitrile; and, two isostructural mixed aluminium-magnesium amidinates[55], $[Me_2Al(Pr^i_2N)Mg\{RNC(Me)NR'\}]$, where R=R'=$Bu^t$ **103** or p-tolyl **104**, prepared from the reaction of alkyl(amido) mixed aluminium-magnesium complexes with selected carbodiimides. The bonding observed in these three structures is that of optimum N-Mg (σ, σ) interactions where each amidinate ligand chelates to the magnesium centre. This more efficient orbital overlap, is counterbalanced by the higher magnesium coordination numbers (5 and 4 respectively c.f. 3 in **3D**), hence the N-Mg bond distances involved (range 2.06-2.13Å) are in the same region as those found in **3D**. In addition to these magnesium examples, amidinate structures of other group 2 metals are reported in the literature e.g. $[\{PhC(NSiMe_3)_2\}_2Ca.2THF]$[56] **105**,

$[\{PhC(NSiMe_3)_2\}_2Sr.2THF]$[57] **106** and $[\{PhC(NSiMe_3)_2\}_2Ba.THF.DME]$[58] **107**, each of which is a monomer whereby the central divalent cation is encapsulated by two trimethylsilyl benzamidinate ligands and donor solvent molecules.

As well as being the first mixed group1/2 metal benzamidinate, complex **3D** also represents the first amidinate structure to contain more than three lithium centres. The monomeric benzamidinates[59], $[PhC(NPh)_2Li.D]$ where D = TMEDA **108** or PMDETA, **109**, resemble the aforementioned magnesium complexes, with symmetrical (σ, σ) N-Li bonding contained within, planar, four-membered NCNLi rings, the anions of which possess diazaallyl (N---C---N) character. This confirms the type of electronic structure when steric constraints are at a minimum. Upon dimerisation, steric factors come more into play so greater electronic and structural variety is observed. Most interestingly, the benzamidinate dimer $[\{PhC(NPh)_2Li.HMPA\}_2]$[59] **110**, exhibits a more localised N=C-N fragment, attributed to the unequal distribution of N-Li bonds (one N atom binds to two Li centres, while the other binds to one Li centre). In structure **3D**, the ligand fragment N3C17N4 also binds to unequal numbers of lithium centres, thus a similar non-uniform delocalisation at its N atoms would be expected, this however is not observed. This apparent conflict can be rationalised if the σ/π nature of the ligand-metal bonding is considered: in the HMPA dimer, **110**, two N-Li bonds are pure σ and the other has a high degree of π-character; whereas in **3D** all the bonds are π-based. Thus as a result the electronic distribution within N3C17N4 is more symmetrical. Dimerisation in two closely related methyl substituted benzamidinates $[\{4\text{-}XC_6H_4C(NSiMe_3)_2Li.base\}_2]$ (X = Me, base = THF[60] **111** or $p\text{-}MeC_6H_4C{\equiv}N$[61] **112**) is achieved differently from that in the HMPA system. Essentially, one NCN unit engages two lithium centres in a (σ, σ) manner, while the other engages them in a (π, π) coordination. To effect this, the dihedral angle between the distinct NCN planes is approximately 90°. The symmetrical nature of the NCN ligation thus leads to a pair of diazaallyl N---C---N bridges. Yet another mode of dimerisation is seen in the acetamidinate, $[\{MeC(NPh)_2Li.HMPA\}_2]$[59] **113**: where two HMPA molecules bridge two lithium centres to form a central $(OLi)_2$

ring. From the perspective of the anion, this structure simply constitutes two joined monomers, each with the familiar NCNLi ring. The trimeric benzamidinate, $[\{PhC(NSiMe_3)_2Li\}_3.N{\equiv}CPh]$[62] **114**, which is unusual in terms of coordination state possesses no special NCN ligating features: one binds in a (σ, σ) manner to two lithium centres, and two others bind in a chelating (π, π) manner to each of two lithium centres. The lithium centre which experiences only the latter type of bonding from two separate NCN ligands is also solvated by a benzonitrile molecule, which renders it five-coordinate, occupying a distorted square based pyramidal geometry.

The triangular-face capping linkage observed for the N3C17N4 ligand in **3D** finds analogy with that of the transition metal cluster, $[Os_3(\mu\text{-}H)(CO)_9\{PhNC(Ph)NH\}]$[63] **115** (figure 3.15). The three osmium centres define an isosceles triangle one edge of which is bridged by the protonated nitrogen atom of the NPhC(Ph)NH ligand; the other nitrogen atom is terminally bound to the third osmium atom in an axial site. By this mode, the amidinide ligand caps one triangular face of the metal framework and formally donates five electrons to the cluster. However the analogy is limited, as compound **115** contains formal metal-metal bonding and **3D** does not.

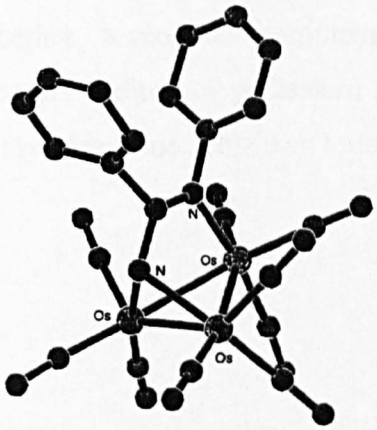

*Figure 3.15- Crystal structure of $[Os_3(\mu\text{-}H)(CO)_9\{PhNC(Ph)NH\}]$ **115**, (hydrogen atoms are omitted for clarity)*

Chapter Three (Part 2) – Macrocyclic Amide Ring Systems Containing a Mixture of S-Block Metals

Aims

- To discuss the analysis and X-ray crystallographic characterisation of several unprecedented macrocyclic ring architectures containing both group 1 and group 2 metals.
- To introduce the crystal structure of the first potassium magnesate, $[\{(Me_3Si)_2N\}_6K_2Mg_2.4\{C_6H_5(CH_3)\}]$, and to discuss its implication for the formation of the aforementioned macrocyclic amides.

3.9 Introduction

The syntheses carried out in this section follows on from the preparation of $[\{(Me_3Si)_2N\}_4Li_2Mg_2(O_2)_x(O)_y]$ **3C** (pg.97) which was found to adopt a $(NM)_4$ heterometallic ring incorporating either oxide or peroxide dianions at its core. It was thus decided to discover whether analogous complexes could be synthesised incorporating the larger alkali metals sodium or potassium accompanied by the bulky secondary amine 2,2,6,6-tetramethylpiperidine. This was found to be the case.

Chapter Three

Experimental (Part 2)

3.10 Chapter Three Experimental (Part 2)

Reaction 3.5: Synthesis of $[\{Me_2\overline{CCH_2CH_2CH_2(Me)_2CN}\}_4Li_2Mg_2(O)]$, 3E

n-BuLi (5mmol in hexane, 3.45ml of a 1.45M solution) was added to a solution of DBM (10mmol in heptane, 10ml of a 1.0M solution). Five equivalents of oxygenated 2,2,6,6-tetramethypiperidine (4.23ml, 25mmol) was then added to the mixture in a dropwise manner. Immediately, a vigorous reaction ensued with the formation of an orange precipitate. This precipitate dissolved upon the addition of oxygenated toluene (10ml) and warming. The solution was left to stand at ambient temperature, overnight, whereby the orange colour deepened to a dark red accompanied by the formation of colourless needle crystals. These crystals were subsequently isolated and identified as a mixture of title complex $[\{Me_2\overline{CCH_2CH_2CH_2(Me)_2CN}\}_4Li_2Mg_2(O)]$ **3E** and the all-lithium derivative, $[\{Me_2\overline{CCH_2CH_2CH_2(Me)_2CN}\}_4Li_4]$ in a ratio of (13:1) respectively.

Yield:	0.34g (10.4%) based on consumption of DBM
Melting Point:	192-194°C (decomp.)
Elemental Analysis:	$0.93(C_{36}H_{72}N_4Mg_2Li_2O)$. $0.07(C_{36}H_{72}N_4Li_4)$
Calculated	C, 68.0; H, 11.4; N, 8.8; Li, 2.4; Mg, 7.1; O, 2.3%
Found	C, 68.0; H, 11.9; N, 7.8; Li, 2.6; Mg, 7.6%

Infrared / cm^{-1} (nujol mull)

2805br, 1230w, 1125s, 998w/s, 889s/w, 789s, 591m/br

On exposure to air a broad signal between 3050-3670cm^{-1} was observed indicating hydrolysis and the regeneration of free amine i.e. $[Mg(OH)_2$, LiOH, H_2O and N-H].

^{1}H NMR (400MHz, d_8-toluene, 300K)

Assignment of protons in TMPH ligand.

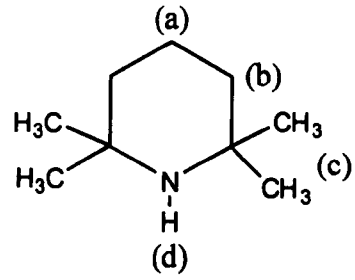

Chemical shift δ/ppm	Splitting pattern	Relative integral	Assignment
1.71	multiplet	1H	CH_2 (a) in **3E**
1.57-1.51	multiplet	2H	CH_2 (b) in **3E**
1.50	multiplet	—	CH_2 (a) in TMPH
1.39	singlet	6H	CH_3 (c) in **3E**
1.27-1.21	multiplet	—	CH_2 (b) in TMPH
1.05	singlet	—	CH_3 (c) in TMPH
0.27	broad singlet	—	N-H in TMPH

In this spectrum a small amount of residual TMPH was present.

^{13}C NMR spectrum (^{1}H-decoupled, 100MHz, d_8-toluene, 300K)

Assignment of carbons in TMPH ligand.

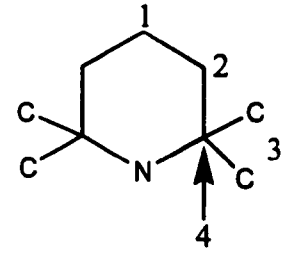

Chemical shift δ/ppm	Assignment
51.8	C – 4 in **3E**
49.6	C – 4 in TMPH
42.4	C – 2 in **3E**
38.7	C – 2 in TMPH
36.9	C – 3 in **3E**
32.0	C – 3 in TMPH
19.7	C – 1 in **3E**
18.9	C – 1 in TMPH

^{7}Li NMR spectrum in d_8-toluene at 300K, 155.50 MHz (externally referenced to LiCl in D_2O, 0.0ppm)

Two sharp lithium signals were observed at 2.52ppm and 0.87ppm with relative integrals 13:1 respectively. Thus the more downfield signal can be assigned to the mixed lithium magnesium complex, [{$Me_2CCH_2CH_2CH_2(Me)_2CN$}$_4Li_2Mg_2(O)$] **3E** and the further upfield signal can be assigned to the all-lithium derivative, [{$Me_2CCH_2CH_2CH_2(Me)_2CN$}$_4Li_4$].

Crystal Structure

X-ray crystallographic studies of a selected crystal with dimensions 0.80x0.40x0.30mm were undertaken. These divulged the, mixed lithium/magnesium, oxide-centred amide, [{$Me_2CCH_2CH_2CH_2(Me)_2CN$}$_4Li_2Mg_2(O)$] **3E** (figure 3.16). The final R factor was 0.049. Other crystallographic parameters are presented in Appendix III.

Table 3.11: Selected bond distances (Å) in **3E**

M(1)-O(1)	1.8616(9)	**M(2)-N(2)**	2.134(15)
M(1)-O(1*)	1.8615(9)	**M(2)-N(1*)**	2.094(15)
M(1)-N(1)	2.159(16)	**M(1)-N(2)**	2.126(16)

Where M1 is the Mg(1)/Li(1) site and M(2) is the Mg(2)/Li(2) site.

Table 3.12: Selected bond angles (°) in **3E**

N(1)-M(1)-N(2)	167.38(7)	**O(1)-M(1)-N(2)**	96.88(5)
M(1)-N(2)-M(2)	76.44(5)	**O(1)-M(1)-N(1)**	95.73(5)
N(1*)-M(2)-N(2)	165.49(6)	**M(1)-O(1)-M(2)**	90.09(4)

Where M1 is the Mg(1)/Li(1) site and M(2) is the Mg(2)/Li(2) site.

Symmetry transformations used to generate equivalent atoms: (*) = 3/2-x, 1/2-y, 1-z

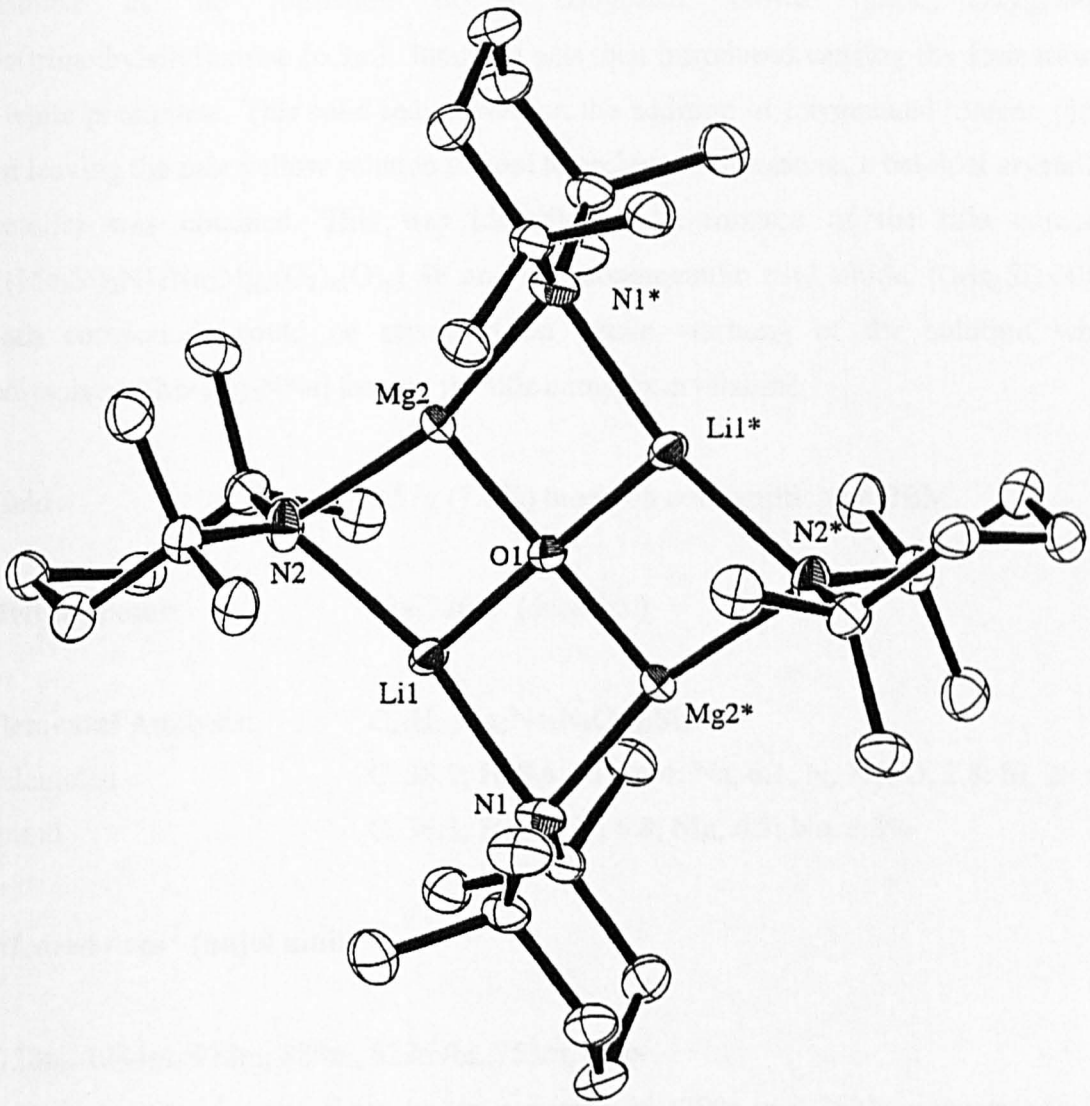

*Figure 3.16- Crystal structure of [{$Me_2CCH_2CH_2CH_2(Me)_2CN$}$_4Li_2Mg_2(O)$] **3E**, (hydrogen atoms are omitted for clarity)*

Reaction 3.6: Synthesis of $[\{(Me_3Si)_2N\}_4Na_2Mg_2(O_2)_x(O)_y]$, 3F

Freshly prepared *n*-BuNa (0.8g, 10mmol) was suspended in oxygenated hexane (10ml) and ultrasounded until a milky suspension formed. To this suspension was added an equimolar amount of DBM (10mmol in heptane, 10.4ml of a 0.96M solution) which resulted in the formation of a congealed brown mass. Oxygenated, bis(trimethylsilyl)amine (6.3ml, 30mmol) was then introduced causing the formation of a white precipitate. This solid redissolved on the addition of oxygenated toluene (8ml). On leaving the pale yellow solution to cool to ambient temperature, a batch of crystalline material was obtained. This was identified as a mixture of the title complex, $[\{(Me_3Si)_2N\}_4Na_2Mg_2(O_2)_x(O)_y]$ **3F** and the monometallic silyl amide, $[(Me_3Si)_2NNa]$. Both compounds could be separated on gentle warming of the solution which redissolved $[(Me_3Si)_2NNa]$ leaving the title complex crystalline.

Yield:	0.57g (7.6%) based on consumption of DBM
Melting Point:	224-226°C (decomp.)
Elemental Analysis:	$C_{24}H_{72}Mg_2Na_2N_4O_{1.32}Si_8$
Calculated	C, 38.1; H, 9.6; Mg, 6.4; Na, 6.1; N, 7.4; O, 2.8; Si, 29.6%
Found	C, 36.3; H, 9.5; N, 6.8; Mg, 6.3; Na, 8.3%

Infrared / cm^{-1} (nujol mull)

2730w, 1244m, 978m, 884m, 829m/br, 753m, 664s

On exposure to air, two sharp bands appeared at 3700s and 3623s corresponding to $Mg(OH)_2$ and Na(OH) respectively. A broad signal also appeared at 3373br which can be assigned as N-H from regeneration of free amine.

^{1}H NMR (400MHz, d_8-toluene, 300K)

Chemical shift δ/ppm	Splitting pattern	Relative integral	Assignment
0.31	multiplet	3H	unknown
0.29	multiplet	4H	unknown
0.17	singlet	18H	$SiMe_3$ (oxide)
0.16	shoulder	—	$SiMe_3$ (peroxide)
0.08	singlet	4H	'Free' $(Me_3Si)_2NH$

^{13}C NMR spectrum (^{1}H-decoupled, 100MHz, d_8-toluene, 300K)

Chemical shift δ/ppm	Assignment
14.49	unknown
12.06	unknown
7.32	unknown
6.47	$SiMe_3$ (oxide)
2.59	'Free' $(Me_3Si)_2NH$

Crystal Structure

X-ray crystallographic studies of a selected crystal with dimensions 0.70x0.40x0.40mm were undertaken. These divulged the, mixed sodium/magnesium, oxide-peroxide amide, $[\{(Me_3Si)_2N\}_4Na_2Mg_2(O_2)_x(O)_y]$, **3F** (figure 3.17). The final R factor was 0.0295. Other crystallographic parameters are presented in Appendix III.

Table 3.13: Selected bond distances (Å) in **3F**

Mg(1)-O(1)	2.007(4)	**Mg(1)-N(2)**	2.049(1)
Na(1)-O(1)	2.328(7)	**Na(1)-N(1*)**	2.549(1)
Mg(1)-N(1)	2.054(1)	**Na(1)-N(2)**	2.595(1)

Table 3.14: Selected bond angles (°) in **3F**

N(1)-Mg-N(2)	141.60(5)	**Mg-N(1)-Na(1*)**	78.76(4)
N(1*)-Na(1)-N(2)	59.84(2)	**Mg(1)-N(2)-Na(1)**	79.86(4)

Symmetry transformations used to generate equivalent atoms: (*) = -x, 1-y, 1-z

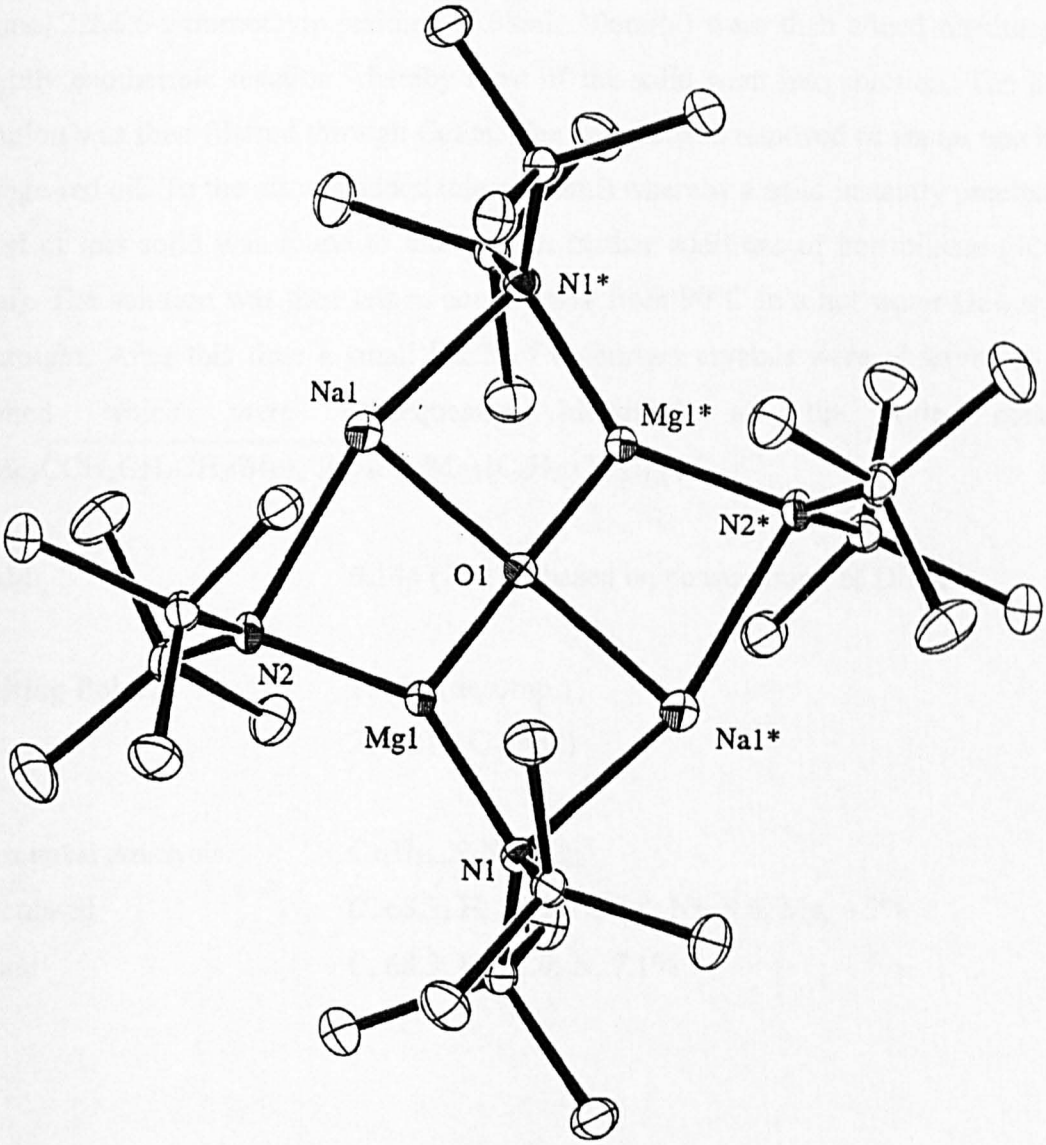

Figure 3.17- Crystal structure of [{(Me$_3$Si)$_2$N}$_4$Na$_2$Mg$_2$(O$_2$)$_x$(O)$_y$] ***3F****, (hydrogen atoms are omitted for clarity)*

Reaction 3.7: Synthesis of $[\{Me_2\overline{CCH_2CH_2CH_2(Me)_2CN}\}_6Na_4Mg_2\{C_6H_3(CH_3)\}]$, 3G

Freshly prepared *n*-BuNa (0.8g, 10mmol) was suspended in hexane (10ml) and ultrasounded for five minutes until a fine, cream-coloured suspension formed. To this was added an equimolar amount of DBM (10mmol in heptane, 10.9ml of a 0.92M solution) resulting in the formation of a congealed brown mass. Three equivalents of the amine, 2,2,6,6-tetramethylpiperidine (5.08ml, 30mmol) were then added resulting in a slightly exothermic reaction whereby most of the solid went into solution. The orange solution was then filtered through Celite. The hexane was removed *in vacuo* leaving an orange-red oil. To the oil was added toluene (5ml) whereby a solid instantly precipitated. Most of this solid was found to dissolve on further additions of hot toluene (40ml in total). The solution was then left to cool slowly from 90°C in a hot water Dewar flask overnight. After this time a small batch of colourless crystals were observed to have formed which were subsequently identified as the title complex, $[\{Me_2\overline{CCH_2CH_2CH_2(Me)_2CN}\}_6Na_4Mg_2\{C_6H_3(CH_3)\}]$ **3G**.

Yield:	0.14g (26.1%) based on consumption of DBM
Melting Point:	180°C (decomp.) 210-211°C (melt)
Elemental Analysis:	$C_{61}H_{114}N_6Na_4Mg_2$
Calculated	C, 68.3; H, 10.7; N, 7.8; Na, 8.6, Mg, 4.5%
Found	C, 68.3; H, 11.0; N, 7.1%

^{1}H NMR (400MHz, d_6-DMSO, 300K)

Assignment of protons in TMP ligand and metallated toluene molecule.

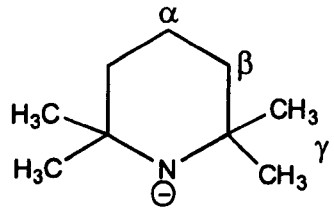

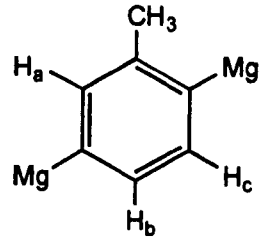

Chemical shift δ/ppm	Splitting pattern	Relative integral	Assignment
7.36	singlet	1/6 H	C_6H_6 (cont.)
7.24	doublet	1H	H_b (tol)
7.17-7.13	singlet / doublet (ovl.)	2H	H_a , H_c (tol)
2.28	multiplet	3H	CH_3 (tol)
1.56	multiplet	17H	H_α (TMP)
1.23	multiplet	34H	H_β (TMP)
1.02	singlet	102H	H_γ (TMP)

Where ovl. = overlap and cont. = contaminant

$^3J_{Hb\text{-}Hc}$=7.2 Hz

Unfortunately, there was not enough sample to carry out ^{13}C NMR studies.

Crystal Structure

X-ray crystallographic studies of a selected crystal with dimensions 0.70x0.40x0.40mm were undertaken. These divulged the mixed sodium/magnesium tetramethylpiperidide complex, $[\{Me_2CCH_2CH_2CH_2(Me)_2CN\}_6Na_4Mg_2\{C_6H_3(CH_3)\}]$ **3G** (figure 3.18). The final R factor was 0.044. Other crystallographic parameters are presented in Appendix III.

Table 3.15: Selected bond distances (Å) in **3G**

Mg(1)-N(1)	2.048(2)	**Mg(1)-C(28)**	2.200(2)	**Na(1)-N(3)**	2.393(2)
Mg(1)-N(2)	2.051(2)	**Na(1)-C(28)**	2.691(2)		
Na(1)-N(2)	2.626(2)	**Na(2)-C(28*)**	2.682(2)		
Na(2)-N(3)	2.350(2)	**Na(2)-N(1*)**	2.596(2)		

Table 3.16: Selected bond angles (°) in **3G**

N(1)-Mg(1)-N(2)	142.85(7)	**N(2)-Na(1)-N(3)**	156.25(6)
N(1)-Mg(1)-C(28)	109.75(7)	**N(2)-Na(1)-C(28)**	80.18(6)
N(2)-Mg(1)-C(28)	107.32(7)	**N(3)-Na(1)-C(28)**	123.31(7)

Symmetry transformations used to generate equivalent atoms: (*) = 1-x, 1-y, 1-z

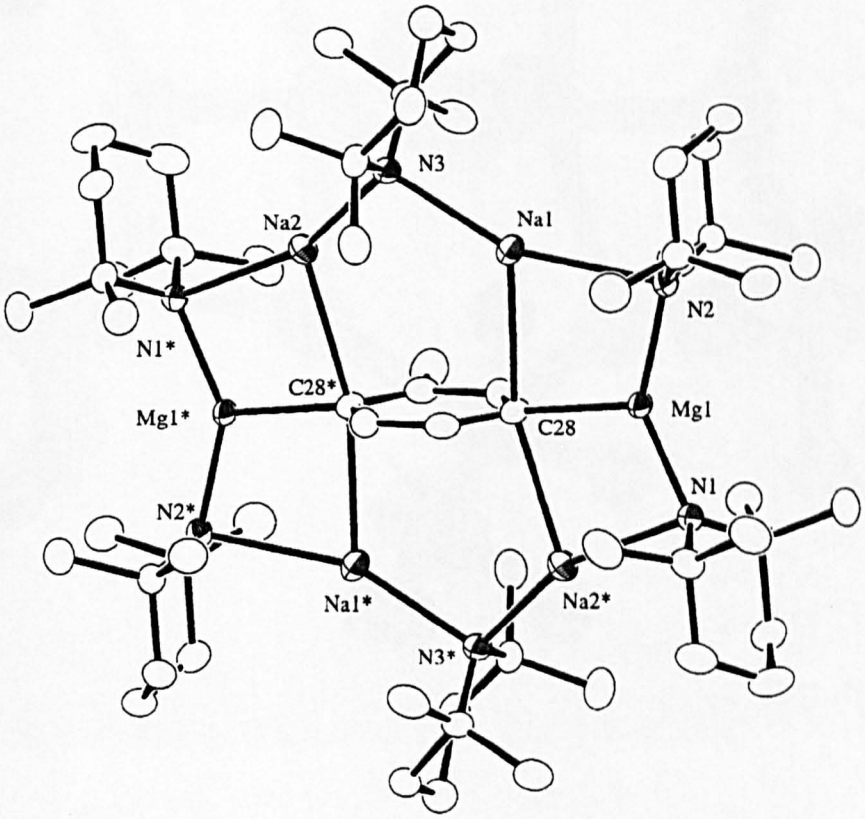

Figure 3.18(a)- Crystal structure of [{Me$_2$CCH$_2$CH$_2$CH$_2$(Me)$_2$CN}$_6$Na$_4$Mg$_2${C$_6$H$_3$(CH$_3$)}] ***3G*** *(in black and white), (hydrogen atoms are omitted for clarity)*

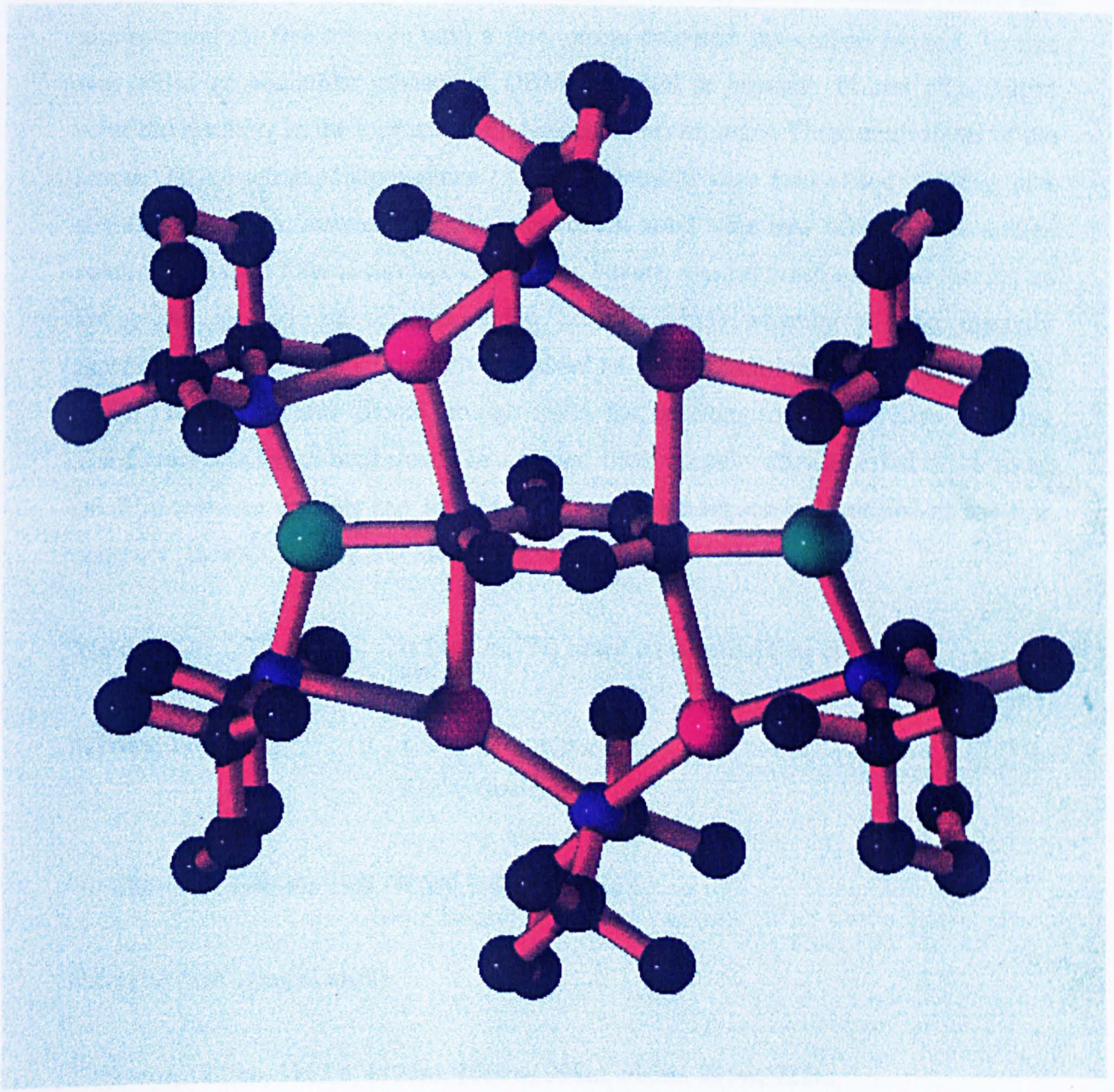

Figure 3.18(b)- Crystal structure of $[\{Me_2CCH_2CH_2CH_2(Me)_2CN\}_6Na_4Mg_2\{C_6H_3(CH_3)\}]$ ***3G*** *(in colour), (hydrogen atoms are omitted for clarity)*

Reaction 3.8: Synthesis of $[\{Me_2\overline{CCH_2CH_2CH_2(Me)_2CN}\}_6Na_4Mg_2(C_6H_4)\}]$, 3H

Freshly prepared *n*-BuNa (0.8g, 10mmol) was suspended in hexane (10ml) and ultrasounded for five minutes until a fine, cream-coloured suspension formed. To this was added an equimolar amount of DBM (10mmol in heptane, 11.2ml of a 0.90M solution) resulting in the formation of a congealed brown mass. Three equivalents of the amine, 2,2,6,6-tetramethylpiperidine (5.08ml, 30mmol) were then added resulting in a slightly exothermic reaction whereby most of the solid went into solution. The orange solution was then filtered through Celite. The hexane was removed *in vacuo* leaving an orange-red oil. To the oil was added benzene (5ml) whereby a solid instantly precipitated. The solid only partially dissolved on further additions of benzene (40ml in total). The solution was filtered through celite, hot, resulting in a clear yellow solution. The filtrate was left to cool slowly in a Dewar flask whereby after a period of 16 hours small needle-like crystals had formed. These were subsequently identified as the title complex $[\{Me_2\overline{CCH_2CH_2CH_2(Me)_2CN}\}_6Na_4Mg_2(C_6H_4)\}]$ **3H**.

Yield: 0.14g (26.7%) based on consumption of DBM

Melting Point: 175°C (decomp.)
222°C (melt)

No elemental analyses were carried out

Infrared / cm^{-1} (nujol mull)

2750w/br, 1229m, 1167w, 1123m, 1069w, 998m, 885m, 855w, 721m
On exposure to air, a very broad band appeared, centred at 3410br. This can be assigned to the hydrolysis products, NaOH, H_2O and free amine. A sharp signal also appeared at 3702m which corresponds to that of $Mg(OH)_2$.

^{1}H NMR (400MHz, d_6-DMSO, 300K)

Assignment of protons in TMP ligand.

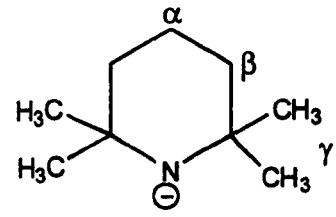

Chemical shift δ/ppm	Splitting pattern	Relative integral	Assignment
7.37	singlet	4H	C_6H_3
1.57	multiplet	19H	H_α (TMP)
1.24	multiplet	38H	H_β (TMP)
1.03	singlet	114H	H_γ (TMP)

^{13}C NMR spectrum (^{1}H-decoupled, 100MHz, d_6-DMSO, 300K)

Assignment of carbons in TMP ligand.

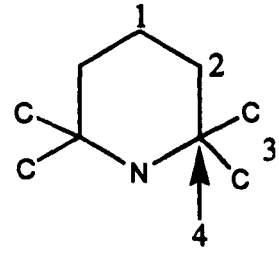

Chemical shift δ/ppm	Assignment
128.3	*ipso*-Ph (C_6H_3)
128.1	C-H (C_6H_3)
48.9	C – 4 (TMP)
37.8	C – 2 (TMP)
31.4	C – 3 (TMP)
18.0	C – 1 (TMP)

Crystal structure

X-ray crystallographic studies of a selected crystal with dimensions 0.40x0.15x0.12mm were undertaken. These divulged the mixed sodium/magnesium tetramethylpiperidide complex, $[\{Me_2CCH_2CH_2CH_2(Me)_2CN\}_6Na_4Mg_2(C_6H_4)]$ **3H** (figure 3.19). The final R factor was 0.062. Other crystallographic parameters are presented in Appendix III.

Table 3.17: Selected bond distances (Å) in **3H**

Mg(1)-N(1)	2.049(4)	**Na(2)-N(1*)**	2.591(4)	**Na(2)-C(28*)**	2.676(5)
Mg(1)-N(2)	2.037(4)	**Na(1)-N(3)**	2.387(4)		
Na(2)-N(3)	2.350(4)	**Mg(1)-C(28)**	2.192(5)		
Na(1)-N(2)	2.603(4)	**Na(1)-C(28)**	2.689(4)		

Table 3.18: Selected bond angles (°) in **3G**

Mg(1)-N(1)-Na(2)	86.6(1)	**N(2)-Mg(1)-C(28)**	107.4(2)
Mg(1)-N(2)-Na(1)	88.1(1)	**N(3)-Na(2)-C(28)**	117.6(1)
Na(1)-N(3)-Na(2)	101.4(1)	**N(1)-Na(2)-N(3)**	159.9(1)

Symmetry transformations used to generate equivalent atoms: (*) = 1-x, 1-y, 1-z

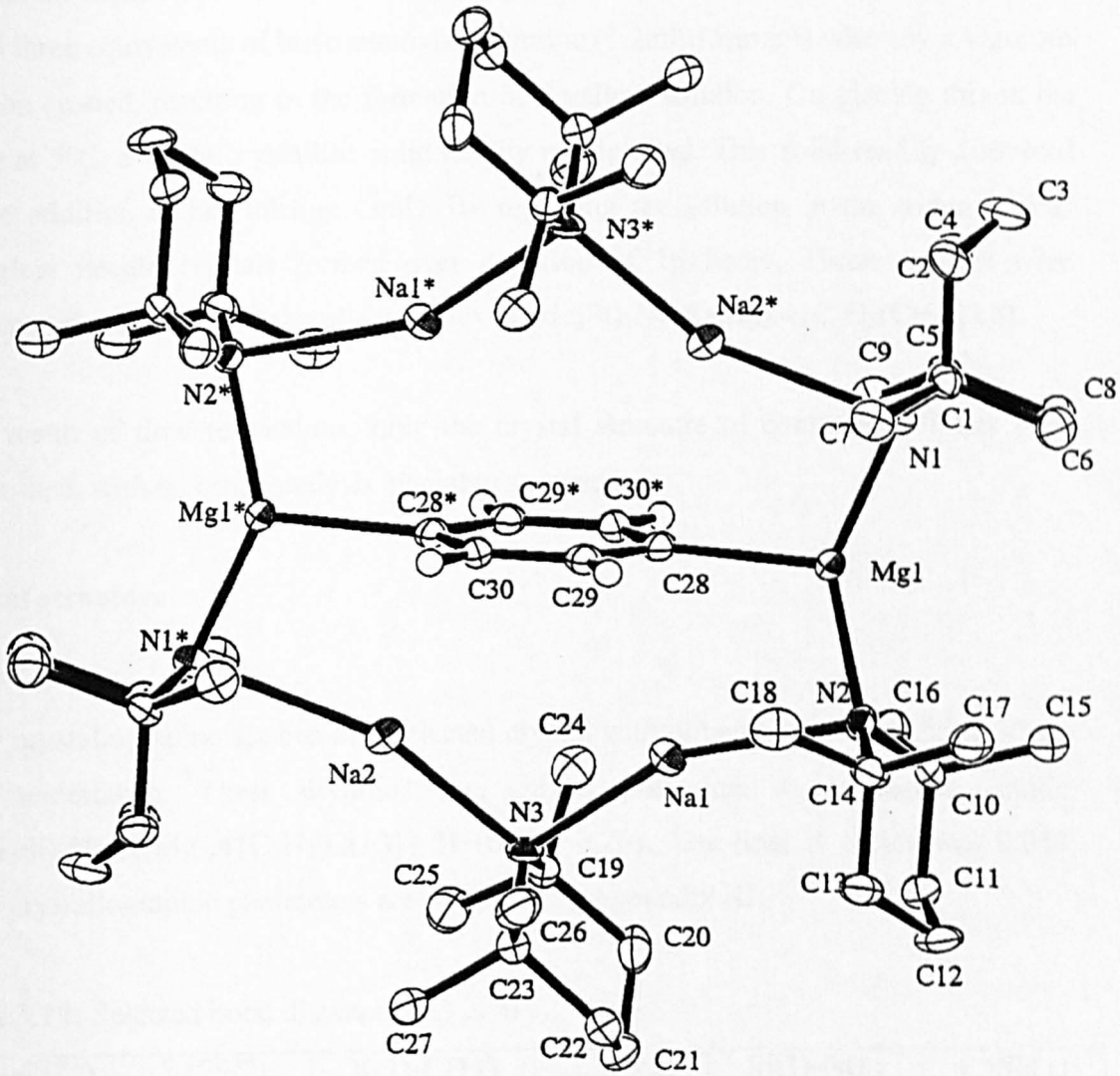

Figure 3.19- Crystal structure of $[\{Me_2\overline{CCH_2CH_2CH_2(Me)_2CN}\}_6Na_4Mg_2(C_6H_4)]$ ***3H***, *(hydrogen atoms omitted for clarity)*

Reaction 3.9: Synthesis of $[\{(Me_3Si)_2N\}_6K_2Mg_2.4\{C_6H_5(CH_3)\}]$, 3I

Freshly prepared *n*-BuK (0.48g, 5mmol) was suspended in hexane (10ml) and ultrasounded until a fine dark suspension formed. An equimolar amount of DBM (5mmol in heptane, 5.0ml of a 1.0M solution) was then added. To this mixture was added three equivalents of bis(trimethylsilyl)amine (3.2ml, 15mmol) whereby a vigorous reaction ensued, resulting in the formation of a yellow solution. On placing this in the fridge at 5°C, a white crystalline solid readily precipitated. This solid readily dissolved on the addition of hot toluene (3ml). By replacing the solution in the fridge at 5°C colourless needle crystals formed over a period of 16 hours. These crystals were subsequently identified as the title complex $[\{(Me_3Si)_2N\}_6K_2Mg_2.4\{C_6H_5(CH_3)\}]$ **3I**.

As a result of time restrictions, only the crystal structure of compound **3I** has been determined, with no other analysis available at present.

Crystal structure

X-ray crystallographic studies of a selected crystal with dimensions 0.75x0.55x0.50mm were undertaken. These divulged the, mixed potassium / magnesium amide, $[\{(Me_3Si)_2N\}_6K_2Mg_2.4\{C_6H_5(CH_3)\}]$ **3I** (figure 3.20). The final R factor was 0.033. Other crystallographic parameters are presented in Appendix III.

Table 3.19: Selected bond distances (Å) in **3I**

K(1)···C(3*)	3.129(2)	**K(1)-C(19)**	3.216(2)	**Si(1)-N(1)**	1.698(1)
K(1)···C(17)	3.399(2)	**K(1)-C(20)**	3.221(2)	**Si(1)-C(3)**	1.900(2)
Mg(1)-N(1)	2.020(1)	**K(1)-C(21)**	3.255(2)	**Si(6)-N(3)**	1.697(1)
Mg(1)-N(3)	2.026(1)	**K(1)-C(22)**	3.282(2)	**Si(6)-C(17)**	1.888(2)

Table 3.20: Selected bond angles (°) in **3I**

N(1)-Mg(1)-N(2)	120.81(6)	**C(3)-K(1)-C(20)**	107.15(6)
N(2)-Mg(1)-N(3)	119.18(6)	**C(3*)-K(1)-C(19)**	82.63(5)
N(1)-Mg(1)-N(3)	120.01(6)	**C(3*)-K(1)-C(23)**	89.95(6)

Symmetry transformations used to generate equivalent atoms: (*) = 2-x, -y, 1-z

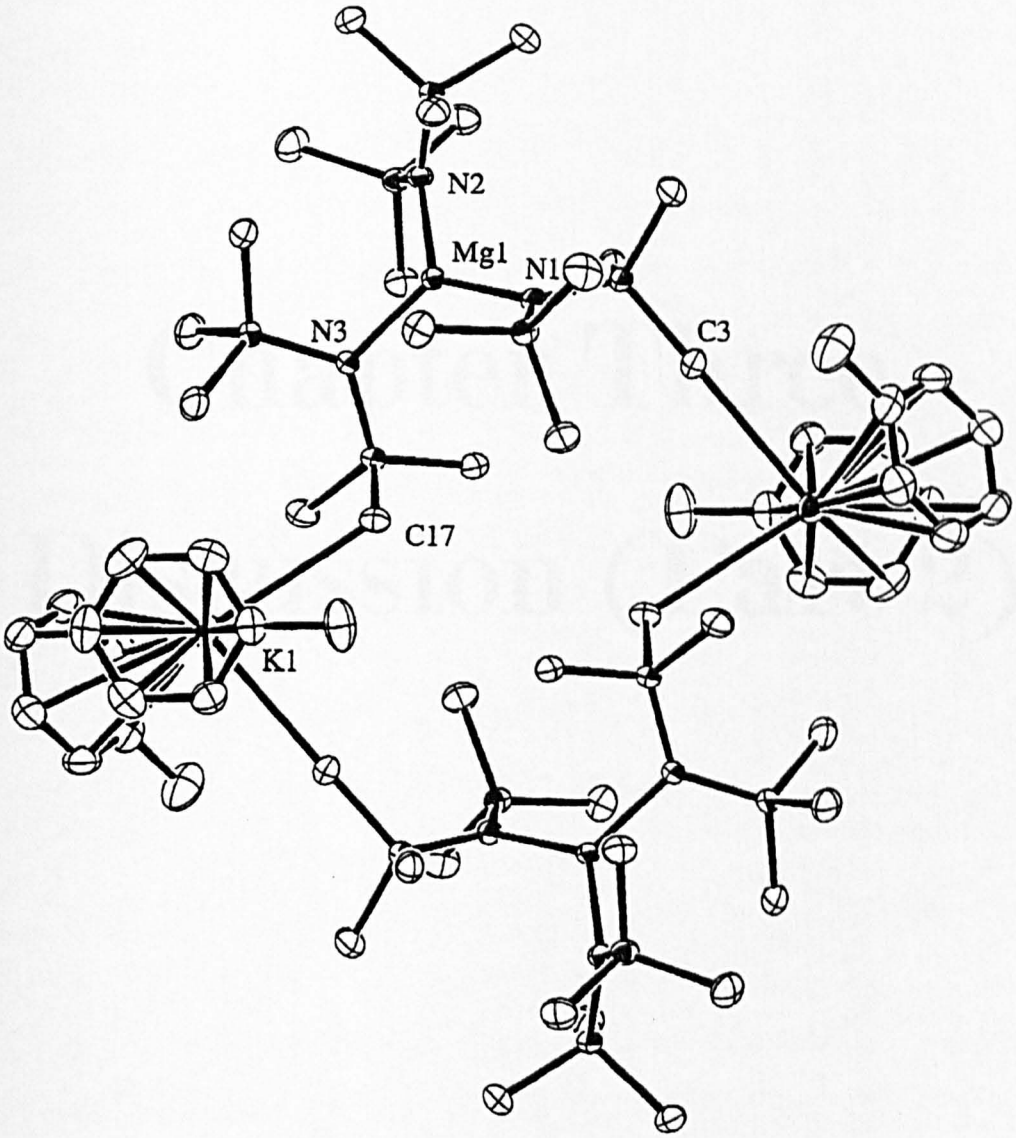

Figure 3.20- Crystal structure of $[\{(Me_3Si)_2N\}_6K_2Mg_2.4\{C_6H_5(CH_3)\}]$ ***3I****, (hydrogen atoms are omitted for clarity)*

Chapter Three

Discussion (Part 2)

3.11 Synthesis and Analysis of Compounds 3E and 3F

The syntheses of both $[\{Me_2\overline{CCH_2CH_2CH_2(Me)_2CN}\}_4Li_2Mg_2(O)]$ **3E** and $[\{(Me_3Si)_2N\}_4Na_2Mg_2(O_2)_x(O)_y]$ **3F** were carried out in a similar manner to that of the aforementioned mixed lithium-magnesium, peroxo-oxo complex **3C** (pg.97), whereby dioxygen was deliberately introduced into the reaction systems, via oxygenation of amines and solvents.

In the synthesis of compound **3E**, five equivalents of TMPH were added to a 1:2 mixture of *n*-BuLi / *n,s*-Bu_2Mg (equation 3.7). A vigorous reaction ensued accompanied by the formation of an orange precipitate. This solid redissolved on the addition of oxygenated toluene. On leaving the solution to stand at ambient temperature, colourless needle crystals formed. The addition of two equivalents of DBM was found necessary as this increased the yield of **3E** in relation to that of the monometallic lithium derivative $[\{Me_2\overline{CCH_2CH_2CH_2(Me)_2CN}\}_4Li_4]$, (LiTMP), which was found to co-crystallise in the unit cell i.e. 1:1 ratio: 61.0% **3E**; 39.0% LiTMP c.f. 1:2 ratio; 93.0% **3E**; 7.0% LiTMP.

$$n\text{-BuLi} + 2\,n,s\text{-}Bu_2Mg + 5\,Me_2\overline{CCH_2CH_2CH_2(Me)_2CNH} \xrightarrow[-(x+y)\,BuH]{O_2} x[\{Me_2\overline{CCH_2CH_2CH_2(Me)_2CN}\}_4Li_2Mg_2(O)] + y[\{Me_2\overline{CCH_2CH_2CH_2(Me)_2CN}\}_4Li_4] + z\,\text{other products} \quad (3.7)$$

The synthesis of complex **3F** was carried out using a 1:1:3 mixture of *n*-BuNa / *n, s* – Bu_2Mg / $(Me_3Si)_2NH$ which produced a white precipitate (equation 3.8). This solid was found to redissolve on the addition of oxygenated toluene. On leaving the solution to cool to ambient temperature a large batch of crystalline material formed, which was found to be a mixture of complex **3F** and that of the monometallic silyl amide, $[(Me_3Si)_2NNa]$, (NaHMDS). The separation of both compounds was easily achieved by

gently heating the solution whereby the monometallic derivative redissolved, leaving the mixed metal complex **3F** unperturbed.

$$n\text{-BuNa} + n,s\text{-Bu}_2\text{Mg} + 3\,(\text{Me}_3\text{Si})_2\text{NH} \xrightarrow{O_2} [\{(\text{Me}_3\text{Si})_2\text{N}\}_4\text{Na}_2\text{Mg}_2(\text{O}_2)_x(\text{O})_y] + [(\text{Me}_3\text{Si})_2\text{NNa}] + \text{other products} \quad (3.8)$$

The formation of both complexes **3E** and **3F**, were confirmed using melting point analysis, where the melting points of these compounds were found to be considerably higher than those of the monometallic derivatives i.e. **3E**, 192-194°C c.f. 165-167°C in LiTMP; **3F**, 224-226°C c.f. 175°C in NaHMDS.

Satisfactory elemental analyses were obtained in both cases. Metal analysis and infrared spectroscopy confirmed the presence of two metals in each complex. On exposure to air metal hydroxide bands were evident which were accompanied with that of the free amine i.e. **3E**, broad band between 3050-3670cm^{-1} corresponding to $Mg(OH)_2$, LiOH, H_2O and N-H; **3F**, two sharp signals were observed at 3700s and 3623s corresponding to $Mg(OH)_2$ and NaOH respectively, free amine was also found at 3373m.

Both compounds **3E** and **3F** were not washed prior to NMR characterisation, thus in these spectra small traces of the free amine were apparent.

The ^{1}H NMR spectrum of compound **3E** in d_8-toluene (figure 3.21) shows clearly the protons of the tetramethylpiperidide ligand, possessing integral values 1:2:6, corresponding to protons of type (a), (b) and (c) respectively as shown below (the N-H (d) is missing as expected).

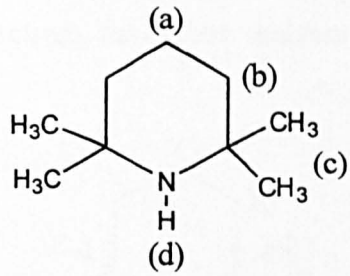

A comparison of the ^{1}H chemical shifts of the parent amine and metallated complex **3E** are shown in table 3.21.

Compound	Protons (a) / ppm	Protons (b) / ppm	Protons (c) / ppm
TMPH	1.50	1.24-1.21	1.05
3E	1.71	1.57-1.51	1.39

Table 3.21- Comparison of ^{1}H chemical shifts

It is observed that on metallation all protons undergo a significant high frequency shift corresponding to a deshielding effect around the TMP ring.

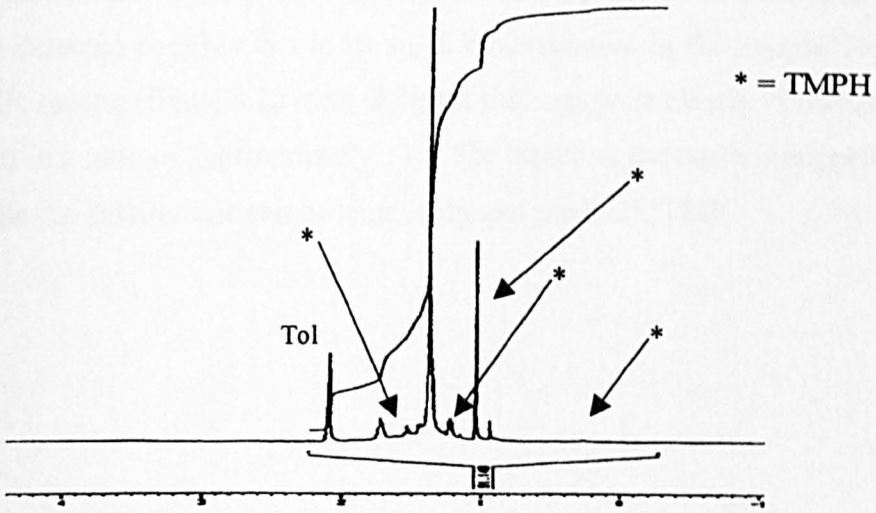

*Figure 3.21- ^{1}H NMR spectrum of compound **3E** in d_8-toluene at 300K*

Turning to the $^{13}C\{^1H\}$ NMR spectrum, the carbon skeleton of the tetramethylpiperidide ligand is shown below.

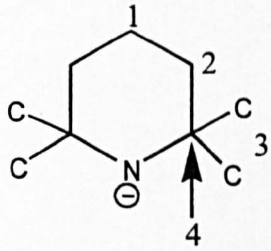

A similar deshielding effect is also observed in the $^{13}C\{^1H\}$ spectrum in comparison to that of the free amine as shown in table 3.22.

Compound	C-4 / ppm	C-3 / ppm	C-2 / ppm	C-1 / ppm
TMPH	49.6	32.0	38.7	18.9
3E	51.8	36.9	42.4	19.7

Table 3.22- Comparison of ^{13}C chemical shifts

In both the ^1H and $^{13}C\{^1H\}$ NMR spectra of **3E** the presence of the all-lithium derivative was not detected possibly due to its small concentration in the sample. However, in the ^7Li NMR spectra (figure 3.22) two different lithiums were clearly visible at 2.52ppm and 0.87ppm in a ratio of approximately 13:1.The larger signal can be assigned to compound **3E**, while the smaller one can be tentatively assigned to LiTMP.

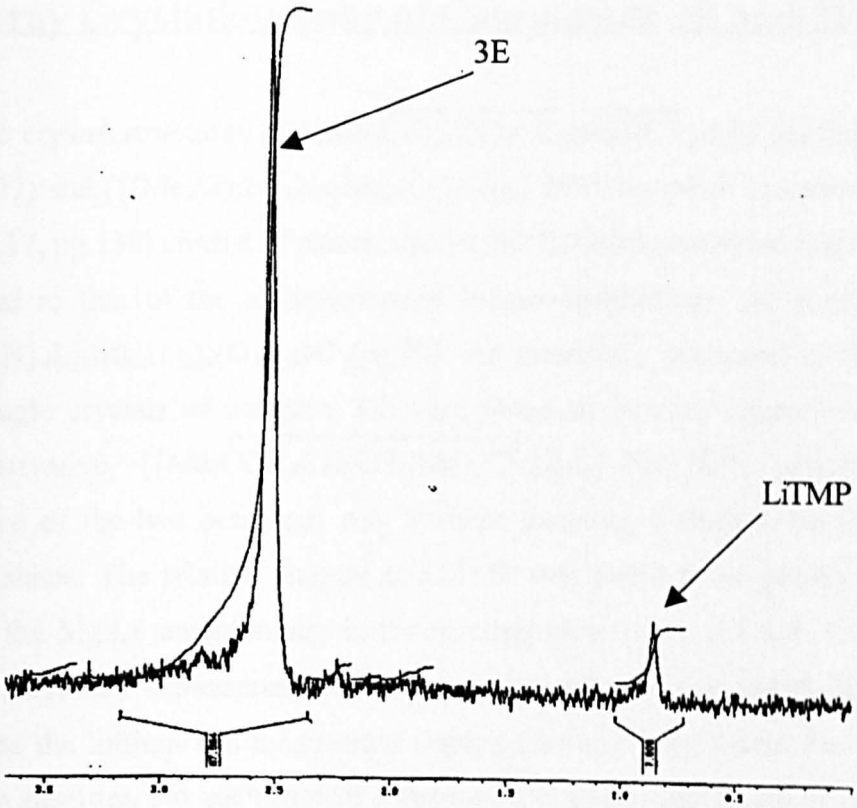

*Figure 3.22 - ^{7}Li NMR spectrum of compound **3E** in d_8-toluene at 300K*

In the ^{1}H NMR spectrum of compound **3F**, a sharp singlet with a definite shoulder 0.01ppm off the main resonance is observed. Thus it is reasonable to assume that the main signal at 0.17ppm belongs to the oxide whereas the signal at 0.16ppm belongs to that of the peroxide species. These are both found to have differing chemical shifts in comparison to the monometallic silyl amides i.e. $[(Me_3Si)_2NNa]$, 0.068ppm, $[\{(Me_3Si)_2N\}_2Mg]$, 0.44ppm and 0.32ppm.

In the $^{13}C\{^{1}H\}$ NMR spectrum, only the oxide complex could be assigned with certainty i.e. at 6.47ppm. The presence of impurities in the sample made assignment of the peroxo component uncertain.

3.12 X-ray Crystallography of Compounds 3E and 3F

The crystal structures of $[\{Me_2\overline{CCH_2CH_2CH_2(Me)_2CN}\}_4Li_2Mg_2(O)]$ **3E** (figure 3.16, pg.127) and $[\{(Me_3Si)_2N\}_4Na_2Mg_2(O_2)_x(O)_y]$ **3F** (only oxide component is shown in figure 3.17, pg.130) consist of planar, cyclic, $(NM)_4$ eight-membered rings, essentially isostructural to that of the aforementioned lithium-magnesium, oxo-peroxo complex $[\{(Me_3Si)_2N\}_4Li_2Mg_2(O_2)_x(O)_y]$ **3C** (pg.99). As previously discussed in the synthesis section, single crystals of complex **3E** were found to be contaminated with the all-lithium derivative, $[\{Me_2\overline{CCH_2CH_2CH_2(Me)_2CN}\}_4Li_4]$ (LiTMP), presumably as a consequence of the two octagonal ring systems adopting a similar, but not identical molecular shape. The relative amount of LiTMP was found to be greatly reduced by increasing the Mg:Li stoichiometry in the reaction from 1:1 to 2:1 [i.e. 1:1, 39%; 2:1, 7%]. The molecular dimensions within the central core of compound **3E** cannot be discussed as the lithium and magnesium centres are indistinguishable due to a mutual substitution disorder. No such mutual substitution disorder was found to be present in compound **3F** due to the pronounced size differential between sodium and magnesium. However site disorder was present in the central core which was refined as 32% peroxide / 68% oxide. In comparison to compounds **3C** and **3E**, the octagonal ring structure of complex **3F** is found to be more asymmetric (but still planar). It is significant that compound **3F** contains more oxide than peroxide. In the lithium derivative, **3C**, this situation is reversed. This implies that the sodium structure is more open and hence there is less steric protection given to the encapsulated peroxo anions, which is suspected to be the kinetic product. The TMP derivative, **3E**, on the other hand, is exclusively oxide (100%), which tends to suggest that the tetramethylpiperidide ligands are less effective at steric shielding than hexamethyldisilazide, (see space-filling diagrams, figure 3.24, pg.150), thus giving only the thermodynamic product.

Complex **3F** represents the first mixed sodium-magnesium amide to be structurally characterised. A search of the Cambridge Crystallographic Database[12] in July 1998 revealed that the only other mixed sodium-magnesium compounds presently

found in the literature are the donor solvated magnesates[64], aryl $[Na(PMDETA)]_2[MgPh_4]$ **116** and the alkynyl complexes $Na_2[Mg(C{\equiv}CBu^t)_3.(D)]_2$ where D = TMEDA **117** or PMDETA **118** prepared by Weiss *et al.*

Due to the larger size of sodium in relation to lithium and magnesium, there exists a higher degree of ionic bonding present in organosodium compounds, thus much longer bonds are observed by comparison. In compound **3F** the N-Na bond distances are observed to be 2.572Å which are considerably longer than those observed in the trimeric polymorph of sodium hexamethyldisilazide, $[\{(Me_3Si)_2NNa\}_3]$[65] **119** i.e. range 2.358-2.394Å, however similar N-Na distances have been observed in the mixed lithium-sodium amide complexes of, $[LiNa\{N(SiMe_3)_2\}_2.3THF]$[26] **120** and $[\{LiNa[N(CH_2Ph)_2]_2.OEt_2\}_2]$[66] **121** [i.e. in **120**, 2.509(4)Å; in **121**, edge contact 2.539(3)Å]. Both sodium and magnesium in complex **3F** are three-coordinate. There are no agostic-type interactions with the silyl methyl groups [i.e. the shortest contact is C(12)···Na(1) at 3.270Å], though such contacts have been found in other hexamethyldisilazide systems, for example in the aforementioned mixed lithium-magnesium complex, $[\{(Me_3Si)_2N\}_3LiMg]$ **3A**, and the trimeric all-sodium complex, mentioned above, which displays both intra- and inter-molecular agostic-type interactions.

The N-Mg bond lengths in compound **3F** are found to be shorter than the bridging N-Mg contacts found in $[\{(Me_3Si)_2N\}_2Mg]$ **23** [i.e. **3F**, 2.052Å c.f. 2.15Å found in **23**]. This can be attributed to the increased negative charge residing on the amido nitrogen centres in complex **3F**. As expected, magnesium is found to approach the central oxide dianion more than sodium [i.e. O-Mg, 2.007(4)Å; O-Na, 2.328(7)Å].

The size differential between the metals in complex **3F** is also highlighted in the bond angles where much larger angles are observed at sodium than at magnesium [i.e. exocyclic N-Mg-N angles, 141.60(5)° and endocyclic N-Na-N angles, 159.84(2)°].

As in the synthesis of compound **3C**, it is expected that in the preparations of both **3E** and **3F** there should be a small amount of oxidation product present in solution as dioxygen is formally being reduced (equation 3.9). It is suspected that this product is a tetrasubstituted hydrazine[67] ($R'_2N\text{-}NR'_2$, where R' = $SiMe_3$ or TMP). Due to time restrictions this identification was not carried out here but will be the subject of further study.

$$[(R'_2N)_6M_2Mg_2] \quad + \quad O_2 \xrightarrow{\text{Redox}} [(R'_2N)_4M_2Mg_2(O_2)] \quad + \quad R'_2N\text{-}NR'_2 \qquad \textbf{(3.9)}$$

In a formal sense, compounds **3C**, **3E** and **3F** can be regarded as products formed from a charge driven process; where two Mg^{2+} ions are substituted for two M^+ ions [i.e. **3C/3E** = Li, **3F** M = Na] which creates a cationic ring with a 2+ charge. Thus in order to gain neutrality the ring hole captures small O^{2-} or O_2^{2-} dianions (scheme 3.3, pg.149). However, this tells us nothing about the mechanism of the process, whether it is concerted or a two-step one. Interestingly, these complexes can also be regarded as antithetical 'crown ether' complexes where the Lewis acid-Lewis base positions have been reversed relative to those in conventional crown ether complexes as such they can be likened to the macrocyclic mercuracarborand compounds prepared by Hawthorne *et al*[68]. The crystal structure of a representative compound of this type is [12]mercuracarborand-4[69] **122** as shown in figure 3.23.

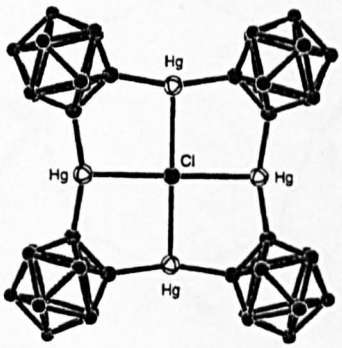

Figure 3.23- Crystal structure of the macrocyclic complex [12]mercuracarborand-4

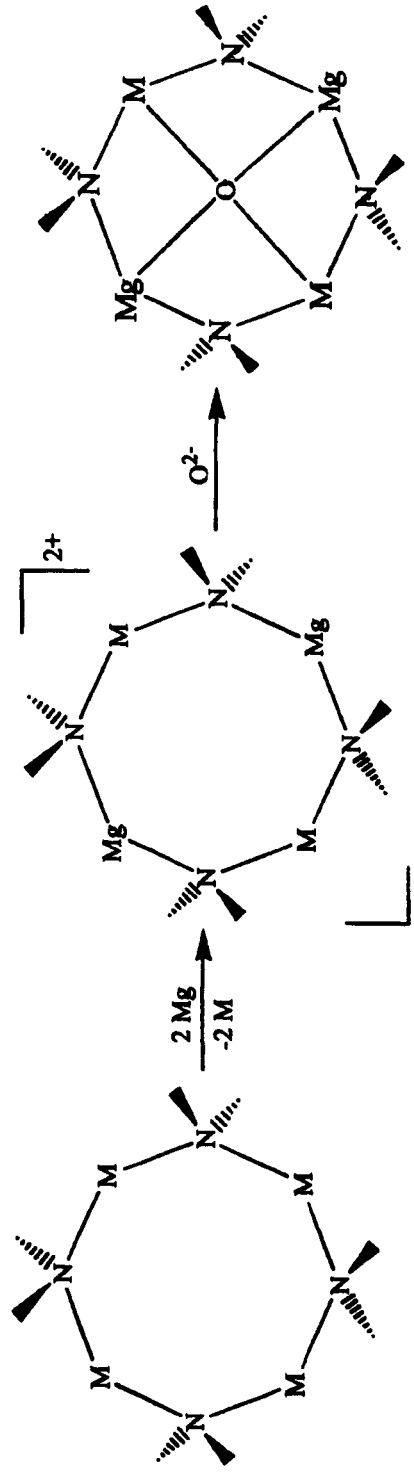

Scheme 3.3- Formal representation of oxide / peroxide incorporation into heterobimetallic cationic rings

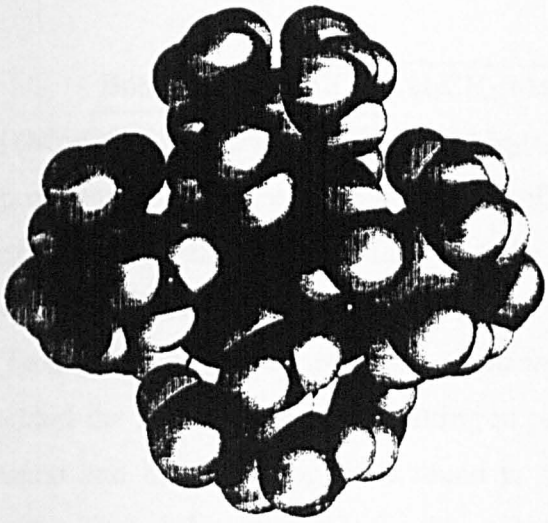

3C

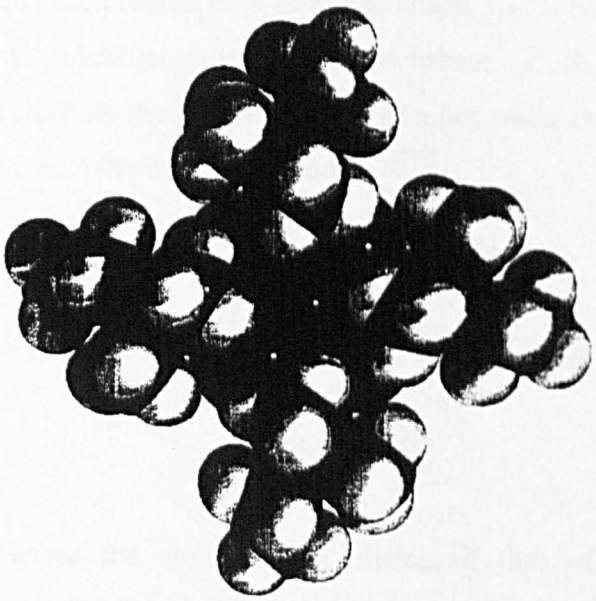

3E

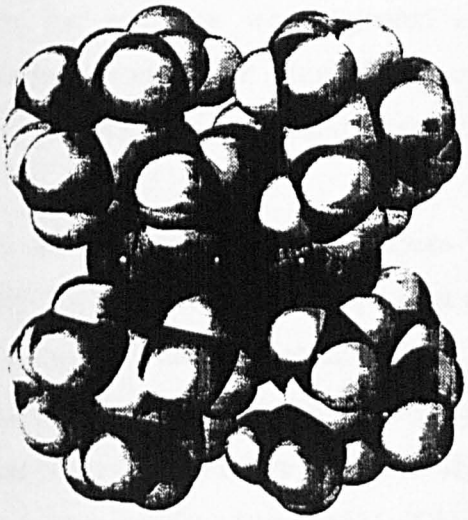

3F

*Figure 3.24 – Space filling representations of compounds **3C**, **3E** and **3F***

3.13 Synthesis and Analysis of Compounds 3G and 3H

Both $[\{Me_2CCH_2CH_2CH_2(Me)_2CN\}_6Na_4Mg_2\{C_6H_3(CH_3)\}]$ **3G** and $[\{Me_2CCH_2CH_2CH_2(Me)_2CN\}_6Na_4Mg_2(C_6H_4)\}]$ **3H** were prepared using the same procedure. To a 1:1 equimolar mixture of *n*-BuNa / DBM were added three equivalents of 2,2,6,6-tetramethylpiperidine whereby an exothermic reaction ensued. The solution was then filtered through a pad of Celite to remove any remaining solids. All solvents (hexane/heptane) were removed *in vacuo* leaving an orange-red oil. To this oil was added the respective arene, resulting in precipitation of a solid (equation 3.10). Excess arene and harsh heating were found to solubilise most of the precipitate, which was again filtered through Celite leaving a clear solution. Slow cooling in a hot water Dewar flask over 16 hours allowed crystallisation of the title compounds.

$$n\text{-BuNa} + n,s,\text{-Bu}_2\text{Mg} + 3\,Me_2CCH_2CH_2CH_2(Me)_2CNH \xrightarrow[\text{-3 BuH}]{\text{arene}} x[\{(Me_2CCH_2CH_2CH_2(Me)_2CN\}_6)Na_4Mg_2\}^{2+}\{\text{arene}\}^{2-}] + \text{other products} \quad (3.10)$$

When the reactions were repeated using the stoichiometry matching that of the crystalline products i.e. ratio of reactants 2:1:3, solubility problems arose both at the amine addition step and on adding the arene.

Satisfactory elemental analyses were obtained for complex **3G**. Compound **3H** readily decomposed in the drybox over a 12 hour period (it turned brown and powdery) thus elemental analysis could not be carried out. On exposure to air the infrared spectrum of compound **3H** showed a broad hydrolysis band centred at 3410br, corresponding to a mixture of NaOH, H_2O and N-H, and a sharp signal also appeared at 3702m corresponding to that of $Mg(OH)_2$.

The ^{1}H NMR spectra of compounds **3G** and **3H**, in d_6-DMSO, showed only one type of tetramethylpiperidide ligand, the chemical shifts of which were found to lie at approximately identical resonances to those of the parent amine (table 3.23).

The protons in the TMP ligand are assigned as follows.

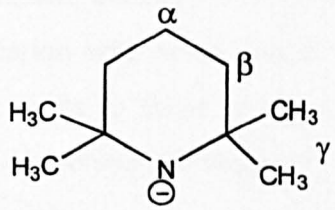

Compound	H_α / ppm	H_β / ppm	H_γ / ppm
$[Me_2CCH_2CH_2CH_2(Me)_2CNH]$	1.58	1.24	1.03
$[\{Me_2CCH_2CH_2CH_2(Me)_2CN\}_6Na_4Mg_2\{C_6H_3(CH_3)\}]$ **3G**	1.56	1.23	1.02
$[\{Me_2CCH_2CH_2CH_2(Me)_2CN\}_6Na_4Mg_2(C_6H_4)\}]$ **3H**	1.57	1.24	1.03

Table 3.23- Comparison of TMP ^{1}H chemical shifts

The dimetallated toluene molecule in compound **3G** is shown below.

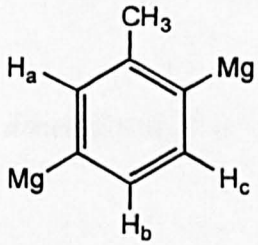

The presence on two symmetrical doublets (at 7.24ppm and 7.16ppm) accompanied by an overlapping singlet (at 7.17ppm) (figure 3.25) is in compliance with the crystal structure whereby toluene is metallated in the 2,5-positions. In this region, a singlet corresponding to benzene is also observed (at 7.36ppm) which integrates to a sixth of a proton, thus can be considered negligible. The coupling constant between protons H_b

and H_c on the toluene molecule is measured at $^3J_{Hb\text{-}Hc}$=7.2 Hz. The methyl group present on toluene is observed at 2.28ppm. In compound **3H**, the 1,4-dimetallated benzene molecule appears as a singlet at 7.37ppm which is identical to that of non-metallated benzene (C_6H_6). It can be thus acknowledged that in deuterated DMSO both structures remain intact. The ratio of metallated arene:TMP is observed to be smaller than expected. This is due to contamination with some parent amine which, as observed above, possesses similar chemical shifts to those in the metallated products (this is highlighted by a small amount of N-H protons at 0.96ppm).

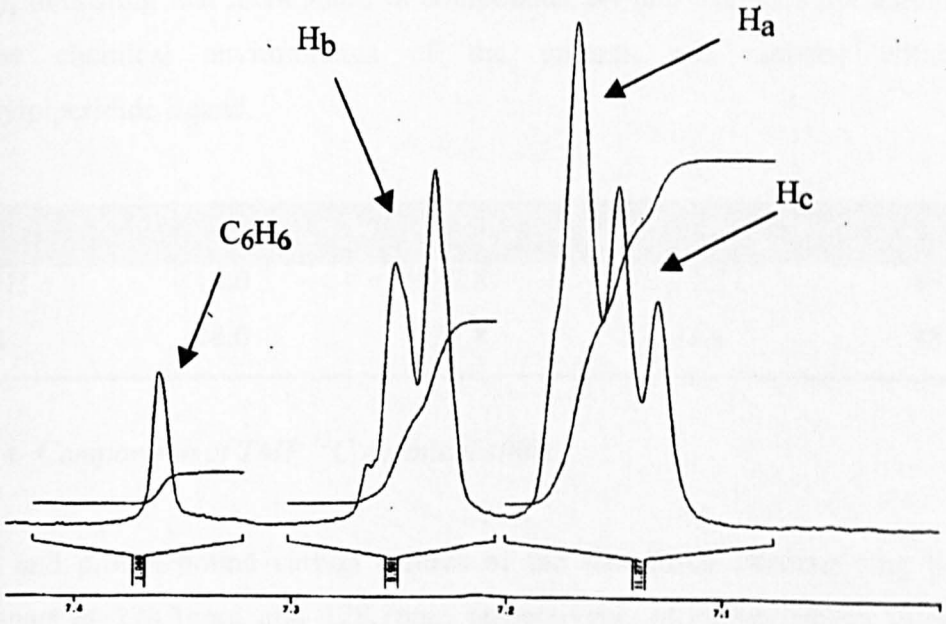

*Figure 3.25 – ^1H NMR spectrum of dimetallated toluene section of **3G** in d_6-DMSO at 300K*

^{13}C NMR studies were carried out on compound **3H** only, as there was not enough of compound **3G** to make a concentrated sample. The carbon skeleton of the tetramethylpiperidide ligand is shown below.

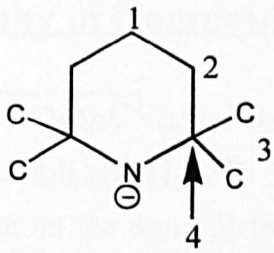

It is observed from table 3.24 that the tetramethylpiperidide carbons have practically identical chemical shifts with those present in the parent amine (akin to ^{1}H NMR spectrum), indicating that metallation in compounds **3G** and **3H** does not significantly affect the chemical environments of the protons and carbons within the tetramethylpiperidide ligand.

Compound	C – 1 / ppm	C – 2 / ppm	C – 3 / ppm	C – 4 / ppm
TMPH	18.0	37.8	31.5	49.0
3H	18.0	37.8	31.4	48.9

Table 3.24- Comparison of TMP ^{13}C chemical shifts

The *ipso* and proton bound carbon centres of the metallated benzene ring lie only 0.2ppm apart at 128.3ppm and 128.1ppm respectively. Moreover, these signals are found at a slightly lower frequency in comparison to non-metallated benzene i.e. at 128.7ppm.

3.14 X-ray Crystallography of Compounds 3G and 3H

Both $[\{Me_2\overline{CCH_2CH_2CH_2(Me)_2CN}\}_6Na_4Mg_2\{C_6H_3(CH_3)\}]$ **3G** and $[\{Me_2\overline{CCH_2CH_2CH_2(Me)_2CN}\}_6Na_4Mg_2(C_6H_4)\}]$ **3H** are essentially isostructural (disregarding the methyl substituent on the dimetallated toluene) as shown in figures 3.18 and 3.19 (pg.133 and 138). An alternative side view of complex **3G** is shown below in figure 3.26.

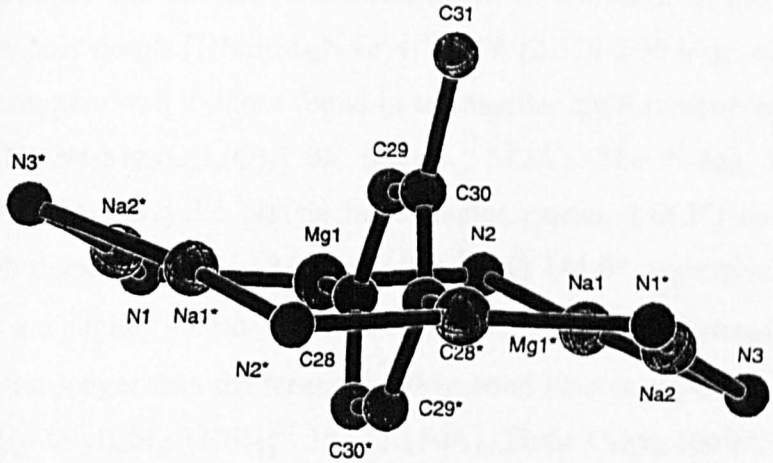

Figure 3.26- Side-view of macrocyclic ring structure 3G

Notable structural features in both compounds include:

(i) the severely puckered twelve-membered, heterometallic, $N_6Na_4Mg_2$ ring possesses crystallographic inversion symmetry;

(ii) the respective arene molecules lie almost orthogonal to the mean plane of the macrocyclic ring;

(iii) the metallation sites of the toluene dianion (2,5-positions) are the same as those of the benzene dianion (1,4-positions);

(iv) two C-H σ-bonds on each arene are replaced by two C-Mg σ-bonds;

(v) these same C atoms each engage in π-interactions with two Na^+ cations lying above or below the aromatic ring.

The similarity between compounds **3G** and **3H** is also shown by their respective dimensions [e.g. mean N-Mg: in **3G**, 2.050Å; in **3H**, 2.043Å; mean N-Na: in **3G**, 2.491Å; in **3H**, 2.483Å]. Other dimensions are listed in tables 3.15-3.18 (pg.133 and pg.137). Significantly, the N-Na bond distances within the homometallic NaNNa units (mean over both structures, 2.370Å) are on average 0.234Å shorter than those within the heterometallic NaNMg units (mean, 2.604Å). This is primarily a consequence of the large difference in the endocyclic bond angles at nitrogen [i.e. mean: 101.5° for N(3); 87.1° for N(1)/N(2)]. The shorter bond distances lie in the range of those found in the cyclic trimeric polymorph [{$(Me_3Si)_2NNa$}$_3$][65] **119** (2.358-2.394Å), while the longer bond lengths compare well to those found in the smaller eight-membered ring structure of [{$(Me_3Si)_2N$}$_4Na_2Mg_2(O_2)_x(O)_y$] **3F** (mean 2.572Å). The N-Mg bond distances (mean, 2.046Å) and exocyclic NMgN bond angles (mean, 143.3°) are also in good agreement with those in complex **3F** [i.e. 2.051Å and 141.6° respectively]. The C-Mg bond distances are slightly shorter (mean, 2.196Å) than those in polymeric [$(Ph_2Mg)_\infty$][70] **123** (2.261Å), but longer than the terminal C-Mg bond distances present in the dimeric THF-solvate [{$(p$-tolyl$)_2$Mg.THF}$_2$][71] **124** (2.130Å). These C-Mg contacts complete the distorted trigonal planar geometry of magnesium [i.e. in **3G**, N(2)Mg(1)C(28), 107.32(7)°; N(1)Mg(1)N(28), 109.75(7)°; N(2)Mg(1)N(1), 142.85(7)° c.f. ideal 120°] where the greatest distortion lies between the amido substituents. The same geometry is also apparent at sodium [i.e. range of summed bond angles, 359.3°-359.7°] which confirms that the NNaN units are coplanar with the metallated carbon atoms so as to maximise C-Na π-interactions (mean, 2.684Å). From the Cambridge Crystallographic Database[72] it is apparent that these interactions lie in the lower limit for bonds of this type (approximate range, 2.6-3.2Å).

There are a number of studies in the literature pertaining to the metallation of toluene and its derivatives using the organometallic reagents BuLi-TMEDA[73] or BuNa[74]. The favoured product is generally that of the resonance stabilised benzyl carbanion (thermodynamic product), which is accompanied by only small amounts of the ring metallated products (kinetic product). Broaddus *et al*[75] found that this ratio was reversed

by increasing the steric bulk at the methyl substituent on toluene i.e. ratio of benzyl product / ring metallation products are 92% / 8% for toluene and 3% / 97% for cumene.

Interestingly, the toluene molecule in **3G** is deprotonated at the diagonal ortho-meta positions, leaving the methyl group intact. This remarkable selectivity can thus be attributed to a special ring template effect. By carrying out *ab initio* MO calculations (at the B3LYP/6-311G++(d,p)level)[76] it was found that there are ten possible isomers formed when toluene is dimetallated. These are shown in figure 3.27.

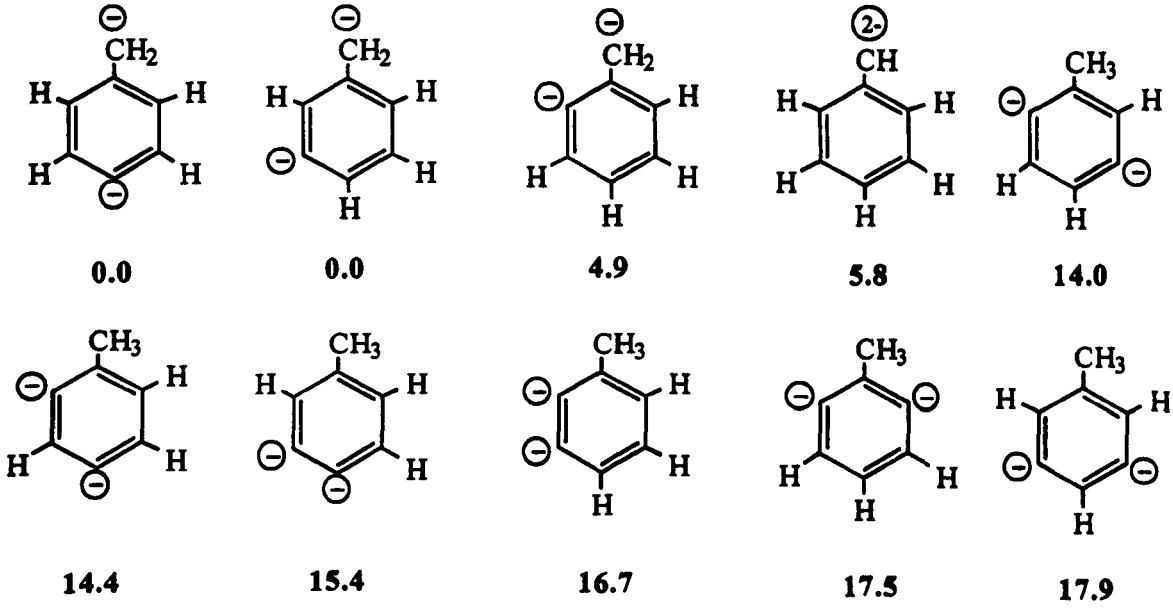

Figure 3.27- Relative energies of toluene-based dianions in kcal mol^{-1}

It is thus observed that an energy deficit of 14 kcal mol^{-1} has to be overcome to form the experimentally observed isomer over the most stable pair (methyl-para or methyl-meta deprotonated) in a thermodynamically controlled reaction. On this evidence, the cationic rings in compounds **3G** and **3H** or more precisely its intermediate precursor of unknown structure must possess exceptional proton abstraction capabilities. Presumably the precursor is $[\{Me_2\overline{CCH_2CH_2CH_2(Me)_2CN}\}_8Na_4Mg_2]$ which abstracts two protons from the arene, with the concomitant elimination of two equivalents of amine. The hypothesised formation of the benzene compound, **3H** is shown in scheme 3.4.

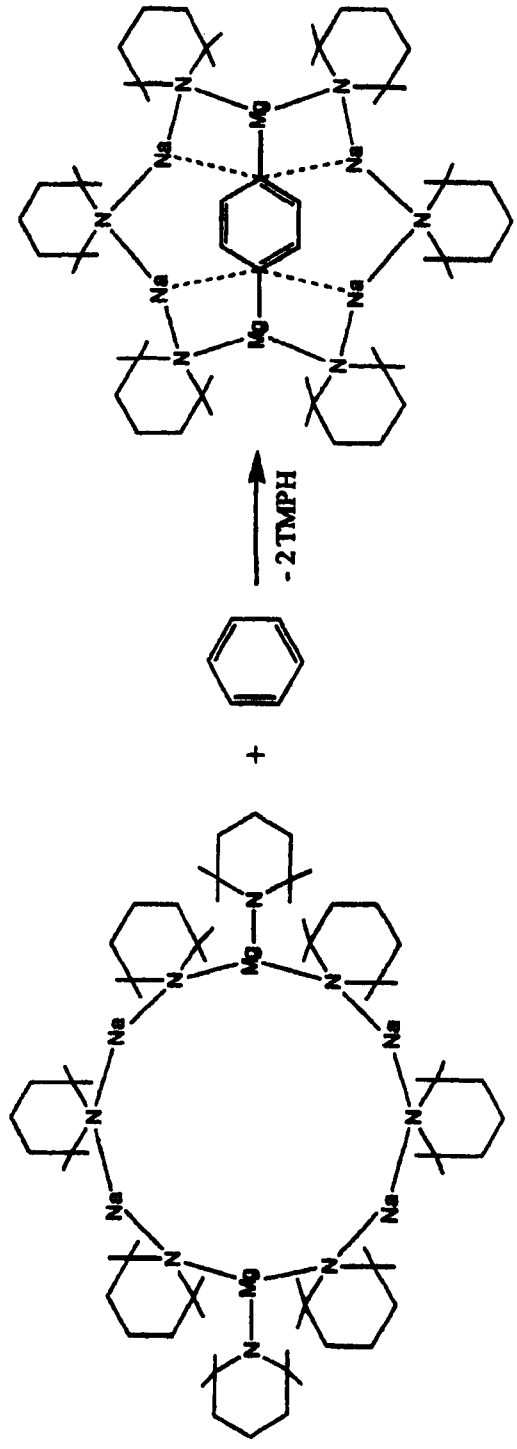

Scheme 3.4- Presumed template reaction for the formation of 3H

3.15 X-ray Crystallography of Compound 3I

The molecular structure of $[\{(Me_3Si)_2N\}_6K_2Mg_2.4\{C_6H_5(CH_3)\}]$ **3I** (figure 3.20, pg.140) is that of a highly puckered, heterobimetallic, sixteen-membered ring containing both formal N-Mg bonds and agostic C···K interactions. This ring can be considered as being formed from the dimerisation of two $[\{(Me_3Si)_2N\}_3KMg.2\{C_6H_5(CH_3)\}]$ moieties. One of these fragments is shown in figure 3.28.

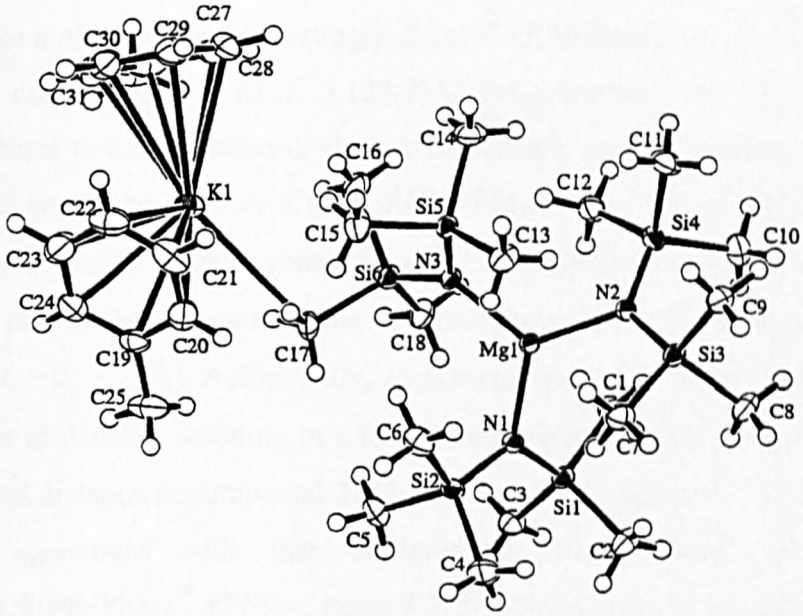

Figure 3.28- View of heterobimetallic ring fragment

Each magnesium centre is bound to three trimethylsilyl amide units, two of which bind agostically through one methyl group to potassium. The third amide unit does not partake in any such agostic interaction, and is solely bonded to magnesium in a terminal site. Together these amide units assume a near-perfect trigonal-planar geometry about the magnesium [i.e. N(1)Mg(1)N(2), 120.81(6)°; N(2)Mg(1)N(3), 119.18(6)°; N(1)Mg(1)N(3), 120.01(6)°; sum of angles 360.0°]. The mean N-Mg distance [2.022Å] is in good agreement with the mean terminal N-Mg bond distance found in

$[\{(Me_3Si)_2N\}_2Mg\}_2]$ **23** [i.e. 1.98Å], there are no significant differences between the terminal and bridging N-Mg bond lengths in compound **3I**. The Si-N and Si-C bond distances within each amide unit are observed to lie within standard deviation of those observed in the aforementioned bis amide [i.e. mean Si-N, 1.701Å; Si-C, 1.877Å in **3I** c.f. range of bond distances, Si-N, 1.705(4)-1.789(6)Å; Si-C, 1.824(12)Å-1.875(8)Å in **23**] and again there is no significant difference between the Si-CH_3 agostic and non-agostic bonds in **3I**.

As mentioned above each potassium cation is bound agostically to a methyl group from two separate amide anions. Interestingly, these C···K distances are asymmetric in length [i.e. short contact: C(3*)···K(1), 3.129(2)Å; long contact: C(17)···K(1), 3.399(2)Å] which suggests that association is via two monomeric species whereby the monomeric unit would appear to involve C(3*)···K(1). The mean C···K distance of 3.264Å is observed to be similar to those contacts present in the lattice structure of $[(MeK)_\infty]$[77] **125** [i.e. 3.2Å] and of those present in the linear chain structure of $[\{(Me_3Si)_3CK\}_\infty]$[78] **126** [i.e. mean C···K, 3.23Å]. Additionally, each potassium is η^6-bound to the π-system of two toluene molecules, resulting in a total coordination number of fourteen. The mean C(π)-K bond distance in compound **3I** (3.246Å, centroid distance 2.94Å) is found to be in good agreement with that observed in the benzene solvated siloxide $[\{(C_6H_6)KOSiMe_2Ph\}_4]$[79] **127** [i.e. mean 3.275Å], but much longer than those found in the tris-benzene solvated, silanide monomer $[KSi(SiMe_3)_3.3C_6H_6]$[33] **128** [i.e. range 3.02-3.08Å]. Interestingly, potassium ion-arene interactions have been reported by the groups of Atwood[80] and of Schaverien[81] in the structures of mixed lanthanide-potassium halides and mixed organoaluminium-potassium salts respectively, where C(π)-K bond distances were found in the range [3.31-3.59Å], of which those observed in compound **3I** are observed to lie at the lower end.

Compound **3I** is the first potassium magnesate to be crystallographically characterised which can be formally represented as $[K\{C_6H_5(CH_3)\}_2]^+[\{(Me_3Si)_2N\}_3Mg]^-$ and is found to possess many structural

differences with that of the aforementioned sodium-toluene macrocyclic complex $[\{Me_2\overline{CCH_2CH_2CH_2(Me)_2CN}\}_6Na_4Mg_2\{C_6H_3(CH_3)\}]$ **3G**.

Key differences are:

(i) the ratio of group 1:group 2 metals is 1:1 in **3I** but 2:1 in **3G**;

(ii) the amide ligands assume different bridging roles i.e. in complex **3I**, as mentioned above, selected methyl groups from the trimethylsilyl amide ligands, directly bound to magnesium, undergo agostic interaction with potassium, whereby the potassium cations do not interact at all with any of the anionic nitrogen centres, however in compound **3G** there is less necessity for agostic interactions as sodium is coordinated by two nitrogen anions.

(iii) toluene in both structures assumes different bonding modes i.e. in complex **3I**, as mentioned above, two toluene molecules are bound in an η^6-fashion to potassium which occupy the periphery of the ring, whereas in compound **3G** one toluene molecule is doubly deprotonated (forming a dianion) which takes up a central position within the ring via two single σC-Mg bonds. In both structures the methyl group is observed to stay intact.

The most interesting feature of the structure of **3I** is its possible implication for the mechanism of the formation of the $[(N_6Na_4Mg_2)^{2+}(arene)^{2-}]$ macrocyclic ring. The first step in the production of the macrocyclic-toluene complex could be the π-interaction of the arene onto the Na atom. The second step could thus be the formation of the amine molecules by interaction of the 'third' amide unit on the magnesium centre with the *ortho*- and *meta*- protons from the arene which orientates to the centre of the ring via two σC-Mg bonds (recall scheme 3.4, pg.158).

3.16 Chapter Three Conclusions

The lithium amidomagnesate complexes, $[\{(Me_3Si)_2N\}_3LiMg]$ **3A** and $[\{(c\text{-}C_6H_{11})_2\}_3LiMg.THF]$ **3B** have been prepared. In both complexes there are three amide units, two bridge both metal centres while the third is bound terminally at magnesium. In complex **3A** additional agostic-type interactions are observed between lithium and one methyl group from both bridging amides; whereas in complex **3B**, a THF donor molecule completes the coordination sphere about the lithium centre.

The first mixed lithium-magnesium N-silylated benzamidinate cage complex, $[\{PhC(NSiMe_3)_2\}_4Li_4Mg(O)]$ **3D**, has been prepared and crystallographically characterised. The structure is found to contain a central Li_4Mg trigonal bipyramidal polyhedron about an oxide (O^{2-}) core. Additionally, the periphery of the structure is observed to consist of two distinct types of amidinate ligand: one type assumes a bridging mode between the lithium and magnesium centres, while the other exhibits an unusual triangular–face capping mode the likes of which has been previously only observed in transition metal amidinate complexes.

Several novel, heterobimetallic, mixed group 1-magnesium ring architectures have also been prepared. These complexes $[\{(Me_3Si)_2N\}_4Li_2Mg_2(O_2)_x(O)_y]$ **3C**, $[\{Me_2\overline{CCH_2CH_2CH_2(Me)_2CN}\}_4Li_2Mg_2(O)]$ **3E** and $[\{(Me_3Si)_2N\}_4Na_2Mg_2(O_2)_x(O)_y]$ **3F** were prepared by reacting a mixture of the respective metal alkyls with the appropriate bulky secondary amine in the presence of dioxygen. The structures consist of planar, eight-membered cationic rings, which are found to encapsulate either peroxide (O_2^{2-}) or an oxide (O^{2-}) dianion.

It has been shown that a (1:1:3) mixture of *n*-BuNa / *n,s*-Bu_2Mg / TMPH is capable of the selective dimetallation of arene rings. Two compounds proving this were crystallographically characterised namely, $[\{(Me_2\overline{CCH_2CH_2CH_2(Me)_2CN})_4Na_4Mg_2\}^{2+}\{arene\}^{2-}]$ (where arene = $\{C_6H_3(CH_3)\}^{2-}$ **3G**

or $\{C_6H_4\}^{2-}$ **3H**). Both structures consist of puckered, heterobimetallic, twelve-membered $N_6Na_4Mg_2$ rings. The metallated arene molecule is located in the centre of each ring whereby metallation occurs at the 2,5-positions and 1,4-positions respectively. Additionally, the sodium centres are observed to interact with the π-system above and below the aromatic ring.

Finally, the first potassium magnesate has been prepared, $[\{(Me_3Si)_2N\}_6K_2Mg_2.4\{C_6H_5(CH_3)\}]$ **3I**, which consists of a highly puckered, sixteen-membered, heterobimetallic ring containing both formal N-Mg bonds and agostic C···K interactions. In contrast with structures **3G** and **3H**, terminal amide units are bound at magnesium with two toluene molecules η^6-bound at each potassium. Consequently, this structure can be thought of as an intermediate in the arene dimetallation process occurring in the aforementioned $N_6Na_4Mg_2$ macrocyclics.

3.17 Chapter Three Further Work

The reactivity of the lithium amidomagnesate complexes, $[\{(Me_3Si)_2N\}_3LiMg]$ **3A** and $[\{(c\text{-}C_6H_{11})_2N\}_3LiMg.THF]$ **3B** requires investigation in comparison to their monometallic analogues e.g. as deprotonating reagents.

The three oxo-containing compounds $[\{(Me_3Si)_2N\}_4Li_2Mg_2(O_2)_x(O)_y]$ **3C**, $[\{Me_2CCH_2CH_2CH_2(Me)_2CN\}_4Li_2Mg_2(O)]$ **3E** and $[\{(Me_3Si)_2N\}_4Na_2Mg_2(O_2)_x(O)_y]$ **3F** should be examined as potentially useful oxo-peroxo transfer agents e.g. to other main group metals, as well as transition metals. Addition reactions similar to the one that produced the amidinate cage complex, $[\{PhC(NSiMe_3)_2\}_4Li_4MgO]$ **3D** should also be studied.

Using a reactive mixture of *n*-BuNa / *n,s*-Bu_2Mg / 3TMPH in the presence of a readily formed dianion, it should be possible to synthesise other heterobimetallic ring systems analogous to **3G** and **3H** e.g. several precursors to dianionic species are shown below.

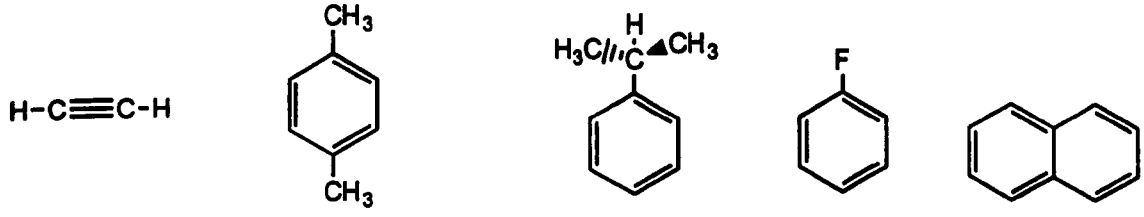

acetylene | 1,4 - dimethylbenzene | isopropylbenzene | fluorobenzene | naphthalene

More organic-type chemistry could be carried out on **3G** and **3H** to form 2,5-substituted toluenes and 1,4- substituted benzenes respectively e.g. as illustrated below for methyl ester substitution.

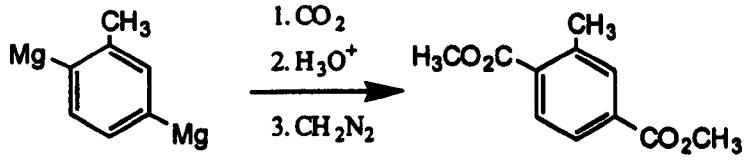

3G | 2,5-substituted methylester

Investigations should also be carried out using bulky primary amines e.g. $DippNH_2$ as well as other secondary amines e.g. diisopropylamine or dibenzylamine. Furthermore, instead of amine groups, bulky carbanionic ligands known to produce alkali metal ring systems could be employed e.g. $(Me_3Si)_3CH$.

Considering the metal centres in all the above compounds, two possible alterations spring to mind. Firstly, the ratio of Li / Na to Mg could be varied so as to produce rings of different size. Secondly, magnesium could be substituted by a range of divalent metal atoms e.g. Ca^{2+}, Zn^{2+}.

Further research is also required on the potassium magnesate complex **3I** to determine whether it is an actual intermediate to dimetallation i.e. by using forcing conditions can the terminal amide groups be eliminated ?. Also, to complete the series, a TMP analogue of the potassium complex should be synthesised analogous to **3G** and **3H**.

Finally, it would be of interest to discover whether the cationic ring systems could be isolated without a core dianion (shown below). This might be achieved by using bulky anions such as BPh_4^- and PF_6^-.

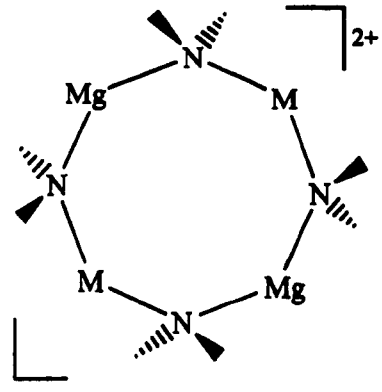

Where M = Li or Na

3.18 Chapter Three References

[1] G. Wittig, R. Ludwig and R. Polster; *Chem. Ber.*, (1955), **88**, 294.

[2] A. Mordini; Advances in Carbanion Chemistry., (ed.) V. Sniekus, Jai Press, London, (1992), **1**, 1., and references therein.

[3] M. Schlosser; *J. Organomet.Chem.*, (1967), **8**, 9.

[4] L. Lochmann and J. Trekoval; *Coll. Czech., Chem. Commun.*, (1988), **53**, 76.

[5] (a) G. Wittig; *Angew. Chem.*, (1958), **70**, 65;
(b) W. Tochtermann; *Angew. Chem., Int. Ed. Engl.*, (1966), **5**, 351.

[6] Uses of lithium organocuprates: G. v. Koten and J. G. Noltes; in *Comprehensive Organometallic Chemistry*, (Eds.) G. Wilkinson, Pergamon, New York, (1982), **4**, 709.

[7] J. A. Wanklyn; *Justus. Leibigs. Ann. Chem.*, (1858), **108**, 67.

[8] (a) S. J. Brown and J. H. Clark; *J. Chem. Soc., Chem. Commun.*, (1985), 672;
(b) A. E. Bayliff, M. R. Bryce, R. D. Chambers and R. S. Mathews; *J. Chem. Soc., Chem. Commun.*, (1985), 1018.

[9] W. Weppner, W. Welzel, R. Kneip and A. Rabenau; *Angew. Chem. Int. Ed. Engl.*, (1986), **25**, 1087.

[10] D. Barr, R. Snaith, D. S. Wright, R. E. Mulvey and K. Wade; *J. Am. Chem. Soc.*, (1987), **109**, 7891.

[11] (a) D. Seebach; *Angew. Chem. Int. Ed. Engl.*, (1988), **27**, 1624;
(b) Y. Yamamoto and J. Yamada; *J. Chem. Soc., Chem. Commun.*, (1988), 802.

[12] F. H. Allen, J. E. Davies, J. J. Galloy, O. Johnson, O. Kennard, C. F. Macrae, E. M. Mitchell, J. M. Smith and D. G. Watson; *J. Chem. Inf. Comp. Sci.*, (1991), **31**, 187.

[13] T. Greiser, J. Kopf, D. Thoennes and E. Weiss; *Chem. Ber.*, (1981), **114**, 209.

[14] D. Thoennes and E. Weiss; *Chem. Ber.*, (1978), **111**, 3726.

[15] B. Schubert and E. Weiss; *Chem. Ber.*, (1984), **117**, 366.

[16] K. M. Waggoner and P. P. Power; *Organometallics.*, (1992), **11**, 3209.

[17] W. Clegg, K. W. Henderson, R. E. Mulvey and P. A. O'Neil; *J. Chem. Soc., Chem. Commun.*, (1993), 969.

[18] W. Clegg, K. W. Henderson, R. E. Mulvey and P. A. O'Neil; *J. Chem. Soc., Chem. Commun.*., (1994), 769.

[19] K. W. Henderson, R. E. Mulvey, F. B. M. Reinhard, W. Clegg and L. Horsburgh; *J. Am. Chem. Soc.*, (1994), **116**, 10777.

[20] M. Motevalli, D. Shah, S. A. A. Shah and A. C. Sullivan; *J. Chem. Soc., Chem. Commun.*, (1994), 2427.

[21] N. H. Buttrus, C. Eaborn, M. N. A. El-Kheli, P. B. Hitchcock, J. D. Smith, A. C. Sullivan and K. Tavakkoli; *J. Chem. Soc., Dalton. Trans.*, (1988), 381.

[22] C. J. Thomas, L. J. H. Zhang, U. Siriwardane, J. A. Maguire, W. Wang, K. A. Brooks, V. P. Weiss and N. S. Hosmane; *Organometallics.*, (1995), **14**, 1365.

[23] A. L. Spek, P. Voorbergen, G. Schat, C. Blomberg and F. Bickelhaupt; *J. Organomet. Chem.*, (1974), **77**, 147.

[24] (a) R. F. Jordan; *Adv. Organomet. Chem.*, (1991), **32**, 325, and references cited therein;

(b) D. J. Cardin, M. F. Lappert and C. L. Raston; *Chemistry of Organo-Zirconium and –Hafnium Compounds.*, Ellis Horwood, England (1986);

(c) W. Kaminsky and H. Sinn; *Transition Metals and Organometallics as Catalysts for Olefin Polymerisation.*, Springer-Verlag, Berlin, (1987), and references cited therein.

[25] L. M. Engelhardt, B. S. Jolly, P. C. Junk, C. L. Raston, B. W. Skelton and A. H. White; *Aust. J. Chem.*, (1986), **39**, 1337.

[26] P. G. Williard and M. A. Nichols; *J. Am. Chem. Soc.*, (1991), **113**, 9671.

[27] M. M. Olmstead, W. J. Grigsby, D. R. Chacon, T. Hascall and P. P. Power; *Inorg. Chim. Acta.*, (1996), **251**, 273.

[28] J. Jubb, P. Berno, S. Hao and S. Gambarotta; *Inorg. Chem.*, (1995), **34**, 3563.

[29] A metastable variant of this structure has also been reported: H. Mack, G. Frenzen, M. Bendikov and M. S. Eisen; *Organomet. Chem.*, (1997), **549**, 39.

[30] L. M. Engelhardt, A. S. May, C. L. Raston and A. H. White; *J. Chem. Soc., Dalton. Trans.*, (1983), 1671.

[31] H. Dietrich; *Acta. Crystallogr.*, (1963), **16**, 681.

[32] T. Kottke and D. Stalke; *Angew. Chem. Int. Ed. Engl.*, (1993), **32**, 580.

[33] K. W. Klinkhammer; *Chem. Eur. J.*, (1997), **3**, 1418.

[34] G. Boche, K. Möbus, K. Harms, J. C. W. Lohrenz and M. Marsch; *Chem. Eur. J.*, (1996), **2**, 604.

[35] C. Drost, C. Jäger, S. Freitag, U. Klingebiel, M. Noltmeyer and G. M. Sheldrick; *Chem. Ber.*, (1994), **127**, 845.

[36] G. D. Stucky and R. E. Rundle; *J. Am. Chem. Soc.*, (1964), **86**, 4821.

[37] K. G. Caulton, M. H. Chisholm, S. R. Drake, K. Folting and J. C. Huffman; *Inorg. Chem.*, (1993), **32**, 816.

[38] H-J. Gais, J. Vollhardt, H. Günther, D. Moskau, H. J. Lindner and S. Braun; *J. Am. Chem. Soc.*, (1988), *110*, 978.

[39] W. Clegg, L. Horsburgh, P. R. Dennison, F. M. Mackenzie and R. E. Mulvey; *J. Chem. Soc., Chem. Commun.*, (1996), 1065.

[40] M. Driess, H. Pritzkow, S. Martin, S. Rell, D. Fenske and G. Baum; *Angew. Chem. Int. Ed. Engl.*, (1996), **35**, 986.

[41] F. M. Mackenzie, R. E. Mulvey, W. Clegg and L. Horsburgh; *Polyhedron.*, (1998), **17**, 993.

[42] P. G. Williard and J. G. MacEwan; *J. Am. Chem. Soc.*, (1998), **111**, 7671.

[43] C. Lambert, F. Hampel, P. v. R. Schleyer, M. G. Davidson and R. Snaith; *J. Organomet. Chem.*, (1995), **487**, 139.

[44] A. Drozdov and S. Troyanov; *Polyhedron.*, (1996), **15**, 1749.

[45] J. R. Rambo, J. C. Huffman and G. Christou; *J. Am. Chem. Soc.*, (1989), **111**, 8027.

[46] F. A. Cotton and M. Shang; *Organometallics.*, (1990), **9**, 2131.

[47] F. A. Cotton and M. Shang; *J. Am. Chem. Soc.*, (1990), **112**, 1584.

[48] T-Y. Her, C-C. Chang, G-H. Lee, S-M. Peng and Y. Yang; *Inorg. Chem.*, (1994), **33**, 99.

[49] R. Han and G. Parkin; *J. Am. Chem. Soc.*, (1992), **114**, 748.

[50] R. W. Chorley, P. B. Hitchcock and M. F. Lappert; *J. Chem. Soc., Chem. Commun.*, (1992), 525.

[51] For reviews see: (a) J. Barker and M. Kilner; *Coord. Chem. Rev.*, (1994), **133**, 219;
(b) F. T. Edelmann; *Coord. Chem. Rev.*, (1994), **137**, 403.

[52] K. Dehnicke; *Chemiker-Zeitung.*, (1990), **114**, 295.

[53] A. R. Sanger; *Inorg. Nucl. Chem. Lett.*, (1997), **9**, 351.

[54] M. Westerhausen and H-D. Hausen; *Z. Anorg. Allg. Chem.*, (1992), **615**, 27.

[55] M-D. Li, C-C. Chang, Y. Yang and G. H. Lee; *Organometallics.*, (1996), **15**, 2571.

[56] M. Westerhausen and W. Schwarz; *Z. Naturforsch.*, (1992), **47b**, 453.

[57] M. Westerhausen, H-D. Hausen and W. Schwarz; *Z. Anorg. Allg. Chem.*, (1992), **618**, 121.

[58] M. Westerhausen and W. Schwarz; *Z. Anorg. Allg. Chem.*, (1993), **619**, 1455.

[59] J. Barker, D. Barr, N. D. R. Barnett, W. Clegg, I. Cragg-Hine, M. G. Davidson, R. P. Davis, S. M. Hodgson, J. A. K. Howard, M. Kilner, C. W. Lehmann, I. Lopez-Solera, R. E. Mulvey, P. R. Raithby and R. Snaith., J. Chem. Soc., Dalton. Trans., (1997), 951.

[60] D. Stalke, M. Wedler and F. T. Edelmann; *J. Organomet. Chem.*, (1992), **431**, C1.

[61] M. S. Eisen and M. Kapon; *J. Chem. Soc., Dalton. Trans.*, (1994), 3507.

[62] T. Gebauer, K. Dehnicke, H. Goesmann and D. Fenske; *Z. Naturforsch.*, (1994), **496**, 1444.

[63] K. Burgess, D. Holden, B. F. G. Johnson and J. Lewis; *J. Chem. Soc., Dalton. Trans.*, (1983), 1199.

[64] M. Geissler, J. Kopf and E. Weiss; *Chem. Ber.*, (1989), **122**, 1395.

[65] (a) J. Knizek, I. Krossing, H. Nöth, H. Schwenk and T. Seifert; *Chem. Ber.*, (1997), **130**, 1053;
(b) M. Driess, H. Pritzkow, M. Skipinski and U. Winkler; *Organometallics.*, (1997), **16**, 5108.

[66] D. R. Baker, R. E. Mulvey, W. Clegg and P. A. O'Neil; *J. Am. Chem. Soc.*, (1993), **115**, 6472.

[67] J. R. Hwu and N. Wang; *Tetrahedron.*, (1988), **44**, 4181.

[68] M. F. Hawthorne and Z. Zheng., *Acc. Chem. Res.*, (1997), **30**, 267.

[69] X. Yang, C. B. Knobler and M. F. Hawthorne; *Angew. Chem. Int. Ed. Engl.*, (1991), **30**, 1507.

[70] P. R. Markies, G. Schat, O. S. Akkerman, F. Bickelhaupt, W. J. J. Smeets, P. van. der. Sluis and A. L. Spek; *J. Organomet. Chem.*, (1990), **393**, 315.

[71] P. R. Markies, O. S. Akkerman, F. Bickelhaupt, W. J. J. Smeets and A. L. Spek., *Adv. Organomet. Chem.*, (1991), **32**, 147.

[72] F. H. Allen and O. Kennard; *Chem. Des. Autom. News.*, (1993), **8**, 31.

[73] (a) A. J. Chalk and T. J. Hoogeboom; *J. Organomet. Chem.*, (1968), **11**, 615.

(b)R. West and P. C. Jones; *J. Am. Chem. Soc.*, (1968), **10**, 2656.

[74] C. D. Broaddus; *J. Am. Chem. Soc.*, (1966), **88**, 4174.

[75] C. D. Broaddus; *J. Org. Chem.*, (1970), **35**, 10.

[76] A. D. Becke; *J. Chem. Phys.*, (1993), **98**, 5646.

[77] E. Weiss and G. Sauermann; *Chem. Ber.*, (1970), **103**, 265.

[78] C. Eaborn, P. B. Hitchcock, K. Izod, A. J. Jagger and J. D. Smith; *Organometallics.*, (1994), **13**, 753.

[79] G. R. Fuentes, P. S. Coan, W. E. Streiss and K. G. Caulton; *Polyhedron.*, (1991), **10**, 2371.

[80] (a) J. L. Atwood and S. K. Searle; *J. Organomet. Chem.*, (1976), **114**, 107.

(b) J. L. Atwood, K. D. Crissinger and R. D. Rodgers; *J. Organomet. Chem.*, (1978), **155**, 1.

[81] C. J. Schaverien and J. B. v. Mechelen; *Organometallics.*, (1991), **10**, 1704.

Chapter Four

Chapter Four – Miscellaneous N-Mg Bonded Structures

Aims

- To discuss the syntheses, analyses and X-ray crystal structures of two isostructural, monomeric magnesium bis(amidinides).
- To discuss the synthesis, analysis and X-ray crystal structure of the heteroleptic magnesium bis(amide) complex $[\{(Me_3Si)_2NMgN(H)C_6H_5.THF\}_2]$.

4.1 Introduction

In the course of three years research, several miscellaneous N-Mg bonded complexes were prepared and fully characterised. As they did not follow the particular themes presented in chapters two and three they are presented in a chapter of their own. The first two structures to be considered are $[\{PhNC(Ph)NPh\}_2Mg.2D.C_6H_5CH_3]$ where D = DMSO or HMPA which are isostructural magnesium bis(amidinides) containing a central six-coordinate magnesium centre. They are prepared by magnesiating two equivalents of N,N'-diphenylbenzamidine with a diorganylmagnesium base in the presence of donor solvent. The third and final compound to be considered is the heteroleptic magnesium bis(amide), $[\{(Me_3Si)_2NMgN(H)C_6H_5.THF\}_2]$ prepared from the transamination reaction of magnesium bis[bis(trimethylsilyl)] amide with aniline, the structure of which is a centrosymmetric dimer, whereby the magnesium centres are four-coordinate occupying distorted tetrahedral environments.

Chapter Four

Experimental

4.2 Chapter Four Experimental

Reaction 4.1: Synthesis of [{PhNC(Ph)NPh}$_2$Mg.2DMSO.$C_6H_5CH_3$], 4A

N, N'-diphenylbenzamidine (0.68g, 2.5mmol) was dissolved in hot toluene (10ml). To this solution was added half an equivalent of DBM (1.25mmol in heptane, 1.25ml of a 1.0M solution). Immediately, a vigorous reaction ensued with the formation of a yellow precipitate. The solid was found to redissolve on the addition of dimethylsulphoxide, DMSO, (0.2ml, 2.5mmol) to give a lime green solution. The solution was then placed in the fridge at 5°C whereby colourless crystals formed over a period of 24 hours. These were subsequently identified as the title complex, [{PhNC(Ph)NPh}$_2$Mg.2DMSO.$C_6H_5CH_3$] **4A**.

Yield:	0.38g (37.3%) based on consumption of DBM
Melting Point:	162-164°C
Elemental Analysis:	$C_{49}H_{50}MgN_4O_2S_2$
Calculated	C, 72.2; H, 6.2; N, 6.9; Mg, 3.0; O, 3.9; S, 7.8%
Found	C, 70.0; H, 6.1; N, 6.8; Mg, 2.6%

Infrared / cm^{-1} (nujol mull)

2731br, 1593s, 1219m/s, 1169w/s, 1011m/s, 941w, 761s

On exposure to air a broad band 3715br appeared corresponding to $Mg(OH)_2$, this was accompanied by a sharp signal at 3304s which can be assigned to that of the free amidine N-H. Signals corresponding to the stretching mode of the amidine ligand, N=C=N, were also observed at 1658v.s and 1588v.s respectively.

^{1}H NMR (400MHz, d_5-pyridine, 300K)

Chemical shift δ/ppm	Splitting pattern	Relative integral	Assignment
7.31-6.79	overlap. multiplets	35H	Ph (tol) / Ph (am)
2.52	singlet	12H	$(CH_3)_2S{=}O$
2.23	singlet	3H	CH_3 (tol)

Where tol = toluene and am = amidinide

^{13}C NMR spectrum (^{1}H-decoupled, 100MHz, d_5-pyridine, 300K)

Chemical shift δ/ppm	Assignment
170.4	N---C---N
151.8-120.6	*o-/m-/p-/ipso*-Ph (tol/am)
41.6	$(CH_3)_2S{=}O$
22.1	CH_3 (tol)

Crystal Structure

X-ray crystallographic studies of a selected crystal with dimensions 0.46x0.42x0.28mm were undertaken. These divulged the, monomeric magnesiated amidine, $[\{PhNC(Ph)NPh\}_2Mg.2DMSO.C_6H_5CH_3]$ **4A** (figure 4.1). The final R factor was 0.0443. Other crystallographic parameters are presented in Appendix III.

Table 4.1: Selected bond distances (Å) in **4A**

Mg(1)-N(1)	2.213(15)	**Mg(1)-N(4)**	2.178(16)
Mg(1)-N(2)	2.202(16)	**Mg(1)-O(1)**	2.076(13)
Mg(1)-N(3)	2.180(15)	**Mg(1)-O(2)**	2.049(14)
N(1)-C(7)	1.328(2)	**N(3)-C(26)**	1.340(2)
N(2)-C(7)	1.338(2)	**N(4)-C(26)**	1.333(2)

Table 4.2: Selected bond angles (°) in **4A**

O(2)-Mg(1)-O(1)	97.94(6)	**N(3)-Mg(1)-N(2)**	111.67(6)
O(2)-Mg(1)-N(4)	89.73(6)	**N(3)-Mg(1)-N(1)**	89.99(6)
N(4)-Mg(1)-N(1)	113.64(6)	**N(2)-Mg(1)-N(1)**	60.63(6)
N(4)-C(26)-N(3)	111.97(15)	**N(1)-C(7)-N(2)**	113.38(15)

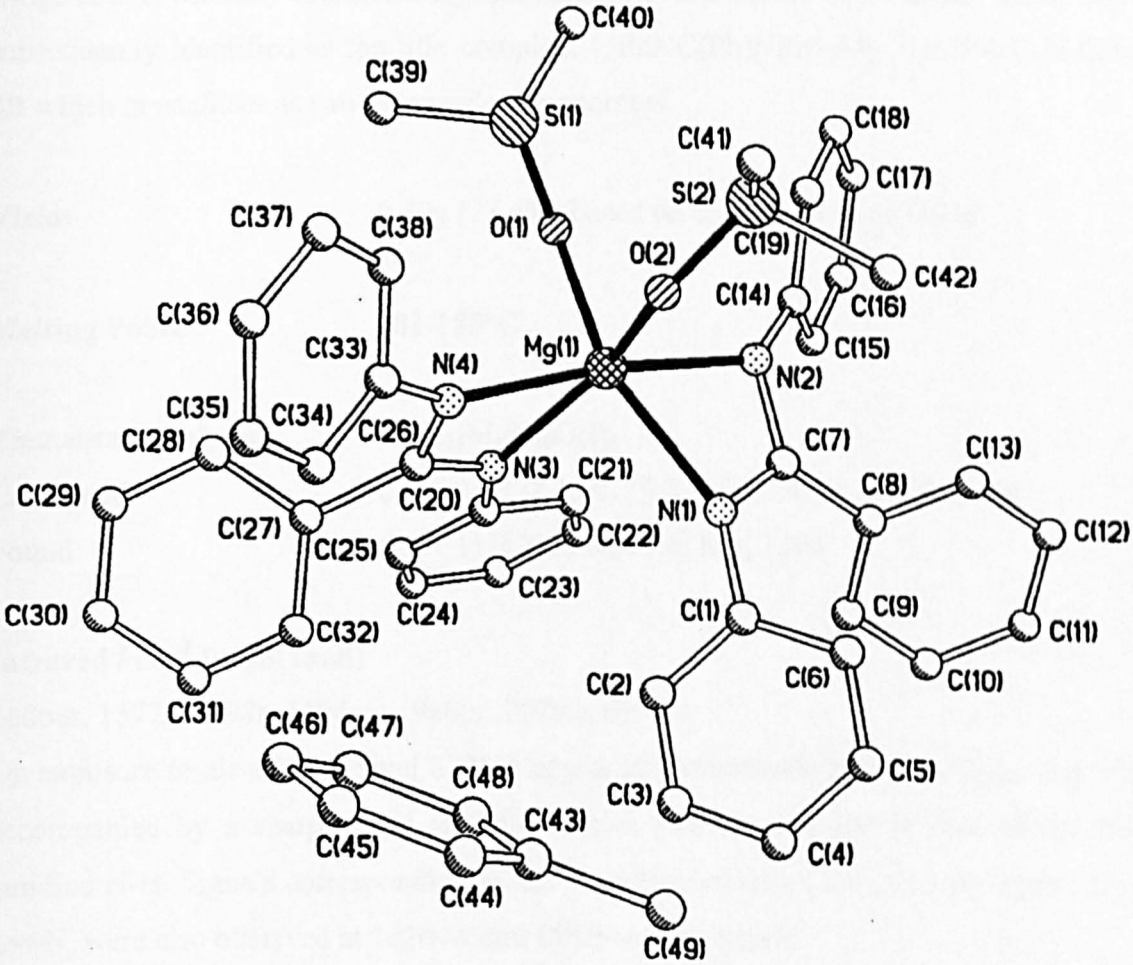

*Figure 4.1- Crystal structure of [{PhNC(Ph)NPh}$_2$Mg.2DMSO.C$_6$H$_5$CH$_3$] **4A**, (hydrogen atoms are omitted for clarity)*

Reaction 4.2: Synthesis of [{PhNC(Ph)NPh}$_2$Mg.2HMPA.$C_6H_5CH_3$] 4B

N, N'-diphenylbenzamidine (0.68g, 2.5mmol) was dissolved in hot toluene (14ml). To this solution was added half an equivalent of DBM (1.25mmol in heptane, 1.25ml of a 1.0M solution). Immediately, a vigorous reaction ensued with the formation of a yellow precipitate. The solid was found to redissolve on the addition of HMPA, (0.5ml, 2.9mmol) to give a lime green solution. The solution was then placed in the fridge at 5°C whereby colourless crystals formed over a period of 24 hours. These were subsequently identified as the title complex, [{PhNC(Ph)NPh}$_2$Mg.2HMPA.$C_6H_5CH_3$] **4B** which crystallises as two independent monomers.

Yield:	0.30g (23.6%) based on consumption of DBM
Melting Point:	183-185°C
Elemental Analysis:	$C_{57}H_{74}MgN_{10}O_2P_2$
Calculated	C, 67.2; H, 7.3; N, 13.8; Mg, 2.4; O, 3.1; P, 6.1%
Found	C, 67.1; H, 6.2; N, 11.6; Mg, 2.2%

Infrared / cm^{-1} (nujol mull)

2686br, 1577s, 1298s, 1194s/m, 988br, 767v.s, 695v.s

On exposure to air a broad band 3725br appeared corresponding to $Mg(OH)_2$, this was accompanied by a sharp signal at 3304s which can be assigned to that of the free amidine N-H. Signals corresponding to the stretching mode of the amidine ligand, N=C=N, were also observed at 1626v.s and 1586v.s respectively.

^{1}H NMR (400MHz, d_5-pyridine, 300K)

Chemical shift δ/ppm	Splitting pattern	Relative integral	Assignment
7.27-6.77	overlap. multiplets	35H	Ph (tol) / Ph (am)
2.53	doublet	36H	$(Me_2N)_3P{=}O$
2.23	singlet	3H	CH_3 (tol)

Where tol = toluene and am = amidinide

^{13}C NMR spectrum (^{1}H-decoupled, 100MHz, d_5-pyridine, 300K)

Chemical shift δ/ppm	Assignment
151.8-120.0	*o-/m-/p-/ipso*-Ph (tol/am)
37.2	$(Me_2N)_3P{=}O$
21.8	CH_3 (tol)

Crystal structure

X-ray crystallographic studies of a selected crystal with dimensions 0.72x0.44x0.42mm were undertaken. These divulged the, monomeric magnesiated amidine, [{PhNC(Ph)NPh}$_2$Mg.2HMPA.$C_6H_5CH_3$] **4B** (figure 4.2). The final R factor was 0.1066. Other crystallographic parameters are presented in Appendix III.

Table 4.3: Selected bond distances (Å) in **4B**

Mg(1)-N(1)	2.233(10)	**Mg(1)-N(4)**	2.236(9)
Mg(1)-N(2)	2.215(9)	**Mg(1)-O(1)**	2.029(9)
Mg(1)-N(3)	2.230(9)	**Mg(1)-O(2)**	2.027(9)
N(3)-C(26)	1.315(14)	**N(1)-C(7)**	1.338(13)
N(4)-C(26)	1.319(14)	**N(2)-C(7)**	1.340(14)

Table 4.4: Selected bond angles (°) in **4B**

O(2)-Mg(1)-O(1)	94.7(4)	**N(3)-Mg(1)-N(2)**	154.9(4)
O(2)-Mg(1)-N(4)	93.1(4)	**N(3)-Mg(1)-N(1)**	101.0(3)
N(4)-Mg(1)-N(1)	91.0(4)	**N(2)-Mg(1)-N(1)**	60.4(3)
N(3)-C(26)-N(4)	114.5(10)	**N(1)-C(7)-N(2)**	113.3(9)

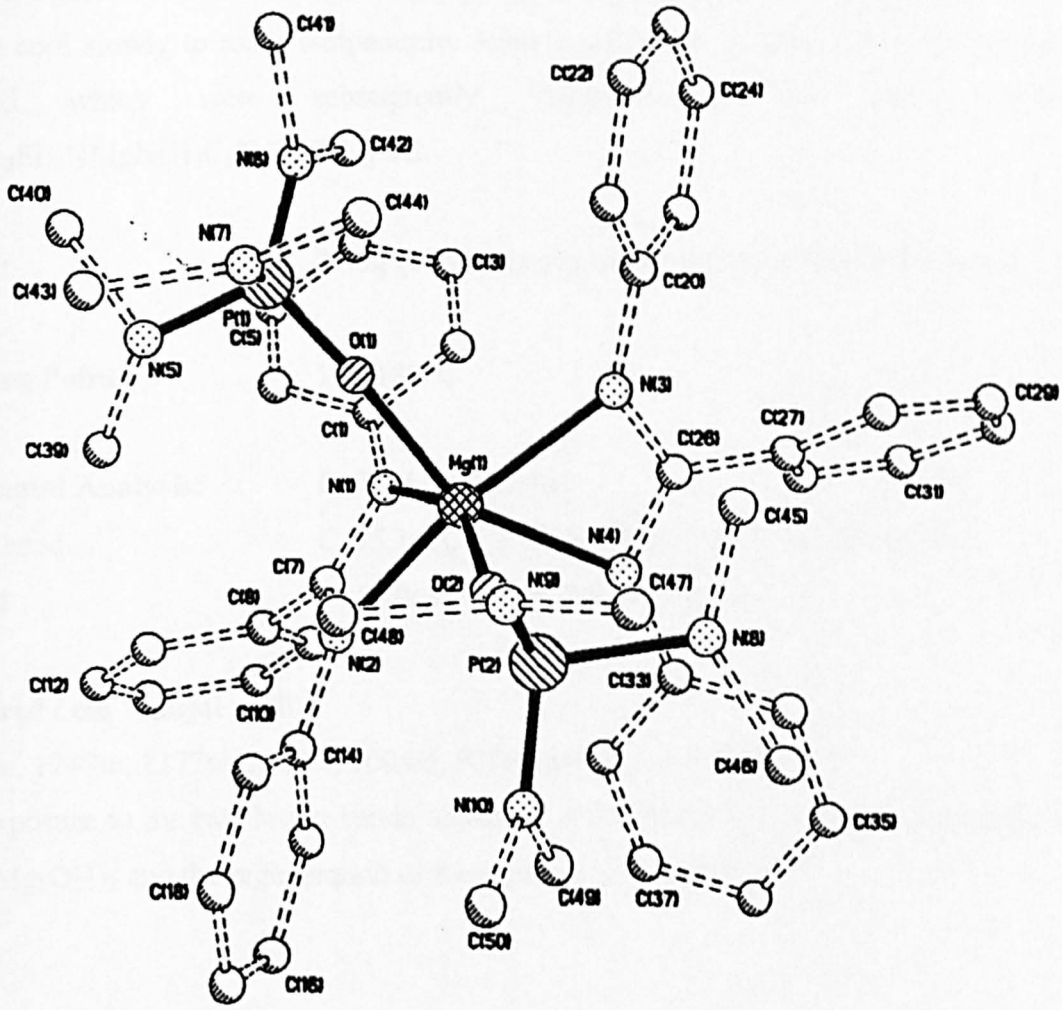

Figure 4.2- Crystal structure of one independent monomer of [{PhNC(Ph)NPh}$_2$Mg.2HMPA.C$_6$H$_5$CH$_3$] ***4B****, (hydrogen atoms are omitted for clarity)*

Reaction 4.3: Synthesis of $[\{(Me_3Si)_2NMgN(H)C_6H_5.THF\}_2]$, 4C

Freshly prepared, crystalline, magnesium bis[bis(trimethylsilyl)]amide (0.69g, 2.0mmol) was dissolved in toluene (9ml). To this colourless solution, an equimolar amount of aniline (0.19ml, 2.0mml) was added, resulting in the formation of a white precipitate. This solid redissolved on the addition of THF (2.5ml, 30mmol) which formed a golden coloured solution. By placing the Schlenk in hot water, the solution was left to cool slowly to room temperature. After a period of 12 hours colourless crystals formed which were subsequently identified as the title complex $[\{(Me_3Si)_2NMgN(H)C_6H_5.THF\}_2]$ **4C**.

Yield:	0.50g (17.9%) based on consumption of Mg bis(amide)
Melting Point:	176-180°C
Elemental Analysis:	$C_{32}H_{64}Mg_2N_4O_2Si_4$
Calculated	C, 55.1; H, 9.2; N, 8.0; Mg, 7.0; O, 4.6; Si, 16.1%
Found	C, 55.0; H, 8.4; N, 7.8; Mg, 6.8%

Infrared / cm^{-1} (nujol mull)

1560m, 1247m, 1177w, 1087w, 1004m, 932m, 840m, 640w, 590w

On exposure to air two broad bands appeared at 3708br and 3383br corresponding to both $Mg(OH)_2$ and the regeneration of free amines (N-H and NH_2).

^{1}H NMR (400MHz, d_5-pyridine, 300K)

Chemical shift δ/ppm	Splitting pattern	Relative integral	Assignment
7.16	multiplet	2H	*meta*-Ph
6.82	multiplet	2H	*ortho*-Ph
6.50	multiplet	1H	*para*-Ph
3.68	multiplet	4H	OCH_2 (THF)
3.62	singlet	1H	N-H
1.65	multiplet	4H	CH_2 (THF)
0.25	singlet	18H	$(Me_3Si)_2N$

Suitable $^{13}C\{^1H\}$ spectra were not recorded due to the poor solubility of the compound.

Crystal structure

X-ray crystallographic studies of a selected crystal with dimensions 0.60x0.50x0.40mm were undertaken. These divulged the, dimeric, four-coordinate, magnesium heteroleptic bis(amide), $[\{(Me_3Si)_2NMgN(H)C_6H_5.THF\}_2]$, **4C** (figure 4.3). The final R factor was 0.0299. Other crystallographic parameters are presented in Appendix III.

Table 4.5: Selected bond distances (Å) in **4C**

Mg-N(1)	2.140(11)	**Mg-O(1)**	2.026(9)
Mg-N(1A)	2.102(10)	**Mg(A)-N(1)**	2.102(10)
Mg-N(2)	2.003(11)		

Table 4.6: Selected bond angles (°) in **4C**

N(2)-Mg-O(1)	105.39(4)	**N(2)-Mg-N(1A)**	124.37(4)
O(1)-Mg-N(1A)	112.03(4)	**N(2)-Mg-N(1)**	120.88(4)
Mg(A)-N(1)-Mg	90.15(4)	**N(1A)-Mg-N(1)**	89.85(4)

Symmetry transformations used to generate equivalent atoms: A: 1-x, 1-y, 1-z

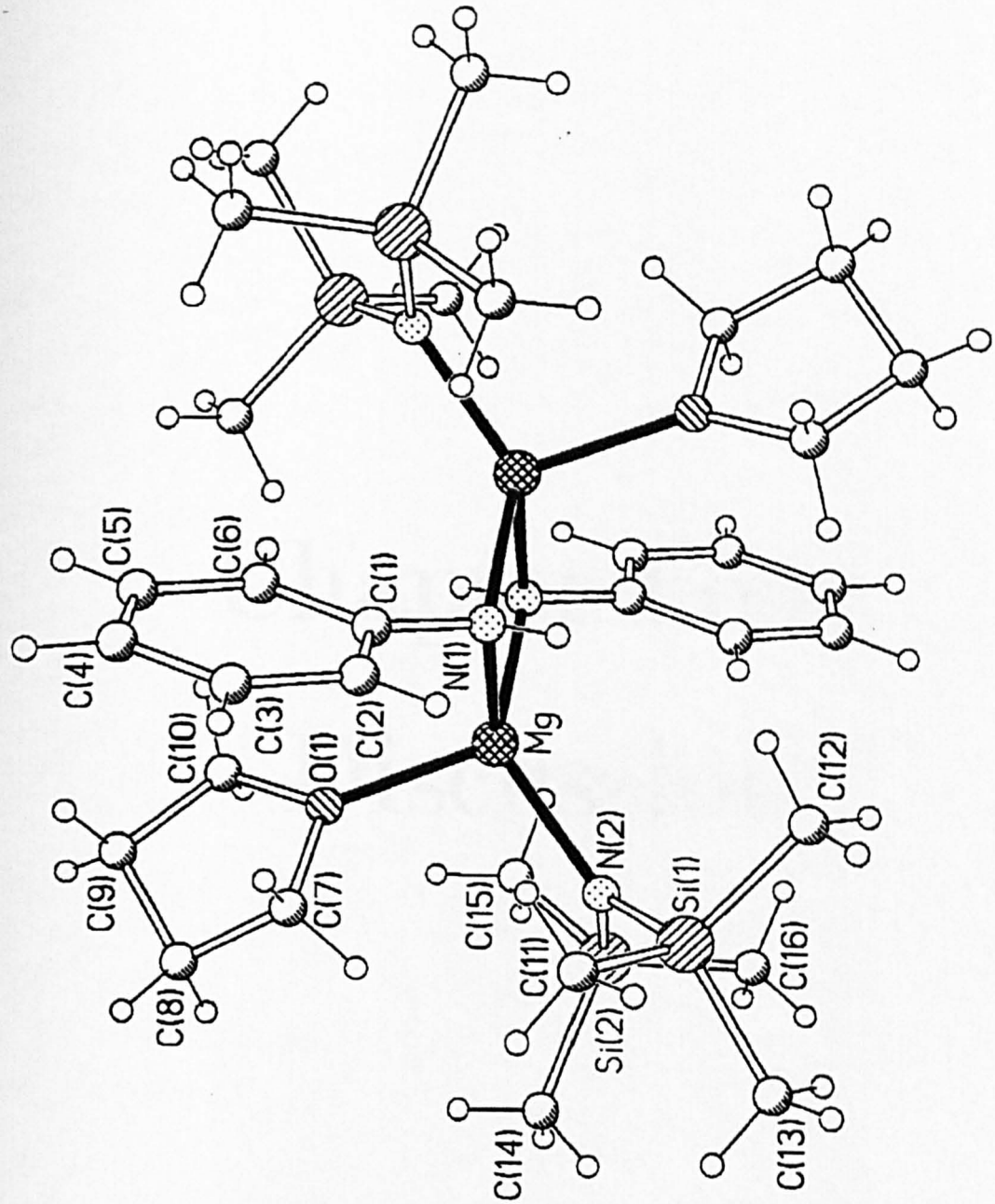

Figure 4.3- Crystal structure of [{$(Me_3Si)_2NMgN(H)C_6H_5.THF$}$_2$] ***4C***

Chapter Four

Discussion

4.3 Synthesis and Analysis of Compounds 4A and 4B

Both compounds, $[\{PhNC(Ph)NPh\}_2Mg.2DMSO.C_6H_5CH_3]$ **4A** and $[\{PhNC(Ph)NPh\}_2Mg.2HMPA.C_6H_5CH_3]$ **4B**, were prepared from the same, facile, metal-hydrogen exchange process whereby two equivalents of N,N'-diphenylbenzamidine were reacted with one equivalent of DBM. This reaction was exothermic resulting in the formation of a yellow precipitate accompanied by butane gas liberation. The, presumably, polymeric solid redissolved on the addition of the donor solvents DMSO and HMPA which in turn led to the crystallisation of the above compounds each of which had a molecule of toluene present in the lattice per monomer (equation 4.1).

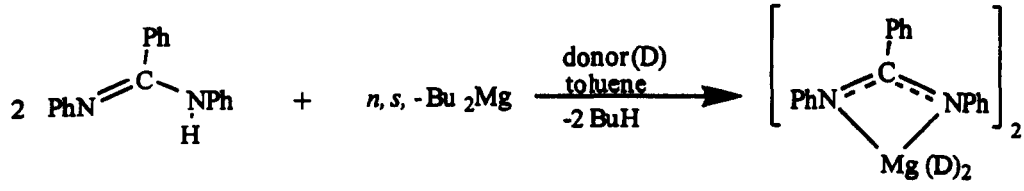

(4.1)

Where D = DMSO or HMPA

Satisfactory elemental analyses were obtained in each case. The infrared spectra of compounds **4A** and **4B** clearly revealed ν(C=N) stretching bands at 1593s and 1577s respectively. On exposure to air, hydrolysis occurred resulting in the formation of $Mg(OH)_2$ and regeneration of the free amidine i.e. N---C---N (asymmetric) stretch at ≈1626v.s and ν(C=N) at ≈1586v.s.

The ^1H NMR spectra of compounds **4A** and **4B** were run in d_5-pyridine. Complete assignment of the amidine-phenyl ring protons proved impossible due to the presence of toluene in the samples which overlapped with these signals. Thus instead of individual assignments, the range of these protons are given in table 4.7.

Compound	Range of phenyl ring protons / ppm
[PhNC(Ph)N(H)Ph]	7.50 – 7.03
[{PhNC(Ph)NPh}$_2$Mg.2DMSO.$C_6H_5CH_3$] **4A**	7.31 – 6.79
[{PhNC(Ph)NPh}$_2$Mg.2HMPA.$C_6H_5CH_3$] **4B**	7.27 – 6.77

Table 4.7- Comparison of phenyl ^1H chemical shifts

From the comparative data, it is observed that on metallation of N,N'-diphenylbenzamidine the protons of the phenyl rings collectively experience a slight low frequency shift which can be attributed to an increase in electron density delocalised around these rings. In both compounds **4A** and **4B** the presence of donor molecules were clearly identified at 2.52ppm for DMSO and 2.53ppm for HMPA respectively. The methyl group from the toluene of crystallisation was also found in this region at 2.23ppm.

In the $^{13}C\{^1H\}$ NMR spectrum of compound **4A**, the N---C---N carbon was clearly observed at 170.4ppm. However in compound **4B** the same signal was not detected, this is presumably the result of a low concentrated sample or insufficient scans. The phenyl protons in compounds **4A** and **4B** are observed to lie at a slightly lower frequency than those present in the free amidine i.e. **4A**, 151.8-120.6ppm c.f. 156.39-122.97ppm in the free amidine. The donor molecules, DMSO and HMPA were found at 41.6ppm and 37.2ppm respectively. The methyl group from the toluene of crystallisation was also found in this region at 22.1ppm.

4.4 X-ray Crystallography of Compounds 4A and 4B

Compounds $[\{PhNC(Ph)NPh\}_2Mg.2DMSO.C_6H_5CH_3]$ **4A** and $[\{PhNC(Ph)NPh\}_2Mg.2HMPA.C_6H_5CH_3]$ **4B** were shown to be monomers by X-ray crystallography. Compound **4B** was found to crystallise as two independent monomers, only one of which will be discussed here. In the crystal lattice of both compounds, toluene was also found to be present (1 molecule per monomer), thus confirming the ^1H NMR formulation.

The six-coordinate magnesium centre in both complexes is bound to two chelating η^2-amidinide units and two monodentate oxygen donor molecules arranged in a distorted octahedral geometry. The ligand sphere about each magnesium centre in both compounds is shown in figure 4.4.

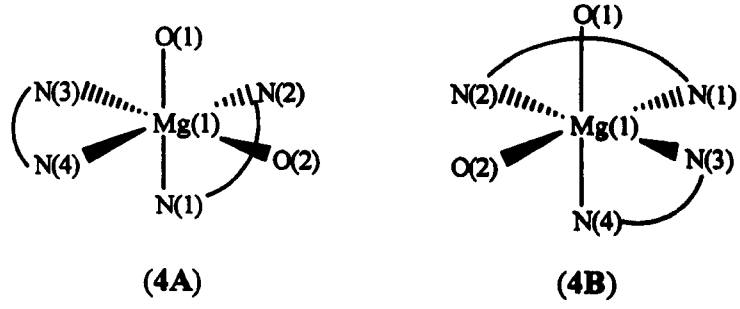

Figure 4.4- Idealised coordination geometries in amidinide monomers

In compound **4A** and **4B**, as drawn, the axial sites are represented by [O(1)/N(1)] and [O(1)/N(4)], and the equatorial sites are represented by [N(2)/N(3)/N(4)/O(2)] and [N(1)/N(2)/N(3)/O(2)] respectively. The amidinide ligands and donor molecules in both complexes are disposed in a *cis* conformation. The core of each structure is made up of two, essentially planar, $\overline{NCNMg}$ four-membered rings. Within each amidinide unit, compounds **4A** and **4B**, display approximately uniform C-N distances [i.e. **4A**, N(1)-C(7), 1.328(2)Å, N(2)-C(7), 1.338(2)Å, N(3)-C(26), 1.340(2)Å, N(4)-C(26), 1.333(2)Å;

4B, N(1)-C(7), 1.338(13)Å, N(2)-C(7), 1.340(14)Å, N(3)-C(26), 1.315(14)Å, N(4)-C(26), 1.319(14)Å] which are almost an exact average of the C=N [1.302(7)Å] and C-N [1.360(8)Å] bond lengths observed in the protonated uncomplexed amidine[1], which suggests the presence of uniform delocalisation throughout the three-atom central unit. Thus the two anions in each structure can be considered as diazaallyl systems. The N-Mg bond distances in compound **4A** are found to be similar to those found in **4B** [i.e. **4A**, mean 2.193Å c.f. **4B**, 2.229Å]. The O-Mg bond distances in compounds **4A** and **4B** are observed to be much shorter than those observed in the aforementioned six-coordinate, THF solvated magnesium bis amide complex [Mg{N(2-pyr)Ph}$_2$.2THF][2] **39** (figure 1.14, pg.26), reflecting the much stronger donor strengths of both DMSO and HMPA in comparison to THF [i.e. **4A**, 2.062Å; **4B**, 2.028Å c.f. 2.212Å in **39**].

As mentioned above, the geometry about the central magnesium in compounds **4A** and **4B** is that of a distorted octahedron [e.g. range of axial-equatorial angles **4A**, 60.63(6)°-113.64(6)°, **4B**, 59.5(3)°-103.1(4)° c.f. 90.0° in an ideal system]. Where the largest distortions are observed between the chelating nitrogen centres of the amidinide ligands [i.e. **4A**, N(2)-Mg(1)-N(1), 60.63(6)°, N(4)-Mg(1)-N(3), 61.11(6)°; **4B**, N(3)-Mg(1)-N(4), 59.5(3)°, N(2)-Mg(1)-N(1), 60.4(3)°] this can be attributed to the steric constraints of the ligand. The distorted NCN angle within the $\overline{\text{NCNMg}}$ four-membered rings in compounds **4A** and **4B** are observed to be slightly smaller than those found in the lithium derivatives[3], [PhC(NPh)$_2$Li.D] where D = TMEDA **102** or PMDETA **103** the ligands of which also show diazaallyl character [i.e. **4A**, N(4)-C(26)-N(3), 111.97(15)°, N(1)-C(7)-N(2), 113.38(15)°; **4B**, N(3)-C(26)-N(4), 114.5(10)°, N(1)-C(7)-N(2), 113.3(9)° c.f. **102**, N-C-N, 115.0(2)°; **103**, N-C-N, 116.7(3)°].

At the time of writing, the only other monomeric magnesium amidinate structure present in the literature is that of the N-silylated derivative[4], [{PhC(NSiMe$_3$)$_2$}$_2$Mg.N≡CPh] **96**, where the central five-coordinate magnesium is encapsulated by two chelating η^2-benzamidinate ligands and one solvating benzonitrile molecule arranged in a distorted trigonal bipyramidal geometry. The N-Mg distances in

compound **96** are observed to be shorter than those in compounds **4A** and **4B** [i.e. 2.115Å c.f. mean 2.193Å in **4A**, mean 2.229Å in **4B**]. This can be explained by the difference in coordination numbers of the magnesium centres involved (6 in **4A/4B** c.f. 5 in **96**) and also due to the different functionalities present on the nitrogen atoms (i.e. large positive silicon groups will polarise the nitrogen centres more than phenyl groups will, therefore stronger bonds to magnesium are expected in the former).

4.5 Synthesis and Analysis of Compound 4C

The heteroleptic magnesium bis(amide) complex $[\{(Me_3Si)_2NMgN(H)C_6H_5.THF\}_2]$ **4C**, was prepared from a 1:1 transamination reaction involving the crystalline magnesium bis(amide) precursor, $[\{(Me_3Si)_2N\}_2Mg]$ and aniline in a toluene/THF solution (equation 4.2).

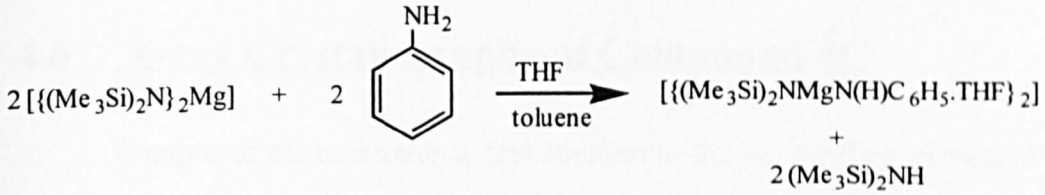

(4.2)

Satisfactory elemental analyses were obtained. On exposure to air the infrared spectrum displayed two broad bands at $3708cm^{-1}$(br) and $3383cm^{-1}$(br) which corresponds to that of $Mg(OH)_2$ and regeneration of the free amines respectively (N-H, NH_2).

The ^1H NMR spectrum, in d_5-pyridine, clearly showed all relevant signals. On metallation of aniline a significant low frequency shift is observed for the N-H proton i.e. 5.39ppm in aniline c.f. 3.62ppm in compound **4C**. By comparison the protons on the phenyl ring only experience a small low frequency shift as a result of charge delocalisation. This is highlighted in table 4.8.

Compound	*meta* – Ph / ppm	*ortho* – Ph / ppm	*para* – Ph / ppm
$C_6H_5NH_2$	7.25	6.97	6.79
$[\{(Me_3Si)_2NMgN(H)C_6H_5.THF\}_2]$ **4C**	7.16	6.89	6.50

Table 4.8- Comparison of phenyl ^1H chemical shifts

The chemical shifts for the donor molecule, THF, were clearly distinguished at 3.68ppm (OCH_2) and 1.65ppm (CH_2). The trimethylsilyl groups were found at lower frequency at 0.25ppm.

As a result of poor solubility, $^{13}C\{^1H\}$ NMR data was not collected.

4.6 X-ray Crystallography of Compound 4C

Compound **4C** represents a new addition to the yet poorly represented family of heteroleptic magnesium bis amide structures of which only two, at present, can be found in the literature, as discussed earlier (figure 1.15, pg.27).

The crystal structure of $[\{(Me_3Si)_2NMgN(H)C_6H_5.THF\}_2]$ **4C** is that of a common dimeric arrangement, the salient feature of which is a central, planar, four-membered $\overline{MgNMgN}$ azamagnesacyclic ring. The magnesium centres are four-coordinate occupying distorted tetrahedral environments [i.e. range of bond angles, 102.21(2)°-124.37(4)°]. In this structure the anilino ligands are observed to bridge the magnesium centres while the bulkier hexamethyldisilazide ligands prefer to bind terminally. This positioning has also been observed in the analogous substituted anilino derivative $[Mg_3\{(\mu\text{-}N(H)Dipp\}_4\{N(SiMe_3)_2\}_2]$[5] **26** which adopts a remarkable trimeric array. Both of these structures can thus be rationalised in terms of the steric bulk of the amide units involved, where the larger hexamethyldisilazide groups prefer terminal positions. In table 4.9 a comparison of the internal ring dimensions of compound **4C** is made with the other heteroleptic bis(amides).

Structure	N_{br}-Mg Bond distances / (Å)	N_{br}-Mg-N_{br} Bond angles / (°)	Mg-N_{br}-Mg Bond angles / (°)
$[\{(Me_3Si)_2NMgN(H)C_6H_5.THF\}_2]$ **4C**	2.102(10)	89.85(4)	90.15(4)
	2.140(11)		
$[\{Mg[\mu\text{-}N(Ph)_2][NPh(2\text{-}pyr)]\}_2]$ **25**	2.080(5)	90.0(2)	90.0(2)
	2.119(5)		
$[Mg_3\{(\mu\text{-}N(H)Dipp\}_4\{N(SiMe_3)_2\}_2]$ **26**	2.095(6)	89.5(2)	90.3(2)
	2.128(6)	90.6(2)	89.5(2)

Where br = bridging

Table 4.9- Comparative geometric data for heteroleptic magnesium bis(amides)

The μN-Mg bond distances in compound **4C** are asymmetrical with short edges and long edges differing by 0.038Å. This could imply that the origin of the dimeric set-up lies in two monomeric moieties, which combine in a transoid arrangement with respect to its amido substituents with the new bonds formed being [Mg-N(1)] and [Mg(A)-N(1A)], and the bridging nitrogen atoms exhibiting sp^3-hybridisation. Alternatively, the bridging nitrogen atoms can be considered as being sp^2-hybridised, whereby two sp^2 orbitals are involved in σ-bonding to the *ipso*-carbon of the phenyl ring and to the hydrogen atom. The two remaining electron pairs thus occupy the remaining hybrid orbital and the unhybridised p-orbital, which lies orthogonal to the anilide plane. The short N-Mg distance (represented by dark lobe) can hence be considered due to the interaction of magnesium with the sp^2 lone pair from the nitrogen while the longer N-Mg distance (represented by the light lobe) can be attributed to interaction of magnesium with the unhybridised p-orbital (figure 4.5). This bonding mode has also been suggested for the dimeric lithium anilide complex[6] $[PhN(H)Li.2THF]_2$ **129**: the distances involved in the asymmetric $\overline{LiNLiN}$ ring [i.e. short N-Li distance, 1.989Å; long N-Li distance, 2.087Å] indicate that the effect is more pronounced in this case.

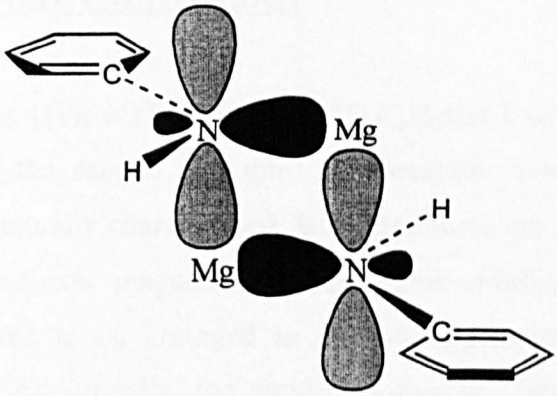

Figure 4.5- Orbital representation of four-membered MgNMgN central ring

It appears significant that all the endocyclic bond angles in compounds **4C**, **25** and **26** are within standard deviations of 90°. This suggests that the longer N-Mg bonds in these structures have considerable p-character.

Unsurprisingly, the terminal N-Mg bond distances in compound **4C** are shorter than the bridging ones [i.e. 2.003(11)Å], indicating that the terminal anions bind more strongly to the magnesium centres. Similar terminal N-Mg bond lengths have been found in other hexamethyldisilazide complexes [i.e. in **25**, 1.966(6)Å; in $[Mg\{N(SiMe_3)_2\}_2]_2$ **23**, 1.98Å; in $[Mg\{N(SiMe_3)_2\}_2.2THF]$ **28**, 2.021Å]. The O-Mg distance is shorter than that in the four-coordinate bis-THF solvated monomer **28** [i.e. 2.026(9)Å in **4C** c.f. 2.093(5)Å in **28**].

4.7 Chapter Four Conclusions

The complexes $[\{PhNC(Ph)NPh\}_2Mg.2D.C_6H_5CH_3]$ where D = DMSO **4A** or HMPA **4B** represent the second and third monometallic magnesium bis(amidinide) compounds to be structurally characterised. Both structures are isostructural and consist of a central six-coordinate magnesium centre. The amidinide ligands and donor molecules are observed to be arranged in a *cis*-arrangement occupying a distorted octahedral geometry. Additionally, the amidinide ligands chelate to the metal centre forming almost planar $\overline{NCNMg}$ four-membered rings, indicating (σ,σ) bonding. These ligands can be considered to be aza-allyl functionalities in view of the C-N bond distances observed within each amidinide unit.

Finally, the heteroleptic, magnesium bis(amide) complex $[\{(Me_3Si)_2NMgN(H)C_6H_5.THF\}_2]$ **4C** has been prepared, which represents only the third such compound to be crystallographically characterised. The structure is found to be that of a dimeric arrangement, whereby each magnesium is four-coordinate occupying a distorted tetrahedral environment. The planar, anilide functions are found to lie in the bridging positions whereas the bulkier bis(trimethylsilyl) amide ligands preferentially occupy terminal positions. The fourth coordination site at magnesium is occupied by a terminally bound THF molecule.

4.8 Chapter Four Further Work

For structural comparison to **4A** and **4B** other solvates of [{PhNC(Ph)NPh}$_2$Mg.D] where D = THF, TMEDA etc should be synthesised. A whole series of magnesium bis(amidinides) can be prepared and investigated using different amidinide ligands e.g.

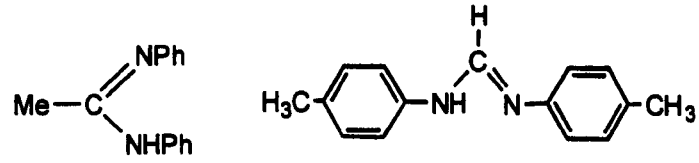

Also the possibility of synthesising mixed-metal analogues using N,N'-diphenylbenzamidine could also be considered e.g.

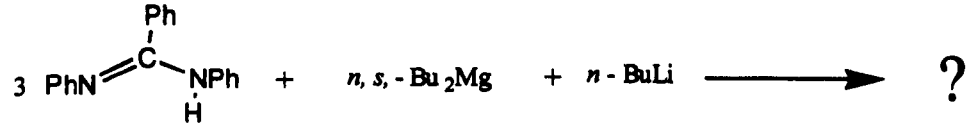

The preparation of compound **4C** in the presence of other donor solvents should be considered to see whether or not the dimeric structure is retained or if a monomeric, heteroleptic structure is formed. Additionally, other mixtures of both primary and / or secondary amides could be employed e.g. bis(trimethylsilyl) amine / dibenzylamine. Variable temperature ^{1}H NMR studies could also be carried out to determine if, the dimeric structure remains intact in solution.

4.9 Chapter Four References

[1] N. W. Alcock, J. Barker and M. Kilner; *Acta. Crystallogr., Section C.* (1988), **44**, 712.

[2] K. W. Henderson, R. E. Mulvey, W. Clegg and P. A. O'Neil; *J. Organomet. Chem.*, (1992), **439**, 237.

[3] J. Barker, D. Barr, N. D. R. Barnett, W. Clegg, I. Cragg-Hine, M. G. Davidson, R. P. Davies, S. M. Hodgson, J. A. K. Howard, M. Kilner, C. W. Lehmann, I. Lopez-Solera, R. E. Mulvey, P. R. Raithby and R. Snaith., *J. Chem. Soc., Dalton. Trans.*, (1997), 951.

[4] M. Westerhausen and H-D. Hausen; *Z. Anorg. Allg. Chem.*, (1992), **615**, 27.

[5] M. M. Olmstead, W. J. Grigsby, D. R. Chacon, T. Hascall and P. P. Power; *Inorg. Chim. Acta.*, (1996), **251**, 273.

[6] R. v. Bülow, H. Gornitzka, T. Kottke and D. Stalke; *J. Chem. Soc., Chem. Commun.*, (1996), 1639.

Appendices

Appendix I

Abbreviations Used Throughout Text:

α	alpha
β	beta
Bu^n	n-butyl
Bu^s	sec-butyl
Bu^t	tert-butyl
Bzl	benzyl
c	cyclo
C.I.P	contact ion pair
DBM	n,s-dibutylmagnesium, Bu_2Mg
Dipp	diisopropylphenyl
DME	dimethoxyethane, $MeOCH_2CH_2OMe$
DMPU	1,3-dimethyl-3,4,5,6-tetrahydro-2(1H)-pyrimidinone
DMSO	dimethylsulphoxide, $Me_2S{=}O$
EDT	ethane-1,2-dithiolate
Et	ethyl
HMPA	hexamethylphosphoramide, $(Me_2N)_3P{=}O$
HTHD	2,2,6,6-tetramethylheptane-3,5-dione
i	iso
J	coupling constant
K	kelvin
LiTMP	lithium tetramethylpiperidide
LDA	lithium diisopropylamide
m	meta
Me	methyl
Mes	mesityl
NaHMDS	sodium hexamethyldisilazide

NMR	nuclear magnetic resonance spectroscopy
o	ortho
p	para
Ph	phenyl
PMDETA	*N,N,N',N',N''-pentamethyldiethylenetriamine,* $(Me_2NCH_2CH_2)_2NMe$
Pr	propyl
Pyr	pyridine
R	variable organic group
s	secondary
S.S.I.P	solvent separated ion pair
t	tertiary
THF	tetrahydrofuran
tmdbtd	7,16-2H-6,8,15,17-tetramethyldibenzo[b,i]-[1,4,8,11]-tetra-azacyclotetradecine
TMCDA	N,N,N',N'-tetramethylcyclohexanediamine, $Me_2N(c\text{-}C_6H_{10})NMe_2$
TMEDA	N,N,N',N'-tetramethylethylenediamine, $Me_2NCH_2CH_2NMe_2$
TMP	tetramethylpiperidide
TMPH	2,2,6,6-tetramethylpiperidine
Tol	toluene
Trip	triisopropylphenyl
X	variable halide group

Abbreviations used in infrared analysis

s	strong
m	medium
w	weak
br	broad
v	very

Appendix II

General Experimental and Instrumentation

Inert Atmosphere Techniques*

Due to the moisture / oxygen sensitivity of organolithium / organomagnesium reagents. Syntheses were carried out using standard Schlenk techniques, whereby all reactions were carried out under an inert argon atmosphere. Air was removed *in vacuo* using an Edwards oil pump. The blanket gas was dried prior to use by passing through two columns, one containing molecular sieves (A4) and the other containing phosphorus pentoxide (which readily converted to phosphoric acid on contact with moisture). Some reaction products were filtered through a sintered glass frit of known porosity, then evacuated prior to storage in the glove box. More often however, crystalline products were left in their mother liquor prior to crystal structure determination so as not to effect the crystal quality by evacuation i.e. solvent loss. Isolated samples were stored in small round bottomed flasks in the argon-filled glove box prior to characterisation.

Solvents and Reactants

All solvents and reactants were distilled and degassed (where applicable) prior to use. Distillation of solvents were carried out over a benzophenone / sodium mix, whereby blue colourisation indicated the formation of ketyl radicals in the presence of moisture. Amines were stirred in calcium hydride for 24 hours, prior to distillation. Degassing procedures involved the freeze-pump-thaw method whereby solvents were frozen in a liquid nitrogen bath then allowed to thaw slowly to room temperature under vacuum. This was repeated several times prior to use

---

* D. F. Schriver and M. A. Drezdzon; *The Manipulation of Air Sensitive Compounds.*, (1986), Wiley-Interscience, New York.

Metallating Reagents

Both *n*-butyllithium (*n*-BuLi) and *n,s*-dibutylmagnesium (DBM) were purchased from the Aldrich Chemical Co as alkane solutions. Periodically, these were standardised in order to determine their exact molarity. This procedure will now be considered. To a known quantity of diphenylacetic acid was added THF (10ml) this solution was then titrated with a known volume of *n*-BuLi. End-point colourless-yellow. For DBM another standardisation procedure was employed whereby to a known volume of reagent was added a few crystals of 1,10-phenanthroline, this was then titrated with a xylene / Bu^sOH solution (1 M) end-point from purple to yellow.

Both *n*-butylsodium (*n*-BuNa) and *n*-butylpotassium (*n*-BuK) were prepared from the transmetallation reaction of *n*-BuLi with an equimolar quantity of the respective metal *tert*-butoxide in hexane solution. The reaction was left to stir for 1 hour at 0°C then filtered and washed (so to remove any soluble $LiOBu^t$) with several aliquots of hexane prior to isolation. *n*-BuNa was isolated as a cream coloured precipitate, whereas the potassium analogue was to be a much darker red / brown solid. Only small batches were prepared on the day as required due to the fierce pyrophoricity and ready decomposition of these compounds.

Instrumentation

Infrared analyses were carried out on a Unicam Mattson 1000 FTIR spectrometer. Samples were prepared as nujol-mulls between either NaCl or KBr plates inside the glove box and transferred to the spectrometer in a dessicator. The nujol was dried over sodium wire. Two spectra were generally recorded for each sample, one before and one after exposure to air. NMR spectra (^1H, ^{13}C and ^7Li) were recorded on either a Bruker AMX or Bruker DPX 400MHz spectrometer. Samples were prepared in the glove box using selected, molecular sieve dried, deuterated solvents. NMR tubes were sealed with a plastic cap reinforced with parafilm prior to analysis. Both ^1H and

^{13}C NMR spectra were referenced to the deuterated solvent signal whereas ^{7}Li NMR spectra were internally referenced to LiCl in D_2O. Elemental analyses (C, H, N) were conducted on a Perkin-Elmer 240 elemental analyser. Samples were prepared by pre-weighing a small tin foil container then filling this with the compound awaiting analysis (1mg). The foil was then rolled up in order to protect the compound from the open atmosphere and re-weighed outside the box prior to analysis. Metal analyses (Li, Mg, Na) were obtained using a Phillips PU 9100X flame absorption spectrometer. Aluminium analysis was carried out on Phillips PU 9400 flame absorption spectrometer. Samples were made up as acidified solutions whereby the concentration of metal was calculated by contrasting with a series of standard solutions containing metal ions. Only analytical grade reagents and distilled water were used.

Appendix III

Crystallographic Data[†]

All crystal structure determinations were carried out at low temperature, whereby crystals were removed from the Schlenk tube under a protective flow of argon or nitrogen gas. These were then coated in an inert perfluorinated oil and transferred to the goniometer head. Once on the diffractometer, a low temperature stream of nitrogen rendered the oil viscous enough to ensure an air tight barrier was achieved during data collection.

X-ray crystallographic studies were carried out at two locations:

1) At Newcastle University, Newcastle, UK, by Prof. Bill. Clegg and co-workers whereby measurements were recorded on either a Stoe-Siemens or Siemens SMART CCD diffractometer using graphite-monochromated MoKα radiation (λ = 0.71073Å) and a cryostream cooler.

2) At Strathclyde University, Glasgow, UK, by Dr. Alan R. Kennedy whereby measurements were recorded on a Rigaku AFC7S diffractometer using graphite-monochromated MoKα radiation (λ = 0.71069Å) and a cryostream cooler.

Important structural parameters of each crystal structure determined are listed below.

[†] G. M. Sheldrick, SHELXL a family of programs for crystal structure refinement, University of Göttingen.

Chapter Two

(1) [{(1,8-$C_{10}H_6(NH)_2$)Mg.HMPA}$_3$.2THF], 2A (Newcastle)

Triclinic colourless prism, space group $\bar{P}1$

a = 14.4134(8)Å	b = 14.7158(8)Å	c = 15.7422(9)Å
T = 160K	Z = 2	V = 3263.6(3)Å^3
α = 86.991(10)°	β = 87.799(10)°	γ = 78.280(10)°

(2) [{MgN(Ph)CH_2CH_2N(Ph).2THF(1.5 THF)}$_2$], 2B (Newcastle)

Monoclinic colourless prism, space group C_2/c

a = 21.035(2)Å	b = 13.682(11)Å	c = 19.439(15)Å
T = 160K	Z = 4	V = 5419.7(7)Å^3
α = 90°	β = 104.368(2)°	γ = 90°

(3) [{MgN(CH_2Ph)CH_2CH_2N(CH_2Ph).HMPA}$_2$], 2C (Newcastle)

Triclinic colourless prism, space group $\bar{P}1$

a = 10.764(2)Å	b = 11.130(2)	c = 11.463(2)
T = 160K	Z = 1	V = 1232.0(4)
α = 89.025(7)°	β = 70.839(4)°	γ = 72.483(6)°

(4) [MgN(Ph)CH_2CH_2N(Ph).2HMPA], 2D (Newcastle)

Triclinic colourless prism, space group $\bar{P}1$

a = 11.116(4)Å	b = 15.945(4)Å	c = 19.872(7)Å
T = 160K	Z = 4	V = 336.4(19) Å^3
α = 73.71(2)°	β = 83.81(2)°	γ = 81.62(3)°

(5) [Mg(HMPA)$_4$.2 AlMe$_4$], 2E (Newcastle)

Orthorhombic colourless prism, space group $P2_12_12_1$

a = 13.796Å	b = 17.468(7)Å	c = 23.691(9)Å
T = 160K	Z = 4	V = 5709.2(4)Å^3
α = 90°	β = 90°	γ = 90°

Chapter Three

(6) [{(Me$_3$Si)$_2$N}$_3$LiMg], 3A (Strathclyde)

Triclinic colourless prism, space group $P1$

a = 8.994(2)Å	b = 11.440(5)Å	c = 16.620(4)Å
T = 123K	Z = 2	V = 1628.3(8)Å^3
α = 98.33(2)°	β = 92.57(19)°	γ = 105.00(3)°

(7) [{(*c*-C$_6$H$_{11}$)$_2$N}$_3$LiMg.THF], 3B (Strathclyde)

Monoclinic colourless prism, space group Cc

a = 11.014(4)Å	b = 18.998(6)Å	c = 19.317(4)Å
T = 123K	Z = 4	V = 3984(2)Å^3
α = 90°	β = 99.70(5)°	γ = 90°

(8) [{(Me$_3$Si)$_2$N}$_4$Li$_2$Mg$_2$(O$_2$)$_x$(O)$_y$], 3C (Strathclyde)

Monoclinic colourless prism, space group $P2/n$

a = 9.161(3)Å	b = 13.785(5)Å	c = 18.139(4)Å
T = 123K	Z = 4	V = 2290.1(12)Å^3
α = 90°	β = 91.17(2)°	γ = 90°

(9) $[\{PhC(NSiMe_3)_2\}_4Li_4Mg(O)]$, 3D (Strathclyde)

Orthorhombic colourless needle, space group *Pbcn*

a = 10.317(3)Å	b = 26.138(15)Å	c = 24.986(14)Å
T = 123K	Z = 4	V = 6738(6)Å^3
α = 90°	β = 90°	γ = 90°

(10) $[\{Me_2\overline{CCH_2CH_2CH_2(Me)_2CN}\}_4Li_2Mg_2(O)]$, 3E (Strathclyde)

Monoclinic colourless needle, space group C_2/c

a = 16.946(3)Å	b = 16.981(3)Å	c = 15.710(3)Å
T = 123K	Z = 4	V = 3957.0(13)Å^3
α = 90°	β = 118.93(10)°	γ = 90°

(11) $[\{(Me_3Si)_2N\}_4Na_2Mg_2(O_2)_x(O)_y]$, 3F (Strathclyde)

Triclinic colourless prism, space group *P*1

a = 10.778(2)Å	b = 12.695(4)Å	c = 8.851(1)Å
T = 123K	Z = 2	V = 1122.8(5)Å^3
α = 108.03(2)°	β = 99.49(2)°	γ = 95.21(2)°

(12) $[\{Me_2\overline{CCH_2CH_2CH_2(Me)_2CN}\}_6Na_4Mg_2\{C_6H_3(CH_3)\}]$, 3G (Strathclyde)

Monoclinic colourless prism, space group $P2_1/n$

a = 15.277(2)Å	b = 8.213(3)Å	c = 25. 541(6)Å
T = 123K	Z = 2	V = 3195(1)Å^3
α = 90°	β = 94.28(1)°	γ = 90°

(13) [{$Me_2CCH_2CH_2CH_2(Me)_2CN$}$_6Na_4Mg_2(C_6H_4)$], 3H (Strathclyde)

Monoclinic colourless needle, space group $P2_1/n$

a = 15.206(2)Å	b = 8.175(3)Å	c = 25.524(3)Å
T = 123K	Z = 2	V = 3165(1)Å^3
α = 90°	β = 93.85(1)°	γ = 90°

(14) [{$(Me_3Si)_2N$}$_4K_2Mg_2$.4{$C_6H_5(CH_3)$}], 3I (Strathclyde)

Triclinic colourless prism, space group $P1$

a = 9.614(8)Å	b = 15.765(2)Å	c = 16.116(2)Å
T = 123K	Z = 1	V = 2223.6(5)Å^3
α = 72.529(10)°	β = 74.898(7)°	γ = 77.439(8)°

Chapter Four

(15) [{$PhNC(Ph)NPh$}$_2$Mg.2DMSO.$C_6H_5CH_3$], 4A (Newcastle)

Triclinic green-coloured prism, space group $P1$

a = 12.594(15)Å	b = 13.928(17)Å	c = 14.758(18)Å
T = 160K	Z = 2	V = 2179.3(5)Å^3
α = 110.78(3)°	β = 95.77(3)°	γ = 111.10(3)°

(16) [{$PhNC(Ph)NPh$}$_2$Mg.2HMPA.$C_6H_5CH_3$], 4B (Newcastle)

Monoclinic green-coloured prism, space group $P2_1$

a = 10.598(13)Å	b = 43.102(6)Å	c = 13.535(17)Å
T = 160K	Z = 2	V = 5675.9(12)Å^3
α = 90°	β = 113.37(3)°	γ = 90°

(17) $[\{(Me_3Si)_2NMgN(H)C_6H_5.THF\}_2]$, 4C (Newcastle)

Monoclinic colourless prism, space group $P2_1/n$

a = 8.934(4)Å	b = 21.311(10)Å	c = 10.806(5)Å
T = 160K	Z = 2	V = 2047.45(16)Å^3
α = 90°	β = 95.62(2)°	γ = 90°